Repeatability of an Integrative Method to Assess Knee Joint Mechanics and Cartilage Health under Load

A Thesis Submitted to the College of

Graduate and Postdoctoral Studies

In Partial Fulfillment of the Requirements

For the Degree of Master of Science

In the Department of Mechanical Engineering

University of Saskatchewan

Saskatoon

By

Ibukunoluwa Olajumoke Elebute

PERMISSION TO USE

In presenting this thesis in partial fulfillment of the requirements for a Postgraduate degree from the University of Saskatchewan, I agree that the Libraries of this University may make it freely available for inspection. I further agree that permission for copying of this thesis in any manner, in whole or in part, for scholarly purposes may be granted by Dr. Emily McWalter, who supervised my thesis project or in her absence, by the Head of the Department or the Dean of the College in which my thesis work was done. It is understood that any copying or publication or use of this thesis or parts thereof for financial gain shall not be allowed without my written permission. It is also understood that due recognition shall be given to me and to the University of Saskatchewan in any scholarly use which may be made of any material in my thesis.

Requests for permission to copy or to make other uses of materials in this thesis in whole or part should be addressed to:

Head of the Department of Mechanical Engineering
57 Campus Drive
University of Saskatchewan
Saskatoon, Saskatchewan S7N 5A9
Canada

OR

Dean
College of Graduate and Postdoctoral Studies
University of Saskatchewan
116 Thorvaldson Building, 110 Science Place
Saskatoon, Saskatchewan S7N 5C9
Canada

ABSTRACT

An integrative and repeatable method that assesses quantitative magnetic resonance imaging (qMRI), mechanical measures by MRI (mechMRI) and gait (kinetics and kinematics) parameters is needed to better understand the mechanics of ACL-injury which is an early model of post-traumatic osteoarthritis. In developing a method that can be used, this research sought to answer three major questions: 1) What is the repeatability of the qMRI, mechMRI and gait analysis measures in healthy individuals? 2) What is the repeatability of the kinematic and kinetic outcomes using a MRI-based anatomical system and a standard gait coordinate system? 3) Is there a link between contact area and qMRI T_2 relaxation times in cartilage?

Addressing the above research questions involved primarily assessing the repeatability of each measure, expressed as the root-mean squared standard deviation (SD_{rms}), as well as evaluating novel measures to determine the link between the different metrics. A MRI-safe loading rig was designed to simulate loading at the knee joint during MRI scanning as well as MRI-lucent gait markers to create a common coordinate system between the MRI and gait systems.

Data was collected three times within a week for five healthy participants for this repeatability study. At the gait lab, participants carried out five motion tasks including walking, stair ascent, descent and chair rise and sit. With the MRI-lucent gait markers still at the same position, qMRI T_2 relaxation time and anatomical MRI scans were carried out. The scans were acquired while the knee was unloaded and fully extended as well as loaded in two flexed positions.

The repeatability results showed a link between qMRI T_2 relaxation times and contact areas with low-SD_{rms} measures in some qMRI-contact integration metrics and coordinate methods of processing dynamic data. qMRI-contact integration metrics were found to have smaller SD_{rms} values for loaded cartilage in the lateral region (Average SD_{rms}: 2.2 ms). Walk peak abduction angle had the smallest SD_{rms} value for kinematics (0.8 degrees) and walk peak flexion moment for the kinetic measures (0.04 N.m/kg). Between dynamic data processed with MRI-based anatomical coordinates and standard gait coordinates systems, functional-based was generally found to have the smaller SD_{rms} values. MRI-based processed data showed smaller SD_{rms} values in kinetic outcome measures compared to that acquired from the standard gait coordinate system.

In conclusion, there are indeed measures across the three different metrics that have smaller SD_{rms} values and therefore may be better suited for use in the study of the ACL-injured population. From the findings of this study, we recommend particular attention be paid to lateral and loaded cartilage conditions for contact mechanics and qMRI T_2 evaluation, and that knee kinematics and kinetics be evaluated with standard gait coordinate system, for the study of healthy and ACL-injured individuals.

ACKNOWLEDGEMENTS

This thesis is first of all dedicated to God, who is the source of all inspiration and discovery. My heart is full of gratitude knowing He was with me every step of the way. And for the many He brought my way to support me on this journey.

I am indeed very grateful for my family – my Dad who has sacrificed so much to make sure I could pursue such a feat. My mum, who has been an amazing support system. All four of my siblings - Eniife, Tolu, Ododo and especially Dara for the opportunity to vent with on similar research challenges. I love every one of you!

I truly appreciate these very special beings – Kirstin, Kadin, Amy, Nima, Dylan, Alvaro, Brennan, Tim, Merhdad, Mahdi, Josje, Jack, Maddie, Chelsey and Dena. I will also like to specially thank Lumeng for all of his help with developing the MRI sequences. My sincere thanks to several friends on campus and to my Calgary family – Ibukun, Ben, Tara and Vicky.

I am truly grateful for Dr. Olubamiji's guidance and insight that has helped make this journey much easier. To Adaora Mbelu whose constant words and life of inspiration has helped shed light on my path, I am truly grateful. I would also use this opportunity to express profound gratitude to Dr. McWalter without whose supervision, this work will not be possible. I truly appreciate all of the sacrifices made and support given to make this happen. Thank you!

TABLE OF CONTENTS

PERMISSION TO USE i
ABSTRACT ii
ACKNOWLEDGEMENTS iv
TABLE OF CONTENTS v
LIST OF TABLES x
LIST OF FIGURES xiv
LIST OF ABBREVIATIONS xvi
Chapter 1 1
INTRODUCTION 1
1.1 Overview 1
1.2 Thesis Organization 2
Chapter 2 3
BACKGROUND 3
2.1 The Knee 3
2.1.1 Anatomy 3
2.1.2 Articular Cartilage under Load 3
2.1.3 Anterior Cruciate Ligament (ACL) 5
2.2 Knee Osteoarthritis (OA) 6
2.2.1 ACL-injury and Post-Traumatic OA (PTOA) 6
2.2.2 Macromolecular Changes of Meniscus and Cartilage in PTOA 7
2.2.3 Radiographic Detection of OA 8
2.3 Quantitative MRI (qMRI) measures in OA pathology 8
2.3.1 Basic Principles of MRI 8
2.3.2 T_2 Relaxation Time Analysis 10
2.3.3 qMRI Analysis Techniques 10
2.3.4 Loading in qMRI Analysis 12
2.4 Mechanical measures from MRI (mechMRI) 14
2.4.1 Load and Motion Conditions in mechMRI Analysis 14

2.4.2 Mechanical measures from MRI 15
2.4.2.1 Contact Area, Centroid and Femoral Tracking 15
2.4.2.2 Image-Based Three-Dimensional Kinematics 21
2.5 Knee Axes Definitions in Three-Dimensional Kinematics and Kinetics 25
2.6 Gait Analysis Measures 26
2.6.1 Relevant Motion Tasks for Gait Analysis 27
2.6.2 Error Measurement in Gait Analysis Measures 27
2.6.3 Key Mechanical Outcomes and Time from Reconstruction Surgery 31
2.7 The Impact of Sex Differences 32
2.8 Some Integrative Studies and Research Motivation 33
2.9 Summary 35
2.10 Research Questions and Objectives 36
Chapter 3 37
METHODOLOGY 37
3.1 Study Design 39
3.2 Data Acquisition 39
3.2.1 MRI 39
3.2.1.1 RF Coil Setup 39
3.2.1.2 Fully-Extended Unloaded Scans 40
3.2.1.3 Flexed Loaded Scans 42
3.2.2 Gait Analysis 42
3.2.2.1 Gait Analysis Apparatus Setup 43
3.2.2.2 Gait Analysis Data Collection Procedure 43
3.3 MRI-safe Loading Rig 45
3.4 MRI-lucent markers 45
3.5 Data Processing 46
3.5.1 qMRI 46
3.5.1.1 Cartilage Segmentation 46

3.5.1.2 Projection Map Generation 46
3.5.1.3 Difference Maps 47
3.5.1.4 Cluster Analysis 48
3.5.1.5 Regional Cartilage Demarcation 49
3.5.2 mechMRI 50
3.5.2.1 Femur Registration and Coordinate System Assignment 50
3.5.2.2 Femur and Contact Segmentation 51
3.5.2.3 Contact Area and Centroid 51
3.5.3 Gait Analysis 51
3.5.3.1 Kinematics 52
3.5.3.2 Kinetics 54
3.6 MRI-Gait Integration 55
3.6.1 Deciding on the Best Approach for Determining MRI-Marker Centroid Position 55
3.6.2 Processing Dynamic Data with MRI-based Landmarks 56
3.7 Integration of qMRI T_2 and Contact Area 58
3.8 Repeatability and Statistical Analysis 59
Chapter 4 61
RESULTS 61
4.1 Patient Characteristics 61
4.2 Quantitative MRI T_2 Repeatability for General, Medial, Lateral and Trochlear Regions at Loaded, Unloaded and Load-Unload Difference 61
4.3 mechMRI Outcomes 63
4.3.1 Repeatability of Contact Centroid Translation 64
4.3.2 Repeatability of Medial and Lateral Contact Area Values at Different Limb Positions 65
4.4 Kinematic and Kinetic Outcomes 67
4.4.1 Repeatability of MRI-based Coordinate System Kinematics Outcomes 67
4.4.2 Repeatability of MRI-based Coordinate System Kinetics 68

4.4.3 Repeatability of Gait-based Coordinate System Kinematics 70
4.4.4 Repeatability of Gait-based Coordinate System Kinetics 71
4.5 MRI-based and Gait-based Outcomes Comparison 73
4.6 Repeatability of qMRI-Contact Integration 78
4.6.1 qMRI-Contact Integration Outcomes – Medial Compartment 78
4.6.2 qMRI-Contact Integration Outcomes – Lateral Compartment 81
4.6.3 Repeatability of Load-Unload qMRI T_2-contact Integration Outcomes – Cluster Maps 83
Chapter 5 86
DISCUSSION 86
5.1 What is the repeatability qMRI, mechMRI and gait analysis measures? 86
5.1.1 qMRI T_2 Relaxation Time 86
5.1.2 Contact Area and Contact Area Centroid Translation (mechMRI) 88
5.1.3 Gait Analysis 91
5.1.3.1 Kinematics 91
5.1.3.2 Kinetics 93
5.1.3.3 Summary 94
5.1.4 What is the repeatability of qMRI, mechMRI and gait analysis measures? - Conclusion 94
5.2 What is the repeatability of the kinematic and kinetic outcomes using a MRI-based anatomical system and a standard gait coordinate system? 94
5.2.1 Kinematics 95
5.2.2 Kinetics 97
5.2.3 What is the repeatability of the kinematic and kinetic outcomes using a MRI-based anatomical system and a standard gait coordinate system? - Conclusions 100
5.3 Is there a link between qMRI T_2 and contact area values in cartilage? 101
5.3.1 Is there a link between contact area and qMRI T_2 values in cartilage? - Conclusions 103

5.4 Study Limitations 104
Chapter 6 106
CONCLUSION 106
6.1 Summary 106
6.2 Conclusions 106
6.3 Clinical Significance 106
6.4 Recommendations for future research 107
6.5 Closing Remarks: 107
REFERENCES 108
Appendix A: Methods Section – Supplementary Material 122
Appendix B: qMRI Results – Supplementary Material 135
Appendix C: mechMRI Results - Supplementary Material 141
Appendix D: Gait Analysis Results - Supplementary Material 148
Appendix E: MRI-Gait Comparison Results – Supplementary Material 166
Appendix F: qMRI-Contact Integration Results – Supplementary Material 174
Appendix G: Consent Form and Ethics Approval 184
Appendix H: Copyright Permission 190

LIST OF TABLES

Table 2-1: Summary of contact area, significant outcomes, how they were defined, corresponding reliability values, findings, and loading condition 17

Table 2-2: Summary of 3-D kinematics significant outcomes, how they were defined, corresponding validation, findings, and loading condition 18

Table 2-3: Summary of MRI-based 3-D Kinematics significant outcomes, how they were defined, corresponding reliability values, findings and loading condition 22

Table 2-4: Summary of repeatability and reliability measures from the literature for knee kinematics 29

Table 2-5: Summary of repeatability and reliability measures for kinetic measures 30

Table 2-6: Summary of studies that have carried out qMRI ($T_{1\rho}$ and T_2 relaxation times) and joint biomechanical studies in the ACL-injured Population 35

Table 3-1: Summary table of details of scans acquired 40

Table 3-2: Summary table of all the outcome measures acquired from knee kinematic and kinetic plots 52

Table 3-3: Summary of how orthogonal vectors were described to define the femur and tibia anatomical coordinate system in the gait-based method. The second cross-product is required to create an orthogonal coordinate system. 53

Table 3-4: Summary of how orthogonal vectors were described to define the femur and tibia anatomical coordinate system in the MRI-based method 57

Table 3-5: Description summary of novel T_2-contact quantitative measures assessed in this study 59

Table 3-6: Details of all repeatability and statistical measures used in the analysis of all outcome measures 60

Table 4-1: Demographics of participants 61

Table 4-2: Mean and SD values of average regional qMRI T_2 values for general, medial, lateral and trochlear regions at loaded and unloaded positions and their difference. SD_{rms} was used for the loaded and unloaded measures while the SD_{diff} was used for the difference measures. The missing values for the unloaded case of three trials for participant 1 and one trial for participant 2 seen in this section is due to MRI sequence errors in the data collection of this data. Therefore, for the unloaded measures, are n = 4 instead of five. The negative values indicate a bigger T_2 in

the smaller region (centroid region or contact) than in the larger region (contact, medial or lateral). 62
Table 4-3: CV% values of loaded and unloaded cartilage means in the global, medial, lateral and trochlear regions..... 63
Table 4-4: Based on our SD_{rms} values, the values in this table represent the minimum change that we expect to see in ACL-injured individuals for regional mean T_2 values that will be considered a clinical change and not just due to measurement error. We express these outcomes with 80%, 90% and 95% statistical confidence based on a two-tailed z-score..... 63
Table 4-5: Mean and SD values of medial and lateral contact centroid translation (absolute distance) at three flexion angle ranges – one-to-two (fully extended to lower flexion angle), one-to-three (fully extended to higher flexion angle), two-to-three (lower to higher flexion angle) .. 64
Table 4-6: Based on our SD_{rms} values, the values in this table represent the minimum change that we expect to see in ACL-injured individuals for contact centroid translation values that will be considered a clinical change and not just due to measurement error. We express these outcomes with 80%, 90% and 95% statistical confidence based on a two-tailed z-score 65
Table 4-7: Mean, SD, SD_{rms} of medial and lateral contact area values at three limb positions – fully extended knee, low flexion angle, high flexion angle..... 66
Table 4-8: CV% values of medial and lateral contact area at fully extended, low flexion and high flexion limb positions 66
Table 4-9: Based on our SD_{rms} values, the values in this table represent the minimum change that we expect to see in ACL-injured individuals for contact area values that will be considered a clinical change and not just due to measurement error. We express these outcomes with 80%, 90% and 95% statistical confidence based on a two-tailed z-score..... 67
Table 4-10: MRI-based mean and SD values per participant and overall mean and SD_{rms} values per measure of peak frontal and sagittal knee angles for walking and stair tasks. The table reports the absolute values of these measures..... 67
Table 4-11: Based on our SD_{rms} values, the values in this table represent the minimum change that we expect to see in ACL-injured individuals for MRI-based kinematic values that will be considered a clinical change and not just due to measurement error. We express these outcomes with 80%, 90% and 95% statistical confidence based on a two-tailed z-score 68

Table 4-12: MRI-based mean and SD values per participant and overall mean and SD_{rms} values per measure of peak frontal and sagittal knee moments for walking, chair, and stair tasks. The table reports the absolute values of these measures. 69
Table 4-13: Based on our SD_{rms} values, the values in this table represent the minimum change that we expect to see in ACL-injured individuals for gait-based kinetic values that will be considered a clinical change and not just due to measurement error. We express these outcomes with 80%, 90% and 95% statistical confidence based on a two-tailed z-score 70
Table 4-14: Gait-based mean and SD values per participant and overall mean and SD_{rms} values per measure of peak frontal and sagittal knee angles for walking and stair tasks. The table reports the absolute values of these measures. 70
Table 4-15: Based on our SD_{rms} values, the values in this table represent the minimum change that we expect to see in ACL-injured individuals for gait-based kinematic values that will be considered a clinical change and not just due to measurement error. We express these outcomes with 80%, 90% and 95% statistical confidence based on a two-tailed z-score 71
Table 4-16: Gait-based mean and SD values per participant and overall mean and SD_{rms} values per measure of peak frontal and sagittal knee moments for walking, chair and stair tasks. The table reports the absolute values of these measures. 72
Table 4-17: Based on our SD_{rms} values, the values in this table represent the minimum change that we expect to see in ACL-injured individuals for gait-based kinetic values that will be considered a clinical change and not just due to measurement error. We express these outcomes with 80%, 90% and 95% statistical confidence based on a two-tailed z-score 72
Table 4-18: Bland Altman limit of agreement values, range and number of points outside of range for all kinematic measures 77
Table 4-19: Bland-Altman limit of agreement values, range and number of points outside of range for all kinetic measures 78
Table 4-20: Means and SDs per participant and overall mean and SD_{rms} of qMRI T_2-contact integration outcomes for loaded and unloaded cases in the medial compartment. Contact-centroid mean difference and SD difference without II represents the geometric-weighted centroid measures while with II indicates the T_2-weighted centroid measures. Negative values indicate a higher T_2 in the larger region; specifically, inside the contact region relative to outside the contact region for measures where contact is the smaller region (i.e. Regional-Contact Area) and

higher T_2 outside the centroid region relative to inside the centroid region where contact is the bigger region (Contact Area-Centroid) 80
Table 4-21: Based on our SD_{rms} values, the values in this table represent the minimum change that we expect to see in ACL-injured individuals for medial loaded and unloaded T_2-contact integration values that will be considered a clinical change and not just due to measurement error. We express these outcomes with 80%, 90% and 95% statistical confidence based on a two-tailed z-score 81
Table 4-22: Means and SDs per participant and overall mean and SD_{rms} of qMRI T_2-contact integration outcomes for loaded and unloaded cases in the lateral compartment. Contact-centroid mean difference and SD difference without II represents the geometric-weighted centroid measures while with II indicates the T_2-weighted centroid measures. Negative values indicate a higher T_2 in the larger region; specifically, inside the contact region relative to outside the contact region for measures where contact is the smaller region (i.e. Regional-Contact Area) and higher T_2 outside the centroid region relative to inside the centroid region where contact is the bigger region (Contact Area-Centroid) 82
Table 4-23: Based on our SD_{rms} values, the values in this table represent the minimum change that we expect to see in ACL-injured individuals for lateral loaded and unloaded T_2-contact integration values that will be considered a clinical change not just due to measurement error. We express these outcomes with 80%, 90% and 95% statistical confidence based on a two-tailed z-score 83
Table 4-24: Mean and SD per participant and overall mean and SD_{rms} values of the number of T_2-increase (unload to load) and T_2-decrease (unload to load) cluster regions present within the contact area under loaded and unloaded cartilage. M - Medial side, L - Lateral side. The decimal values are from finding the mean of an integer number of clusters from each trial. 83
Table 5-1: SD_{rms} and Bland-Altmann Rank Table for Kinematic Measures. The numbers in the parentheses indicate the measures rank from smallest to biggest values 96
Table 5-2: SD_{rms}, and Bland-Altmann Rank Table for Kinetic Measures – the numbers in the parentheses indicates the measures rank from smallest to biggest values 100

LIST OF FIGURES

Figure 2-1: Articular Cartilage different zonal collagen and PG orientations (With permission from Chelsey Thorson) 4

Figure 2-2: a) Diagram of the knee showing the ACL and other ligaments and tissue. b) Knee motions supported by the ACL (With permission from Dr. Uche Monu)..... 6

Figure 2-3: Basic principles of MRI. a) Polarization - Static magnetic field has a net magnetization of M due to hydrogen protons by either being in a parallel or anti-parallel state b) Precession - Hydrogen protons spin about the z-axis at the larmor frequency. c) Excitation – RF pulses tip the magnetization into the transverse plane. d) Relaxation - The time it takes for the magnetization to recover to its state of equilibrium. T_1 recovers along the logitudinal axis and T_2 decays in the transverse plane. (With permission from Dr. Uche Monu)..... 9

Figure 2-4: Key mechanical outcomes of gait analysis (walking activity) from three recent meta-analysis papers of ACLR studies with increasing time (months) from surgery. : Kaur et al [11], : Slater et al [12], : Hart et al [13]. Up-arrow: Measure increased over time-period it covers. Equal-sign: Measure did not change over time-period it covers. KFM – Knee Flexion Moment, KEM – Knee Extension Moment, KFA – Knee Flexion Angle, HFA – Hip Flexion Angle, KAA – Knee Adduction Angle, KAM – Knee Adduction Moment..... 32

Figure 3-1: Methodology flowchart giving an overview of the major processes carried out in this study..... 38

Figure 3-2: Two body RF coils arranged in cage-like form to accommodate knee for MR scanning 40

Figure 3-3: Labelled image of the gait force plate set up for all the motion tasks carried out. The stool was only used for the chair tasks..... 43

Figure 3-4: Labelled image of lower limb markers used for motion capture (although image shows lower limb markers, full-body marker set was used for visualization)..... 44

Figure 3-5: Condyle-Cylinder Radial Projection Illustration (courtesy of Dr. Uche Monu)..... 47

Figure 3-6: The cluster analysis map flowchart in this figure shows the output image at every stage used to develop the cluster map. The individual loaded and unloaded cluster maps are generated and then they are subtracted from each other which gives the difference maps. Finally, using pixel size and intensity thresholds, clusters and their centroids were defined on the map. The red outline shows the outer boundary of the loaded contact region and the blue outline in the

difference map image represents the outer boundary of the unloaded contact region. These contact regions were always overlaid on the cartilage map outputs. 49
Figure 3-7: Regional cartilage demarcation for T_2 regional analysis 50
Figure 3-8: Shank segment free body diagram with forces and moments 55
Figure 3-9: a) Left: MRI-marker centroid generated from segmentation (Analyze 12.0, Analyze Direct, Overland Park, KS, USA) – red arrows show the centroid positions in each of the planes – coordinates (36, 202, 114). b) Right: MRI-marker centroid that was visually-determined - red arrows show the centroid positions in each of the planes – coordinates (37, 204, 115) 56
Figure 3-10: Flowchart showing process of transforming MRI-based landmarks to motion capture (gait) coordinate system. $T_{MRI\text{-}Gait}$ is the homogenous transformation matrix to go from MRI to gait coordinate system 57
Figure 3-11: 2-D Cartilage map illustrating the regions used in defining the T_2-contact measures 59
Figure 4-1: SD_{rms} plot for all kinematic measures for MRI-based and gait-based values. 74
Figure 4-2: SD_{rms} plot for all kinetic measures for MRI-based and gait-based values. 76
Figure 4-3: Sample of 2-D visualization map of particularly big difference between loaded and unloaded cartilage represented as clusters. The red boundaries indicate the outer boundary of the contact region. Top: T_2-decrease cluster maps with a) contact under loaded cartilage and b) contact under unloaded cartilage. Bottom: T_2- increase cluster maps with a) contact under loaded cartilage and b) contact under unloaded cartilage. The white arrows show the cluster centroid counts in and around the contact area region 85
Figure 5-1: An example of a T_2-increase (from unloaded to loaded case) cluster projection map showing cluster centroids away from the centroid of the contact region of loaded cartilage. The red contour indicates the outer boundary of the unloaded contact region. The contact region is seen to overlay over a region where there is no cartilage because cartilage regions not present in loaded and unloaded cartilage are removed. Interpolation of the cartilage map also plays a role in this. 103

LIST OF ABBREVIATIONS

ABS - Acrylonitrile Butadiene Styrene

ACL - Anterior Cruciate Ligament

ACLD - Anterior Cruciate Ligament Deficient

ACLR - Anterior Cruciate Ligament Reconstructed

AL - Anatomical Landmarks

AMB - Anteromedial Band

ATD - Anterior Tibial Displacement

BW - Body Weight

CA - Cluster Area

CMC - Coefficient of Multiple Correlation

CV_{rms} - Root Mean Square Coefficient of Variation

DESS – Double Echo Steady State

ECM - Extracellular Matrix

EPG - Extended Phase Graph

FOV - Field of View

GAG - Glycosaminoglycan

ICC - Intra-Reliability Coefficient

JSN - Joint Space Narrowing

JSW - Joint Space Width

KL - Kellgren Lawrence

MRI - Magnetic Resonance Imaging

mechMRI - Mechanical Magnetic Resonance Imaging

MoCap - Motion Capture

OA – Osteoarthritis

PG - Proteoglycans

PGA - Proteoglycan Aggregate

PLB - Posterolateral Band

PTOA – Post Traumatic Osteoarthritis

qMRI – Quantitative Magnetic Resonance Imaging

RF – Radio Frequency

ROI - Region of Interest

RSA - Roentgen Stereophotogrammetric analysis

SAR - Specific Absorption Rate

SD_{rms} - Root Mean Square Standard Deviation

TSL - Spin Lock Time

Chapter 1

INTRODUCTION

The introduction section below provides an overview of this project 'repeatability of an integrative method to assess knee joint mechanics and cartilage health under load'. The organization of the thesis is also described.

1.1 Overview

Anterior cruciate ligament (ACL) injury is an important model of post-traumatic osteoarthritis (PTOA) because research has revealed that 50% of ACL-injured individuals will end up with radiographic osteoarthritis (OA), within 10-20 years of injury [1-3]. However, currently there is a lack of validated tools to comprehensively study this group early in the OA disease process. Identifying important changes early is important because it presents the best opportunity for meaningful intervention. Development of a repeatable method to study this population has the potential to give more insight into how the degeneration occurs over time; especially early in the disease process.

Individuals with ACL injury display changes in articular cartilage health and joint biomechanics. Knee articular cartilage has been shown to degenerate in the ACL-injured and radiographic OA populations [4, 5]. Specifically, advanced quantitative magnetic resonance imaging (qMRI) techniques, such as $T_{1\rho}$ and T_2 relaxation times, show elevated values in the ACL-injured population as compared to healthy individuals [6-8]. These measures which can show early changes in cartilage (within 6 months of ACL reconstruction) [9], appear to be important in the long-term health of the joint. Joint biomechanics in ACL-injured individuals is often investigated by gait analysis [10-13] and also by contact area and its translation obtained from magnetic resonance image (MRI) or 3-D models [14, 15]. These methods have shown statistically significant differences in ACL-injured as compared to healthy groups (for instance, more posterior contact patterns from MRI and changes in peak knee flexion angles and moments for gait analysis) [14, 15].

qMRI, contact area and its translation from MRI and gait analysis, have all been shown to change with ACL-injury but there has been limited work studying these metrics together. Most studies assess one or two of these metrics at a time [16, 17]. Therefore, the objective of this work

was to create an integrative method to assess qMRI, contact area from MRI and gait analysis measures; the repeatability was then assessed in healthy individuals. A MRI-safe loading rig and MRI-lucent gait markers, required for the method, was also designed and constructed.

1.2 Thesis Organization

The thesis is organized as follows:

Chapter 2: Background

This chapter provides an overview of the knee joint and the macromolecular structure of cartilage under load. The relationship between post-traumatic OA (PTOA) and ACL-injury is described. The basic principles of MRI are reviewed as well as mechanical outcomes and their analysis techniques from both gait and MR images. The chapter concludes by stating the specific research questions of this project.

Chapter 3: Methods

This chapter describes the study design, data acquisition steps and tools for MRI and gait analysis, as well as data processing procedures for this data. The statistical and repeatability analysis methods used are also justified.

Chapter 4: Results

In this chapter, measure outcome key findings are summarized and tabulated for qMRI, mechMRI, gait analysis and qMRI-contact.

Chapter 5: Discussion

In this chapter, each of the research questions (detailed in section 1.2) are addressed with reference to each of the metrics – qMRI, mechMRI, gait analysis (kinematics and kinetics) and qMRI-contact integration – highlighting major findings and how they fit in the broader body of literature.

Chapter 6: Conclusions and Future Recommendations

This chapter highlights the conclusions for each of the three objectives described in section 1.2. The clinical significance and future recommendations of this integrative repeatability study are also discussed.

Chapter 2
BACKGROUND

This chapter includes a description of the knee anatomy and key tissue function, knee OA, a review of the literature in the areas of qMRI, image-based mechanics and gait analysis in ACL-injury and knee OA. It discusses the literature on the ACL-injured population. The reason for this is because although this work is limited to assessing the repeatability of a technique in healthy participants, it is important to understand what should be expected in the ACL-injured population as this is the final application of the method developed from this work.

2.1 The Knee

This section provides a general overview of the knee. It reviews specifically its anatomy, the tissues involved in loadbearing including the articular cartilage which is the focus of this work, and the ACL since this is the future application of the methodology designed from this project.

2.1.1 Anatomy

The knee joint is a joint with primarily flexion-extension motion, as well as internal-external and abduction-adduction rotations occurring concurrently. Its complex structures enable it to bear large amounts of loads that are present while performing daily activities like running, walking or climbing. The knee is made up of two articulating joints – one between the tibia and femur (the tibiofemoral joint) and another between the patella and femur (the patellofemoral joint) – that aid in its unique motion of rotating internally and externally at the same time as it bends and straightens. Bones, joint capsule, tendons, ligaments, meniscus and articular cartilage are the major tissues that make up the knee joint and enable the transmission of loads to efficiently facilitate stability, lubrication and low friction during motion.

2.1.2 Articular Cartilage under Load

The articular cartilage which is a specialized connective tissue that overlays joint surfaces, has unique structures that facilitate transmission of large loads as well as motion with a low coefficient of friction. Due to a lack of blood vessels and nerves, the tissue is prone to continuous degeneration because it cannot heal itself naturally [18]. The organized architecture of the tissue is important to how the load is transmitted and the mechanical loading influences the degeneration of the tissue [19]. Chondrocytes are the only cells present in articular cartilage and they are surrounded

by an extracellular matrix (ECM) which is a fibrillar network of collagens and proteoglycans (PG) within a viscous water-based substance called synovial fluid [20, 21]. The articular cartilage is made up of various zones – the superficial, middle, deep and calcified zones – the orientations of fibers varies by zone and this affects the mechanical response of the ECM to load [18, 22, 23] (Figure 0-1 below).

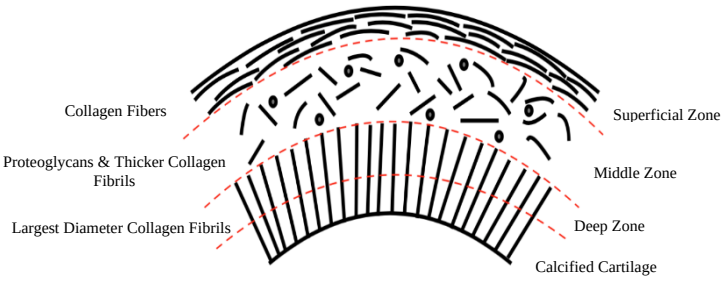

Figure 0-1: Articular Cartilage different zonal collagen and PG orientations (With permission from Chelsey Thorson)

The superficial zone: Collagen fibers are tightly packed and aligned parallel to the articular surface in this zone. It is the thinnest zone yet has the highest proportion of collagen and helps protect the deeper layers from shear stresses [18, 22, 23].

The middle zone: The middle zone is made up of PG and thicker collagen fibrils that are oriented randomly. It has a much higher volume than the superficial zone and it helps maintain a highly stable hydrated structure of the cartilage. The PG present are negatively charged, and by attracting positively charged ions, it creates swelling pressures (because there is a difference in charge across the membrane) that help in resisting compressive loads [18, 22, 23].

The deep zone: The collagen fibrils in the deep zone are the thickest and are perpendicular to the bone surface. PG concentration is the highest in this zone and with the lowest water concentration [18, 22, 23].

The calcified zone: This zone has collagen fibrils with the primary function of anchoring the cartilage to the subchondral bone [18, 22, 23].

The mechanical properties of the ECM are highly dependent on two main macromolecules present – type II collagen and PG. Stability through shear and tensile properties are provided by the collagen which makes up to 60 % of the dry cartilage weight [22]. The PGs are part of large

proteoglycan aggregates (PGAs) made from hyaluronic acid [24, 25]; each PG is composed of a core protein with oligosaccharide and glycosaminoglycan (GAGs) chains attached to it [24, 25]. The GAGs are what attract cations and water, resulting in swelling that gives articular cartilage high compressive strength [24, 25]. When the joint is loaded, the compression of the PGAs allow force distribution to the rest of the joint surface and thereby reduce pressure on the articular cartilage [26]. Lubricin produced by chondrocytes and synoviocytes, line the joint surface and facilitate the low friction interface of the articular cartilage during motion [27-29]. The pathogenesis of cartilage degeneration can also be attributed to the loss of lubricin in the synovial joint [27-29].

2.1.3 Anterior Cruciate Ligament (ACL)

Stability of the tibiofemoral joint is primarily provided by four ligaments within the knee – ACL, posterior cruciate ligament (PCL), medial collateral ligament (MCL) and the lateral collateral ligament (LCL). In particular, the ACL which runs from the posterior and lateral side of the femur to the anterior and medial side of the tibia, helps to prevent excessive anterior translation of the tibia due to its location and non-isometric behavior through different ranges of motion [30, 31]. With the help of the posterolateral band (PLB) and anteromedial band (AMB) that give it its non-isometric properties [30], the ACL has an average restraint value that decreases with increasing flexion, with maximum forces between 15 and 30 degrees of flexion [31]. Being that the tibiofemoral joint is a joint experiencing internal and external rotation, the ACL also acts as a secondary restraint against these rotations (Figure 0-2) [31]. The ACL is more prone to injury because it is half as strong as the PCL [32]. Also, anterior translation, which is restricted by the ACL, is more vulnerable in a traumatic event [32]. Injury to the ACL usually occurs in various sporting activities where there is an abrupt and forceful twist of the knee joint under full body weight.

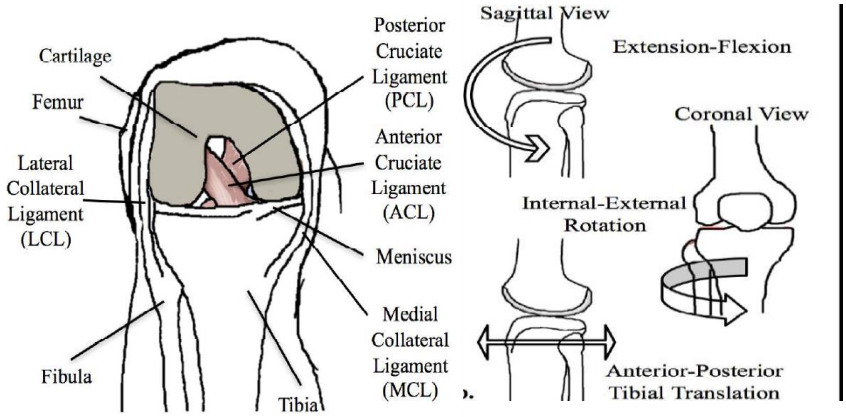

Figure 0-2: a) Diagram of the knee showing the ACL and other ligaments and tissue. b) Knee motions supported by the ACL (With permission from Dr. Uche Monu)

2.2 Knee Osteoarthritis (OA)

Knee Osteoarthritis (OA), can be categorized into idiopathic and post-traumatic OA. Acute joint injury from abrupt, rigorous activity is the primary cause of PTOA [33]. This form of OA is 4.2 times more likely to occur in people with knee injury than those with femur fractures or other lower leg injuries [34]. ACL-injury is a major knee injury that leads to PTOA with 0-39% of cases leading to PTOA from isolated injuries [1, 2, 35-37] and 21-100% with concomitant meniscal injuries [35, 37-40]. The association of ACL-injury to PTOA can be attributed to several risk factors such as age, sex, knee alignment and meniscal tears [41-43]. With PTOA being diagnosed in approximately 50% of ACL-injured individuals within 10-20 years of initial injury [1-3], ACL-injury is a major cause of radiographic PTOA occurring in the younger population. This early onset of OA drastically reduces the quality of life due to inability to participate in physical activities and increases the chances of the need for early total knee replacement surgery.

2.2.1 ACL-injury and Post-Traumatic OA (PTOA)

The critical role of the ACL in providing anterior-tibial stability is an indication of how injury to the ligament could affect the mechanical function of the joint. The change in loading patterns due to ACL deficiency or rupture alters joint motion (which will be discussed in chapter 2.6) and affects surrounding menisci, chondral and subchondral articular cartilage [44], thereby predisposing the joint to PTOA. Although it is expected that there is a relationship between altered

loading patterns from ACL-injury and PTOA, it is yet unknown how the change in joint mechanics might affect cartilage and meniscus under load, and the role it plays in the PTOA pathology.

2.2.2 Macromolecular Changes of Meniscus and Cartilage in PTOA

Due to the collaborative role of the meniscus and articular cartilage in the load-bearing function of the knee joint, degeneration occurs in both tissues over the OA pathology. Articular cartilage damage affects meniscal tissue health [45] and meniscal damage affects articular cartilage [46]. One study that probed regional similarities using double-contrast macro-radiographs of damage severity between meniscus and articular cartilage, found that the degenerative changes of both tissues are mostly concomitant with meniscal damage preceding articular cartilage changes [47]. It is important to understand the relationship between meniscus and articular cartilage macromolecular changes early in the OA pathology to gain insight to how it might affect load-bearing and kinematic changes.

OA cartilage in contrast to healthy cartilage, has a degenerated surface with soft areas and increase in synovial fluid production [48-50]. Macromolecular breakdown of PG and GAGs present in articular cartilage are characteristic of earlier stages of the disease where fibrillation begins to occur in the superficial zone. The depletion causes more water to diffuse into the cartilage [51] causing some form of swelling. The synovial membrane also begins to thicken causing infiltration of inflammatory cells. Abnormal bone growths (osteophytes) can also be seen at the earlier stages of OA. Later in the disease process, the surface of the cartilage becomes uneven with fissures and cracks. Depletion of PG also extends to the deep zone causing the whole ECM to be completely disordered. Thus, radiographic OA is defined as joint space narrowing due to the thinning of the cartilage and wearing down of the meniscus.

Although loss of articular cartilage is a structural hallmark of OA, it is a whole-joint disorder, including meniscal damage and changes to other tissues. A strong association between degenerated menisci and OA has been seen in macroscopic and histopathological studies [52-55], where it is suspected that even a healthy knee could develop OA due to meniscal damage. Regardless of which tissue damage precedes which, macromolecular changes in meniscus is seen to begin from the matrix itself with no apparent changes on the surface [56].

2.2.3 Radiographic Detection of OA

The gold standard for assessing OA clinically is from symptoms and two-dimensional radiographic images which are used to evaluate traits like joint space width (JSW) and osteophytes which are bony growths that occur from the degeneration. For the purpose of research, grading schemes such as the KL grading scheme [57, 58], are used to diagnose the severity of OA from the radiographic images. Below is the interpretation of what the different KL grades (0-4), represent:

- KL grade 0: No radiographic features
- KL grade 1: doubtful joint space narrowing (JSN) and possible osteophytic lipping
- KL grade 2: definite osteophytes and possible JSN on anteroposterior weight-bearing radiograph
- KL grade 3: multiple osteophytes, definite JSN, sclerosis, possible bony deformity
- KL grade 4: large osteophytes, marked JSN, severe sclerosis and definite bony deformity

The issue with radiographic grading schemes such as KL is that features like JSW, cannot be standardized as some arthroscopically normal joints in some patients, have been seen to exhibit 'pathological' JSW [59]. Furthermore, as cartilage cannot be delineated from those images, it is impossible to detect early cartilage pathologies, from which disease can more easily be treated. A more sensitive imaging modality that can provide this function of detecting early cartilage pathologies is MRI.

2.3 Quantitative MRI (qMRI) measures in OA pathology

qMRI is a powerful research tool that can provide surrogate measures of the macro-molecular structure, content and function of tissues. qMRI can distinguish between healthy and degenerating tissues earlier than radiographic images. Examples of qMRI sequences that have been used in the study of meniscus and cartilage biomechanical behavior, are T_2 and $T_{1\rho}$ relaxation times. These two measures are important in ACL-injury studies because they can distinguish between ACL-injured and heathy population tissue as early as 6 months after injury [9].

2.3.1 Basic Principles of MRI

Tissues within the body contain water which have a hydrogen nucleus (^{1}H) that acts like a tiny magnet with a nuclear spin and a magnetic dipole moment, μ (Figure 0-3). The net magnetization within the body is zero because all the protons are randomly oriented. In a very strong and static magnetic field, all the nuclei become either parallel or anti-parallel to the magnetic

field lines. With slightly more nuclei in the parallel than anti-parallel direction, the net magnetization is no longer zero and is in the direction of the static magnetic field, B_0. Each of the spins precess about the B_0 direction at a unique frequency called the Larmor frequency (given by the gyromagnetic ratio multiplied by B_0). As seen in Figure 0-3, the main magnetic field in the longitudinal direction (z-direction) is considered the reference frame and a tip of the nuclei away from this direction into the transverse plane is what makes imaging possible. Radiofrequency pulses are applied to tip the magnetization out of the B_0 direction into the transverse plane. Receiver coils detect the signals due to the change in the magnetic flux as it relaxes back to its original state and collects spatial frequency data. The spatial frequency data is stored as an array which is called k-space. To go from the k-space (i.e. the frequency domain) to image space, an inverse Fourier transform is applied.

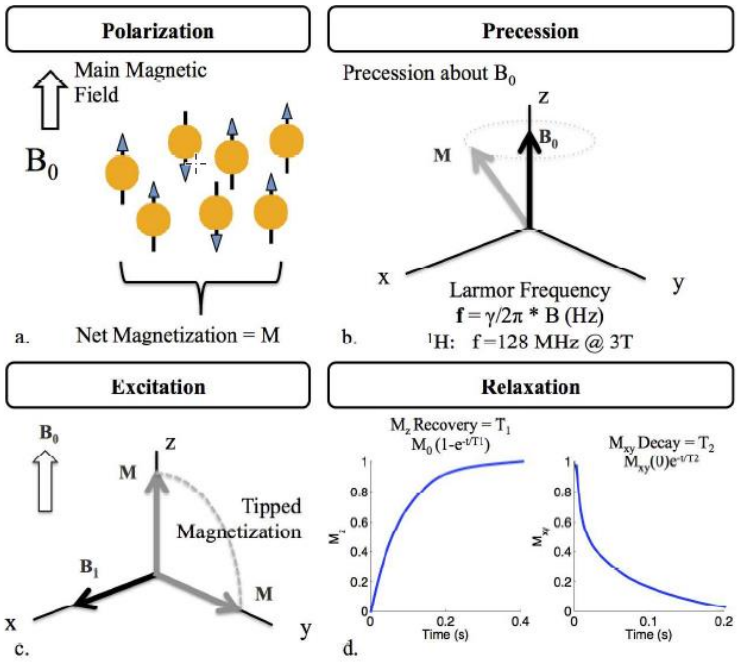

Figure 0-3: Basic principles of MRI. a) Polarization - Static magnetic field has a net magnetization of M due to hydrogen protons by either being in a parallel or anti-parallel state b) Precession - Hydrogen protons spin about the z-axis at the larmor frequency. c) Excitation – RF pulses tip the magnetization into the transverse plane. d) Relaxation - The time it takes for the magnetization to recover to its state of equilibrium. T_1 recovers along the logitudinal axis and T_2 decays in the transverse plane. (With permission from Dr. Uche Monu)

T_2 and $T_{1\rho}$ relaxation times (the time it takes for the perturbed magnetization to return to its state of equilibrium) are commonly used measures in knee qMRI studies. T_2 relaxation time is the time that it takes the magnetization to return to equilibrium in the transverse plane. $T_{1\rho}$ is a variation on this, where the magnetization is locked in the transverse plane before it is allowed to relax back. This spin-lock frequency is typically a 500 Hz pulse and it locks the magnetization in the transverse direction and prevents it from dephasing. Both T_2 and $T_{1\rho}$ decay mono-exponentially and occur as a result of the energy exchange that occurs between spins and their macromolecular environment, as they return to their natural state (aligned with B_0). T_2 relaxation time is the focus of this study.

2.3.2 T_2 Relaxation Time Analysis

T_2 relaxation time has been extensively used in knee research, including in large cohort studies such as the Osteoarthritis Initiative, and is known to be moderately correlated with water content and collagen organization in both meniscus and articular cartilage. A breakdown in the collagen structure is reflected by elevated T_2 relaxation times in articular cartilage [9, 60-62] and meniscus [4, 43, 63]. Some studies show however, a relationship with PG content as well [9, 64, 65]. Abnormal T_2 relaxation time values have been seen to be correlated with severity of OA [9, 61, 63, 66]. T_2 relaxation time of articular cartilage in mild and severe OA (37.7±2.9ms) is higher compared to that of healthy cartilage (34.2±1.4ms) [61, 65]. Meniscus T_2 measures are also significantly elevated in OA cases with meniscal tears than those without meniscal tears and healthy knee [4, 63]. In ACL-injured cases, T_2 has been seen to discriminate between healthy articular cartilages as early as 6 months post-reconstructive surgery [9]. However, some other studies, using a different T_2 analysis technique, did not find any significant difference for 1-year after reconstruction [6, 67]. The usual way of measuring T_2 is to carry out a series of spin echo scans with varying echo times. This process takes about an hour and so different groups have come up with more efficient ways such as using multiple echoes, T_2 preparations, and steady state sequences. In this study, we use one of these more efficient methods, specifically a modified double echo steady state (DESS) sequence.

2.3.3 qMRI Analysis Techniques

qMRI analysis of tissue is a non-trivial task and one of the challenges is being able to represent the information in a meaningful way. In most qMRI studies, only 1 to 3 slices each from the medial and lateral sides are analyzed; averages of qMRI measures are then made over segmented regions

[68, 69]. The issue with this method is that when only 1-3 slices are studied, a focal defect or degeneration elsewhere in the tissue may be missed. There are some methods that try to make use of qMRI data from the entire cartilage plate. One example is voxel based relaxometry which is a post-processing approach that compares voxels across subjects by fitting each subject's data to a common template; the technique performs analysis on defined compartments and does not characterize focal defects [70]. Additionally, focal lesions have been identified as important indicators of different stages of the OA disease process and have been included in semi-quantitative scoring systems [71]. In response to this, our group previously developed a novel quantitative approach for identifying clusters particularly big longitudinal T_2 changes. This approach was used to identify focal lesions in cartilage of the ACL-injured population and showed changes as early as 6 months post ACL-reconstruction [9]. This method is adopted in this study in a modified manner to identify focal changes with load.

We used a cluster analysis technique developed by our group. Our cluster analysis method is a qMRI-based analysis technique that involves the identification of focal lesions or clusters in articular cartilage. First, data from two or more time points is acquired and two-dimensional projection maps are created which allows for normalization and registration of the data. Clusters are defined as change in qMRI value, based on running a kernel with particular intensity and size thresholds across the dataset. One defined outcome measure is termed percent cluster area (%CA) which is simply the percent area of the projection map covered by clusters above (%CA+) or below (%CA-) the set thresholds. %CA is a preferable form of presenting results in the cluster analysis technique as compared to a global compartmental mean because these values may not capture the elevated contiguous areas which are likely very important in the OA disease process. This is a limitation of other analysis techniques. Results can also be presented as mean compartmental and regional values. Projection maps can be categorized into regions and compartments for easy comparisons – global, lateral (anterior, central and posterior), medial (anterior, central and posterior), and trochlear regions – which is also similar to regional compartmentalization of other analysis techniques [9]. Thus, it is easy to compare results from the cluster technique to the literature.

The reproducibility measured by root-mean squared coefficient of variation (CV_{rms}) of the cluster analysis technique, has been assessed in the previous study for inter/intra subject and observer variability, for both the pixel-wise and global mean outcomes, and these are comparable to values from other T_2 analysis techniques [9]. Intra-subject and intra/inter-observer variability were found to be less than 9% and 6% respectively for the global mean values. The pixel-wise method was seen to be less precise with less than 15% and 10% for intra-subject and intra/inter-observer variability respectively. Variability due to consecutive scans and noise was seen to be less than 6% for the global mean and less than 11% for the pixel-wise outcomes [9]. T_2 relaxation time measurements techniques in the literature have displayed reproducibility values between 4 – 29% [72-74]. The qDESS method which was used to acquire T_2 in our past work, had reproducibility values of 6.4 – 10.7% [75] and root-mean square error measurements compared to the reference standard, of 4.6 ms [76]. The literature discussed in the past few paragraphs show that the qDESS and cluster technique show good reproducibility as compared to other approaches.

Using cluster analysis or other techniques, $T_{1\rho}$ and T_2 relaxation time have been seen to track early degeneration of articular cartilage with no particular advantage of one relaxation time measure over the other. In our previous study using the cluster analysis technique, both $T_{1\rho}$ and T_2 relaxation time %CA+, was seen to be significantly elevated longitudinally in ACL-injured knees when compared to healthy knees ($T_{1\rho}$: 8.5 ± 6.8% (ACL-injured) vs 1.44 ± 1.37% (healthy), T_2: 6.4 ± 3.7% (ACL-injured) vs 1.24 ± 1.30 % (healthy)). Similarly, studies that used a non-cluster approach have found higher values of T_2 and $T_{1\rho}$ relaxation times in diseased cartilage than in healthy cartilage [68, 69, 77-79]. From past literature, there is no clear indication as to which one of the relaxation time analysis measures is better than the other in assessing early cartilage damage, however, T_2 relaxation time sequences are known to be more easily acquired and available than $T_{1\rho}$ and so there is the potential for broader adoption of the technique. $T_{1\rho}$ values also vary depending on the magnitude of the spin lock pulse applied and, at higher spin lock frequencies, have higher specific absorption rate (SAR).

2.3.4 Loading in qMRI Analysis

qMRI of cartilage under load may provide more information than when unloaded and may give more insight about the mechanical behavior of the tissue. Normal cartilage under load, is

compressed, causing water to exude out of the solid matrix, creating osmotic pressure that becomes the major (90%) means of load-bearing [80, 81]. T_2 relaxation time analysis of healthy cartilage, between loaded and unloaded condition, have shown a decrease in T_2 values under load, and significantly in the tibial cartilage contact region of the medial femur and the medial and lateral regions of the tibia [82, 83]. In damaged cartilage, breakdown of collagen causes swelling of PG which results in cartilage permeability and water increase [65]. When the water increases, the cartilage matrix becomes more compressible [84], causing a greater portion of the load to be carried by the ECM and leading to increased stress in the cartilage [85]. Because T_2 relaxation is sensitive to collagen anisotropy and water content [9, 60-62], it should be able to distinguish the different responses of damaged cartilage under load from healthy. Although T_2 may not be as sensitive to PG concentration, it can be used alongside $T_{1\rho}$ to gain more insight into pathological changes of cartilage under load. Souza et al found a greater reduction in both $T_{1\rho}$ and T_2 relaxation times under load in the medial and lateral femur of OA cartilage (13-19%) when compared to healthy cartilage (3-13%) [16], indicating reduced ability of the collagen-PG matrix to properly distribute the joint load.

The integration of qMRI analysis with joint mechanics under load, will give insight into the effect of abnormal loading patterns present in ACL-reconstructed (ACLR) knees. Within the ACL injured population, high knee adduction moment (KAM) cohorts were found to have higher $T_{1\rho}$ and T_2 relaxation time values (~5ms more than low KAM) during walking in the posterior medial femur articular cartilage [86]. Knee kinematics of ACLR knees, evaluated from MR images under 125 N axial load at 30 degrees of flexion and extension, found increased $T_{1\rho}$ relaxation in the medial femoral condyle of the weight-bearing cartilage for abnormal tibial rotation range and anterior tibial translation, as compared to the contralateral knee [87]. These studies indicate an existing link between gait mechanical measures and qMRI relaxation time measures.

Since mechMRI and gait analysis have shown correlations with qMRI relaxation times in these studies [86, 87] with standard qMRI analysis techniques (averaging pre-defined regions and compartments), it is expected that an exploratory study that integrates all three metrics and uses the cluster analysis approach would provide additional, more specific local relationships.

2.4 Mechanical measures from MRI (mechMRI)

Evaluating knee joint kinematics with MRI scans that depict soft tissue and bony structures, can be used to better understand the change in loading patterns that may occur in the ACL-reconstructed (ACLR) or ACL-deficient (ACLD) knee compared to healthy knees. Mechanical measures from MR images have been termed 'mechMRI' by our group and this will be the terminology used throughout this thesis. The normal healthy kinematic movement of the knee joint involves flexion and extension motion, where femoral condyles roll and glide over the tibial plateau while the tibia itself rotates involuntarily in the axial plane (internally or externally), guided by the ACL [88, 89]. Studies of ACLR and ACLD MRI-based knee kinematics, have mostly shown an increased range of axial rotation and antero-posterior laxity when compared with healthy knees [17, 90-99]. The change in such kinematics is what is suspected to be the cause of OA development seen to occur 10-20 years after ACL-injury [1-3] and ACL-reconstruction [100, 101]. mechMRI has been used to evaluate measures such as three-dimensional kinematics under static loads, two-dimensional kinematics under dynamic loads and cartilage contact patterns under static loads [15, 95, 102-106].

2.4.1 Load and Motion Conditions in mechMRI Analysis

For accurate *in vivo* measurements of knee joint mechanics with MRI, it is necessary to simulate joint loading and motion during scans. Studies have shown that static unloaded conditions are not representative of physiological conditions and could be misleading [107, 108]. The abnormal response of ACL-injury needs to be instigated by simulating joint loading and movement, in order to understand both treatment efficacy and potential future pathology. Supine closed-bore MRI scanners allow quasi-static load simulation where a MRI-compatible loading device is used to exert axial [17, 95, 109] or torsional loads [102] at the knee at different flexion angles. Dynamic load conditions in a closed-bore MRI with Cine-PC MRI, are also used to study knee mechanics [110, 111]. The limitations of scanning the knee loaded in a closed-bore scanner while lying in the supine position, is that, sustaining the load in such position is more difficult than while standing even with similar flexion angles. This is because unlike the usual activity of standing or walking where the quadriceps muscles support the full body weight with the foot firmly planted and in the direction of gravity, lying supine and sustaining a load is unusual to the body. Other muscles such as the hip flexors and the core which are not normally used to sustain loads, are engaged. Other

knee stabilizers are also required to maintain the raised leg position, such as the hamstrings, sartorius and abductors are also likely engaged. This loading pattern differs from maintaining an upright position and thus joint loading patterns may differ even if relative magnitude does not. Upright open-bore MRI scanners enable scans to be taken under normal gravitational conditions and can be 2-D dynamic but these scanners have a lower magnetic field strength, which leads to lower resolution images and/or longer scan times [103, 105]. Hares et al [106] was able to use a combination of both MRI scanner types by registering high-resolution open-bore scans to low-resolution upright weight-bearing scans for kinematic analysis. As motion artifacts can be present in loaded image scans, keeping the loaded imaging times short is essential. Registering high resolution unloaded images to flexed loaded lower resolution ones, is often used for kinematic analyses in order to minimize motion artifact effects. In spite of the atypical loading limitations of quasi-static MRI kinematic analyses, several studies have shown significant differences between healthy and ACLR or ACLD knees with unique kinematic measures such as tibiofemoral contact area and tibiofemoral 3-D translation and rotations [17, 95, 102, 103, 109].

2.4.2 Mechanical measures from MRI

With the imaging capabilities of MRI, mechanical measures in ACL-injured and OA individuals can be assessed and compared to healthy individuals. The section below discusses some of these measures and their outcomes in the literature and comparison with other imaging mechanics methods. Some tibiofemoral mechanical measures acquired from MRI that will be discussed in this section are three-dimensional kinematics, contact area, contact area centroid, and femur tracking.

2.4.2.1 Contact Area, Centroid and Femoral Tracking

Contact area size, centroid, and femoral tracking are some mechanical measures that have been acquired from MRI in the literature and have been used in the study of knee OA pathology. Contact area gives an idea as to how load is distributed across the joint and is usually assessed with loaded knee joint during MRI scan (see Table 0-1). Table 0-1 shows two studies that found contact area from the integration of B-spline lines created on each sagittal image along the line of contact [14, 15, 17]. Carpenter et al used this measure to assess ACLR and contralateral knees and found no significant difference of contact area between them when assessing from 40 degrees flexion to full extension [15, 17]. In Patel et al's work, the normal contact area change from flexion to extension

was assessed and it is seen that contact area decreases slightly with flexion in the medial compartment and changes more in this compartment than in the lateral [14]. Contact centroid and femur tracking (i.e. tracking of the femoral condyle center) have also been assessed with similar results across studies of more posterior patterns seen in the ACL-injured knee than healthy and contralateral knee particularly in the lateral compartment (Table 0-2) [14, 95, 103, 104, 109, 112]. A slightly different outcome is tibia contact having more anterior patterns in injured than contralateral. This was seen in one study that assessed tibiofemoral contact pattern in OA knees [112]. This difference may be due to adaptive mechanical changes that may have already occurred in the contralateral knee of an individual with knee OA. *Although the methods of defining contact centroids or femoral points may be different across studies, the similar results in the ACL-injured group and the error values (see Table 0-2 for details) indicate that contact area, centroid, and femoral tracking are good measures that can be used in the study of early OA knee mechanics.*

Table 0-1: Summary of contact area, significant outcomes, how they were defined, corresponding reliability values, findings, and loading condition

	Paper Reference	Type	Population Type	Activity/Task	How measure was defined	Validation	Summary of Findings
Contact Area	Carpenter et al [15]	Contact Area	ACLR and Contralateral	Full extension and 40° - 125 N compressive force - MRI	Cartilage-on-cartilage computed by connecting all spline points with a set of triangles and then summing the triangle areas.	Not Reported	No significant difference in contact area between ACLR and contralateral
	Patel et al [14]	Contact Area	Healthy	0° to 60° (0°, 20°, 30°, 35°, 50°, 60°) 133N compressive load - MRI	B-spline lines created on each sagittal image along the line of contact and integrating the lines across all the images	InterCV: (Medial) - 11.4%, 6.3 % (Lateral), IntraCV: (Medial) - 3.8%, (Lateral) - 6.1%	Contact area (medial) started at 374 mm^2 and decreased to 308 mm^2 with flexion of 60°, while lateral compartment contact area did not change significantly from 276 mm^2

Table 0-2: Summary of 3-D kinematics significant outcomes, how they were defined, corresponding validation, findings, and loading condition

	Paper Reference	Type	Population Type	Activity/Task	How measure was defined	Validation	Summary of Findings
Contact Area Centroid Translation /Femur Tracking	Shefelbine et al [95]	Contact Area Centroid Tracking	Healthy/ACLD - TF kinematics under axial load	Full extension and 45° flexion - 125 N compressive (MRI)	Mid-point of contact line in each sagittal slice determined and centroid calculated as the weighted average of contact width	Not Reported	*Contact area centroid (tibia) in ACLD knees @extension, more posterior to uninjured *Significantly less posterior translation of contact centroid in medial tibial condyle in ACLD knee
	Scarvell et al [109]	Contact Area Centroid/ Femoral Condyle Tracking	ACLD and Healthy	0° to 90° (15° intervals) - 150N compressive load - MRI	*Femoral condyle position on tibial plateau measured as distance from posterior tibial cortex to point of tibiofemoral contact of medial/lateral femoral condyle *Where contact occurred over a wide area, area centroid was used	ICC: 0.94 - 0.96 (CI 99% 0.91 - 0.97)	*Tibiofemoral contact pattern of loaded knees did not differ from unloaded knees *Difference in tibiofemoral contact pattern in the ACL-injured knee was associated with more severe knee symptoms
	Logan et al [103]	Femoral Condyle Tracking	ACLD and Contralateral	0° to 90° Progressive squat - MRI	**Position of posterior femoral condyles relative to the tibia:** *Centers of the posterior circular surfaces of the femoral condyles *Distance between this center and a vertical line drawn from the ipsilateral posterior tibial cortex for each flexion position. *Changes in distance between increments of flexion equate to relative motion of the femur on the tibia with flexion.	1.5 mm - Accuracy	More posterior in the lateral compartment of ACLD than normal knees

	Paper Reference	Type	Population Type	Activity/Task	How measure was defined	Validation	Summary of Findings
Contact Area Centroid Translation /Femur Tracking	Carpenter et al [15]	Contact Area Centroid Tracking	ACLR and Contralateral	Full extension and 40° - 125 N compressive force - MRI	Contact centroid in each compartment was defined as the area centroid for the corresponding set of triangles. Expressed w.r.t the tibial origin and centroid translations when moving from extended to flexed position as the difference between the 2 positions.	Intra/Inter-observer reproducibility: 0.6 - 0.9 mm	No significant difference between contact location between ACLR and contralateral
	Scarvell et al [104]	Contact Area Centroid and Femoral Flexion Center Tracking comparison	ACLD and Contralateral	0° to 90° (15° intervals) - 150N compressive load – MRI	**Position of posterior femoral condyles relative to the tibia** – *Centers of the posterior circular surfaces of the femoral condyles *Distance between this center and a vertical line drawn from the ipsilateral posterior tibial cortex for each flexion position. *Changes in distance between increments of flexion equate to relative motion of the femur on the tibia with flexion. **Tibiofemoral contact mapping** - Distance from posterior tibial cortex to the point of tibiofemoral contact of medial and lateral femoral condyle. Where contact occurred over a wide area, the area centroid was used.	Intra-observer CV – Femoral Flexion Centre: 0.94 (95% C.I, 0.83 - 0.97) Intra-observer CV - Contact mapping: 0.94 (95% C.I, 0.91 - 0.97)	*More posterior contact pattern in injured knee in lateral compartment. *FFC moved back very little during flexion (medial) and FFC moved back throughout flexion (lateral)

	Paper Reference	Type	Population Type	Activity/Task	How measure was defined	Validation	Summary of Findings
Contact Area Centroid Translation /Femur Tracking	Scarvell et al [112]	Tibiofemoral Contact Pattern	OA and Contralateral	0° to 90° (15° intervals) - 150N compressive load - MRI	**Tibiofemoral contact point** - distance from posterior tibial cortex to point at which femoral condyle contacted the tibial plateau	Intraclass Correlation - 0.94 (99% C.I, 0.91 - 0.97)	*Contact in the lateral and medial compartments of OA knee more anterior on tibial plateau than healthy in knee extension and 90° flexion. *Anterior contact pattern associated with OA
	Patel et al [14]	Contact Area Centroid Tracking	Healthy	0° to 60° (0°, 20°, 30°, 35°, 50°, 60°) 133N compressive load - MRI	Centroid of each compartment contact area relative to the tibial plateau was calculated for each position and transformed to the straight leg position coordinate frame of reference - enables calculation of change in position of contact area with flexion of the knee.	Not reported	*With 60° flexion: *Medial contact area centroid - moved posteriorly 8 mm *Lateral contact area - moved posteriorly 5.2 mm

2.4.2.2 Image-Based Three-Dimensional Kinematics

The outcome of three-dimensional knee kinematics analyzed from MRI under different loading conditions has given insight into knee motion and changes in ACL-injured knees. Normal knee kinematics assessed from MRI with 125 N quasi-static load has shown that, with increased flexion, femoral roll back increases by about 18.5 mm and the tibia translates medially by about 2.5 mm with frontal and axial rotations of up to 8° [14]. The magnitude of rotation however, in the axial plane, is seen to be more (11.55 ± 3.2°) when the knee is not loaded [113]. Deviation from normal kinematics have been seen in ACLD knees where the femur is seen to translate more anteriorly than in healthy knees [95]. This is in line with findings from dynamic Roentgen Stereophotogrammetric Analysis (RSA) studies which are considered to be a gold standard for 3-D kinematics, but are invasive due to the requirement for radiolucent beads to be attached to the bone [114, 115]. In another MRI-based study with similar findings, the loading activity was designed to activate isometric muscular contraction [102]. This study found specifically more posterior translation of the medial femoral condyle than the lateral. Another finding that stands out and is consistent across studies, is increased tibial internal rotation in ACLD knees when moving from extended to flexed position [15, 92]. *The consistency in these findings, in spite of the different loading conditions, indicate that anterior/posterior translation is an important measure to acquire when developing an integrated method to further explore the mechanics of early OA.*

Apart from the different loading conditions, 3-D kinematic analysis methods and coordinate system definition vary across studies, which likely leads to differences in results (see Table 0-3). In MRI kinematics, high resolution fully extended knee images can be registered to the lower resolution flexed and loaded images to create a transformation matrix from which 6 degrees of motion values can be derived [14]. Fixed coordinate systems can also be created in the femur and tibia based on visible anatomical landmarks in the MRI, from which translations and rotations can be described [15, 92, 95]. The fixed coordinate system method has results with root mean square error (RMSE) values ranging from 0.04 – 2.2 mm [15, 92, 95, 102]. Within the fixed coordinate system method, there are also differences in the way the axes may be defined that might contribute to differences in study findings. The likely result of this is that patterns can be compared across studies, but absolute values cannot.

Table 0-3: Summary of MRI-based 3-D Kinematics significant outcomes, how they were defined, corresponding reliability values, findings and loading condition

	Paper Reference	Type	Population Type/Summary of objectives	Activity/Task	How measure was defined	Validation	Summary of Findings
3-D Kinematics	Shefelbine et al [95]	*Anterior/Posterior Femoral Translation *Medial/Lateral Femoral Translation *Femoral Rotation	Healthy/ACLD - TBF kinematics under axial load	Full extension and 45° flexion - 125 N compressive (MRI)	Two coordinates fixed in the femur and tibia. **Femur:** *M-L axis: Line joining centers of the posterior femoral condyles *Origin: Mid-point of M-L line *Temp Longitudinal: Line through the mid-diaphysis in single image slice at knee center *A-P axis: Cross product of M-L axis and temp longitudinal *I-S axis: Cross product of M-L and A-P axes **Tibia:** *M-L axis: Line connecting posterior tibial condyles *Origin: Mid-point of M-L axis *A-P axis: Cross product between M-L axis and line through tibial shaft I-S axis: Cross product between the M-L and A-P axes	Intra/Inter Observer: <0.8mm (RMSE)	*Femur more posterior to tibia than contralateral at extension (2.6 mm) *In flexion, translated more anteriorly than uninjured (4.3mm)
	Eisenhart et al [102]	*Femoro-Tibial Translations (translations beween tibia and femoral condyles)	ACLD with contralateral - Femorotibial translations under muscle activity	30° and 90° of flexion - isometric contraction of flexor muscle groups (10 N.m about knee joint) - MRI	Tibia-based local coordinate system with femoral reference points to track femur w.r.t the tibia coordinate system. ***Tibia Coordinate System:** Tibial plateau segmented per slice and area centroid of used as origin. 3-D coordinate system defined from spatial orientation of tibia. ***Femoral reference point:** Mid-point of trans-epicondylar axis (least unaffected by knee flexion)	Tibia-based CS: SD - 0.22 mm, CV% - 0.2% | Translation - SD: 0.12mm and CV% - 4.7%	*Posterior translation of femur between 30° and 90° relative to tibia *In ACLD (+1.3 ± 3.8mm), posterior translation of MFC was larger than in healthy (-0.9 ± 2.9 mm) *Under extensor isometric contraction -increased posterior position of femur at 30° not at 90° in both ACLD and contralateral

	Paper Reference	Type	Population Type	Activity/Task	How measure was defined	Validation	Summary of Findings
3-D Kinematics	DeFrate 06, [92]	*6-degrees of freedom knee kinematics	ACLD - Kinematics of ACLD	Quasi-static lunge - full extension to 90° of flexion (15°, 30°, 60°, 90°) - dual orthogonal fluoroscopic system	Two coordinates fixed in the femur and tibia. **Femur:** I-S axis: Long axis of the femur M-L axis: Transepicondylar line **Tibia** I-S axis: Long-axis of tibial shaft M-L axis: Perpendicular to long axis A-P axis: Perpendicular to both I-S and M-L axes Origin: Center of tibial plateau Translations as mid-transepicondylar relative to tibial coordinate system - converted to tibia w.r.t femur	Average error - Displacement - 0.04 +/- 0.06 mmn| Rotations: < 0.3°	*ACLD - significant tibial anterior shift (~3mm) and internal rotation (~2°) at low flexion angles. *Medial tibial translation (1mm) between 15° and 90°
	Brandsson et al [97]	*Internal/External Tibial Rotations *Abduction/Adduction Tibial Rotations *M-L, I-S and A-P translations	ACLD and Contralateral	Ascent 8cm platform - RSA X-ray	Translations: Tantalum markers in fixed reference segment and reference points in tibia/femur **Tibia reference points:** Two tips of tibial intercondylar eminence. **Femur reference points:** Circular centers of the medial and femoral condyles	SD Rotation: 1.6° - 2.3° | SD Translation from 1.2 - 2.2 mm. 10 times > than measurement error.	*Tibial center more posteriorly displaced and externally rotated in ACLD *Increased Anterior displacement of the lateral femoral condyle in ACLD *Lateral femoral condyle less A-P translation in extension *Medial femoral condyle same on both injured and contralateral
	Carpenter et al [15]	*Femoral condyle position *Tibial Rotation	ACLR and Contralateral	Full extension and 40° - 125 N compressive force - MRI	Fixed tibia coordinate system. Tibia:***M-L axis:** Line connecting most posterior points of medial and lateral sides of tibial plateau|***Origin:** Mid-point of M-L axis line|***A-P axis:** Cross product of M-L axis and tibial shaft axis from mid-sagittal slice|**I-S:** Cross product between M-L and A-P axes	TBF Rotation Accuracy: 0.1°|Inter/Intra observer rotation: 1.5°|Inter/Intra observer translation: 0.6 to 0.9 mm	*In fully extended, tibia in ACLR more externally rotated (3.6° ± 4.2°) than contralateral *Extension to flexion - ACLR more internal tibial rotation (3.5° ± 5.9°) than contralateral

	Paper Reference	Type	Population Type	Activity/Task	How measure was defined	Validation	Summary of Findings
3-D Kinematics	Patel et al [14]	*Axial Rotation *A-P Translation *M-L Translation	Healthy	0° to 60° (0°, 20°, 30°, 35°, 50°, 60°) 133N compressive load - MRI	Tibias and femurs were registered to the same 3-D space including all 6 motions to give transformational matrix from which 3-D motions were calculated	*Roll back: 13.3% (Inter-observer), 15.6% (Intra-observer) *Tibial Translation Lateral: 26% (Inter-observer), 14% (Intra-observer) *Valgus angle: 6.3% (Inter-observer), 6.9% (Intra-observer) *Internal rotation: 8.1% (Inter-observer), 6.2% (Intra-observer)	*Tibial Rotation ~ 4.8° at 40° flexion and the n decreased *Tibial valgus increased by 8° at 60° *Femoral roll back increased to 18.5 mm at average 60° flexion. *Tibia translated medially 2.5 mm at 60° flexion
	Chen et al [113]	*Axial Rotation of tibia during flexion-extension	Healthy	0° to 40° and 40 to 0° (0° , 8° ,16° , 24° , 32° , 40°) - no load - MRI	Images were acquired in the transverse plane and tibial rotation angle defined as the angle through the line from the tibial tubercle midpoint to the upper tibiofibular joint midpoint	SD: 2.97°	Tibia rotated internally (11.55 +/- 3.2) during knee flexion and rotated externally (11.40 +/- 3.0 degrees) during knee extension *Tibial rotation differed significantly between 0 to 24° and 24 to 40°

2.5 Knee Axes Definitions in Three-Dimensional Kinematics and Kinetics

The biggest challenge in defining axes for femur and tibia anatomical coordinate systems is that there is no actual fixed axis of rotation that exists as the knee moves. Different methods have been proposed to optimally describe knee motion. One of such one is by Grood and Suntay's joint coordinate system (JCS) [116], where motion is described with two fixed-body axes in the femur and tibia and one floating axis normal to both. The proposition of this method was that it was sequence-dependent unlike the Euler angles or cardan sequence methods of extracting the motion and translation values from the relevant transformation matrices. It has however been proven in later work, that the joint coordinate system is equivalent to the Cardan XYZ sequence [117]. The International Standard of Biomechanics has proposed the JCS as a standard because of its clinically relevant way of reporting joint motion [118]. There has however been other work that has proposed axes definitions, particularly for the flexion axis, that would reduce kinematic "cross-talk" which is where the component of one rotation in a particular plane is interpreted as rotation from another plane. Churchill et al's [119] proposition of an optimal compound flexion axis is an estimation by a trans-epicondylar axis. The study uses cadaver specimens to compare the outcomes of a computer-based optimal flexion axis, to outcomes of an anatomical-based trans-epicondylar axis with similar results. The optimal flexion axis is said to keep residual components the same during the entire flexion-extension cycle on the basis that the optimal flexion and longitudinal axes are properly placed [119]. There are other flexion axes definitions including the instantaneous helical axis [120]. A study that compared the different flexion axis definition outcomes found that motion in the frontal plane was most sensitive to these different axes definitions [121].

The longitudinal axis for femur or tibia can be described as going from the knee joint center to the hip joint center or ankle joint center respectively (mechanical long axis) or from the femur/tibia origin through the femoral shaft centroid (anatomical long axis). For the tibia, this difference in long axis definition is less of a concern than the difference in the femoral long axis. This is because there is a higher distinction between the vectors of the mechanical and anatomical axes of the femur than those of the tibia. It is not apparent which of the femoral axes definitions better describes axial rotations or longitudinal translations. In gait analysis, the hip joint center can be easily estimated from assumptions that it is a ball and socket joint [122]. While femoral shaft centers to define an anatomical long axis cannot be accurately described in

gait analysis, it can easily be seen and used in MRI 3-D kinematics coordinate definitions. ISB recommends a functional approach of defining the hip joint center in gait analysis, however, variation can occur in the long axis if the definition of the origin point differs [118]. Lenz et al [121] showed that axial (antero-posteral) motion is most sensitive to different locations of the femoral origin. Between functional and anatomically defined coordinate system models, Besier et al [123] showed that gait data processed from a functional model is more repeatable than that processed from an anatomical-landmark model. Different femoral longitudinal axis definitions have been explored by Stagni et al and it was found that it can affect calculations of both angles and moments of the hip and knee joints with the antero-posterior direction being more sensitive to the errors [124]. *These findings show that more investigation is needed in coordinate system definitions that will be more ideal for knee kinematics and kinetic description.*

2.6 Gait Analysis Measures

Some biomechanical (kinematics and kinetics) adaptations of the ACL-injured (ACLD and ACLR) joint, while carrying out activities of daily living, can be captured with gait analysis. Literature has revealed that these adaptations are sensitive to time from injury. Please note that the term 'gait analysis', in this thesis, will be used to refer to both kinematic and kinetic measures calculated from motion capture and force plate data or reconstruction. A "quadriceps avoidance" phenomenon in ACL injury, where knee flexion moment is lower in order to control anterior tibial translation, has been hypothesized and observed in some studies [125, 126]. However, further work has shown that, for chronic injury, this is not the case. Knoll et al demonstrated that pre-injury walking patterns in sagittal plane kinetics and kinematics were restored, 8 months post-surgery [126]. Another study that assessed sagittal-plane knee kinematics and kinetics of chronic ACLD and healthy-matched controls with different activities, found similar biomechanical patterns (between healthy and ACLD), even though the ACLD group had lower joint functionality and strength deficits [127-129].These studies reveal that sagittal-plane measures may not be sufficient in distinguishing between ACL-injured and healthy groups.

Axial and frontal plane movements seem to be more sensitive to biomechanical differences between the healthy and ACL-injured groups. Georgoulis et al found that ACLD individuals had greater internal tibial rotation than healthy individuals during walking [96]. In studies with higher demand activities (stair descent, drop-landing and pivoting), ACLR individuals were seen to have a significantly higher tibial rotation than the uninjured contralateral knee and the healthy

group's knees but not as much as the ACLD group even though they had normal levels of anterior tibial translation [130, 131]. Increased knee adduction moments have also been observed in the ACL-injured population [125, 132, 133]. Higher internal tibial rotation and knee adduction moments present in the ACL-injury than healthy may be linked to cases of medial compartment OA [133]. It is important to know that in spite of these findings, movements in the axial and frontal planes are most susceptible to kinematic cross-talk.

2.6.1 Relevant Motion Tasks for Gait Analysis

Certain motion tasks assessed with gait analysis reveal more information on mechanical differences than other activities in the study of the ACL injured population. Low-demand activities like walking have been seen to distinguish ACLD and healthy knees [96] but not for ACLR. In spite of seeming restoration of normal kinematics from walking gait analysis, ACLR cases do not return to pre-injury levels of activity [134], have high re-injury rates [135] and still end up with PTOA [101, 136, 137]. This makes it evident that while standard activities like walking are recommended, slightly higher demand tasks for gait analysis are also required to understand OA pathology in ACLR individuals. Furthermore, studies that have investigated different activities in ACL-injury found that activities such as stair negotiation, pivoting and landing activities, showed increased tibial rotation of ACLR and ACLD than healthy, where walking did not [96, 130]. A recent systematic review paper that took into consideration time after reconstruction surgery in assessing ideal activities for the study of the ACLR population, recommends stair negotiation and landing tasks for early stages of ACLR surgery and pivoting or landing tasks for 6 months after ACLR surgery [138]. In deciding ideal activities for ACLR gait analysis studies, one needs to consider that motion tasks do not worsen injury. Also, activities that increase errors from skin-motion artifacts (undesirable motion between marker and skin) are of concern which can be up to 16 mm in walk and cut activities [139]. *In this light, walking, stair negotiation, and chair tasks may be activities worth investigating further for the study of ACL-injured biomechanics as they include low-demand and reduced skin-motion task activities.*

2.6.2 Error Measurement in Gait Analysis Measures

Understanding measurement error in gait analysis is important for knowing what differences are meaningful. Sources of error include inconsistent marker placement, variation in walking speed across sessions, data-processing, and measurement equipment errors [140]. As seen in Table 0-5, in the sagittal plane for kinematics, ICC (Inter/Intra Class Correlation Coefficient) varies from 0.77 – 0.98 across different studies with standard error measurement

(S.E.M) and standard deviation (SD) values of 1.7 to 7.94 degrees in walking and stair activities [141-146]. This is worse than the frontal error measurements (~2 degrees), which is expected because motion that occurs in this plane is much smaller than that which happens in the sagittal plane [141, 144]. Stair ICC (0.77 – 0.88) and SD values (2.4 – 7.11 degrees) are slightly worse than walking, perhaps due to more skin motion artifacts that occur during this activity [142, 144-146].

A similar trend follows for kinetic measures (Table 0-5), where the standard deviation values are worse in the stair activity (0.40 – 0.51 N.m/kg) sagittal measures than in the walk sagittal measures (0.11 – 0.22 N/m/kg) [141, 142, 147-152]. The frontal moments have similar ICC values between the chair and walking activities (0.72-0.95) with S.E.M and SD following a similar trend (0.06 - 0.13 N.m/kg) [141, 142, 147-152]. Coefficient of multiple correlation (CMC) was used as an error measurement in some studies as can be seen in Table 0-4 and Table 0-5. CMC is a measure that expresses the proportion of how much the dependent variable varies in relation to the independent variable [153]. One study that compared ICC and CMC values for the same study, showed a conflict in the repeatability outcomes [154]. While ICC takes into account the standard error of measurement and minimum detectable change, CMC does not. For this reason, though it was included in the tables for completeness, it will not be discussed further.

Table 0-4: Summary of repeatability and reliability measures from the literature for knee kinematics

	Measure	Repeatability	Mean	Details of Study	Reference	Motion Capture System
Walk	Peak Flexion Angle	**ICC:** 0.77 **SEM:** 3.73° **SD:** 6.4°	12.4°- 13.0°	OA | Two days	Robbins et al [141]	Optoelectronic motion capture system (acquired at 100 Hz)
		CMC: 0 .985 +/-0.009	18°	Healthy | Within/Between days (3)	Kadaba et al [142]	5-infrared camera system (acquired at 50 Hz)
		ICC: 0.892	12.6°	Healthy | Two days	Van der Linden [143]	Two flexible electrogoniometers
		SD: 3.2° **ICC:** 0.93	17.8°	Healthy | Three times (days)	Scheys et al [144]	8 – 14 infrared cameras (acquired at 100 Hz)
	Peak Extension Angle	**SD:** 1.7° **ICC:** 0.98	2.8°	Healthy | Three times (days)	Scheys et al [144]	8 – 14 infrared cameras (acquired at 100 Hz)
		ICC: 0.74 **SEM:** 3.79° **SD:** 6.5°	5°-5.4°	OA | Two days	Robbins et al [141]	Optoelectronic motion capture system (acquired at 100 Hz)
	Peak Abduction Angle	**CMC:** 0 .783 +/-0.159	16°	Healthy | Within/Between days (3)	Kadaba et al [142]	5-infrared camera motion capture system (acquired at 50 Hz)
	Peak Adduction Angle	**SD:** 1.9°|**ICC:** 0.93	8.8°	Healthy | Three times (days)	Scheys et al [144]	8 – 14 infrared cameras (at 100 Hz)
		ICC: 0.60 **SEM:** 1.98° **SD:** 2.1°	3.8 -4.3°	OA | Two days	Robbins et al [141]	Optoelectronic motion capture system (acquired at 100 Hz)
Stair	Stair Ascent – Peak Extension Angle	**SD:** 7.40° **Mean CV:** 2.35	93.9°	Healthy | Within a day	Protopapadaki et al [145]	8-camera infrared cameras (acquired at 120 Hz)
		SEM: 1.5° Injured **SEM:** 2.5° Contralateral	87.6° (Injured) 85.2° (Contralateral)	ACLD/Contralateral | Within Day	Maryam et al [146]	6-camera infrared cameras (acquired at 100Hz)
		SD: 6°|**ICC:** 0.84	63.1°	Healthy | Three times (days)	Scheys et al [144]	8 – 14 infrared cameras (at 100 Hz)
		SD: 12.6	89.4	Healthy| Two days	Van der Linden [143]	Two-flexible electrogoniometers
	Stair Descent – Peak Extension Angle	**SD:** 2.4°|**ICC:** 0.77	64.6°	Healthy |Three times (days)	Scheys et al [144]	8 – 14 infrared cameras (at 100 Hz)
		SD: 7.11°	90.5°	Healthy | Within a day	Protopapadaki [145]	8-camera infrared cameras (120 Hz)
		SD: 13.6°	84.5°	Healthy | Two days	Van der Linden [143]	Two-flexible electrogoniometers

Table 0-5: Summary of repeatability and reliability measures for kinetic measures

Motion Task	Measure	Repeatability	Mean	Details of Study	Reference	Motion Capture Systems
Walk	Peak Flexion Moment	**ICC:** 0.57 **SD:** 0.18 N.m/kg	0.29 N.m/kg	OA Two days	Robbins et al [141]	Optoelectronic motion capture system (100 Hz) and force plate (2000 Hz)
		CMC: 0 .936 +/-0.03	2 % N.m/(BW*LL)	Healthy Within/Between days (3)	Kadaba et al [142]	5-infrared camera system and force plate (both sampled at 50 Hz)
		SD: 0.14 N.m/kg	0.54 N.m/kg	Healthy Same Day	Costigan et al [147]	Optoelectronic motion capture system and force plate (50 Hz)
	Peak Extension Moment	**ICC:** 0.78 **SD**: 0.22 N.m/kg	0.25 N.m/kg	OA Two days	Robbins et al [141]	Optoelectronic motion capture system (100 Hz and force plate (2000Hz)
		CMC: 0 .936 +/-0.03	7 %N.m/(BW*LL)	Healthy Within/Between days (3)	Kadaba et al [142]	5-infrared camera system and force plate (50 Hz)
	Peak Abduction Moment	**ICC:** 0.93 **SEM:** 0.05 N.m/kg **SD:** 0.13 N.m/kg	0.29 N.m/kg	OA Two days	Robbins et al [141]	Optoelectronic motion capture system sampled at (100 Hz), force plate (2000Hz)
		CMC: 0 .916 +/-0.093	3 %N.m/(BW*LL)	Healthy Within/Between days (3)	Kadaba et al [142]	5-infrared camera system and force plate (50 Hz)
	Peak Adduction Moment	**ICC:** 0.92 **SEM:** 0.06 N.m/kg **SD:** 0.13 N.m/kg	0.38 N.m/kg	OA Two days	Robbins et al [141]	Optoelectronic motion capture system (100 Hz) and force plate (2000 Hz)
		CMC: 0 .916 +/-0.093	1.5 %N.m/(BW*LL)	Healthy Within/Between days (3)	Kadaba et al [142]	5-infrared camera system and force plate (50 Hz)
Chair	Chair Rise: Peak Adduction Moment	**ICC:** 0.72 **SD:** 5.8 x 10^{-3} N m $BW^{-1}H^{-1}$	2.5 x 10^{-3} N m $BW^{-1}H^{-1}$	Healthy Between days (3)	Gilleard et al [148]	8-infrared camera system (60 Hz) and force plate at (960 Hz)
	Chair Rise: Peak Knee Extension Moment	**SD:** 0.10 - 0.13 N.m/kg (Healthy) **SD:** 0.09 - 0.25 N.m/kg (Palsy)	0.49 – 0.51 N.m/kg (Healthy) 0.09 – 0.15 N.m/kg (Palsy)	Healthy/Palsy Same day	Suriyaamarit et al [149]	8-infrared camera system sampled at 120 Hz and force plate (1200 Hz)
	Chair Sit (squat): Peak Abduction Moment	**ICC:** 0.95 **SEM:** 0.06 N.m/kg	0.41 N.m/kg	Healthy Two days	Alenezi et al [150]	10-infrared camera system (240 Hz) and force plate (1200 Hz)
	Chair Sit (squat): Peak Knee Extension Moment	**ICC:** 0.77 **SEM:** 0.06 N.m/kg	0.96 N.m/kg	Healthy Two times	Alenezi et al [150]	10-infrared camera system sampled (240 Hz) and force plate (1200 Hz)
Stair	Stair Ascent – Peak Extension Angle	**SD:** 0.24 N.m/kg	1.16N.m/kg	Healthy Two days	Costigan et al [147]	Optoelectronic motion capture system and force plate (both 50 Hz)
		SD: 0.13 - 0.21 N.m/(Body mass*height)	0.71 – 0.75 N.m/(Body mass*height)	Uninjured ACLR Same Day	Hooper et al [151]	3-infrared camera system (50 Hz) and force plate (200 Hz)
	Stair Descent – Peak Extension Angle	**SD:** 22 N.m	63.1 N.m	Healthy Same day	Spanjaard et al [152]	9-infrared camera system and force plate (sampling rate not reported)
		SD: 0.11	0.65 – 0.68 N.m/(Body mass*height)	Uninjured ACLR Same Day	Hooper et al [151]	3-infrared camera system (50 Hz) and force plate (200 Hz)

2.6.3 Key Mechanical Outcomes and Time from Reconstruction Surgery

Time from ACL-reconstruction surgery and reliability of axial plane kinematics have been seen to affect the mechanical outcomes in gait analysis. Figure 0-4 shows key mechanical outcomes from meta-analysis studies of gait (walking) in the ACLR population including – peak knee extension/flexion moments, peak knee/hip flexion angle, and peak knee adduction/abduction moment – which are sagittal and frontal kinetic and kinematic values [11-13]. Hart et al reported that no conclusions could be drawn about axial plane kinematics due to inconsistencies across the literature [13]. This may be expected considering that axial plane kinematics have the lowest reliability [140]. From the mechMRI literature, it is seen that axial kinematics are of importance in the ACL-injured study. Being able to analyze ACLR mechanics with both tools (gait analysis and mechMRI) could be insightful. Furthermore, Figure 0-4 below summarizes the findings of three recent meta-analysis/systematic review papers that assessed past work in the study of the ACLR population while walking [11-13], using motion capture and force plates. There appears to be a slight discrepancy in the findings, except within a time range 9 – 36 months post-surgery, and because of the consistency across the studies, this may be an indication that this time-period may be an ideal time to carry out a biomechanical study of the ACLR population. From the comprehensive meta-analysis that the Slater et al study gave on progressive mechanical changes after ACLR, the ideal time range post-surgery also falls within the same 9 – 36-month period discovered from the meta-analysis comparisons i.e. the biggest difference between all the outcome measures and healthy controls fall within this period (9-36 months) [12]. Being able to assess the mechanics of ACLR individuals within this ideal time period post-surgery, and with both mechMRI (which gives more reliable axial kinematic information) and gait analysis, would maximize interesting findings in the exploratory study of ACL-injury and reconstruction.

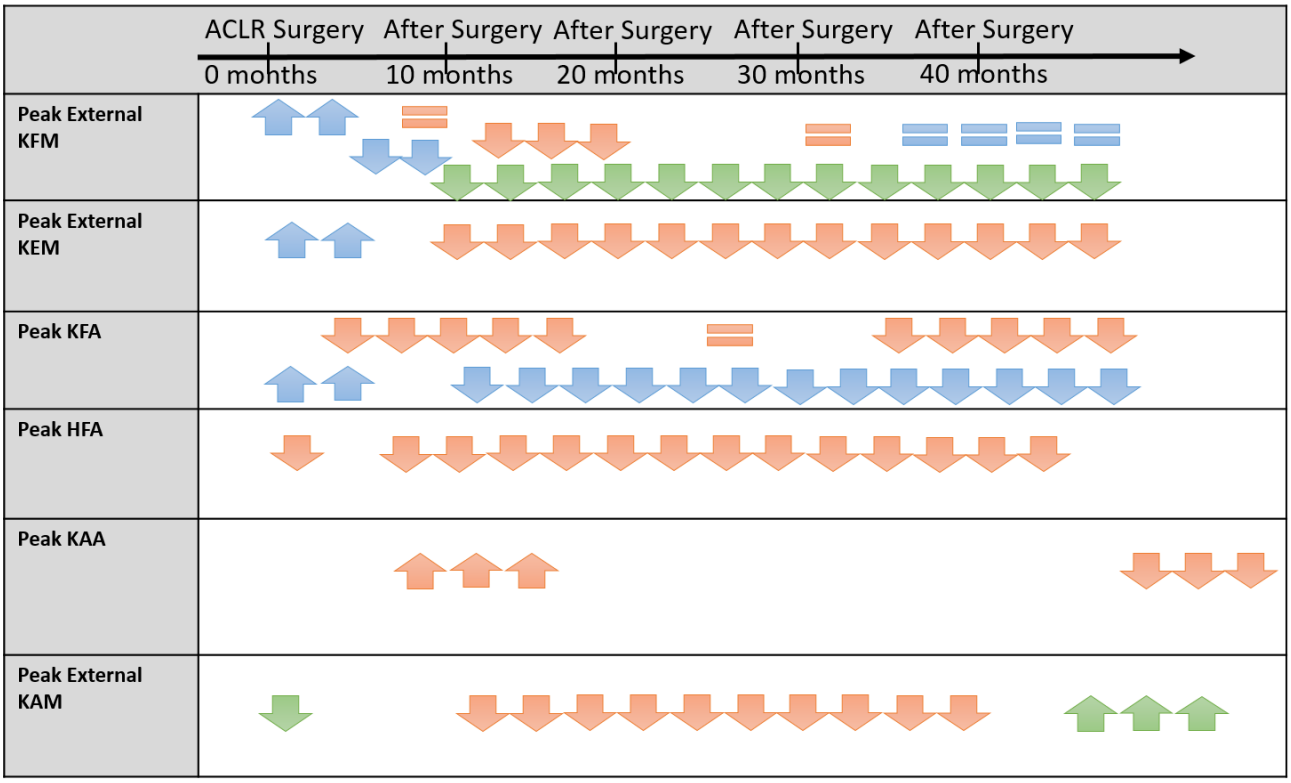

Figure 0-4: Key mechanical outcomes of gait analysis (walking activity) from three recent meta-analysis papers of ACLR studies with increasing time (months) from surgery. : Kaur et al [11], : Slater et al [12], : Hart et al [13]. Up-arrow: Measure increased over time-period it covers. Equal-sign: Measure did not change over time-period it covers. KFM – Knee Flexion Moment, KEM – Knee Extension Moment, KFA – Knee Flexion Angle, HFA – Hip Flexion Angle, KAA – Knee Adduction Angle, KAM – Knee Adduction Moment

2.7 The Impact of Sex Differences

As the focus of this study is to apply the developed method to the ACL-injured population, it is important to know the impact of sex differences in this group. Gianotti et al's show that the number of ACL-injuries sustained by males is greater than that sustained by females [155]. However, the risk of females incurring ACL-injury in the same sports is greater than males. In terms of recovery, women have been seen to be worse [156, 157] and are more likely to incur a second ACL-injury [158, 159]. One study that looked at the impact of sex differences on gait mechanics before and after ACL reconstructive surgery found both men and women had significant differences in hip excursions and knee moments compared to the un-injured knee but only women had a decreased in knee excursion from pre- to post-surgery [160]. There are no known studies that have investigated the impact of sex differences on qMRI and mechMRI metrics in ACL-injured individuals. Deepak et al studied sex differences in knee cartilage composition and walking mechanics in healthy and OA populations and found higher

lateral articular cartilage and lower peak adduction moment in women than in men for both cohorts [161]. These findings indicate that there might be an impact of sex differences on ACL-injured and healthy individuals while studying the knee.

2.8 Some Integrative Studies and Research Motivation

Studies have found correlations between qMRI measures (T_2 relaxation times) and joint biomechanical measures from gait analysis [86, 162-164] and mechMRI [87, 165, 166] in the ACL-injured population, but there is limited work integrating these findings. An example of the limitations in other studies is single slice qMRI analysis methods that do not capture the full cartilage plate and limited mechanical outcomes being explored.

Table *0-6* below shows an increase of qMRI relaxation times with higher mechanical measures from the results of past studies. These studies assessed only certain regions of cartilage, and none assessed all three parameters of mechMRI, qMRI and gait analysis in the study of the ACL-injured population. Being able to carry out an exploratory study on the link between joint mechanics (measured with both mechMRI and gait analysis) and qMRI T_2 relaxation times (with an analysis method that assesses the full cartilage plate), may reveal the most relevant measures across the three parameters (qMRI, mechMRI and gait analysis), that can then be used in larger studies of the ACL-injured population. But before any of this can occur, a repeatable method needs to be developed and this is the primary objective of this work. The scope of this thesis is limited to the development of the technique and validation in healthy participants.

Table 0-6: Summary of studies that have carried out qMRI ($T_{1\rho}$ and T_2 relaxation times) and joint biomechanical studies in the ACL-injured Population

Authors	Kinematic/Kinetic Findings	Gait/mechMRI	Correlations with qMRI $T_{1\rho}$ and T_2 – Cartilage Region
Haughom et al [87]	Increased Anterior Tibial Translation	mechMRI	Increased $T_{1\rho}$ relaxation times – Medial Femoral Condyle of Weight-bearing region (30 degrees flexion under load)
Samaan MA et al [162]	Greater Knee Flexion Moment	Gait	Increased $T_{1\rho}$ relaxation times – Central Medial Tibia
	Greater Knee Flexion Moment Impulse	Gait	
Teng HL et al [163]	Higher Knee Flexion Moment	Gait	Increased $T_{1\rho}$ and T_2 relaxation times - Medial Femoral Condyle
	Higher Knee Flexion Angle	Gait	
Zaid et al [165]	Increased Anterior Tibial Position	mechMRI	Increased $T_{1\rho}$ relaxation time– Medial Compartment
Landsdown DA et al [166]	Increased Anterior Tibial Position	mechMRI	Increased $T_{1\rho}$ relaxation time– Central Medial Tibia
Kumar et al [86]	Higher Knee Adduction Moment	Gait	Increased $T_{1\rho}$ relaxation time – Medial Tibia, Central Medial Tibia, Posterior Medial Tibia and Posterior Medial Femur Increased T_2 relaxation time – Medial Tibial, Medial Femur, Posterior Medial Femur and Posterior Medial Tibia
Kumar et al [164]	Increased Knee Adduction Moment impulse	Gait	Increased $T_{1\rho}$ and T_2 relaxation time – Medial Compartment

2.9 Summary

In this chapter, the following points were highlighted:

- OA is a degenerative disease of the joint that affects tissue (meniscus and cartilage) and currently has no cure
- ACL-injury can be used as an early model for OA as 50% of the population develop PTOA within 10-20 years of injury
- Quantitative MRI $T_{1\rho}$ and T_2 relaxation measures can be used as a surrogate measure of tissue (cartilage and meniscus) health
- Newer qMRI analysis techniques, such as cluster analysis, provide local information about tissue degeneration as compared to more widely used approaches that use global or compartmental averages; since focal defects are important in OA, more localized analysis approaches may provide different and interesting results in the ACL population
- mechMRI analysis of loaded and unloaded conditions can distinguish between healthy knee and ACL-injured kinematics

- Gait analysis mechanical measures distinguish between ACL-injured and healthy population, however, there are varied outcomes depending on time from reconstructive surgery as well as the type of motion task analyzed
- Limited work has been carried out in exploring the relationships of qMRI, mechMRI and gait analysis metrics.
- A repeatable and integrative method to explore qMRI, mechMRI and gait analysis measures is needed to better understand PTOA.

2.10 Research Questions and Objectives

As mentioned in chapter 1 our research objectives are:

i) To create an integrative method to assess qMRI, contact area from MRI (mechMRI) and gait analysis measures

ii) To assess its repeatability in healthy individuals

We addressed these objectives through three specific research questions:

i) What is the repeatability of the qMRI, mechMRI and gait analysis measures in healthy individuals?

ii) What is the repeatability of the kinematic and kinetic outcomes using a MRI-based anatomical system and a standard gait coordinate system?

iii) Is there a link between contact area and qMRI T_2 relaxation times in articular cartilage

Chapter 3
METHODOLOGY

The methodology developed in this study as shown in Figure 0-1 below, is grouped into three categories – the study design (section 3.1), the data acquisition (section 3.2) and the data processing (section 3.5). Data was collected in five healthy participants, three times each, on three different days. Data were acquired for qMRI, mechMRI and gait analysis (sections 3.2.1 – 3.2.3). A MRI-safe loading rig (section 3.3) and a MRI-lucent gait marker (section 3.4) were developed specifically for this work. For data processing, we modified a novel method for the qMRI analysis (section 3.5.1) and used standard methods for the mechMRI (section 3.5.2) and gait analysis (section 3.5.3). We developed a method to integrate data from MRI and gait analysis (section 3.6), so as to compare which coordinate system may be better in processing kinematic and kinetic data. A novel method was also developed to integrate qMRI and contact area data (section 3.7).

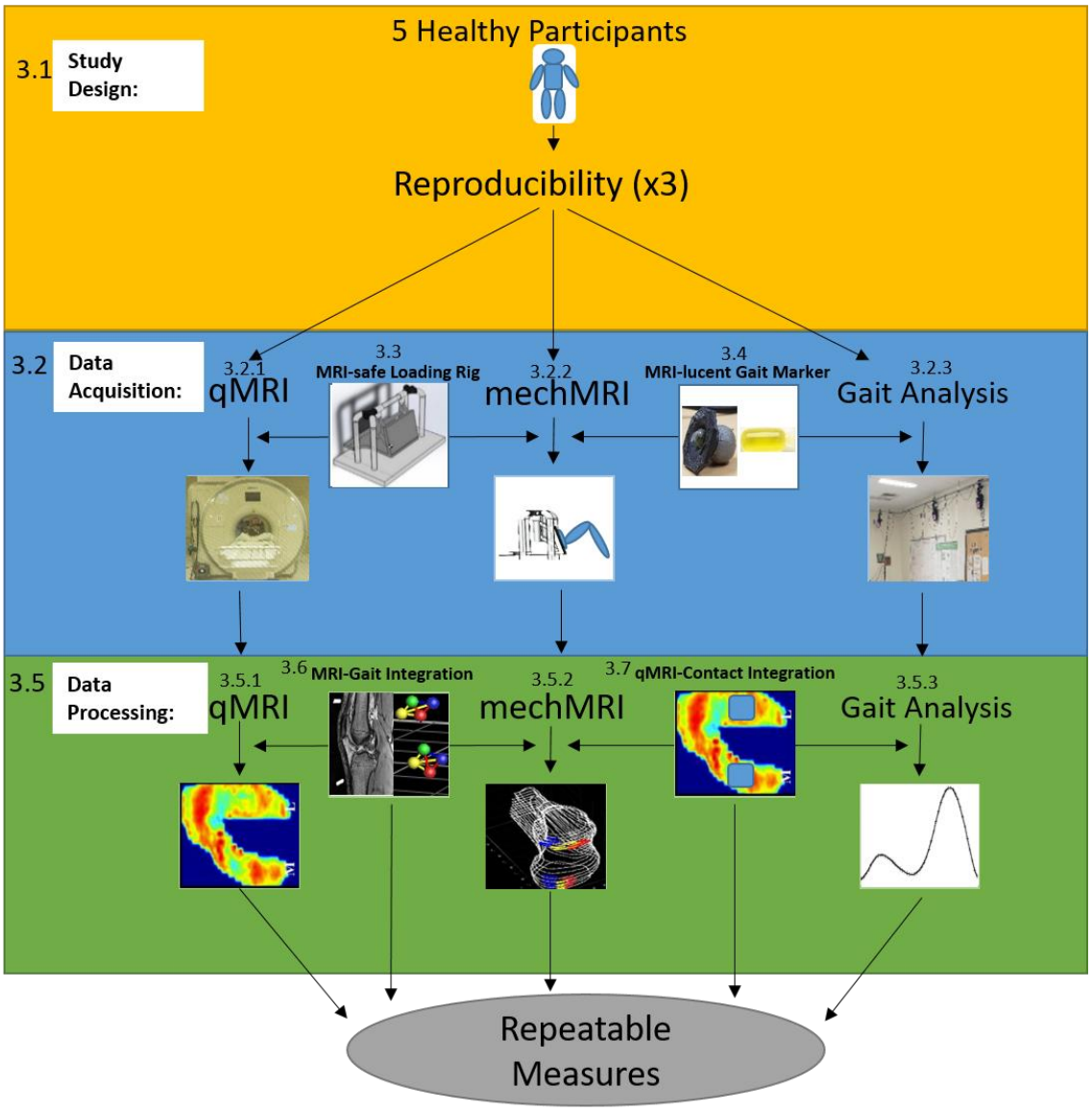

Figure 0-1: Methodology flowchart giving an overview of the major processes carried out in this study.

3.1 Study Design

To determine the repeatability, data for five healthy participants were acquired for qMRI, mechMRI and gait analysis each on three separate days within one week. The inclusion criteria for all our participants included no history of knee injury, pain, surgery or musculoskeletal disease. Participants also had to be 18 or older to be included in the study. The study protocol was approved by our institutional ethics review board and all participants gave informed consent (see Appendix G).

3.2 Data Acquisition

Data collection was carried out using a 3T MRI scanner (MAGNETOM-Skyra, Siemens Healthcare, Erlangen, Germany) at the Royal University Hospital and with a motion capture system (VICON, Oxford, UK) at the biomechanics of balance and movement lab (at the Physical Activity Complex building), both at the University of Saskatchewan campus in Saskatoon. Depending on how each individual was scheduled, the motion capture data collection was carried out either immediately before or after the MRI data collection. Scheduling was limited by the availability of MRI scan time.

3.2.1 MRI

In this section, the procedures followed to acquire the mechMRI and qMRI data are detailed. The section begins with describing the RF coil setup used for the knee scans and then describes the setup and data collected for the knee while fully extended and unloaded and while flexed and loaded.

3.2.1.1 RF Coil Setup

The radiofrequency (RF) coils used for this project were prepared to accommodate both fully extended and flexed knee orientations. This was done using two flexible 18-Channel transmit-receive body coils (Body-18, Siemens Healthcare, Erlangen, Germany) arranged in a cage-like form (see Figure 0-2). The coils were held in place by a plastic parachute buckle and Velcro straps which were wrapped around both coils. The participant then inserted his or her knee into the coil for scanning. This essentially created a knee coil with a larger radius to accommodate both positions. The signal-to-noise ratio (SNR) of the setup was verified previously by our group was shown to be equivalent, and in some instances better, than a standard 15-channel knee coil setup.

Figure 0-2: Two body RF coils arranged in cage-like form to accommodate knee for MR scanning

3.2.1.2 Fully-Extended Unloaded Scans

Three sequences were used to acquire three MRI scans of the knee in a fully extended, unloaded position. The participants were instructed to remain as still as possible during the scans. Table 0-1 below shows details of these sequences.

Table 0-1: Summary table of details of scans acquired

	High Resolution Isotropic Scan	**mechMRI Scan**	**Quantitative T_2 Relaxation Time Scan**
Name of Scan	SPACE	MEDIC	qDESS
TE (Echo Time) - milliseconds	29	8	6 and 38
TR (Repetition Time) - milliseconds	1200	14	22
Resolution - millimeters	0.6 x 0.6 x 0.6	0.5 x 0.72 x 3	0.625 x 0.625 x 3
# of Signal Averages	1	1	1
Bandwidth - Hertz	385	465	300
Scan Time – minutes:seconds	15:00 – 16:00	1:32	3:22

High Resolution Isotopic Anatomy Scan: The purpose of this scan was to visually determine the centroid of the MRI-lucent ellipsoid markers as well as to spatially describe the anatomical landmarks used to create the MRI-based anatomical coordinate system. The sequence used is a Siemens product sequence called Sampling Perfection with Application optimized Contrasts using different flip-angle Evolution (SPACE). With this scan, it was important that the MRI-lucent gait markers were placed close to the knee joint so that it was within the coverage of the RF coil setup. Because of this, the scan had to have a larger field of view and higher isotropic resolution than other scans and was the longest scan (15-16 minutes). It was only in this scan that the MRI-lucent markers were required to remain on the limb except if the participant had not carried out the gait analysis tasks yet. This scan was taken first, before other sequence scans that were acquired.

Baseline for mechMRI data: A scan was acquired for the purpose of contact area, contact area centroid translation, and three-dimensional pose analysis (mechMRI). This sequence was also a product sequence called Multiple Echo Recombined Gradient Echo (MEDIC). As this scan did not need to capture the markers, the field-of-view (FOV) was smaller and was focused on the tibiofemoral joint. The scan time for this sequence was the shortest at 1 minute and 32 seconds; which was by design since this was one of the scans acquired in the loaded condition, which will be described below.

T_2 relaxation time assessment: The purpose of this scan was to generate a T_2 relaxation time map that was optimized for articular cartilage. A modified Double Echo Steady-State (DESS) scan was used; this sequence is gradient-spoiled steady state based but acquires two echoes (images) per repetition time with a spoiler gradient separating them [167]. The principle of this sequence is described by Staroswiecki et al and the analytical formula used to generate T_2 relaxation time maps for cartilage was described in Sveinsson et al [78, 167]. Briefly, the T_2 estimation is created using extended phase graph (EPG) modelling from which a linear approximation of the relationship between two DESS signals can be acquired. The benefit of quantitative cartilage T_2 estimation with this method is that it can be acquired with scan times as short as 3 to 4 minutes. Other details of this sequence not contained in Table 8 below, include gradient duration of 3.4 ms, flip angle of 25 degrees and gradient area of 313.2 mT/m*ms. The qDESS scan, unlike the above-mentioned scans, is a custom research sequence written by a member of our research group for use with the 3T scanner available at RUH.

3.2.1.3 Flexed Loaded Scans

For the flexed loaded scans, the MRI-lucent markers were removed, and the participant was repositioned in the scanner with their foot on the loading rig (see section 3.3 below for a detailed description of the device design) which simulated approximately 20% of the participant's body weight at the knee. The knee was first flexed to an angle determined by limb length and comfort within the scanner and while maintaining the desired foot position on the pedal. With a permanent marker, three points were identified: a rough estimation of the knee joint from the side of the limb, a point along the femoral shaft and a point along the tibial shaft. The flexion angle was measured using a goniometer and these points. The purpose of this was so that the flexion angle could be re-created for subsequent data acquisitions. Important to note is that it is challenging to re-create the same angles across different participants with the hand-held MRI-safe goniometer. The goniometers usually have an error of 10 or more degrees and so it was determined that the method of marking up the points be used to keep consistent angles within trials of each participant. This was suitable since repeatability within a participant is being assessed. Furthermore, we did not want to limit the maximum angle to the tallest participant as we would not have known what this large angle would be beforehand. MRI-safe pillows and wedges were placed within the coil, under the participant's knee for support.

Two flexed loaded scans were carried out – one at a low flexion angle and one at a high flexion angle. In the low flexion angle position, the only scan acquired was the mechMRI scan described in section 3.2.1.3 above. In the high flexion angle position, two scans were acquired – the mechMRI scan and the T_2 scan. The T_2 scan was only acquired in one flexed and loaded knee angle position because it is a longer scan than the mechMRI scan and we did not want to have our participants hold the three-and-a-half minute scan at two loaded angles. Also, this was a preliminary study looking at understanding how T_2 will change within the contact area and we needed to know if it is an important metric before committing valuable MRI scan time to it.

3.2.2 Gait Analysis

The gait analysis data acquisition was carried out with a motion capture system (Nexus, VICON, Centennial, CO, USA), made of 8 infrared cameras stationed at strategic positions around the room and two force plates (AMTI, model OR6-7, Watertown, MA). Knee kinematics and kinetics were assessed with sampling rates of 100 Hz for the camera and 2000 Hz for the force plate. In this section, the gait analysis apparatus setup will be described as well as the data collection procedure.

3.2.2.1 Gait Analysis Apparatus Setup

The motion tasks carried out in this project included walking, chair rise, chair sit, stair ascent, and descent. The motion capture room had to be set up in such a way that all the motion tasks could be carried out with the force plates in one configuration. In order to do this, a force plate, labelled force plate 1 (as seen in the Figure 0-3 below), was stationed in the floor. This enabled force readings for the walking activity. A second force plate was stationed on top of an elevated platform (wooden block 1) to enable force readings for the stair ascent and descent tasks. For the chair rise and sit task, a stool was placed across the elevated force plate platform and a second wooden block (wooden block 2) of similar height. With this setup, the participant could carry out the chair rise and sit tasks while the force readings were taken from the force plate 1 in the floor. Force plate 2 was used in the chair tasks, to identify in what frames from the force readings, the participant began and ended the tasks.

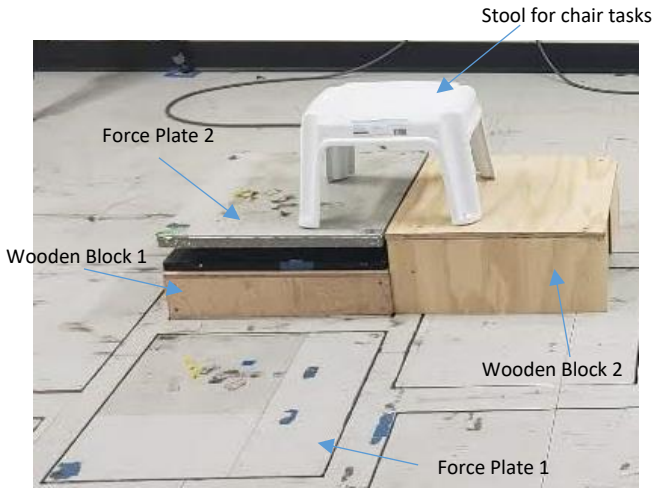

Figure 0-3: Labelled image of the gait force plate set up for all the motion tasks carried out. The stool was only used for the chair tasks.

3.2.2.2 Gait Analysis Data Collection Procedure

Before data collection, the cameras were calibrated following a standard calibration procedure. After this, an origin was set by placing a wand at the origin position in the room and capturing this into the motion capture system. With markers placed on the corners of force plate 2, the current orientation and position of the elevated force plate was acquired from custom software (Matlab, the mathworks, Natwick, MA) created by Dr. Lanovaz. The location and orientation of force plate 1, being located in the floor, was already calibrated and registered in the gait analysis system.

Each participant was prepared for motion data collection by affixing reflective markers (9 mm and 14 mm diameter markers) to different segments of their body. For the purpose of this project, a total of thirty-six markers (including the MRI-lucent gait markers on the right limb- described in detail in Section 3.4 below), were used for motion capture during the activities and an additional eight for static calibration. Figure 0-4 below shows the positions of the lower limb markers. Other markers not seen in the image include a cluster of 4 markers at the sacrum attached with a belt used to track the motion of the pelvis. Also, upper body markers were only used for visualization purposes and were located around the head (3), at the shoulders, elbows and wrists (one marker on each side).

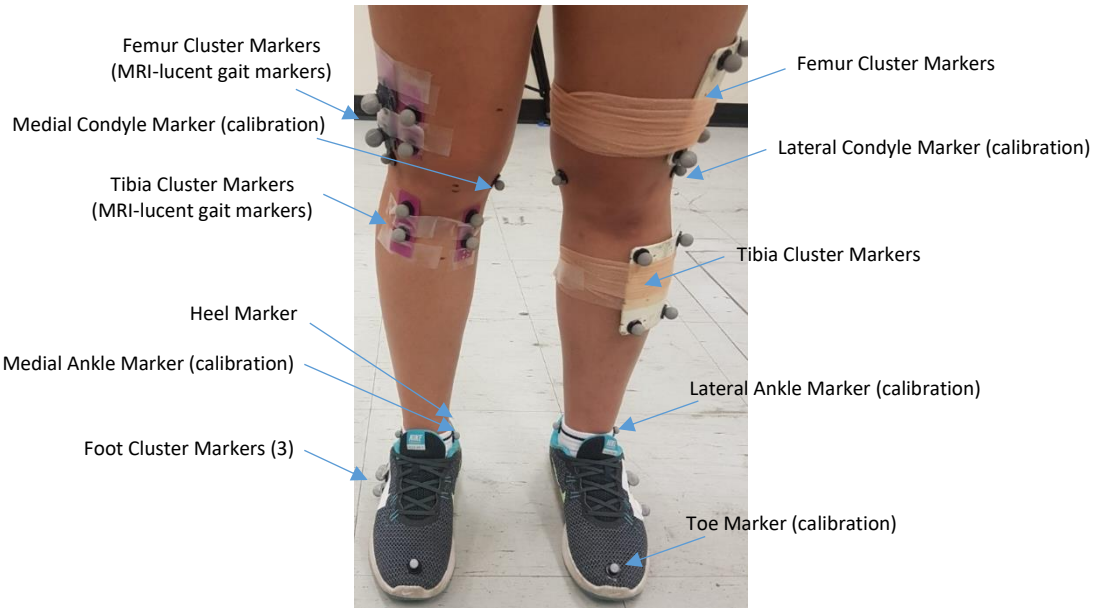

Figure 0-4: Labelled image of lower limb markers used for motion capture (although image shows lower limb markers, full-body marker set was used for visualization)

Once the markers were affixed to the individual, a static calibration was carried out where they were instructed to stand in a 'T-pose' position while a few frames of data were captured. The additional 8 calibration markers (palpated knee condyles, ankles and toes) were present only for this capture. With the static calibration pose, the relative positions of the markers were used to create the gait-based coordinate system. The static calibration markers were then removed in preparation for functional calibration.

Functional calibration was done in order to identify the hip joint center and knee joint center and flexion axis by assuming ball-socket and hinge joint motion, respectively. This approach was presented in O'Brien and Ehrig who showed that the knee flexion axis and hip joint center can be found with the stated assumptions, from taking a few frames of data where limb is swung back and forth about the hip and knee joints [122, 168]. The individual was instructed to carry out this back and forth motion while frames of data were captured. This protocol was repeated two to three times for the knee and hip joints for each limb to pick out the best trial where the participant was most steady and performing the motions the correct way. This was visually determined from the replay of the motion task.

After the functional calibration was carried out, the participant was instructed on how the motion tasks should be done. Each of the motion tasks was carried out several times, to get at least three good trials. For the walking task, the participant was instructed to walk in a natural way at a regular pace over a distance of approximately 3 meters. The walking speed of our participants ranged from 1.2 to 1.4 m/s. Any of the trials where the full foot did not land within the force plate were excluded and another trial was acquired. Instead of making the stair and chair tasks self-paced, these tasks were carried out over a 2-second period measured by a metronome (Sound Brenner Limited, Berlin, Germany) set at 60 beats per minute, hence the tasks were done over two beats. The focus of the stair tasks was the right foot climbing onto the step for ascent and the right foot leaving the step for descent. Bad trials were noted for cases where the wrong limb was used. For the chair tasks, participants were instructed to lift the right limb up for a few seconds just before rising from the chair and just after sitting back down. This was necessary for zeroing the force plates later in the data processing step. Bad trials were noted as trials where the limb was not lifted appropriately or where the foot was not properly placed on the force plate.

3.3 MRI-safe Loading Rig

The design of an MRI-safe loading rig was a secondary objective of this work. More details on the design process can be seen in Appendix A-2.

3.4 MRI-lucent markers

The design of an MRI-lucent gait marker was another secondary objective of this work. The details of the design can be seen in Appendix A-6.

3.5 Data Processing

Raw data collected from the MRI and gait systems was processed with different tools and methods in order to interpret the data. The sections below describe the methods and tools used to process qMRI, mechMRI and gait data. The novel methodology developed for integrating the data from the three metrics is also described in this section.

3.5.1 qMRI

T_2 relaxation time maps were generated from the modified DESS images (detailed in section 3.2.1.2). As previously mentioned, a signal ratio was calculated from the two echoes (images) acquired within a single repetition time [167] . The equation 3-2 below describes the relationship between the signal ratio and the MRI parameter [167]. The T_2 relaxation time for each pixel was determined using this analytical approach defined in the equation below. Custom software (Matlab, the mathworks, Natwick, MA) was used to carry out these calculations to generate the quantitative T_2 values for each voxel.

$$\frac{s_2}{s_1} = e^{-\frac{2(TR-TE)}{T_2}} \frac{1+e^{-\frac{TR}{T_1}}}{2} \quad \text{---------- (3-2)}$$

Where s_2 is the signal from the second echo and s_1 is the signal from the first echo, TR is repetition time, TE is echo time, T_1 is T_1 relaxation time and T_2 is T_2 relaxation time.

3.5.1.1 Cartilage Segmentation

Manual segmentation of the cartilage was carried out, slice-by-slice, on the generated quantitative T_2 relaxation time maps. This was done for ease of segmentation as the cartilage stands out clearly in these images. From the segmentations made with the Image Edit module of Analyze 12.0 (Analyze Direct Inc., Overland Park, KS, USA), binary masks were created which were then superimposed on the T_2 map. The segmentation of the cartilage was done following guidelines originally described by Monu et al [9]. These included ensuring a smooth crescent shape of the cartilage, avoiding partial-volume effects at the bone-cartilage boundary and excluding regions of high T_2 relaxation times which likely contain synovial fluid. These rules were followed to ensure consistent segmentations for all participants.

3.5.1.2 Projection Map Generation

The purpose of representing the quantitative values of T_2 relaxation time of the cartilage as a two-dimensional projection map was for better visualization. In our experience, clinicians generally prefer this to having to rotate a three-dimensional rendering. This method of qMRI data representation and corresponding custom software (Matlab, the mathworks, Natwick, MA)

was developed by Monu et al [9]. It involves extracting the bone-cartilage interface from each segmented slice and collapsing it into one sagittal plane. From this, a circle was created with center and radius to fit through the femoral condyles using a least-squares approach (see Figure 0-5). Bins of one-degree increments from the most anterior proximal point of the cartilage to 245 degrees, were then made. A qMRI value was assigned to each bin, if the bin had more than one voxel within it, the average of all voxels was assigned. The projection map was then created by plotting angular bins vs the slice number. This projection map protocol was carried out on the T_2 relaxation time data collected for this study.

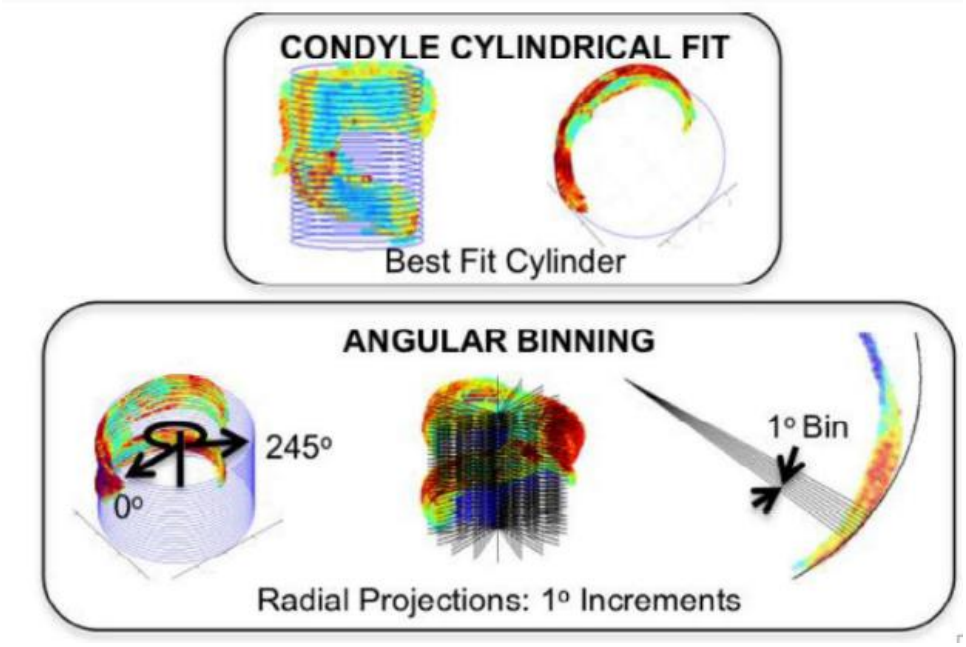

Figure 0-5: Condyle-Cylinder Radial Projection Illustration (courtesy of Dr. Uche Monu)

3.5.1.3 Difference Maps

Difference maps were created between the unloaded and loaded T_2 relaxation time scans. This was where the approach in the current study diverged from that of Monu et al. In the Monu et al study, the difference map was created between images from two different time points post-ACL injury to identify the changes in cartilage health over time. For this project, the same principle was applied but to study changes in cartilage properties with load. Thus, the difference map was created between the loaded and unloaded T_2 relaxation time maps, specifically loaded minus unloaded. Within this map both positive and negative differences emerged. The difference map was facilitated by an alternate registration step described below.

Projection Map Template – An Alternate Solution to Cartilage Registration:

The projection map allowed the data to be presented in a normalized manner and also facilitated comparison to different time-points and data acquisition conditions. It was an alternate form approach to a 3D rigid body registration. Since the projection map has a consistent number of slices for each participant and angular bins (245 degrees), this acted as a template to which all cartilage data for every trial was mapped. The data was also normalized across the slice direction. This can be observed by the fact that the cartilage reaches the edge of both sides of the projection map in the slice direction. In this study, we used this approach to carry out the comparison between the loaded and unloaded conditions. Any pixels in the projection map that were not present in both conditions were removed. By projecting onto the same slice-bin template and only taking data present in both images, direct pixel comparisons were possible.

3.5.1.4 Cluster Analysis

The cluster analysis approach was used to identify focal regions of change that might be missed in single slice analyses [9]. Figure 0-6 below shows the steps involved in creating the cluster maps for this analysis. First, the T_2 maps for the loaded and unloaded cartilage were created. Next, positive and negative difference maps were created implying increasing and decreasing T_2 from unloaded to loaded cases, respectively. From each of these maps, a cluster map was created which displays significant or focal regions of change, as well as the centroid of this cluster region. Focal regions of change or 'clusters', were defined by setting thresholds of intensity-difference and size. A cluster size of 12 mm^2 and intensity-difference of 5 ms, were used as the thresholds for this project. These numbers were initially acquired by Monu et al to be ±2 SDs from the mean intensity-difference from their study, with clusters defined as a set of contiguous pixels above or below the T_2 threshold [9]. It was determined that the same numbers will be appropriate for our study by carrying out a sensitivity analysis where we assessed how the clusters changed with varying pixel-difference area and fixed intensity-difference at the defined threshold and varying intensity-difference with a fixed pixel-difference area size at the defined threshold (see Appendix A-4). By visual inspection, the output maps were similar and therefore we used the same thresholds that had been used previously.

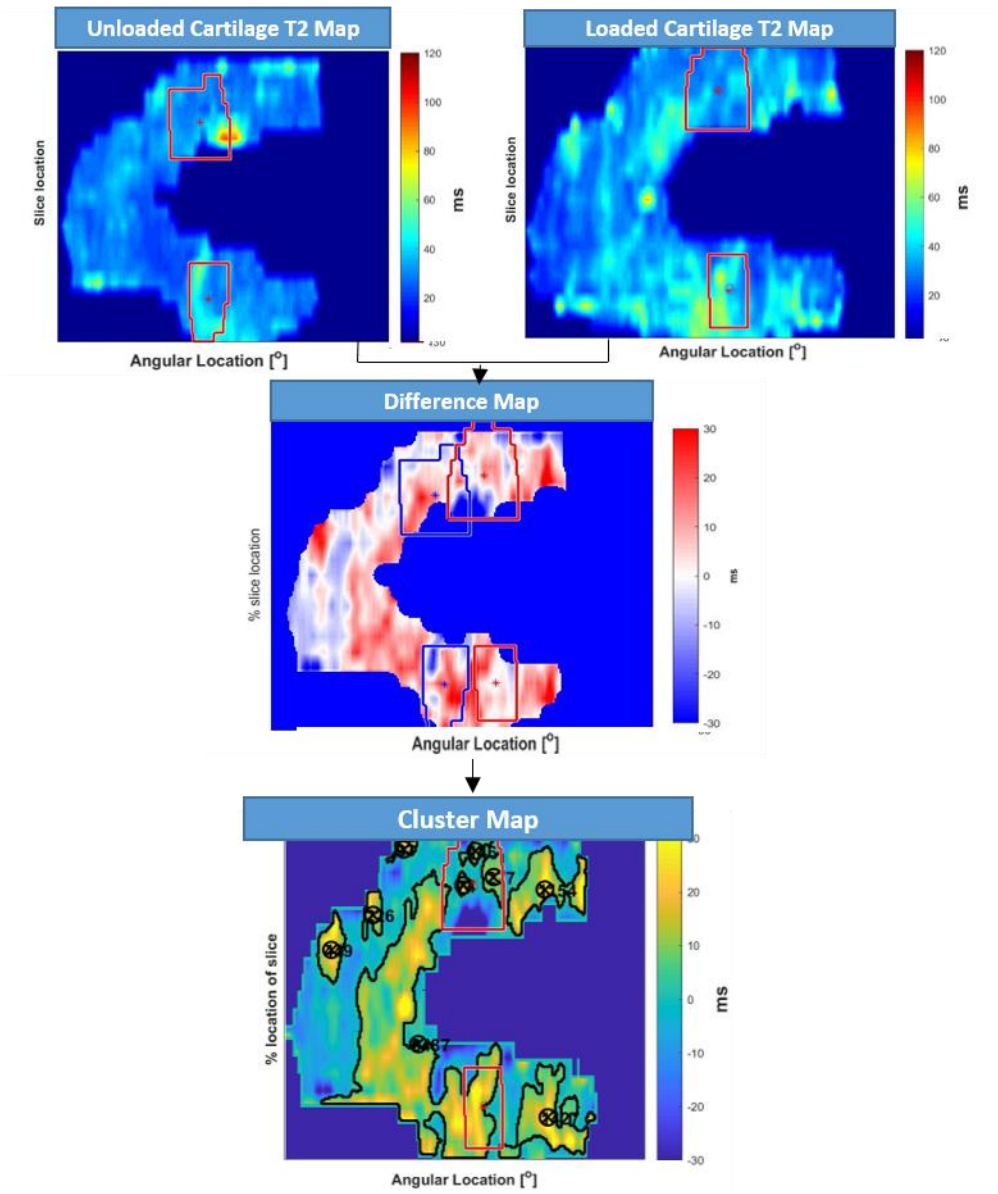

Figure 0-6: The cluster analysis map flowchart in this figure shows the output image at every stage used to develop the cluster map. The individual loaded and unloaded cluster maps are generated and then they are subtracted from each other which gives the difference maps. Finally, using pixel size and intensity thresholds, clusters and their centroids were defined on the map. The red outline shows the outer boundary of the loaded contact region and the blue outline in the difference map image represents the outer boundary of the unloaded contact region. These contact regions were always overlaid on the cartilage map outputs.

3.5.1.5 Regional Cartilage Demarcation

A regional analysis was carried out by dividing the projection map into medial, lateral and trochlear regions. This was done to be able to compare with the literature. The regions were divided by the midpoint in the slice direction and at 85 degrees in the bin direction (see Figure 0-7). The 85 degree bin was chosen from assessing all the maps created and finding that it falls approximately where the outer edge of the anterior medial cartilage turns into the trochlear as see

in Figure 0-7 below. The medial region T_2 relaxation time value was then defined as the mean of all the non-zero values within 85 to 245 degrees and 0 to half of the number of cartilage slices. The lateral region was defined as all non-zero values within 85 to 245 degrees and half to the total number of cartilage slices present.

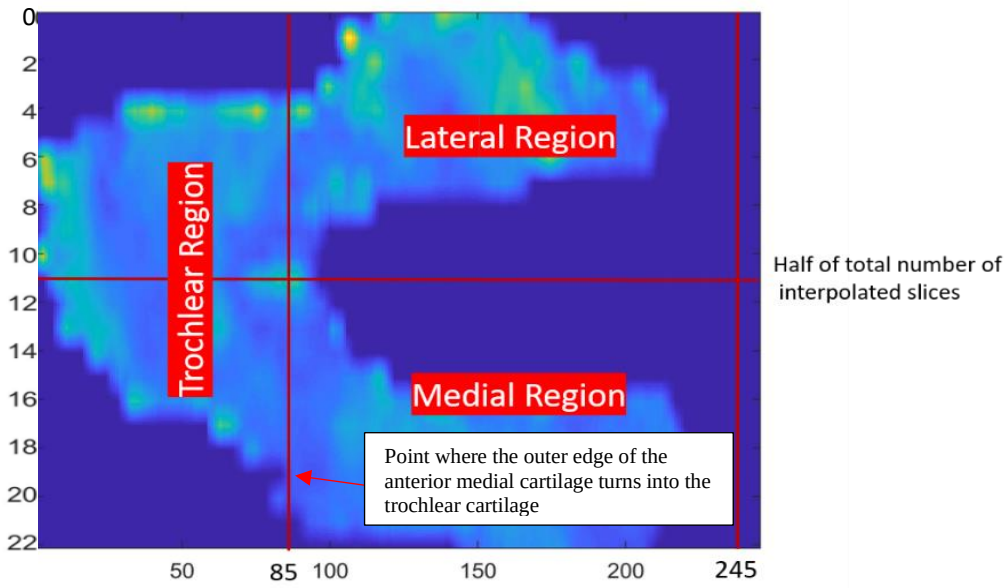

Figure 0-7: Regional cartilage demarcation for T_2 regional analysis

3.5.2 mechMRI

The mechMRI analysis for this study consisted of assessing the flexion angle of the knee, the tibiofemoral contact area and the translation of the contact area centroid at three knee positions. To do this, cartilage contact regions were segmented and centroid position determined, then the femurs were registered to determine the flexion angle. The femur was also segmented and together with the contact segmentation and centroid position, point clouds were generated for visualization. Details of these analyses are described in the sections below.

3.5.2.1 Femur Registration and Coordinate System Assignment

The femur registration of the high and low knee flexion position scans to the fully extended knee scan, was done to determine the flexion angle and to have all the femoral contact positions within the same femur coordinate system for point cloud visualization. The mechMRI scans of the femur in the knee flexed positions were each manually registered to the femur of the

high-resolution isotropic scan, with the Registration module of Analyze 12.0 (Analyze Direct Inc., Overland Park, KS, USA). With the alignment of the femurs after registration, a common femur long-axis was created by joining the femoral origin (described in Table 0-3 below) and the centroid on the most proximal slice of the femoral shaft which was visually determined. The tibial long axis for each of the flexed positions was also created, going from the knee origin to the centroid on the most distal slice of the tibial shaft which was also visually determined. The flexion angle for each of the knee positions was calculated as the angle between the femoral and tibial long axes lines.

3.5.2.2 Femur and Contact Segmentation

Segmentation was carried out in the fully extended femur, the tibiofemoral contact area in the extended position, as well as the contact area in the transformed (post-registered) flexed knee scans. All segmentation was carried out using the Image Edit module of Analyze 12.0 (Analyze Direct Inc., Overland Park, KS, USA). For the femur segmentation, the outline of the femur was traced for every slice of the fully extended knee scan. The contact area was identified in the medial and lateral compartments using a validated approach [169]. This process involves directly delineating tibiofemoral contact in a slice-by-slice manner and then applying slice-thickness multiplication. After segmenting the contact, the slice thickness multiplication to report the contact area was automatically generated by the ROI module of Analyze 12.0 (Analyze Direct Inc., Overland Park, KS, USA). From this module, the contact centroid coordinates for each of the medial and lateral compartments were acquired, as well as the boundary coordinates for both the femur outline and the medial and lateral contact areas of all the knee positions.

3.5.2.3 Contact Area and Centroid

Point cloud models of the femur and the contact areas were created for each knee position. Point-cloud images were generated from the boundary coordinates, with custom software (Matlab, the Mathworks, Natwick, MA). The centroids were superimposed on the contact areas and the translation of the centroid was calculated by finding the absolute distance between positions. This distance was calculated for the fully-extended to low flexion contact centroid, the fully-extended to high flexion contact centroid, and low flexion to high flexion contact centroid for the medial and lateral compartments.

3.5.3 Gait Analysis

The collected gait lab data were used to calculate knee kinematics and kinetics for the walk, stair, and chair tasks. Table 0-2 below details all the kinematic and kinetic outcome

measures used for these tasks from the kinematic and kinetic plots. These tasks were identified as important in the study of ACL-injured individuals as described in the background, section 2.6.1 above. To calculate the kinematics, the ZXY cardan sequence was used. For kinetics, standard 3D inverse dynamics was used.

Table 0-2: Summary table of all the outcome measures acquired from knee kinematic and kinetic plots

Kinematics	
Walk	Peak Flexion Angle
	Peak Extension Angle
	Peak Abduction Angle
	Peak Adduction Angle
Stair Rise	Peak Extension Angle
Stair Descent	Peak Flexion Angle
Kinetics	
Walk	Peak Flexion Moment
	Peak Extension Moment
	Peak Abduction Moment
	Peak Adduction Moment
Chair Rise	Peak Extension Moment
	Peak Adduction Moment
Chair Sit	Peak Flexion Moment
	Peak Abduction Moment
Stair Ascent	Peak Extension Moment
Stair Descent	Peak Flexion Moment

3.5.3.1 Kinematics

The positions of the gait markers with respect to the global coordinate system were used to create transforms from which the knee angles were derived for every frame of data. To create the knee coordinate system for each segment, the knee flexion axis and the hip and knee joint centers needed to be found. Using custom software (Matlab, the Mathworks, Natwick, MA) written by Dr. Lanovaz, the symmetrical axis of rotation approach (SARA) described in Ehrig et al's work [122] was used. In this approach, the knee flexion axis and hip and knee joint centers were found from applying single value decomposition (SVD) to the segment-to-marker-cluster transformation matrices. The segment-to-marker-cluster transformation matrices to which SVD was applied, were acquired from applying a routine described by Soderkvist et al, where the transform going from one coordinate system to the other, can be found when given the segment markers described in those two coordinate systems [170]. The advantage of the SARA approach

to determine hip and knee joint centers and flexion axis, is that it can be used to interpret ball or hinge joints, hence it could be used to find the parameters at the hip and the knee from the back and forth motions described in the section 3.2.2.1 [122]. The outcomes of SARA included flexion axis vectors and the joint center described with respect to the cluster coordinates of the closest distal and proximal segment (femur and tibia in our case). Although the joint center may not amount to exactly the same point, it is expected that the joint center described in the most important segment is chosen. In our case, we chose this as the joint center described in the femur coordinate system over the tibia coordinate system.

Table 0-3 below describes how the anatomical coordinate system was defined for each of the femur and tibia segments. As can be seen, a slight modification was applied to the knee joint center or origin found from the SARA approach. This modification involves projecting the mid-point of the palpated condyle markers onto the flexion axis vector line acquired from the SARA approach [171].

Table 0-3: Summary of how orthogonal vectors were described to define the femur and tibia anatomical coordinate system in the gait-based method. The second cross-product is required to create an orthogonal coordinate system.

Origin/Axis	Femur	Tibia
Flexion	Determined from back and forth motion (flexion/extension) of the knee and applying symmetrical axis of rotation approach	Determined from back and forth motion (flexion/extension) of the knee and applying symmetrical axis of rotation approach
Knee Origin	Mid-point projection of the line joining the medio-lateral palpated condyle markers onto the flexion axis vector	As for Femur
Long	Cross Product 1: Vector from the knee origin to the hip joint center and the flexion axis Cross Product 2: Cross Product 1 vector and the flexion axis vector	Cross Product 1: Vector from the mid-point of the line joining the palpated mediolateral ankle markers to the knee origin and the flexion axis vector Cross Product 2: Cross Product 1 vector and the flexion axis vector

Next, the marker cluster-to-functional coordinate system transforms were found for each segment. With this transform, all the cluster markers for each segment could be described with respect to the functional coordinate system. Again, the routine described by Soderkvist et al was used to find the transform to go from each of the functional coordinate systems to the global coordinate system as the cluster markers were already described in these two coordinate systems

[170]. The transforms of the femur and tibia functional coordinate system to the global coordinate system were then multiplied together to find the transform between the two coordinate systems (femur and tibia). Knee angles could then be identified from this final transformation matrix for each frame of data. This was done by applying the ZXY Cardan sequence to the rotational portion of the transformation matrix as described in the equation (3-3) below. By multiplying out this Cardan sequence, angles about the three rotational axes were found from the three equations. Custom software (Matlab, the Mathworks, Natwick, MA) code written by Dr. Reinshmidt was used to derive these angles as described [172].

Rotational portion of $T_{tiba\text{-}fema}$ =

$$\begin{bmatrix} cos\theta_3 & sin\theta_3 & 0 \\ -sin\theta_3 & cos\theta_3 & 0 \\ 0 & 0 & 1 \end{bmatrix} \begin{bmatrix} 1 & 0 & 0 \\ 0 & cos\theta_1 & sin\theta_1 \\ 0 & -sin\theta_1 & cos\theta_1 \end{bmatrix} \begin{bmatrix} cos\theta_2 & 0 & -sin\theta_2 \\ 0 & 1 & 0 \\ sin\theta_2 & 0 & cos\theta_2 \end{bmatrix} \text{ ---------- (3-3)}$$

Θ_3 = Rotation about the z-axis

Θ_1 = Rotation about the x-axis

Θ_2 = Rotation about the y-axis

Where $T_{tiba\text{-}fema}$ is the transformation matrix to go from tibia functional to femur functional coordinate system.

3.5.3.2 Kinetics

The kinetic measures at the knee were found by assuming a 3-D link-segment model with each segment connected by joints defined by a single point. Figure 0-8 below shows the forces and moments of the shank segment used to find the unknown moment at the knee from standard inverse dynamics. Equations 3-4 and 3-5 below show how this value was calculated. The segment mass (m), center of mass position and segment length were found using anthropometric data from De lava et al [173]. The acceleration value (a) was found from the second derivative of the marker position vectors at each frame after a fourth-order low-pass butterworth filter was applied (cut-off frequency – 300Hz). Distal force and moment values (F_d and M_d) were worked out from the force plate reading. It was assumed that the angular acceleration was zero considering the low speed at which the shank moves in each of the activities. With these assumptions, the moment at the knee which in this case was M_p was found for each frame of data. The moment value was then normalized by the mass of the participant.

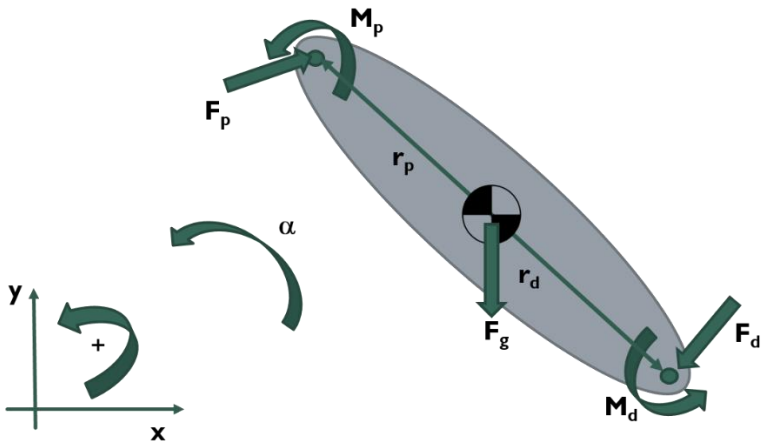

Figure 0-8: Shank segment free body diagram with forces and moments

$$\sum \vec{F} = m\vec{a} = \overrightarrow{F_d} + \overrightarrow{F_g} + \overrightarrow{F_p} \quad \text{---------- (3-4)}$$

$$\sum M = I\alpha = M_p + M_d + (r_p \, x \, F_p) + (r_d \, x \, F_d) \quad \text{---------- (3-5)}$$

where r_p is the proximal length from the center of mass position, r_d is the distal length from the center of mass position, m is mass of the segment (these inertial properties were acquired from De lava et al [173]), a is acceleration, I is the mass moment of inertia, α is the angular acceleration (these values both go to zero as explained above), F_g is the force of gravity, F_d and M_d are force and moment at the distal end of the segment respectively, F_p and M_p are force and moment at the proximal end of the segment respectively.

3.6 MRI-Gait Integration

The MRI-lucent gait marker clusters present on the femur and tibia segments of each trial facilitated data integration between the MRI and gait systems. In order to effectively do this, the markers needed to be described in both systems. In this section, the rationale for the selected method of determining the marker centroid in the MRI is explained. The method of processing dynamic data with MRI-based landmarks is also described.

3.6.1 Deciding on the Best Approach for Determining MRI-Marker Centroid Position

The ellipsoid center of the MRI-lucent marker was visually identified from the high-resolution isotropic MR image (Analyze 12.0, Analyze Direct, Overland Park, KS, USA). This approach was chosen, as opposed to segmenting the ellipsoid in all visible slices and having packaged software calculate the centroid (Analyze 12.0, Analyze Direct, Overland Park, KS, USA), because it was significantly quicker and provided similar results. In visually identifying the ellipsoid marker centroid, there were rules followed to maintain consistency. This involved

finding the mid slice in the frontal and sagittal planes and taking a point in the center, being guided by the axial plane view. Figure 0-9 below shows the outcome of an investigation that was done to compare these two methods. As can be seen, there was a slight difference in these positions (1.5 mm difference). The visually determined method was much quicker while the process of segmenting the markers in each slice (of an average of 200 slices) took significantly more time. For these reasons, the visual method of determining the ellipsoid centroid was chosen for this study.

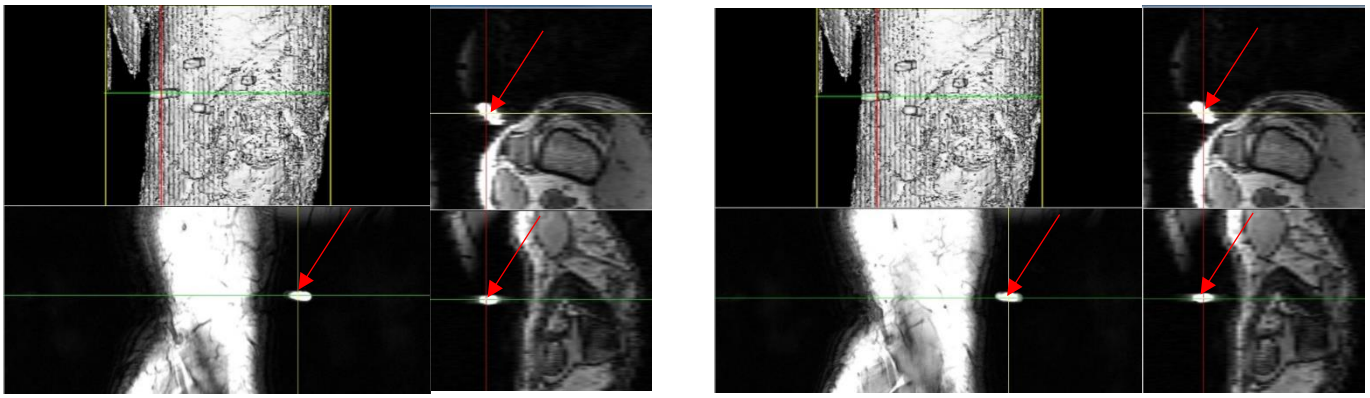

Figure 0-9: a) Left: MRI-marker centroid generated from segmentation (Analyze 12.0, Analyze Direct, Overland Park, KS, USA) – red arrows show the centroid positions in each of the planes – coordinates (36, 202, 114). b) Right: MRI-marker centroid that was visually-determined - red arrows show the centroid positions in each of the planes – coordinates (37, 204, 115)

Additional details on this process can be found in Appendix A-5.

3.6.2 Processing Dynamic Data with MRI-based Landmarks

Figure 0-10 below shows a flowchart of the steps followed in transforming the MRI-based anatomical landmarks from being expressed in the MRI-based coordinate system to the gait-based coordinate system, in order to process dynamic data. With all the MRI-based landmarks converted to the gait space, the same steps as described in sections 3.5.3.1 and 3.5.3.2 were used to create the anatomical landmarks of the femur and tibia, which were then used to process knee kinematic and kinetic data. Table 0-4 below summarizes the MRI-based landmarks used to define the femur and tibia anatomical coordinate systems. As can be seen in the table, the flexion axis from gait analysis (determined from SARA) was used in defining this MRI-based coordinate system. The flexion axis from gait analysis was chosen for MRI-based data processing so that only the long axes definition is different between the two coordinate system definitions. This way we can confirm the difference in outcomes between choosing anatomical

(femur shaft centroid - MRI-based) and mechanical (hip joint center - gait-based) long axes. All other points (femur origin, femur and tibia shaft centroid) described, were acquired from the MR image. This approach allowed kinematic and kinetic data to be described in both knee coordinate systems (one derived from gait measures and the other from MRI measures), with the purpose of determining the method that provides the most repeatable results.

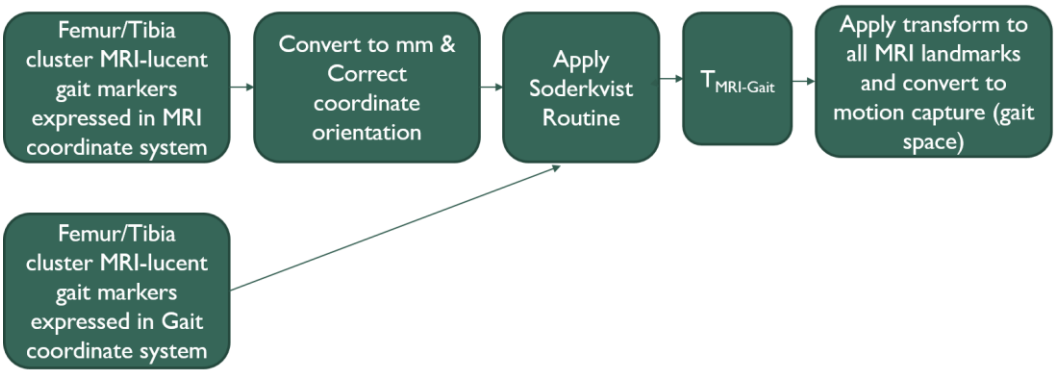

Figure 0-10: Flowchart showing process of transforming MRI-based landmarks to motion capture (gait) coordinate system. $T_{MRI-Gait}$ is the homogenous transformation matrix to go from MRI to gait coordinate system

Table 0-4: Summary of how orthogonal vectors were described to define the femur and tibia anatomical coordinate system in the MRI-based method

Origin/Axis	Femur	Tibia
Flexion	Determined from back and forth motion (flexion/extension) of the knee and applying symmetrical axis of rotation approach	Determined from back and forth motion (flexion/extension) of the knee and applying symmetrical axis of rotation approach
Knee Origin	MRI-based femur origin: Most proximal point in the intercondylar notch, defined in the sagittal plane. Knee Origin: Projection of MRI-based femur origin onto the flexion axis	As for Femur
Long	Cross Product 1: Vector going from the knee origin to the femur shaft centroid in the most proximal axial slice and the flexion axis Cross Product 2: Cross Product 1 vector and the flexion axis vector	Cross Product 1: Vector going from the tibia shaft centroid in the most distal axial slice, to the knee origin and the flexion axis vector Cross Product 2: Cross Product 1 vector and the flexion axis vector

3.7 Integration of qMRI T_2 and Contact Area

Visualizing the medial and lateral contact positions and their centroids on the projection and cluster maps is one of the integrative pipelines developed for this project. In order to do this, the tibiofemoral contact was segmented from the T_2 relaxation time images (i.e. the same images used to segment the cartilage). From the segmentation, contact binary masks were created, and the boundaries and their corresponding geometric and T_2-weighted centroids were mapped onto the 2D projection maps. The geometric centroids of the medial and lateral regions were found from the shape of the contact on the map while the T_2-weighted centroid was found using equation 3-6 below. The position of the geometric centroid was compared with that of the weighted centroid.

$$X_{w.c} = \frac{\sum x_i(\frac{1}{T_{2(xi,yi)}})}{\sum \frac{1}{x_i}}, Y_{w.c} = \frac{\sum y_i(\frac{1}{T_{2(xi,yi)}})}{\sum \frac{1}{y_i}} \quad \text{---------- (3-6)}$$

where $X_{w.c}$ and $Y_{w.c}$ are the x and y positions of the weighted centroid, x_i is the x position and y_i is the y position. $T_{2(x,yi)}$ is the T_2 value in the relevant x and y position.

The contact outer boundary was plotted onto the original projection map as well as on the cluster maps. With the contact region and centroid visualized on the maps, the link between contact area and changes in T_2 relaxation times with load, could be assessed visually. A cluster was said to be within a contact region if there was any overlap between any part of the clusters and the contact area.

The link between the location of the contact area, contact centroid, and T_2 relaxation time values was also explored quantitatively. Table 0-5 below summarizes the novel measures that were explored and how they were acquired. Each of these measures were assessed in the medial and lateral compartments in both loaded and unloaded conditions. Figure 0-11 below shows the definition of each of the regions used to calculate the measures.

Table 0-5: Description summary of novel T_2-contact quantitative measures assessed in this study

T_2-contact quantitative measure	Description Summary of measure
Regional-Contact Mean Difference	In either of the medial or lateral regions, the mean T_2 outside the contact region minus the mean T_2 inside the contact region.
Regional-Contact Standard Deviation (SD.) Difference	In either of the medial or lateral regions, the SD. of T_2 outside the contact region minus the SD. T_2 inside the contact region.
Regional-Contact Maximum Difference	In either of the medial or lateral regions, the maximum T_2 outside the contact region minus the maximum T_2 inside the contact region.
Regional-Contact Minimum Difference	In either of the medial or lateral regions, the minimum T_2 outside the contact region minus the minimum T_2 inside the contact region.
Contact-Centroid Mean Difference - geometric centroid	In either of the medial or lateral regions, the mean T_2 inside the contact area excluding that of the geometric contact centroid (8 adjacent pixels points around centroid point), minus the mean T_2 of the geometric contact centroid (8 adjacent pixels around centroid point).
Contact-Centroid Standard Deviation (SD.) – geometric contact centroid	In either of the medial or lateral regions, the SD. of T_2 inside the contact area excluding that of the geometric contact centroid (8 adjacent pixels points around centroid point), minus the SD. of T_2 of the geometric contact centroid (8 adjacent pixels around centroid point).
Contact-Centroid Mean Difference T_2-weighted centroid	In either of the medial or lateral regions, the mean T_2 inside the contact area excluding that of the T_2-weighted contact centroid (8 adjacent pixels points around centroid point), minus the mean T_2-weighted contact centroid (8 adjacent pixels around centroid point).
Contact-Centroid Standard Deviation (SD.) Difference - T_2-weighted centroid	In either of the medial or lateral regions, the SD. of T_2 inside the contact area excluding that of the T_2-weighted contact centroid (8 adjacent pixels points around centroid point), minus the SD. T_2-weighted contact centroid (8 adjacent pixels around centroid point).

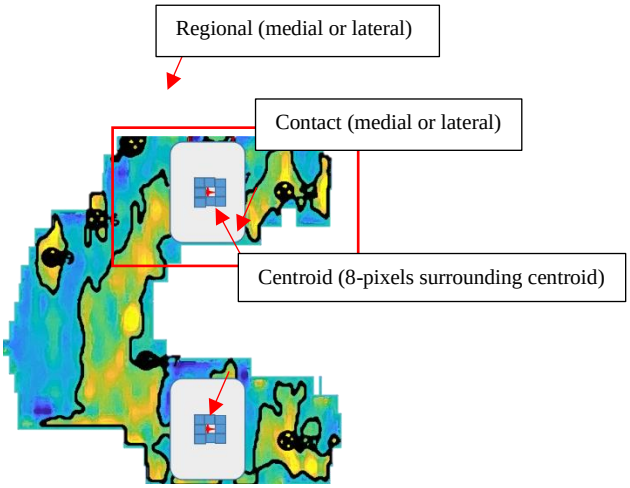

Figure 0-11: 2-D Cartilage map illustrating the regions used in defining the T_2-contact measures

3.8 Repeatability and Statistical Analysis

Table 0-6 below shows repeatability and agreement measures used in this thesis. The justifications for using these measures are described in the table. As can be seen, the measures acquired are SD_{rms} and CV_{rms} for repeatability and Bland-Altman analysis for showing agreement between the MRI-based and gait-based kinematic and kinetic outcomes.

Table 0-6: Details of all repeatability and statistical measures used in the analysis of all outcome measures

	SD_{rms}	**SD_{diff}**	**CV_{rms}**	**Confidence Interval**	**Bland-Altman Analysis**
Outcome Measures Applied to	Standard measures	Difference measures	Regional T_2 and Contact Area	All measures	Kinematic and kinetic measures
Justification	This is the primary measure of repeatability used in this study. · Chosen for reporting in units of measure it is applied to · Expresses how widely spread from mean the data is · The smaller the standard deviation, the more repeatable a measure is	Standard deviation calculation for difference measures as it squares negative values	Measure data dispersion from the mean · Used in addition to SD_{rms} to be able to compare repeatability to relevant literature	Used to calculate the minimum change required to obtain a statistical difference in future studies. Based on two-tailed z-score	Used to show agreement between two methods; here between results generated with the MRI-based and the gait-based knee coordinate systems.
Equation	$SD_{rms} = \sqrt{\sum_{j=1}^{m} \frac{S_{Dj}^2}{m}}$	$SD_{diff} = \sqrt{((SD_{rms1})^2} + \sqrt{(SD_{rms2})^2)}$	$\%Cv_{rms} = \frac{SD_{rms}}{\sum_{j=1}^{m} \left(\bar{x}_{j/m}\right)} \cdot 100$	80%: ±SD*1.28 95%: ±SD*1.96 99%: ±SD*2.58 (SD can be either SD_{rms} or SD_{diff})	X-axis: Mean value of the two methods for each trial Y-axis plot: Difference between the values of the two methods for each trial Upper and lower limits of agreement: ±2 SD from the mean difference between the values of the two methods
Equation Terms	SD: Standard standard-deviation j: Given subject i: Number of repeated measures m: Total number of subjects	SD_{rms1}, SD_{rms2}: Root-mean squared standard deviation for the first and second measures used to calculate the difference measure	SD_{rms}: Root mean square standard deviation x_j: Mean value per subject j: Given subject m: Total number of subjects	SD: Standard standard-deviation	n/a

Chapter 4
RESULTS

This section reports the key results from each of qMRI, mechMRI and gait measures. All raw data acquired are reported in tables as well as the repeatability and statistical outcomes. Sample figures are also included in this section, with reference to additional figures in the Appendix.

4.1 Patient Characteristics

Five healthy volunteers (two male, three female mean age 22.8 ± 2.5 years, mean height = 1.71 ± 0.1m, mean mass = 70.0 ± 12.3 kg, mean BMI = 23.8 ± 3.5 kg/m^2) (Table 0-1) participated in the repeatability study. The study was reviewed by the institutional ethics board and all participants gave informed consent (see Appendix G).

Table 0-1: Demographics of participants

Characteristics of Participants						
	Number	Age (years)	Sex	Height (m)	Weight (Kg)	BMI (kg/m^2)
Healthy Participants	5	22.8±2.5	3F, 2M	1.71±0.1	70.0±12.3	23.8±3.5

4.2 Quantitative MRI T_2 Repeatability for General, Medial, Lateral and Trochlear Regions at Loaded, Unloaded and Load-Unload Difference

The SD_{rms} tended to be higher in the medial compartment than in other regions (Table 0-2). The overall SD_{rms} and SD_{diff} values ranged from 2.4ms to 4.9ms. The smallest SD_{rms} occurred in the lateral loaded cartilage (2.4ms). The mean T_2 relaxation times for the global, medial, lateral and trochlear regions did not appear to change much with load. The overall mean difference values were positive for all regions (higher loaded value), except for in the medial region, but the differences were small ranging from -1 ms to 1.9 ms. Some individual cases did show negative differences (higher unloaded value) and this was relatively consistent within the individual. The largest positive difference between loaded and unloaded mean T_2 was in the trochlear region (1.9 ms) and the smallest in the global region (0.6 ms).

Except in the trochlear region, loaded cartilage had the smaller SD_{rms} value than loaded cartilage. The overall SD_{rms} T_2 values ranged from 2.8ms to 4.1ms for loaded cartilage and 2.8ms to 4.2ms for unloaded cartilage. Mean T_2 relaxation times ranged from 26.0ms to 27.7ms for loaded cartilage and 25.3ms to 27.5ms for unloaded cartilage. The lateral cartilage had the highest overall mean T_2 values and medial loaded, the lowest. Data was missing for unloaded

case of three trials for participant 1 and unloaded case of one trial for participant 2 due to an error running the MRI sequence during data collection. Cartilage T_2 relaxation time maps as well as data for each trial for each participant can be found in Appendix B.

Table 0-2: Mean and SD values of average regional qMRI T_2 values for general, medial, lateral and trochlear regions at loaded and unloaded positions and their difference. SD_{rms} was used for the loaded and unloaded measures while the SD_{diff} was used for the difference measures. The missing values for the unloaded case of three trials for participant 1 and one trial for participant 2 seen in this section is due to MRI sequence errors in the data collection of this data. Therefore, for the unloaded measures, are n = 4 instead of five. The negative values indicate a bigger T_2 in the smaller region (centroid region or contact) than in the larger region (contact, medial or lateral).

	Participant 1		Participant 2		Participant 3		Participant 4		Participant 5		Overall Values	
	Mean	SD	Mean	SD	Mean	SD	Mean	SD	Mean	SD	Overall Mean	SD_{rms} or SD_{diff}
	Global											
Loaded (ms)	25.8	2.1	24.3	0.6	30.8	0.7	23.5	1.8	30.2	2.8	26.9	2.8
Unloaded (ms)			26.9	6.5	26.8	0.8	25.8	4.0	27.1	0.8	26.7	3.5
Difference (ms)			-2.3	6.1	4.0	0.7	-2.4	5.4	3.0	2.4	0.6	3.0
	Medial											
Loaded (ms)	28.9	6.0	20.0	1.8	29.9	1.6	23.1	3.6	28.2	0.9	26.0	3.4
Unloaded (ms)			26.3	7.7	28.4	1.6	25.5	4.3	25.6	2.1	26.4	4.6
Difference (ms)			-5.9	5.2	1.5	1.3	-2.4	7.9	2.7	2.4	-1.0	4.9
	Lateral											
Loaded (ms)	24.2	2.1	25.4	2.4	34.0	1.6	25.6	3.4	29.5	2.3	27.7	2.4
Unloaded (ms)			28.8	4.6	27.2	0.9	27.2	3.8	27.0	1.8	27.5	3.2
Difference (ms)			-4.7	5.6	6.8	1.3	-1.6	7.3	2.5	2.4	0.8	4.8
	Trochlear											
Loaded (ms)	25.1	2.2	26.2	3.2	27.5	3.5	22.0	2.3	31.2	5.4	26.4	3.5
Unloaded (ms)			23.5	4.6	25.2	1.6	24.5	3.8	28.0	1.2	25.3	2.8
Difference (ms)			4.5	3.9	2.3	4.8	-2.4	3.7	3.2	5.3	1.9	4.0

The loaded cartilage CV% was lower than that of unloaded cartilage in all regions except in the trochlear region (Table 0-3). In the loaded scans, the CV% did not show the same pattern of regional lowest and highest as the unloaded scans. The highest CV% for loaded cartilage occured in the trochlear region (13.4%) and the lowest occurs in the global region (6.6%). In the unloaded cartilage, the lowest CV% occured in the lateral region (12%) and the highest CV% in the medial region (16.7%). The loaded CV% ranged from 6.6% - 13.4% while that of unloaded cartilage ranges from 11% - 16.7%.

Table 0-3: CV% values of loaded and unloaded cartilage means in the global, medial, lateral and trochlear regions

	Loaded CV%	Unloaded CV%
Global	6.6%	14.4%
Medial	12.1%	16.7%
Lateral	9.4%	12.0%
Trochlear	13.4%	11.0%

For all regions, the confidence interval values for the loaded cartilage were smaller than that of the corresponding unloaded cartilage (Table 0-4). The smallest confidence interval for the loaded cartilage was in the global region (±2.3ms) and for the unloaded cartilage was in the trochlear region (±3.6ms). The statistical confidence ranges were ±2.3ms to ±14.0ms for the global measure, ±4.3ms to ±18.8ms for the medial region, ±3.1ms to ±13.2ms for the lateral region and ±4.5ms to ±14.9ms for the trochlear region. The largest confidence interval was in the medial difference measure with ±7.3ms for 80% confidence, ±11.2ms for 95% confidence and ±18.8ms for 99% confidence.

Table 0-4: Based on our SD_{rms} values, the values in this table represent the minimum change that we expect to see in ACL-injured individuals for regional mean T_2 values that will be considered a clinical change and not just due to measurement error. We express these outcomes with 80%, 90% and 95% statistical confidence based on a two-tailed z-score

	Confidence Interval		
	80%	95%	99%
	Global		
Loaded (ms)	±2.3	±3.5	±5.9
Unloaded (ms)	±4.9	±7.5	±12.7
Difference (ms)	±5.4	±8.3	±14.0
	Medial		
Loaded (ms)	±4.3	±6.6	±11.1
Unloaded (ms)	±5.9	±9.0	±15.2
Difference (ms)	±7.3	±11.2	±18.8
	Lateral		
Loaded (ms)	±3.1	±4.8	±8.1
Unloaded (ms)	±4.1	±6.2	±10.5
Difference (ms)	±5.1	±7.9	±13.2
	Trochlear		
Loaded (ms)	±4.5	±6.9	±11.7
Unloaded (ms)	±3.6	±5.5	±9.2
Difference (ms)	±5.8	±8.8	±14.9

4.3 mechMRI Outcomes

The mechMRI outcomes including contact area and centroid at three different knee positions are reported in the sections below. For this study, the lower flexion angle was 21.5° on average (range: 17.4 – 26.2°) and the higher flexion angle was 35.0° on average (range: 28.2 –

37.2°); all flexion angles were relative to the full extension position for the particular individual which was set to zero.

4.3.1 Repeatability of Contact Centroid Translation

The SD_{rms} ranged from 2.6 – 4.4 mm for contact area centroid translation between the three knee flexion angles (Table 0-5). The low to high flexion range had the smallest SD_{rms} and the extended to low flexion range, had the largest SD_{rms}. Overall, the centroid translated between 8.1mm and 20.2mm. Comparing the translation of the centroid points between the medial and lateral sides, the lateral side translated more posteriorly than the medial in all flexion ranges. The translation from fully extended to the high flexion angle (one-to-three), had the most centroid translation in both medial and lateral sides. The centroid translated more from the fully extended to the lower flexion angle (one-to-two) than from the lower to the higher flexion angle (two-to-three) in both medial and lateral sides. See Appendix C for point cloud images of the contact area and centroid positions at each of the limb orientations as well as the three trial values for each participant.

Table 0-5: Mean and SD values of medial and lateral contact centroid translation (absolute distance) at three flexion angle ranges – one-to-two (fully extended to lower flexion angle), one-to-three (fully extended to higher flexion angle), two-to-three (lower to higher flexion angle)

	Participant 1		Participant 2		Participant 3		Participant 4		Participant 5		Overall Values	
	Mean	SD	Mean	SD	Mean	SD	Mean	SD	Mean	SD	Overall Mean	SD_{rms}
	Medial											
One-to-Two (Medial) – mm	14.5	5.9	6.8	5.9	11.3	2.5	12.1	3.0	9.1	3.7	10.8	4.4
One-to-Three (Medial) – mm	22.4	1.5	19.7	3.9	21.9	4.8	19.2	6.2	18.1	0.7	20.2	4.0
Two-to-Three (Medial) – mm	9.1	4.3	14.2	4.8	10.9	2.5	7.2	3.2	9.6	3.6	10.2	3.9
	Lateral											
One-to-Two (Lateral) – mm	10.0	1.6	7.3	5.8	7.9	2.1	7.9	2.8	7.3	1.7	8.1	3.1
One-to-Three (Lateral) – mm	12.5	1.6	14.3	2.8	16.0	2.6	12.1	4.3	12.2	0.8	13.4	2.7
Two-to-Three (Lateral) - mm	6.0	3.9	7.2	3.2	9.3	0.6	4.3	2.1	5.4	2.6	6.5	2.6

The lateral region confidence intervals were smaller than those of the medial region (Table 0-6). In the medial region, the two-to-three centroid translation had the smallest confidence interval (±4.8mm) and in the lateral region, the one-to-three centroid translation has the smallest for the lateral region (±3.4mm). The medial confidence interval values range from ±4.8mm to ±14.7mm and those of the lateral range from ±3.4mm to ±10.5mm. The highest confidence interval values occurred at medial one-to-two centroid translation with all other

values being less than ±5.7mm at 80% confidence, ±8.7mm at 95% confidence and ±14.7mm at 99% confidence.

Table 0-6: Based on our SD_{rms} values, the values in this table represent the minimum change that we expect to see in ACL-injured individuals for contact centroid translation values that will be considered a clinical change and not just due to measurement error. We express these outcomes with 80%, 90% and 95% statistical confidence based on a two-tailed z-score

	Confidence Interval		
	80%	95%	99%
	Medial		
One-to-Two (Medial) – mm	±5.7	±8.7	±14.7
One-to-Three (Medial) – mm	±5.1	±7.8	±13.2
Two-to-Three (Medial) – mm	±4.8	±7.3	±12.4
	Lateral		
One-to-Two (Lateral) – mm	±4.1	±6.2	±10.5
One-to-Three (Lateral) – mm	±3.4	±5.2	±8.8
Two-to-Three (Lateral) - mm	±3.5	±5.3	±9.0

4.3.2 Repeatability of Medial and Lateral Contact Area Values at Different Limb Positions

The repeatability, expressed as SD_{rms}, for the medial side had a range of 45.9 mm^2 – 49.6 mm^2 and for the lateral side a range of 41.8mm^2 – 105.9mm^2 (Table 0-7). The low flexion SD_{rms} for the lateral contact area had the overall largest value (105.9 mm^2) and the fully extended lateral contact area had the smallest (41.8 mm^2). The medial contact area had bigger SD_{rms} with increasing flexion angle. The overall mean of contact area ranged from 262.7 mm^2 to 513.3 mm^2 for all limb positions. The lateral contact area appeared to be bigger in all limb positions with low flexion lateral having the overall largest contact area. The contact area value for the medial side was smallest in the high flexion position and for the lateral, smallest in low flexion position. The difference between the contact area of the medial side between low flexion angle and high flexion angle positions, however, was not very different (0.2mm^2). See Appendix B-3 and B-4 for point cloud images of the contact area and centroid positions at each of the limb orientations as well as the three trial values for each participant.

Table 0-7: Mean, SD, SD_{rms} of medial and lateral contact area values at three limb positions – fully extended knee, low flexion angle, high flexion angle

	Participant 1		Participant 2		Participant 3		Participant 4		Participant 5			
	Mean (mm^2)	SD (mm^2)	Mean (mm^2)	SD (mm^2)	Mean (mm^2)	SD (mm^2)	Mean (mm^2)	SD (mm^2)	Mean (mm^2)	SD (mm^2)	Overall Mean (mm^2)	SD_{rms} (mm^2)
Fully Extended (°)	0.0	0.0	0.0	0.0	0.0	0.0	0.0	0.0	0.0	0.0	0.0	0.0
Medial Contact Area	413.7	69.8	420.8	19.9	278.8	5.9	430.8	30.3	392.2	24.5	387.2	41.8
Lateral Contact Area	460.8	98.8	342.6	7.0	212.5	8.8	202.8	21.6	195.8	14.9	282.9	45.9
Low Flexion (°)	**26.2**	**6.9**	**26.1**	**2.6**	**19.7**	**5.5**	**17.4**	**8.0**	**17.9**	**4.0**	**21.5**	**5.4**
Medial Contact Area	476.9	45.6	521.4	135.8	358.2	33.2	714.2	76.9	496.0	51.4	513.3	105.9
Lateral Contact Area	411.1	63.7	249.4	34.9	175.8	13.0	299.0	27.6	178.0	17.6	262.7	46.4
High Flexion (°)	**37.2**	**2.1**	**34.5**	**2.2**	**43.4**	**12.2**	**28.2**	**10.1**	**31.8**	**4.6**	**35.0**	**6.2**
Medial Contact Area	477.7	131.3	430.7	57.4	295.8	21.5	382.6	39.1	438.7	18.3	405.1	82.1
Lateral Contact Area	332.7	54.6	225.8	18.8	258.0	19.2	324.3	25.4	159.4	15.2	260.0	49.6

The CV% of the medial region contact area was lower than that of the lateral region except in the high flexion limb position (Table 0-8). The highest CV% for medial contact area occured in the high flexion limb position (19.6%) and the lowest occured in the fully extended limb position (11.1%). For the lateral contact area, the lowest CV% occured in the high flexion limb position (11.6%) and the highest CV% in the fully extended limb position (16.3%).

Table 0-8: CV% values of medial and lateral contact area at fully extended, low flexion and high flexion limb positions

	Medial CV%	Lateral CV%
Fully Extended	11.1%	16.3%
Low Flexion	15.1%	15.7%
High Flexion	19.6%	11.6%

For all limb positions, the confidence intervals for the lateral region contact area were smaller than that of the medial contact area except in the fully extended limb position (Table 0-9). For the 80% to 99% statistical confidence, intervals ranged from $\pm 55.2mm^2$ to $\pm 151.9mm^2$ for the fully extended knee, from $\pm 53.0mm^2$ to $\pm 256.6mm^2$ for the low flexion knee, and $\pm 38.8mm^2$ to $\pm 262.0mm^2$ for the high flexion knee. The largest confidence interval occurred at high flexion medial contact with all other values being less than $\pm 101.7mm^2$ at 80% confidence, $\pm 155.5\ mm^2$ at 95% confidence, and $\pm 262.0mm^2$ at 99% confidence.

Table 0-9: Based on our SD_{rms} values, the values in this table represent the minimum change that we expect to see in ACL-injured individuals for contact area values that will be considered a clinical change and not just due to measurement error. We express these outcomes with 80%, 90% and 95% statistical confidence based on a two-tailed z-score

	Confidence Interval		
	80%	95%	99%
	Fully Extended		
Medial Contact Area (mm2)	±55.2	±84.3	±142.1
Lateral Contact Area (mm2)	±59.0	±90.2	±151.9
	Low Flexion Angle		
Medial Contact Area (mm2)	±99.6	±152.3	±256.6
Lateral Contact Area (mm2)	±53.0	±81.0	±136.5
	High Flexion Angle		
Medial Contact Area (mm2)	±101.7	±155.5	±262.0
Lateral Contact Area (mm2)	±38.8	±59.3	±100.0

4.4 Kinematic and Kinetic Outcomes

The kinematic and kinetic results from MRI-based and gait-based processing methods are shown in the following sections. At the end of the section, comparisons between the two methods are shown in Bland-Altman plots for the different measures and SD_{rms}.

4.4.1 Repeatability of MRI-based Coordinate System Kinematics Outcomes

The SD_{rms} showed the smallest values to occured in in the walk peak adduction angle (1.4°) and the largest in the stair descent peak flexion angle (10.8°). The walking speed of our participants ranged from 1.2 to 1.4 m/s. The walk-related measures generally had smaller SD_{rms} values than the stair-related measures (Table 0-10). The overall mean values for each of the measures ranged from 2.8° to 77°. The largest values occurred in the stair ascent and descent peak extension and flexion angle measures (52.7° and 77.0° respectively). The lowest occurred in the peak adduction angle measure (2.8°). See Appendix D for the three trial values for each of the participants.

Table 0-10: MRI-based mean and SD values per participant and overall mean and SD_{rms} values per measure of peak frontal and sagittal knee angles for walking and stair tasks. The table reports the absolute values of these measures.

	Participant 1		Participant 2		Participant 3		Participant 4		Participant 5		Overall Values	
	Mean	SD	Mean	SD	Mean	SD	Mean	SD	Mean	SD	Overall Mean	SD_{rms}
Walk - Peak Flexion Angle (degrees)	25.3	3.5	20.7	1.1	15.7	1.5	7.2	6.7	4.3	1.1	14.7	3.5
Walk - Peak Extension Angle (degrees)	7.4	3.7	4.4	2.8	2.5	2.2	3.5	1.2	10.2	1.4	5.6	2.4
Walk - Peak Abduction Angle (degrees)	7.3	2.8	14.0	0.6	9.2	4.1	4.5	5.6	2.9	3.3	7.6	3.7
Walk - Peak Adduction Angle (degrees)	3.3	2.5	4.0	1.1	2.9	1.2	1.7	0.9	2.0	1.5	2.8	1.5
Stair Up - Peak Extension Angle (degrees)	51.4	7.8	52.8	6.2	54.3	3.9	45.5	9.3	59.2	7.1	52.7	7.1
Stair Down - Peak Flexion Angle (degrees)	71.2	7.8	77.8	1.8	76.9	3.7	72.3	10.4	87.0	11.7	77.0	8.0

For all the walk kinematic measures, the confidence intervals were smaller than those of the stair kinematic measures (Table 0-11). The smallest confidence interval for walk activity kinematics occurred in the walk peak extension angle measure (±2.0 degrees) and for the stair activity occurred in the stair ascent peak extension angle (±9.1 degrees). The statistical confidence ranged from ±2.0 degrees to ±12.1 degrees walk activity and from ±9.1 degrees to ±26.5 degrees for stair activities. The largest confidence intervals were for stair descent peak flexion angle, with ±10.3 degrees at 80% confidence, ±15.7 degrees at 95% confidence and ±26.5 degrees at 99% confidence.

Table 0-11: Based on our SD_{rms} values, the values in this table represent the minimum change that we expect to see in ACL-injured individuals for MRI-based kinematic values that will be considered a clinical change and not just due to measurement error. We express these outcomes with 80%, 90% and 95% statistical confidence based on a two-tailed z-score

	Confidence Interval		
	80%	**95%**	**99%**
Walk - Peak Extension Angle (degrees)	±3.1	±4.8	±8.1
Walk - Peak Extension Angle (degrees)	±2.0	±4.0	±5.6
Walk - Peak Abduction Angle (degrees)	±4.7	±7.2	±12.1
Walk - Peak Adduction Angle (degrees)	±2.0	±3.0	±5.1
Stair Up - Peak Extension Angle (degrees)	±9.1	±13.9	±23.4
Stair Down - Peak Flexion Angle (degrees)	±10.3	±15.7	±26.5

4.4.2 Repeatability of MRI-based Coordinate System Kinetics

The SD_{rms} showed the smallest value to occur in the walk peak flexion moment measure (0.04N.m/kg) and the largest to occur in the stair descent peak extension moment (0.26N.m/kg) (Table 0-12). The walk sagittal moment measures generally had smaller SD_{rms} values than all other measures. The overall mean values for all of the measures ranged from 0.07N.m/kg to 0.86N.m/kg. The largest values occurred in the walk peak adduction moment and stair descent peak flexion moment measures (0.81N.m/kg and 0.80N.m/kg respectively). The smallest occurred in the walk peak flexion moment measure (0.07N.m/kg). See Appendix D for the three trial values for each of the participants.

Table 0-12: MRI-based mean and SD values per participant and overall mean and SD_{rms} values per measure of peak frontal and sagittal knee moments for walking, chair, and stair tasks. The table reports the absolute values of these measures.

	Participant 1		Participant 2		Participant 3		Participant 4		Participant 5		Overall Values	
	Mean	SD	Mean	SD	Mean	SD	Mean	SD	Mean	SD	Overall Mean	SD_{rms}
Walk - Peak Flexion Moment (N.m/kg)	0.15	0.02	0.03	0.01	0.07	0.01	0.02	0.01	0.09	0.08	0.07	0.04
Walk - Peak Extension Moment (N.m/kg)	0.27	0.02	0.24	0.01	0.32	0.08	0.23	0.04	0.13	0.02	0.24	0.05
Walk - Peak Abduction Moment (N.m/kg)	0.46	0.01	0.31	0.24	0.42	0.15	0.84	0.18	0.51	0.03	0.51	0.21
Walk - Peak Adduction Moment (N.m/kg)	0.75	0.05	0.62	0.23	1.03	0.36	0.99	0.19	0.92	0.09	0.86	0.21
Chair Rise - Peak Extension Moment (N.m/kg)	0.43	0.01	0.73	0.09	0.64	0.10	0.82	0.24	0.53	0.04	0.63	0.13
Chair Rise - Peak Adduction Moment (N.m/kg)	0.19	0.07	0.24	0.06	0.40	0.14	0.76	0.16	0.26	0.08	0.37	0.20
Chair Down - Peak Flexion Moment (N.m/kg)	0.36	0.03	0.49	0.07	0.63	0.20	0.61	0.18	0.36	0.11	0.49	0.13
Chair Down - Peak Abduction Moment (N.m/kg)	0.28	0.17	0.13	0.05	0.47	0.10	0.59	0.07	0.18	0.05	0.33	0.15
Stair Up - Peak Extension Moment (N.m/kg)	0.34	0.08	0.37	0.21	1.19	0.22	1.27	0.29	0.44	0.10	0.72	0.26
Stair Down - Peak Flexion Moment (N.m/kg)	0.75	0.39	1.09	0.12	1.37	0.15	0.64	0.26	0.19	0.05	0.81	0.25

The confidence intervals for the walk sagittal kinetic measures were smaller than those of other activities (Table 0-13). The smallest confidence interval occurred for the walk activity kinetics in the walk peak flexion moment measure (±0.1 N.m/kg), for the chair activity in the frontal moment measures (±0.5 N.m/kg), and for the stair activity in the stair ascent peak extension moment (±1.1 N.m/kg). The 80% to 99% statistical confidence intervals were ±0.1 N.m/kg to ±2.9 N.m/kg for the walk activities, ±0.5 N.m/kg to ±2.1 N.m/kg for chair activity, and ±1.1 N.m/kg to ±3.3 N.m/kg for stair activity. The stair descent peak flexion moment had the largest confidence intervals with ±1.2 N.m/kg at 80% confidence, ±1.8 N.m/kg at 95% confidence and ±3.0 N.m/kg at 99% confidence.

Table 0-13: Based on our SD_{rms} values, the values in this table represent the minimum change that we expect to see in ACL-injured individuals for gait-based kinetic values that will be considered a clinical change and not just due to measurement error. We express these outcomes with 80%, 90% and 95% statistical confidence based on a two-tailed z-score

	Confidence Interval		
	80%	95%	99%
Walk - Peak Flexion Moment (N.m/kg)	±0.1	±0.2	±0.3
Walk - Peak Extension Moment (N.m/kg)	±0.3	±0.5	±0.8
Walk - Peak Abduction Moment (N.m/kg)	±0.7	±1.1	±1.8
Walk - Peak Adduction Moment (N.m/kg)	±1.1	±1.7	±2.9
Chair Rise - Peak Extension Moment (N.m/kg)	±0.8	±1.3	±2.1
Chair Rise - Peak Adduction Moment (N.m/kg)	±0.5	±0.8	±1.4
Chair Down - Peak Flexion Moment (N.m/kg)	±0.6	±1.0	±1.7
Chair Down - Peak Abduction Moment (N.m/kg)	±0.5	±0.7	±1.2
Stair Up - Peak Extension Moment (N.m/kg)	±1.1	±1.6	±2.8
Stair Down - Peak Flexion Moment (N.m/kg)	±1.2	±1.8	±3.0

4.4.3 Repeatability of Gait-based Coordinate System Kinematics

The smallest SD_{rms} was for the walk peak adduction angle measure (0.7°) and the largest was for the stair ascent peak extension angle measure (6.4°) (Table 0-14). The walk-related measures generally had a smaller SD_{rms} than the stair-related measures. The overall mean values for each of the measures ranged from 1.7° to 77.6°. The biggest values occurred in the stair ascent and descent peak extension and flexion angle measures (56.0° and 77.6° respectively). The lowest occurred in the peak adduction angle measure (1.7°). See Appendix D for the three trial values for each of the participants.

Table 0-14: Gait-based mean and SD values per participant and overall mean and SD_{rms} values per measure of peak frontal and sagittal knee angles for walking and stair tasks. The table reports the absolute values of these measures.

	Participant 1		Participant 2		Participant 3		Participant 4		Participant 5		Overall Values	
	Mean	SD	Mean	SD	Mean	SD	Mean	SD	Mean	SD	Overall Mean	SD_{rms}
Walk - Peak Flexion Angle (degrees)	22.7	1.2	17.1	1.5	17.8	1.2	7.4	7.5	13.0	1.3	15.6	3.5
Walk - Peak Extension Angle (degrees)	4.3	0.9	3.3	1.5	1.6	1.2	2.1	0.9	0.5	0.2	2.4	1.0
Walk - Peak Abduction Angle (degrees)	3.2	3.6	1.4	0.8	0.2	0.1	2.4	2.3	3.1	3.6	2.1	2.5
Walk - Peak Adduction Angle (degrees)	2.8	1.2	2.6	0.8	1.3	0.3	0.5	0.4	1.5	0.5	1.7	0.7
Stair Up - Peak Extension Angle (degrees)	47.9	11.6	56.2	7.4	56.7	2.6	53.4	1.7	66.0	1.9	56.0	6.4
Stair Down - Peak Flexion Angle (degrees)	67.8	11.2	72.3	3.4	78.4	4.1	77.5	2.3	92.2	4.8	77.6	6.0

The walk kinematics confidence intervals were smaller than those of the stair kinematics (Table 0-15). The smallest confidence interval for walk activity kinematics occurred in the walk peak adduction angle measure (0.9 degrees) and for the stair activity, stair descent peak flexion angle (±7.8 degrees). The statistical confidence ranges were ±0.9 degrees to ±11.7 degrees for walk activities, and ±7.8 degrees to ±21.0 degrees for stair activities. The largest confidence interval was for stair ascent peak extension angle, being ±8.2 degrees at 80% confidence, ±12.5 degrees at 95% confidence and ±21.0 degrees at 99% confidence.

Table 0-15: Based on our SD_{rms} values, the values in this table represent the minimum change that we expect to see in ACL-injured individuals for gait-based kinematic values that will be considered a clinical change and not just due to measurement error. We express these outcomes with 80%, 90% and 95% statistical confidence based on a two-tailed z-score

	Statistical Confidence		
	80%	95%	99%
Walk - Peak Flexion Angle (degrees)	4.5	6.9	11.7
Walk - Peak Extension Angle (degrees)	1.3	2.0	3.4
Walk - Peak Abduction Angle (degrees)	3.2	4.9	8.3
Walk - Peak Adduction Angle (degrees)	0.9	1.4	2.4
Stair Up - Peak Extension Angle (degrees)	8.2	12.5	21.0
Stair Down - Peak Flexion Angle (degrees)	7.8	11.8	20.0

4.4.4 Repeatability of Gait-based Coordinate System Kinetics

SD_{rms} showed the smallest value to occur in the walk peak abduction moment and chair sit peak flexion moment measures (both 0.05N.m/kg). The largest SD_{rms} was seen to occur in the chair ascent peak adduction moment (0.18N.m/kg) (Table 0-16). The overall mean values for each of the measures ranged from 0.11N.m/kg to 0.67N.m/kg. The biggest values occurred in the stair ascent peak extension moment and stair descent peak flexion moment measures (0.67N.m/kg and 0.62N.m/kg respectively). The lowest occurred in the walk peak abduction moment measure (0.04N.m/kg). See Appendix D for the three trial values for each of the participants.

Table 0-16: Gait-based mean and SD values per participant and overall mean and SD_{rms} values per measure of peak frontal and sagittal knee moments for walking, chair and stair tasks. The table reports the absolute values of these measures.

	Participant 1		Participant 2		Participant 3		Participant 4		Participant 5		Overall Values	
	Mean	SD	Mean	SD	Mean	SD	Mean	SD	Mean	SD	Overall Mean	SD_{rms}
Walk - Peak Flexion Moment (N.m/kg)	0.23	0.05	0.14	0.08	0.04	0.00	0.02	0.01	0.15	0.06	0.11	0.07
Walk - Peak Extension Moment (N.m/kg)	0.30	0.09	0.26	0.03	0.17	0.04	0.18	0.04	0.27	0.05	0.24	0.07
Walk - Peak Abduction Moment (N.m/kg)	0.17	0.02	0.17	0.01	0.15	0.07	0.24	0.04	0.14	0.03	0.18	0.05
Walk - Peak Adduction Moment (N.m/kg)	0.32	0.02	0.43	0.06	0.48	0.14	0.30	0.03	0.26	0.07	0.36	0.08
Chair Rise - Peak Extension Moment (N.m/kg)	0.14	0.05	0.24	0.01	0.17	0.12	0.12	0.02	0.09	0.00	0.15	0.06
Chair Rise - Peak Adduction Moment (N.m/kg)	0.42	0.07	0.65	0.05	0.57	0.21	0.96	0.11	0.39	0.03	0.60	0.18
Chair Down - Peak Flexion Moment (N.m/kg)	0.13	0.05	0.14	0.03	0.25	0.04	0.11	0.02	0.12	0.05	0.20	0.05
Chair Down - Peak Abduction Moment (N.m/kg)	0.43	0.10	0.39	0.05	0.60	0.06	0.75	0.15	0.26	0.06	0.48	0.14
Stair Up - Peak Extension Moment (N.m/kg)	0.32	0.14	0.39	0.26	1.10	0.20	1.23	0.13	0.33	0.10	0.67	0.16
Stair Down - Peak Flexion Moment (N.m/kg)	0.76	0.13	0.77	0.19	0.66	0.09	0.43	0.03	0.49	0.03	0.62	0.11

The walk sagittal kinetic measures had the smallest confidence intervals (Table 0-17). The smallest confidence intervals were for chair sit peak abduction moment and stair descent peak flexion moment (±0.1 N.m/kg for both). The statistical confidence ranged from ±0.1 N.m/kg to ±0.6 N.m/kg for walk activity, ±0.2 N.m/kg to ±0.6 N.m/kg for chair activity, and ±0.3 N.m/kg to ±0.7 N.m/kg for stair activity. The largest confidence intervals were for stair ascent peak extension moment; they were found to be ±0.3 N.m/kg at 80% confidence, ±0.4 N.m/kg at 95% confidence and ±0.7 N.m/kg at 99% confidence.

Table 0-17: Based on our SD_{rms} values, the values in this table represent the minimum change that we expect to see in ACL-injured individuals for gait-based kinetic values that will be considered a clinical change and not just due to measurement error. We express these outcomes with 80%, 90% and 95% statistical confidence based on a two-tailed z-score

	Statistical Confidence		
	80%	95%	99%
Walk - Peak Flexion Moment (N.m/kg)	±0.1	±0.1	±0.2
Walk - Peak Extension Moment (N.m/kg)	±0.1	±0.1	±0.2
Walk - Peak Abduction Moment (N.m/kg)	±0.1	±0.1	±0.1
Walk - Peak Adduction Moment (N.m/kg)	±0.1	±0.2	±0.3
Chair Rise - Peak Extension Moment (N.m/kg)	±0.1	±0.1	±0.2
Chair Rise - Peak Adduction Moment (N.m/kg)	±0.2	±0.3	±0.5
Chair Down - Peak Flexion Moment (N.m/kg)	±0.2	±0.4	±0.6
Chair Down - Peak Abduction Moment (N.m/kg)	±0.1	±0.2	±0.4
Stair Up - Peak Extension Moment (N.m/kg)	±0.3	±0.4	±0.7
Stair Down - Peak Flexion Moment (N.m/kg)	±0.1	±0.2	±0.4

4.5 MRI-based and Gait-based Outcomes Comparison

SD_{rms} for the MRI-based and gait-based coordinate system were most similar in the walk peak flexion angle measure (MRI: 3.6° and gait: 4.1°) (Figure 0-1). They differed the most in the stair ascent peak extension angle measure (MRI: 9.7° and gait: 7.2°) and the stair descent peak flexion angle (MRI: 10.8° and gait: 7.6°). In the walk peak abduction and adduction angle measures, the difference between the two measures was 1.1° and 0.6°, respectively. In all but the walk peak flexion angle measure, the gait-based outcome measures had a better repeatability than the MRI-based outcome measures.

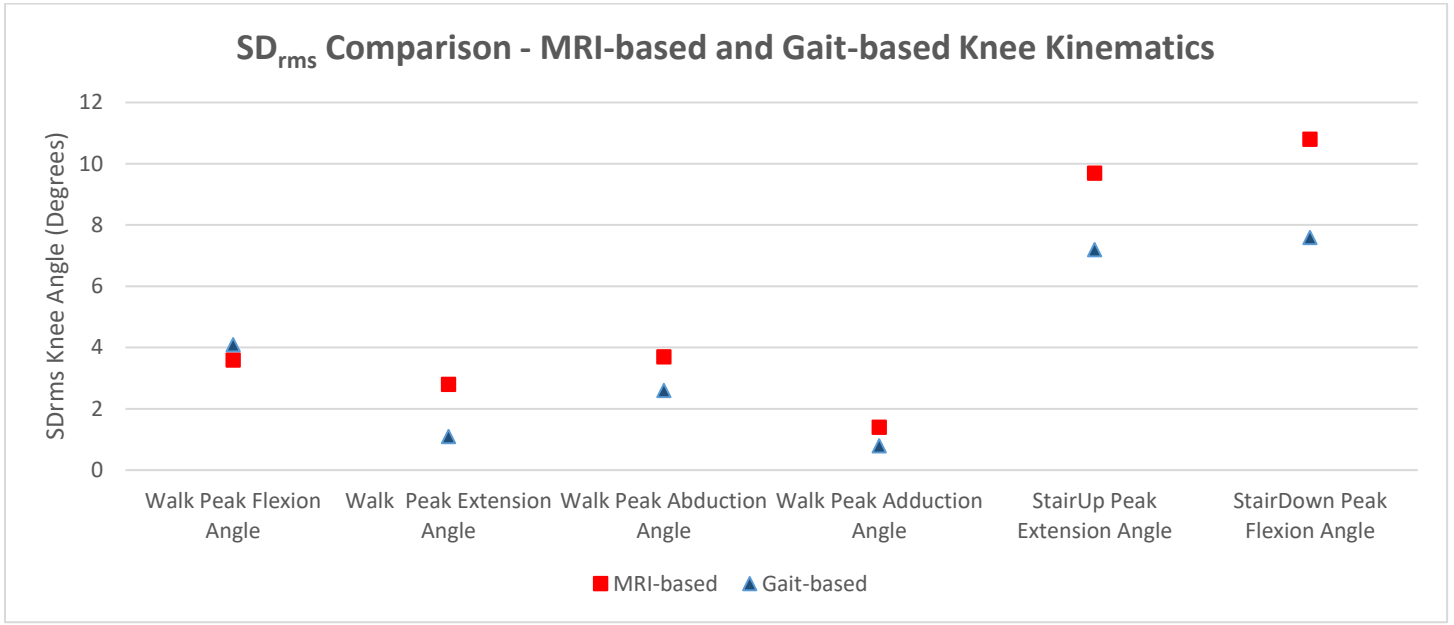

Figure 0-1: SD_{rms} plot for all kinematic measures for MRI-based and gait-based values.

The MRI-based and gait-based SD_{rms} for the kinetic measures were seen to be most similar in the walk sagittal moments (difference: 0.02N.m/kg – 0.03N.m/kg) and the chair frontal moments (difference: 0.01N.m/kg – 0.02N.m/kg) (Figure 0-2). The repeatability values of the two methods differed the most in walk frontal moments (difference: 0.13N.m/kg – 0.16N.m/kg) and stair descent peak flexion moment (difference: 0.14N.m/kg). The gait-based outcome measures had lower SD_{rms} in seven out of ten of the measures including the walk sagittal moment measures and the stair ascent peak extension moment measure. In the seven measures where gait-based SD_{rms} was lower, the difference between the SD_{rms} of the two methods ranged from 0.07N.m/kg to 0.16N.m/kg. In the other three measures where MRI-based was lower, the difference ranged from 0.02N.m/kg to 0.06N.m/kg. The difference in SD_{rms} between the two methods was as low as 0.01N.m/kg and 0.02N.m/kg in the chair frontal moments.

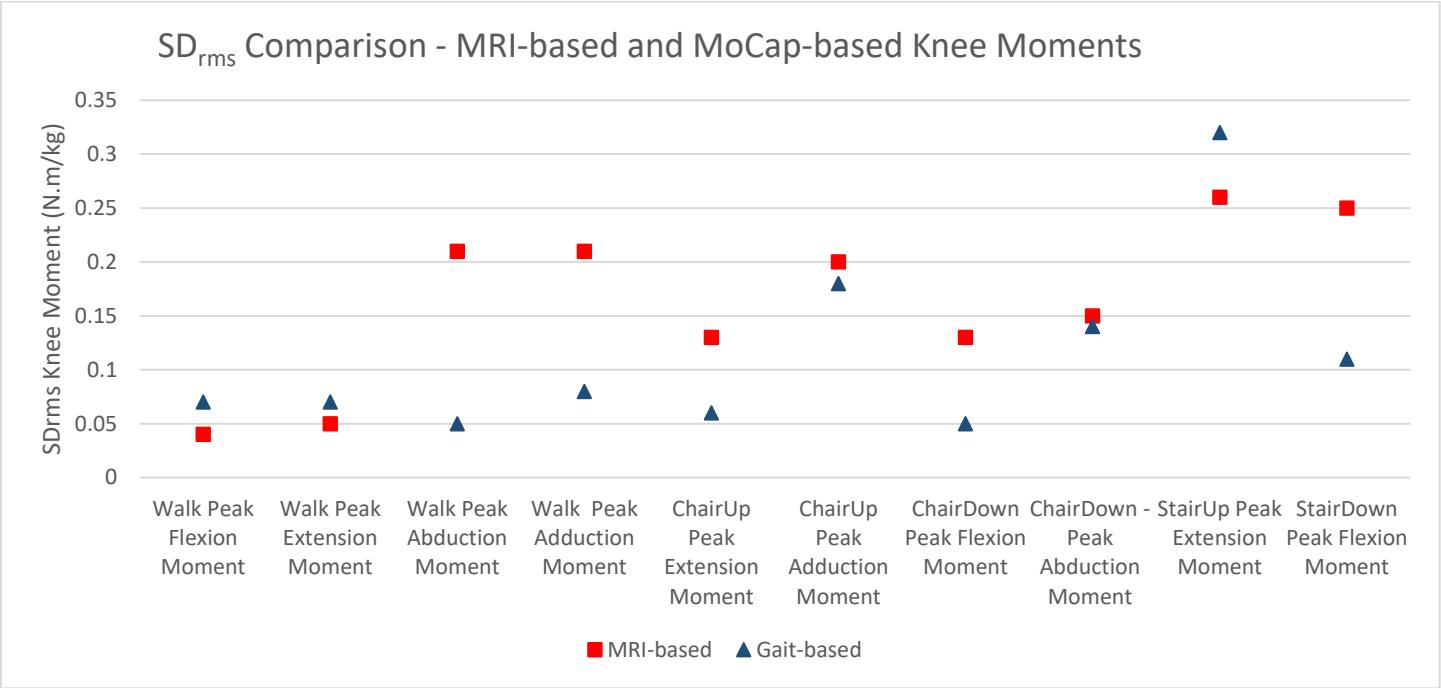

Figure 0-2: SD_{rms} plot for all kinetic measures for MRI-based and gait-based values.

The Bland-Altman analysis outcomes for kinematic measures showed only the stair ascent peak extension angle measure to have more than one mean difference point outside of the limits of agreement (Table 0-18). The upper limit of agreement ranges from 3° to 17.4° and the lower limit of agreement to range from -19.1° to -1°. The limit of agreement range values ranged from 4.0° to 31.4° and the overall mean difference values ranges from -1° to 5.5°. Walk peak extension and abduction angle Bland-Altman plots had a slight skew to the right. Bland-Altman plots for all measures can be seen in Appendix E.

Table 0-18: Bland Altman limit of agreement values, range and number of points outside of range for all kinematic measures

	Upper Limit of Agreement	Lower Limit of Agreement	Limit of Agreement Range	Overall Mean Difference (Bias)	Number of Points Outside the Limits
Walk - Peak Flexion Angle (degrees)	9.0	-11.0	20.0	-1.0	1
Walk - Peak Extension Angle (degrees)	11.3	-4.8	16.1	3.4	1
Walk - Peak Abduction Angle (degrees)	17.4	-6.4	23.8	5.5	1
Walk - Peak Adduction Angle (degrees)	3.0	-1.0	4.0	1.0	1
Stair Up - Peak Extension Angle (degrees)	12.3	-19.1	31.4	-3.4	2
Stair Down - Peak Flexion Angle (degrees)	11.8	-13.1	25.0	-0.6	1

The outcomes of the Bland-Altman analysis for kinetic measures showed only the walk peak flexion moment and walk peak abduction moment measures to have more than one mean difference point outside the limits of agreement (Table 0-19). The upper limit of agreement ranged from 0.10N.m/kg to 1.05N.m/kg. The lower limit of agreement ranged from -0.83N.m/kg to 0.14N.m/kg. The limit of agreement range values ranged from 0.32N.m/kg to 1.88N.m/kg and the overall mean difference values ranged from -3.4N.m/kg to 5.5N.m/kg. Walk peak abduction and abduction moment Bland-Altman plots had a slight skew to the right. Bland-Altman plots for all measures can be seen in the Appendix E.

Table 0-19: Bland-Altman limit of agreement values, range and number of points outside of range for all kinetic measures

	Upper Limit of Agreement	Lower Limit of Agreement	Limit of Agreement Range	Overall Mean Difference (Bias)	Number of Points Outside the Limits
Walk - Peak Flexion Moment (N.m/kg)	0.13	-0.19	0.32	-0.02	2
Walk - Peak Extension Moment (N.m/kg)	0.22	-0.22	0.44	0.001	0
Walk - Peak Abduction Moment (N.m/kg)	0.72	-0.05	0.77	0.33	2
Walk - Peak Adduction Moment (N.m/kg)	0.99	0.02	0.97	0.56	0
Chair Rise - Peak Extension Moment (N.m/kg)	0.82	0.14	0.68	0.5	0
Chair Rise - Peak Adduction Moment (N.m/kg)	0.42	-0.76	1.18	-0.17	0
Chair Down - Peak Flexion Moment (N.m/kg)	0.83	-0.25	1.08	0.29	0
Chair Down - Peak Abduction Moment (N.m/kg)	0.1	-0.41	0.51	-0.15	1
Stair Up - Peak Extension Moment (N.m/kg)	0.64	-0.43	1.07	0.11	0
Stair Down – Peak Flexion Moment (N.m/kg)	1.05	-0.86	1.88	0.11	0

4.6 Repeatability of qMRI-Contact Integration

In this section, results from novel qMRI-contact integration measures are reported for the medial and lateral compartments. All of the measures are difference measures where the negative values indicate a higher T_2 in the larger region; specifically, inside the contact region relative to outside the contact region for measures where contact is the smaller region (i.e. regional-contact area) and higher T_2 outside the centroid region relative to inside the centroid region where contact is the bigger region (contact-area centroid). The missing values for the unloaded case of three trials for participant 1 and one trial for participant 2 seen in this section are due to MRI sequence errors in the data collection of this data.

4.6.1 qMRI-Contact Integration Outcomes – Medial Compartment

The SD_{diff} of the qMRI-contact integration outcomes for the medial compartment was generally smaller in unloaded than loaded cartilage (Table 0-20).The SD_{diff} in the loaded case ranged from 0.7 ms to 25.6 ms and the unloaded case ranged from 0.5 ms to 20.6 ms. The

repeatability of the qMRI-contact integration outcomes for the loaded and unloaded cases follow almost the same patterns of smallest to largest with regional-contact maximum difference being the largest SD_{diff} and regional-contact minimum difference being the lowest SD_{diff}. Although regional-contact minimum difference had the smallest SD_{diff}, the overall mean of the difference measure is also small in these measures (loaded: -0.7ms and unloaded: -0.3ms).

The biggest overall mean value (absolute difference), occurred in the contact-centroid SD difference (9.5ms and 10.1ms in loaded and unloaded, respectively) and were both negative values (meaning that the T_2 is larger in the area around the centroid). This measure was 3.5ms in the loaded and 2.4ms in the unloaded compartment. The overall mean for loaded and unloaded medial mean difference measures (regional-contact mean difference, contact-centroid mean geometric difference, contact-centroid mean T_2-weighted difference (denoted with II in table)), ranged from -3.3ms to 2.1ms. For the maximum and minimum difference (regional-contact maximum difference, regional-contact minimum difference) the overall mean values ranged from -0.7 to 0.6ms. For the standard deviation difference values (regional-contact standard deviation difference, contact-centroid standard deviation difference, contact-centroid standard deviation difference II), the overall mean values ranged from -10.1ms to 0.7ms. See Appendix F for the three trial values for each of the participants.

Table 0-20: Means and SDs per participant and overall mean and SD_{rms} of qMRI T_2-contact integration outcomes for loaded and unloaded cases in the medial compartment. Contact-centroid mean difference and SD difference without II represents the geometric-weighted centroid measures while with II indicates the T_2-weighted centroid measures. Negative values indicate a higher T_2 in the larger region; specifically, inside the contact region relative to outside the contact region for measures where contact is the smaller region (i.e. Regional-Contact Area) and higher T_2 outside the centroid region relative to inside the centroid region where contact is the bigger region (Contact Area-Centroid)

	Participant 1		Participant 2		Participant 3		Participant 4		Participant 5		Overall Values	
	Mean	SD	Mean	SD	Mean	SD	Mean	SD	Mean	SD	Overall Mean	SD_{diff}
	Medial Loaded											
Regional-Contact Mean Diff. (ms)	-6.5	8.3	4.0	6.9	-1.6	2.2	-5.2	1.9	-2.6	2.7	-2.4	7.2
Regional-Contact SD Diff. (ms)	0.4	2.6	2.2	2.0	2.5	2.3	0.5	1.5	-2.8	5.7	0.5	4.6
Regional-Contact Max Diff. (ms)	2.7	17.6	16.4	11.3	7.1	15.7	-3.5	24.9	-19.7	13.3	0.6	25.6
Regional-Contact Min Diff. (ms)	-1.6	0.6	-0.2	0.2	-0.9	1.2	-0.2	0.2	-0.4	0.5	-0.7	0.7
Contact-Centroid Mean Diff. (ms)	-4.4	8.4	-11.5	7.2	4.6	2.8	5.6	1.4	-1.3	3.1	-1.4	11.7
Contact-Centroid SD Diff (ms)	-9.6	3.5	-5.6	2.9	-7.7	0.4	-10.0	1.9	-14.6	6.0	-9.5	7.6
Contact-Centroid Mean Diff. II (ms)	-0.4	5.7	-9.4	3.5	2.8	3.7	-1.1	8.8	12.9	16.2	1.0	11.1
Contact-Centroid SD Diff II (ms)	-10.0	3.2	-8.2	4.4	-9.1	1.6	-9.3	1.7	-10.1	5.4	-9.3	7.6
	Medial Unloaded											
Regional-Contact Mean Diff. (ms)			18.1	11.6	-5.8	2.9	-0.9	6.1	-3.2	3.2	2.1	5.2
Regional-Contact SD Diff. (ms)			8.9	6.6	-2.3	1.6	0.8	4.2	-4.7	2.1	0.7	4.5
Regional-Contact Max Diff. (ms)			48.5	10.5	-30.8	2.4	1.3	18.8	-20.7	17.1	-0.4	20.6
Regional-Contact Min Diff. (ms)			0.1	0.2	-1.0	1.2	-0.1	0.2	-0.1	0.2	-0.3	0.5
Contact-Centroid Mean Diff. (ms)			-5.9	1.3	-3.2	1.0	6.8	10.5	0.8	7.5	-0.4	6.8
Contact-Centroid SD Diff (ms)			-3.4	1.3	-11.8	2.3	-11.2	3.6	-14.2	2.0	-10.1	5.1
Contact-Centroid Mean Diff. II (ms)			9.4	6.7	-1.5	2.3	-15.2	11.6	-5.7	1.0	-3.3	8.2
Contact-Centroid SD Diff II (ms)			-5.7	2.1	-11.2	1.7	-9.9	2.9	-12.7	3.3	-9.9	5.1

For both loaded and unloaded cases, the regional-contact minimum measure had the smallest confidence intervals (Table 0-21); the value of these were ±0.8ms and ±0.7ms, respectively. The statistical confidence intervals ranged from ±6.7ms to ±30.1ms for the mean difference measures, ±5.7ms to ±19.6ms for SD difference measures, ±26.3ms to ±66ms for maximum difference measures, and ±0.7ms to ±1.7ms for minimum difference measures. The largest confidence intervals were for loaded contact-centroid mean difference, with values of ±32.7ms at 80% confidence, ±50.1ms at 95% confidence and ±66ms at 99% confidence.

Table 0-21: Based on our SD_{rms} values, the values in this table represent the minimum change that we expect to see in ACL-injured individuals for medial loaded and unloaded T_2-contact integration values that will be considered a clinical change and not just due to measurement error. We express these outcomes with 80%, 90% and 95% statistical confidence based on a two-tailed z-score

	Confidence Interval		
	80%	95%	99%
	Medial Loaded		
Regional-Contact Mean Diff. (ms)	±9.2	±14.0	±18.5
Regional-Contact SD Diff. (ms)	±5.8	±8.9	±11.8
Regional-Contact Max Diff. (ms)	±32.7	±50.1	±66.0
Regional-Contact Min Diff. (ms)	±0.8	±1.3	±1.7
Contact-Centroid Mean Diff. (ms)	±14.9	±22.9	±30.1
Contact-Centroid SD (ms)	±9.7	±14.9	±19.6
Contact-Centroid Mean Diff. II (ms)	±14.2	±21.8	±28.6
Contact-Centroid SD II (ms)	±9.7	±14.8	±19.5
	Medial Unloaded		
Regional-Contact Mean Diff. (ms)	±6.7	±10.2	±13.4
Regional-Contact SD Diff. (ms)	±5.7	±8.8	±11.5
Regional-Contact Max Diff. (ms)	±26.3	±40.3	±53.1
Regional-Contact Min Diff. (ms)	±0.7	±1.1	±1.4
Contact-Centroid Mean Diff. (ms)	±8.8	±13.4	±17.7
Contact-Centroid SD (ms)	±6.5	±10.0	±13.2
Contact-Centroid Mean Diff. II (ms)	±10.5	±16.1	±21.1
Contact-Centroid SD II (ms)	±6.5	±9.9	±13.0

4.6.2 qMRI-Contact Integration Outcomes – Lateral Compartment

Unlike the medial compartment qMRI-contact integration measures, the loaded repeatability were smaller than the unloaded (Table 0-22). The lateral repeatability values were generally smaller than the medial repeatability except in the regional-contact min difference measure. The SD_{diff} values ranged from 3.0ms to 12.9ms in loaded cartilage and 2.6ms to 20.8ms in unloaded cartilage. The repeatability of the loaded qMRI-contact integration outcomes followed almost the same patterns of smallest to largest as the unloaded with regional-contact maximum difference being the largest SD_{diff} and regional-contact minimum difference being the smallest.

The overall mean values for loaded and unloaded lateral mean difference measures (regional-contact mean difference, contact-centroid mean difference, contact-centroid mean difference II) ranged from -6.9ms to 2.2ms. For the maximum and minimum difference (regional-contact maximum difference, regional-contact minimum difference), overall means ranged from -3.4 to 20.8ms. For the standard deviation difference values (regional-contact standard deviation difference, contact-centroid standard deviation difference, contact-centroid standard deviation difference II), overall means ranged from -9.1ms to 6.2ms. See Appendix F for the three trial values for each of the participants.

Table 0-22: Means and SDs per participant and overall mean and SD_{rms} of qMRI T_2-contact integration outcomes for loaded and unloaded cases in the lateral compartment. Contact-centroid mean difference and SD difference without II represents the geometric-weighted centroid measures while with II indicates the T_2-weighted centroid measures. Negative values indicate a higher T_2 in the larger region; specifically, inside the contact region relative to outside the contact region for measures where contact is the smaller region (i.e. Regional-Contact Area) and higher T_2 outside the centroid region relative to inside the centroid region where contact is the bigger region (Contact Area-Centroid)

	Participant 1		Participant 2		Participant 3		Participant 4		Participant 5		Overall Values	
	Mean	SD	Mean	SD	Mean	SD	Mean	SD	Mean	SD	Overall Mean	SD_{diff}
	Lateral Loaded											
Regional-Contact Mean Diff. (ms)	-4.3	4.6	0.4	4.6	-9.0	6.0	-1.5	4.0	-1.8	1.8	-3.2	5.2
Regional-Contact SD Diff. (ms)	1.7	2.7	3.3	1.9	5.8	2.7	9.3	4.5	2.9	2.0	4.6	3.0
Regional-Contact Max Diff. (ms)	13.1	10.1	23.6	8.6	9.3	14.1	38.9	17.6	14.8	13.0	19.9	12.9
Regional-Contact Min Diff. (ms)	-4.4	4.3	-1.2	1.6	-13.9	2.5	-0.8	1.0	-0.8	1.0	-4.2	2.4
Contact-Centroid Mean Diff. (ms)	-5.8	3.1	-0.9	3.0	-10.4	5.1	3.3	7.6	-1.5	6.5	-3.0	8.8
Contact-Centroid SD Diff (ms)	-7.9	0.9	-6.8	2.1	-7.9	2.2	-7.7	0.8	-12.1	2.1	-8.5	4.0
Contact-Centroid Mean Diff. II (ms)	-0.9	8.5	-3.1	2.2	-3.9	2.8	-0.6	9.9	-8.6	10.7	-3.4	9.1
Contact-Centroid SD Diff II (ms)	-6.8	2.7	-5.9	0.8	-8.3	2.1	-6.5	1.4	-11.6	0.9	-7.8	3.8
	Lateral Unloaded											
Regional-Contact Mean Diff. (ms)			-9.4	2.7	-7.5	4.6	-11.3	1.8	0.8	4.9	-6.9	5.6
Regional-Contact SD Diff. (ms)			2.6	2.2	4.8	2.8	2.4	1.0	4.8	3.8	3.7	3.7
Regional-Contact Max Diff. (ms)			25.8	14.5	11.3	18.9	2.9	1.8	43.6	14.2	20.8	20.8
Regional-Contact Min Diff. (ms)			-0.7	0.6	-11.1	5.7	-1.5	0.9	-0.2	0.1	-3.4	2.6
Contact-Centroid Mean Diff. (ms)			6.9	4.2	-1.8	1.9	-2.4	8.5	6.1	7.1	2.2	10.5
Contact-Centroid SD (ms)			-9.9	0.4	-6.0	2.2	-10.6	4.4	-9.9	3.3	-9.1	6.0
Contact-Centroid Mean Diff. II (ms)			4.3	3.8	-3.6	5.4	-9.6	6.9	-4.4	4.6	-3.3	9.7
Contact-Centroid SD II (ms)			-7.9	1.7	-6.3	2.3	-9.6	4.5	-8.8	2.9	-8.1	6.2

For both loaded and unloaded cases, the regional-contact minimum measure had the smallest confidence interval measure (Table 0-23); the value of these were ±3.1ms and ±3.3ms, respectively. The statistical confidence ranged from ±6.6ms to ±23.5ms for the mean difference measure, ±3.8ms to ±10.3ms for SD difference, ±16.5ms to ±53.5ms for maximum difference and ±3.1ms to ±6.7ms for minimum difference. The largest confidence interval was for loaded contact-centroid mean difference with values of ±26.6ms at 80% confidence, ±40.7ms at 95% confidence and ±53.5ms at 99% confidence.

Table 0-23: Based on our SD_{rms} values, the values in this table represent the minimum change that we expect to see in ACL-injured individuals for lateral loaded and unloaded T_2-contact integration values that will be considered a clinical change not just due to measurement error. We express these outcomes with 80%, 90% and 95% statistical confidence based on a two-tailed z-score

	Confidence Interval		
	80%	95%	99%
	Lateral Loaded		
Regional-Contact Mean Diff. (ms)	±6.6	±10.2	±13.4
Regional-Contact SD Diff. (ms)	±3.8	±5.8	±7.7
Regional-Contact Max Diff. (ms)	±16.5	±25.3	±33.2
Regional-Contact Min Diff. (ms)	±3.1	±4.8	±6.3
Contact-Centroid Mean Diff. (ms)	±11.3	±17.3	±22.8
Contact-Centroid SD (ms)	±5.1	±7.8	±10.3
Contact-Centroid Mean Diff. II (ms)	±11.7	±17.9	±23.5
Contact-Centroid SD II (ms)	±4.9	±7.4	±9.8
	Lateral Unloaded		
Regional-Contact Mean Diff. (ms)	±7.2	±11.0	±14.5
Regional-Contact SD Diff. (ms)	±4.7	±7.2	±9.5
Regional-Contact Max Diff. (ms)	±26.6	±40.7	±53.5
Regional-Contact Min Diff. (ms)	±3.3	±5.1	±6.7
Contact-Centroid Mean Diff. (ms)	±13.4	±20.5	±27.0
Contact-Centroid SD (ms)	±7.7	±11.8	±15.5
Contact-Centroid Mean Diff. II (ms)	±12.4	±19.0	±25.0
Contact-Centroid SD II (ms)	±7.9	±12.2	±16.0

4.6.3 Repeatability of Load-Unload qMRI T_2-contact Integration Outcomes – Cluster Maps

The SD_{rms} indicate the T_2-increase cluster maps were more repeatable, particularly on the lateral side (0.0 – 0.3 # of clusters). The measure with the highest SD_{rms} was the number of clusters in and around the loaded contact on the medial side (0.9) (Table 0-24). The medial side had overall mean number of clusters ranging from 1.3 – 1.4 and in the lateral side the overall mean clusters range from 0.3 to 0.8. The number of clusters within and around the contact in loaded cartilage is generally higher (0.8 to 1.4) than that found within and around the unloaded cartilage (0.25 – 1.4).

Table 0-24: Mean and SD per participant and overall mean and SD_{rms} values of the number of T_2-increase (unload to load) and T_2-decrease (unload to load) cluster regions present within the contact area under loaded and unloaded cartilage. M - Medial side, L - Lateral side. The decimal values are from finding the mean of an integer number of clusters from each trial.

	Participant 1		Participant 2		Participant 3		Participant 4		Participant 5		Overall Values	
	Mean	SD	Mean	SD	Mean	SD	Mean	SD	Mean	SD	Overall Mean	SD_{rms}
	Unloaded Contact											
T_2-increase (from unloaded to loaded)			0.5M, 1.0L	0.7M, 0.0L	1.3M, 0.0L	0.6M, 0.0L	2.0M, 0.0L	1.0M, 0.0L	1.3M, 0L	0.6M, 0.0L	1.3M, 0.25L	0.2M, 0L
T_2-decrease (from unloaded to loaded)			1.5M, 0.5L	0.7M, 0.7L	1.3M, 0.5L	0.6M, 0.6L	1.0M, 1.3L	0.0M, 0.6L	1.7M, 0.3L	0.6M, 0.6L	1.4M, 0.7L	0.3M, 0.1L
	Loaded Contact											
T_2-increase (from unloaded to loaded)			0.5M, 0.5L	0.7M, 0.7L	2.7M, 1.0L	0.6M, 1.0L	0.6M, 1.2L	0.6M, 1.2L	1.7M, 0.3L	0.6M, 0.6L	1.4M, 0.8L	0.3M, 0.3L
T_2-decrease (from unloaded to loaded)			1.5M, 0.5L	0.7M, 0.7L	2.0M, 1.3L	0M, 0.6L	0.0M, 0.6L	0.0M, 0.6L	2M, 0.7L	1M, 0.6L	1.4M, 0.8L	0.5M, 0.1L

To provide some context, an illustrative example of how the number of clusters in and around the cluster region was determined is shown for one participant (Figure 0-3). From this figure, it can be seen that the cluster areas and their centroids were close to and around the contact area centroids (T_2-weighted and geometric) and within and around the edges of the contact regions. In the case of the T_2-increase maps at the top (Figure 22 a and b), there were two cluster centroids within and around the fully extended contact and three cluster centroids within and around the flexed contact region on the medial side and none on the lateral. For the T_2-decrease maps at the bottom (Figure 22 c and d), there was one cluster centroid within and around the fully-extended contact on both sides and two each in and around the flexed contact area on both sides.

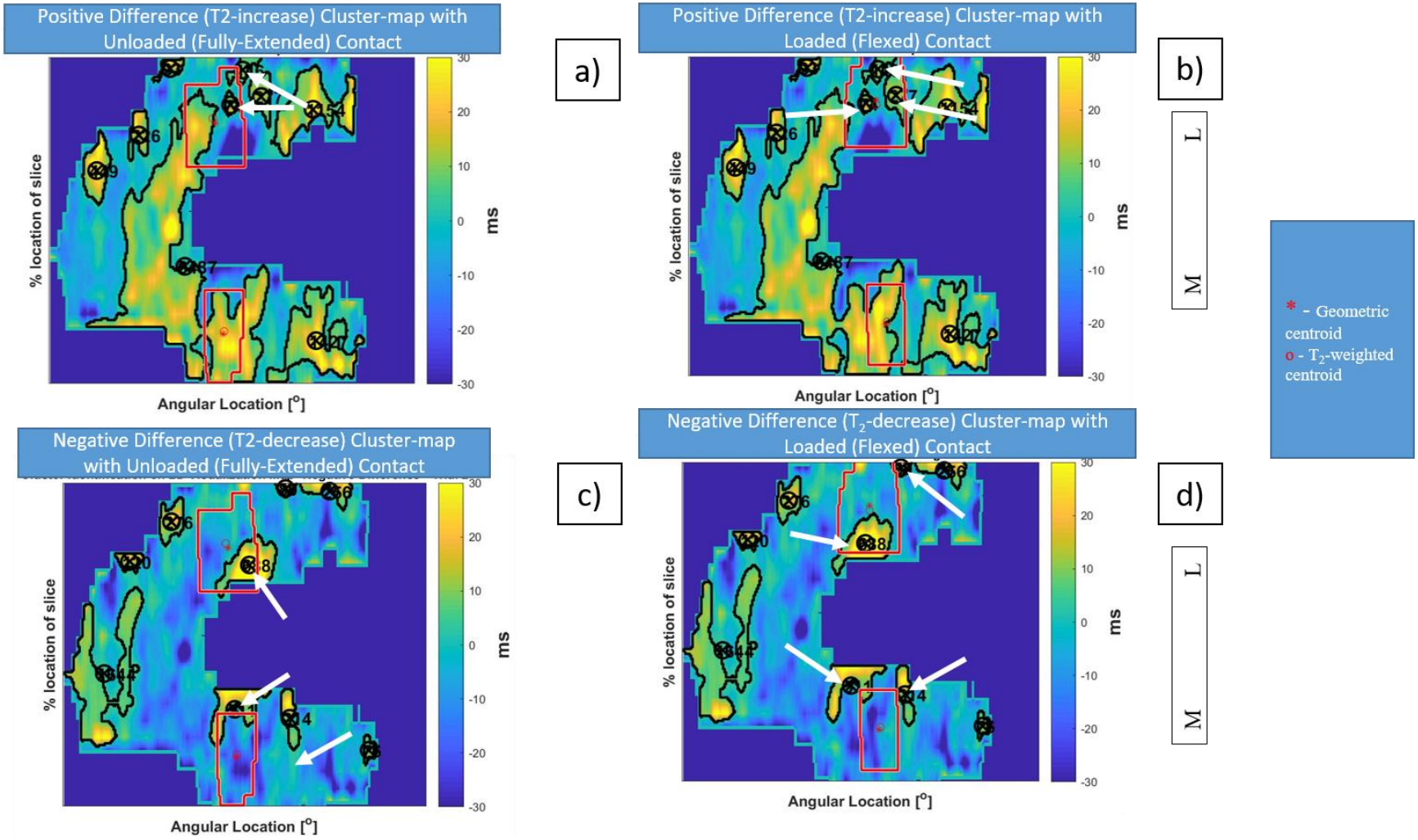

Figure 0-3: Sample of 2-D visualization map of particularly big difference between loaded and unloaded cartilage represented as clusters. The red boundaries indicate the outer boundary of the contact region. Top: T_2-decrease cluster maps with a) contact under loaded cartilage and b) contact under unloaded cartilage. Bottom: T_2- increase cluster maps with a) contact under loaded cartilage and b) contact under unloaded cartilage. The white arrows show the cluster centroid counts in and around the contact area region

Chapter 5
DISCUSSION

In this section, insights from the results with respect to the literature are expounded upon. The discussion is guided by the study's three research questions: 1) What is the repeatability of qMRI, mechMRI and gait analysis measures? 2) What is the repeatability of the kinematic and kinetic outcomes using a MRI-based anatomical system and a standard gait coordinate system? 3) Is there a link between qMRI T_2 and contact area values in cartilage?

5.1 What is the repeatability qMRI, mechMRI and gait analysis measures?

The overarching objective of this work is to show the repeatability, expressed as SD_{rms} and SD_{diff}, of specific qMRI, mechMRI and gait analysis measures that can be used to guide future work in the study of the ACL-injured population. This section goes over each of the three measurement systems to discuss repeatability and how the results may be applied to the study of ACL-injured individuals.

5.1.1 qMRI T_2 Relaxation Time

Our qMRI T_2 relaxation time and repeatability values fall within the same range as the literature. From the literature, the T_2 relaxation time of healthy cartilage has been seen to range from 22 – 47ms [9, 72, 73, 75]. T_2 relaxation times depend on the sequence used, and so direct comparisons of magnitude cannot be made between studies [76]. The mean T_2 values from this study range from 25.3ms – 26.9ms which falls within the expected range of values. The CV_{rms} for T_2 in our study ranges from 10.2% to 16.3%. This aligns with repeatability values from the literature which have been seen to range from 4% – 29 % [72, 74]. Past work from our research group with similar techniques, found CV_{rms} of less than 15% [9]. All of our measures were less than this, except lateral unloaded cartilage which had a slightly higher CV_{rms} of 16.7%. The slightly higher CV_{rms} values may be due to our lower mean values compared to results from past work in our research group, however, the SD_{rms} is within a similar range. The difference in magnitude is likely due to the different MRI parameters used in the present study. In the literature, the medial region generally has larger CV_{rms} than the lateral region which agrees with our findings [9, 72, 73, 75].

The confidence intervals for the T_2 relaxation time measures (Table 0-4) are useful because they represent the minimum detectible difference to show a true effect between groups or conditions in future studies. For example, the difference between healthy and ACL-injured T_2

relaxation times range from 3 – 5ms in the literature [6, 174]. Looking at our confidence interval table (Table 0-4), this falls within 80% confidence (unloaded: ±4.9ms); all other confidence intervals were greater than this. It should be noted that our results are for only five participant and could potentially be an over-estimate of the repeatability; however, our findings are within the range of most studies in the literature.

Some conditions were seen to have larger SD_{rms} than others. Loaded T_2 measures are seen to have a slightly smaller SD_{rms} than unloaded measures as well as lateral having smaller SD_{rms} than medial. The measures with smaller SD_{rms} could be of interest in the study of ACL-injured individuals.

It is important to assess regional mean T_2 relaxation times as well as differences in T_2 relaxation times between loaded and unloaded conditions, in order to identify regions where the difference are not only most pronounced but have smaller SD_{rms}. Comparing the SD_{rms} values of the difference measures (between loaded and unloaded), the trochlear region has the smallest value even though its overall mean showed that the loaded trochlea had a higher T_2 relaxation time. This may be because the trochlear region loads were small. Monu et al found interesting results in the trochlear region with clusters of increased T_2 relaxation times, which may indicate degeneration, in ACL-injured individuals over time [9]. The loaded-unloaded difference measure of the medial compartment had the largest SD_{rms} value, as do the medial loaded and unloaded compartments separately. It is interesting to note that this same medial compartment is the only measure with a negative overall mean value (generally higher unloaded than loaded T_2 relaxation times) and so it is possible that the negative value may be due to measurement error.

Previous studies that have assessed T_2 relaxation times in loaded and unloaded conditions have seen lower values in the loaded case. When studying the whole plate or compartment, our results however show only a few cases where the loaded T_2 relaxation time is lower than the unloaded. This occurred in two cases in the general, three cases in medial, five cases in lateral, and four cases in trochlear regions ranging from -0.1ms to -0.8ms. An increase in T_2 (from unloaded to loaded) was observed more often and ranged from 0.3ms to 8ms. The inconsistency of our results with the literature may be due to the fact that our assessment was carried out specifically within the contact area over which there is a pressure gradient under load. It is expected that some regions within the contact region may in fact increase, while other areas decrease, and this highlights the importance of exploring the change within the contact area. A

limitation, however, is that the resolution may not be sufficient to clearly distinguish between cartilage that is adjacent versus within the loaded region. Schoenbauer et al [83] found consistently lower T_2 relaxation times after the cartilage was loaded for greater than 7 minutes. Nishii et al [82] found similar results for cartilage that was pre-loaded for 6 – 9 minutes before scan. Also, significant change in T_2 was detected under dynamic loading only after high knee loading activities such as deep knee bending and running [175]. The knees of participants in the present study were only loaded at approximately 20% body weight which may not be a large enough load. Further, they held the load for approximately 3.5 minutes which may not have been a long enough time to see similar trends as in the literature. Our scans were also carried out in the evening, meaning that the participants had been loading their joints all day. A longer period of offloading before the unloaded scan and a longer period of loading before the loaded scan may be required to see an effect. One challenge with this approach is that since our method will be used to assess individuals with knee injury, the loading task must be limited. Exploring the unloading and loading protocols, pre-loading activities before MRI scan may be useful in future studies.

In the ACL-injured population, it is expected that T_2 relaxation times will be higher in the unloaded cartilage compared to the healthy population [136]. As ACL-injury causes a breakdown in the cartilage matrix, it is likely that there will be a clearer distinction between loaded and unloaded cartilages [9, 136]. This would even be better if loading conditions are more carefully created such as preloading for loaded cartilage and offloading limb before unloaded cartilage scan.

5.1.2 Contact Area and Contact Area Centroid Translation (mechMRI)

Our findings for contact area show similar magnitudes and trends as in the literature with reasonable repeatability for most measures. In Patel et al's work, contact area for healthy individuals taken at six angles of flexion between 0 and 60 degrees, ranges from 370 mm^2 – 440 mm^2 [14]. Similarly, in our study, contact area ranged from 387.2 mm^2 – 405.1 mm^2 except in the lower flexion angle medial contact area where it is 513.3 mm^2. The reason for this particularly large medial contact area in the lower flexion angle as compared to Patel's work, may be due to the difference in our loading mechanisms. While our study loaded participants' knees at a load proportional to their body weight (20% BW – 110N – 144N), in Patel's work, participants maintained a load of 133 N applied to the foot [14]. It is possible that bigger joint

sizes in participants of higher body weight could contribute to why contact area in our study was larger at such flexion angles (mean: 21.5° degrees of flexion). This factor may also be the reason for higher CV_{rms} in our study - they reported CV values of 6.3% - 11.4% while our study reports CV_{rms} values of 11.1% - 19.6%. Also, unlike our study that based our CV_{rms} on three trials on different days, their CV values are based on 3 trials within the same day and within the same MR session. Carpenter et al report SD values (52 mm^2 – 77 mm^2) that are more similar in range to our SD_{rms} values (41.8 mm^2 – 82.1 mm^2) except in our medial contact area of the lower flexion angle (105.9 mm^2). The Carpenter et al study, however, only evaluated contact area at full extension and 60 degrees of flexion which may also explain their smaller contact area values ranging from 81mm^2 to 361mm^2.

The confidence intervals calculated for contact area (Table 0-8) are useful for defining the minimum detectible difference between groups or conditions in future studies. For example, the difference between healthy and ACL-injured for contact area measures have been seen to average 62 mm^2 overall [14, 15]. Looking at our confidence interval table in Table 0-8, this only falls within 80% confidence of fully extended limb and not for any other measure or confidence interval. Thus, in this case one could be 80% confident that this was a true statistical difference. It is difficult to know if, if we had a bigger population (greater than n = 5), we would still get these confidence interval numbers.

Like Carpenter and Patel's work, our contact area is larger in the medial side with the lateral side not changing much from fully extended to higher flexion angles. Interesting to note is that in general, our lateral contact area has a lower SD_{rms} (45.9 mm^2 - 49.6 mm^2) than our medial contact area (41.8 mm^2 – 105.9 mm^2) which lines up with the findings of Patel et al and Carpenter et al [14, 15]. Carpenter et al found a larger mean difference in contact area change from extension to flexion, between that of ACLR and contralateral knees for the medial side to be 8 mm^2 and that of the lateral side to 37 mm^2 [15]. From Carpenter et al's study, the larger difference in the lateral side may indicate that it is more sensitive to differences in injured and healthy knees. This together with the smaller repeatability for lateral measures seen in our study, may give us more confidence in applying these measures in the study of ACL-injured individuals. Furthermore, medial contact area and particularly at the lower flexion angle had the largest SD_{rms}. The smallest SD_{rms} for contact area occurred in the fully extended measures

(medial and lateral) and these measures as well as the lateral measures (in the low and high flexion angle positions), are conditions with the smallest SD_{rms}.

Our contact area centroid translation patterns seen between the fully extended and the two flexed knee positions (low and high flexion) align with what is seen in the literature with smaller SD_{rms} on the lateral side where the centroid translation occurs between the lower and higher knee flexion angles. Our overall mean translation values were seen to range from 10.2 mm – 20.2 mm on the medial side and 6.5 mm – 13.4 mm on the lateral side. Patel et al who also assessed contact centroid translation in healthy individuals from fully extended to 60 degrees of flexion, found the medial contact centroid to translate up to 8mm and the lateral contact centroid to translate up to 5.2 mm [14]. The difference in values between our study and Patel's work may be due to the fact that these translation positions were taken with reference to the tibia as opposed to the centroid in the fully extended limb, as was done in our study. It may be for the same reason that other studies that reported accuracy and repeatability found smaller values than ours, being that the translation was also taken from an anatomical landmark. While our method has two points susceptible to variability – the start and end of the translation – choosing an anatomical landmark as a reference point only has the end point that is susceptible to variability. Examples of studies that assessed centroid translation this way are Logan et al who found accuracy of 1.5 mm and Carpenter et al who found reproducibility of 0.9 mm [15, 103]. Our SD_{rms} on the other hand, range from 3.9 mm – 4.4 mm on the medial side and 2.6 mm – 3.1 mm on the lateral side. Another reason for our larger SD_{rms} may be because it was taken and analysed over three days unlike these other studies. It should be noted however, that this data is more representative of longitudinal studies that are commonly done when studying ACL-injured individuals. Regardless of the difference in repeatability, our translation patterns align with what is seen in the literature with more posterior translation of the medial than the lateral side [14, 15, 176]. Comparing the repeatability of the absolute distances of the contact centroid between the three different limb positions, the measures for the lower to higher flexion angle has the smallest repeatability value (medial: 10.2 mm and lateral: 6.5 mm). The lateral centroid translation values are also have smaller SD_{rms} (6.5 mm – 13.4mm) than the medial (10.2 – 20.2 mm). This may be of particular interest in the study of ACL-injured individuals because Logan et al, Carpenter et al, and Scarvell et al found more posterior translations of the lateral side of ACL-injured individuals than the lateral side of contralateral or healthy individuals [15, 103, 176].

5.1.3 Gait Analysis

This section has been broken down into kinematic and kinetic sections each discussing primarily the SD_{rms} values of the measures.

5.1.3.1 Kinematics

The overall mean values of all our measures are close to the expected values from the literature. For walk peak flexion and extension angle the mean values from past literature range from 12.4°- 17.8° and 2.8°- 5.4° respectively [141-144]. Our mean peak flexion and extension angles fall close to the literature ranges with 14.7° for walk peak flexion angle and 5.6° for walk peak extension angle. The same goes for the frontal walk kinematics with values ranging from 3.8° to 16° [141, 142, 144] and our mean values falling close to these values at 2.8° and 7.6° for peak abduction and adduction angles respectively. Our stair ascent peak extension angle has an overall mean of 52.7°and the literature mean values range from 63.1° to 93.4°. Stair descent peak extension angle mean in the literature ranges from 64.6° - 90.5° [143-145] and our mean value for this measure falls within this range at 77.0°. Scheys et al defined good repeatability to be SD values that fall below 5° for all kinematic measures [144]. Using this criterion, all but our stair flexion angles are smaller than this number (7.2 – 10.8°).

Most of our kinematic values fall within the expected range for healthy individuals with most with SD_{rms} being less than 5°. The most repeatable measures in our study are the walk peak adduction angle and peak extension angle which aligns with another study with a similar experimental setup. Scheys et al did a repeatability study in heathy individuals over three days and found walk peak extension and peak adduction angles to have the lowest SD amongst other measures that we also assessed. For our walk peak adduction angle, the MRI-based and gait-based coordinate outcomes have SD_{rms} of 1.4 and 0.8 degrees respectively and for walk peak extension angle, 2.8 and 1.1 degrees respectively. Scheys et al's study found standard deviation values to be 1.9 degrees for peak adduction angle and 1.7 degrees for peak extension angle [144]. The walk peak adduction and peak extension angles particularly stand out for us because both coordinate system methods agree on these two measures as having the smallest SD_{rms}. Although the gait-based coordinate outcomes have smaller SD_{rms} than the MRI-based, it is interesting to see that for the walk peak adduction angle, both methods show smaller SD_{rms} than that reported in Scheys et al's study. For the walk peak extension angle, Scheys et al's SD is smaller than our MRI-based SD_{rms} but not as small as our gait-based SD_{rms}. These findings are similar to Robbins et al's work with repeatability over two days in OA participants [141], who found smaller

repeatability values in walk peak adduction angle measures than walk peak extension angle although the SD values are bigger in this study than ours or Scheys et al's findings (2.1 degrees for walk peak adduction and 6.5 degrees for walk peak extension angle). It is expected that in the diseased or injured group, repeatability may be larger because of differences in pathological factors between injured individuals and so it is clear that the next study in this project needs to be repeatability in the ACL-injured population.

The highest SD_{rms} were the flexion and extension angles from the stair activity for the standard gait- and MRI-based coordinate systems. Further, stair descent was higher than stair ascent for both methods (stair ascent peak extension angle SD_{rms}: 9.7° and 7.2°; stair descent peak flexion angle SD_{rms}: 10.8° and 7.6°). The stair activities also had the highest SD_{rms} in Scheys et al's study (stair ascent peak extension angle: 6°; stair descent peak flexion angle: 2.4°) although the stair descent SD_{rms} is lower than that of stair ascent which is the reverse in our case [144]. Our SD_{rms} values for the stair flexion angles are higher than that found in Scheys et al's study and this may be due to the fact that with a wider range of motion as in stair activities, there is a higher possibility of kinematic cross-talk. The stair sagittal kinematics SD_{rms} of our study for gait based outcomes, was more similar to Protopapadaki et al's [145] finding of SD of 7.4° for stair ascent and 7.11° for stair descent. Protopapadaki's study, however, was a within day repeatability study. From these findings, our gait-based stair sagittal kinematics is better recommended than MRI-based because of how close it is to and even lower SD_{rms} than a within-session repeatability study which is expected to have a lower repeatability value.

The minimum detectible difference for kinematics, as described by confidence intervals (Table 0-15), show that it is likely that we will only be able to detect differences between groups or conditions in future studies with 80% confidence. The difference between healthy and ACL-injured kinematics have been have been seen to average 5º [12, 96]. Looking at our confidence interval table in Table 0-15, this only falls within 80% confidence of the walk kinematic measures. Again, a larger sample size may alter the values in this table; however, the SD_{rms} reported in this thesis are in the range of those reported in the literature.

A factor that may have increased variability in our study is functional calibration across the trials. The functional calibration outcomes (flexion axis, hip and joint center) are dependent on the placement of markers on the limb [177]. As no method was taken to ensure that the markers were placed at the exact same position across the trials but standard postioning

techniques based on using anatomical landmarks were employed. However, there is a possibility that this may have impacted our results.

5.1.3.2 Kinetics

The overall mean and repeatability values of all our measures in this study, are close to the values reported in the literature. To make comparison to the literature, some assumptions had to be made to convert to common units. From previous literature, peak sagittal moment mean values have been seen to range from 0.28 – 5.6 N.m/kg for walking (SD: 0.11 – 0.23 N.m/kg), 0.49 – 1.98 N.m/kg for chair tasks (SD: 0.10 – 0.23 N.m/kg) and 0.05 – 0.3 N.m/kg for stair tasks (SD: 0.24 – 0.51 N.m/kg) [141, 142, 147, 149, 150]. Results from our study were found to have mean values of 0.11 – 0.36 N.m/kg for walking (SD_{rms}: 0.04 – 0.08 N.m/kg), 0.15 – 0.60 N.m/kg for chair tasks (SD_{rms}: 0.06 – 0.19 N.m/kg) and 0.62 – 0.67 N.m/kg for stair tasks (SD_{rms}: 0.11 – 0.22 N.m/kg). The frontal plane kinetic mean values are comparable, with walking values of 0.38 – 3.2 N.m/kg and chair task values of 0.41 – 2.56 N.m/kg in the literature [141, 142, 148, 150-152] and walking values of 0.17 - 0.86 and chair task values of 0.33 – 0.56 N.m/kg in our study. The slight discrepancy in our values compared to the literature might be a result of having the femur and tibia clusters closer to the knee joint than typical. This was done due to the limitation of the size of the knee joint field-of-view in MRI scanning. Functional axes generated in this condition tend to be steeper than normal when the femur and tibia cluster markers are closer together and with this, the knee joint center would have been positioned higher since it was defined as lying along the flexion axis. Like in our study, the largest SD and SD_{rms} values from the literature are seen to occur in stair ascent peak extension moment and stair descent peak flexion moment when compared with the other measures assessed in this study (literature: 0.24 – 0.51 N.m/kg; our study: 0.11 – 0.22 N.m/kg). All other repeatability values for the measures in our study are less than 0.23 N.m/kg.

Given the confidence intervals calculated for kinetics, the minimum detectible differences were less than 0.3 N.m/kg, 0.4 N.m/kg and 0.7 N.m/kg for 80%, 95% and 99% confidence, respectively (Table 0-17). From the literature, the difference between healthy and ACL-injured kinetic measures is 0.14 N.m/kg on average [12]. Our confidence interval table in Table 0-17 shows that this value will fall between 80% and 95% confidence for all walk measures except 95% confidence for walk peak adduction moment as well as 80% confidence for chair sit peak abduction moment and stair descent peak flexion moment.

5.1.3.3 Summary

In summary, kinematics and kinetics showed different measures with highest and lowest SD_{rms}. For kinematics, walk peak adduction and peak extension angles showed the lowest SD_{rms} and peak stair flexion angles showed the highest SD_{rms}. For kinetics, the measure with the lowest SD_{rms} and best agreement in performance ranks between the methods is peak chair sagittal moments and the highest SD_{rms} is seen in the peak sagittal stair moments. For both kinetics and kinematics, the highest SD_{rms} occurs in the peak sagittal stair measures and this may identify measures of less priority in the study of ACL-injured individuals. From our findings, the walk sagittal and frontal measures should be explored in kinetics and kinematics studies of ACL-injured individuals.

5.1.4 What is the repeatability of qMRI, mechMRI and gait analysis measures? - Conclusion

The qMRI, mechMRI and gait analysis measures found to have the lowest SD_{rms} from the study of our healthy population may be of particular interest in the study of ACL-injured individuals. qMRI T_2 relaxation times lateral and loaded measures appear to be have the lowest SD_{rms} than other qMRI T_2 measures. Contact area and centroid translation SD_{rms} comparison reveals lowest SD_{rms} for the medial than the lateral side. Walk sagittal and frontal measures are seen to have the lowest SD_{rms} in both coordinate system methods for kinematics and sagittal chair measures for kinetics. Another reason for larger repeatability values for some measures is sex differences within our population.

5.2 What is the repeatability of the kinematic and kinetic outcomes using a MRI-based anatomical system and a standard gait coordinate system?

Some of the greatest sources of error in the literature in gait analysis have been associated with imprecise location of anatomical landmarks and joint centers and these contribute to key differences between the MRI-based and gait-based coordinate systems [124, 177, 178]. The functional flexional axis is a common definition between the two methods of defining the coordinate systems, hence it is not discussed in comparing the measure outcomes of both methods. With the aid of MRI, anatomical landmarks have been defined and used to create a coordinate system that have been used to process dynamic data. In this section, SD_{rms} has been used to assess and compare the repeatability of the outcomes of processing kinematic and kinetic data from MRI-based and gait-based coordinate systems. The outcomes of the Bland-Altman analysis used to compare the two methods have also been discussed in this section.

5.2.1 Kinematics

The Bland-Altman analysis for the kinematic measures between the methods shows good agreement for some of the measures. Giavarina et al described that three factors are to be considered when determining agreement between two methods with Bland-Altman [179]. These are the proximity of the overall mean difference to zero (the closer to zero, the less bias), the width of the limits of agreement range (smaller than a clinically acceptable range, the better), presence of a skew in the plot (skewed nullifies assumption of normal distribution of the mean differences) and the number of mean difference points outside the limits of agreement (95% of total points should fall within the limits of agreement range). All measures were seen to have a normal distribution, hence slight skews seen in any of the plots were not of concern. Walk peak extension and peak abduction angles have a non-significant skew in their Bland-Altman plots, which does not affect the assumption of normal distribution for these measures. These same measures have overall mean difference values that are farthest away from zero. Using an acceptable SD criteria of 5°, any limit of agreement range greater than 20° (2 SDs on either side of the mean difference) will be considered to have a bias and therefore questionable agreement between the two methods for this study. Using this criterion, only the walk peak abduction angle, stair ascent peak extension angle, and stair descent peak flexion angle measures have limits of agreement greater than 20°. The other four measures have less. In particular, the stair ascent peak extension angle measure not only has a mean difference greater than 20 but also the farthest away from zero for the overall mean difference (-3.4°) and two points outside of the limits of agreement which is greater than 5% of the total number of points. It can be said that for the stair ascent peak extension angle measure, the two methods do not have a good agreement. Two measures have a limit of agreement range of 20 or less. These include the walk peak flexion angle measure (20°) and the walk peak adduction angle measure (4°). These measures also have reasonably small overall mean difference (-1.0° and 1.0°) and 95% of the total points fall within the limits of agreement. These include the walk peak flexion angle measure and the peak adduction angle measure which can be said to have a good agreement between the two methods for these measures. For the methods that have a good agreement, any of the knee coordinate systems should be okay to use to process data of these measures. This is however solely based on the performance of repeatability. It is still unclear which of these coordinate systems may be

more accurate. Table 0-1 below shows a ranking of each of the measures' limit of agreement range and SD_{rms} values for the two methods.

Table 0-1: SD_{rms} and Bland-Altmann Rank Table for Kinematic Measures. The numbers in the parentheses indicate the measures rank from smallest to biggest values

	Limit of Agreement Range	MRI-based SDrms	Gait-based SDrms
Walk - Peak Flexion Angle (degrees)	19.9 -- (3)	3.5 -- (3)	3.5 -- (4)
Walk - Peak Extension Angle (degrees)	16 -- (2)	2.4 -- (2)	1.0 -- (2)
Walk - Peak Abduction Angle (degrees)	23.8 -- (4)	3.7 -- (4)	2.5 -- (3)
Walk - Peak Adduction Angle (degrees)	3.93 -- (1)	1.5 -- (1)	0.7 -- (1)
Stair Up - Peak Extension Angle (degrees)	31.3 -- (6)	7.1 -- (5)	6.4 -- (5)
Stair Down - Peak Flexion Angle (degrees)	24.9 -- (5)	8.0 -- (6)	6.0 -- (6)

The lower SD_{rms} of most gait-based kinematic outcomes compared to MRI-based may be due to marker localization error. Comparing the SD_{rms} values of the gait-based and MRI-based outcomes shows a lower SD_{rms} in gait-based outcomes. From the plot and table, it can also be seen that the ranks across the measures for the two methods, are similar. This again shows that while the SD_{rms} of the gait-based outcomes is lower, there is a good agreement between the two methods as illustrated by the Bland-Altman plots described earlier. Della et al [177] and Leardini's work [180] highlight the importance of correct marker localization in landmark determination in gait systems for kinematic outcomes. The higher SD_{rms} in the MRI-based outcomes particularly in the stair sagittal kinematic outcome measures, may be due to inaccurate localization of the femur and tibia cluster MRI-lucent markers determined from MRIs. This is evident in the error reported in Table A-5-1, of Appendix A-5 where deviation from the VICON-generated marker centroids is seen (4.6mm – 9.4mm). Also, the marker centroid was determined visually in the MRI and this is also subject to more variability than marker localization conducted by the VICON system in the gait-based method. Marker centroid localization in the VICON system is subject to how well the calibration was done with accuracy in the range of 0.5mm – 0.8mm. It is possible that the higher the range of motion (as is the case with stair activity compared to walk), there is more kinematic crosstalk. Also, as stair activities are not a routine task as is walking, the participants might have had a harder time carrying it out repeatably. It might have also been more difficult as the task involved only one step as opposed to the typical series of steps that participants might be used to doing.

From these findings, it can be concluded that while we may be concerned about which of the MRI-based and gait-based kinematic outcome measures may be more appropriate from the assessment of the repeatability, most of the outcomes can be said to be systematically equivalent from the Bland-Altman analysis. The lower SD_{rms} seen in the gait-based measures may be due to data acquisition and definition as described, yet, it remains unclear which of these methods may be better for kinematic and kinetic analysis.

5.2.2 Kinetics

The Bland-Altman analysis of the two methods in the kinetic outcome measures shows agreement between the methods in some of the measures. The acceptable limit of agreement for this study is 0.6N.m/kg which is from a SD of 1.5 N.m/kg, which is the highest value of the 85th percentile of SD_{rms} that was acquired from all measures given that limit of agreement is +/- 2 SDs. All measures were seen to have a normal distribution, hence slight skews seen in any of the plots were not of concern. Two measures, including walk peak abduction and adduction moment measures, have a limit of agreement range value greater than 0.6N.m/kg (0.77N.m/kg and 0.97N.m/kg) with overall mean differences that are the farthest away from zero (0.33N.m/kg and 0.56N.m/kg). Walk peak abduction moment particularly has 2 points outside of the limits of agreement which is greater than 5% of the points within the limit. This implies that walk peak abduction and adduction moment, the two methods do not systematically agree. For the measures that do agree between the two methods, the analysis shows that this occurs in walk peak extension moment and chair sit peak abduction moment, where both measures have limit of agreement ranges of less than 0.6 N.m/kg (0.44N.m/kg, and 0.52 N.m/kg), overall mean differences not too far from zero (0.001 N.m/kg and -0.15 N.m/kg) and less than 2 points outside of the limits of agreement. These are measures for which the choice of coordinate system to process the data may not have a significant impact on the results.

SD_{rms} comparison between the two coordinate systems generally shows lower SD_{rms} for measures of gait-based than MRI-based outcomes. MRI-based kinetic outcome measures had lower SD_{rms} values in walk peak flexion moment, peak extension moment, and in stair descent peak flexion moment. Gait-based outcomes had lower SD_{rms} for walk peak abduction and adduction moments (frontal-plane moments). Interesting to note is that MRI-based kinetic outcome measures had lower SD_{rms} in the sagittal-plane moments for the stance-inclusive activities (walk and stair) and higher SD_{rms} in the frontal plane moments when compared to the

gait-based. Sagittal knee moments have been seen to be more sensitive to knee joint center locations with increased variability at slower walking speeds [181]. The reason stated is that at slower speeds, the moment magnitude is smaller and the sign of the moment changes such that one cannot tell it from the knee center location variation effect. This may explain the SD_{rms} differences between the two methods for the sagittal moments of chair and stair activities, as these were carried out at slower speeds than the walking activity. The difference in the SD_{rms} of the MRI-based and gait-based kinetic outcomes may also be due to the knee joint center differences between the two methods. While the MRI-based method defined it as the flexion axis projection of the most proximal point of the intercondylar notch, the gait-based defined it as the flexion axis projection of the mid-point between the palpated femoral condyles. The MRI-based method may be more subject to differences in bone shapes and soft tissue behaviour. This highlights the importance of a functional joint center as is the case in gait-based and as recommended by the International Society of Biomechanics [118].

The difference in the long-axis definition also plays a role in the difference in repeatability between the two methods. The long-axis with the MRI-based system is an anatomical long axis, running from the knee joint center to the actual shaft of the femur (anatomical axis) as opposed to the functional-based system which runs from the knee joint center to the hip joint center (mechanical axis). The difference in defining the long axis between the two methods can be comparable to findings of different methods used to define the hip joint centers. Stagni et al [124] and Leardini et al [182] confirm that knee joint moments are largely affected by hip joint center estimations due to the inaccuracies in determining the pelvic and femoral anatomical landmarks when it is determined functionally. Significant differences of up to 4.9% have been observed with different long axis definitions, particularly in knee flexion moments [183]. This may explain the different SD_{rms} values for peak knee flexion moments of chair and stair activities. Richards et al found different knee external moments to be especially sensitive in squat activity which can be likened to our chair activity and can be related to the difference between the two SD_{rms} values (Chair rise: 0.07 N.m/kg and Chair sit: 0.035 N.m/kg) [184].

The SD_{rms} comparison between the two coordinate system methods and Bland-Altman analysis show a similar trend of stronger agreement between the two methods where the repeatability values least differ in the measure with the strongest agreement (see Table 0-2

below). Comparing the SD_{rms} values between the two methods shows that they least differ in the walk sagittal moments. Also, Bland-Altman analysis shows the smallest range of limits of agreements with overall mean difference in these measures which are each closest to zero. It is also in the measures of the most repeatability difference (walk frontal moments and stair descent peak flexion moment), that the Bland-Altman analysis shows the weakest agreement (most bias) between the two methods. Important to note also is that in the measures of most repeatability difference between the two measures, MRI-based outcomes performed better. This could indicate that MRI-based coordinates will be better in processing these measures (walk frontal moments and stair descent peak flexion moment) since it gives the lower SD_{rms} for these measures as compared to the gait-based results.

The measures with the smallest SD_{rms} and good agreement between the two methods (gait-based and MRI-based coordinates), are the peak sagittal moments for chair activities. These values are much larger in the MRI-based outcomes (chair rise peak extension moment: 0.49 N.m/kg; chair sit peak flexion moment: 0.63 N.m/kg) than the gait-based outcomes (chair rise peak extension moment: 0.14 N.m/kg; chair sit peak flexion moment: 0.14 N.m/kg). Moreover, our gait-based outcome SD_{rms} (chair rise peak extension moment: 0.06 N.m/kg and chair sit peak flexion moment: 0.05 N.m/kg) for these measures are not only smaller than that of MRI-based (chair rise peak extension moment: 0.13 N.m/kg and chair sit peak flexion moment: 0.13 N.m/kg) but also smaller than what is seen in the literature (chair rise peak extension moment: 0.10 – 0.13 N.m/kg and chair sit peak flexion moment: 0.23 N.m/kg) [150]. This could mean that though coordinate definitions are particularly sensitive in chair task sagittal moment values, this is not the case for their repeatability, given the agreement between the two methods on the performance rank.

The least agreement in repeatability performance ranks between the two methods compared to other measures is in the walk peak abduction moment and peak flexion moment. For the walk peak flexion moment, the SD_{rms} ranks best in the MRI-based outcomes (0.04 N.m/kg) and fourth in the gait-based outcomes (0.07 N.m/kg). The difference in SD_{rms} ranks for walk peak flexion moment in the two methods given how close the kinetic values are to themselves, (MRI-based: 0.07 N.m/kg and gait-based: 0.12 N.m/kg) may imply that this measure's repeatability is particularly sensitive to the coordinate system setup. For the walk peak abduction moment, with a big difference in the value (MRI-based: 0.34 N.m/kg and gait-based:

0.86 N.m/kg), the implication may be that the coordinate system setup affects both the accuracy and repeatability. Caution must be taken for the walk peak abduction moment outcomes with the coordinate system that is used to process it because of this finding.

Table 0-2: SD_{rms}, and Bland-Altmann Rank Table for Kinetic Measures – the numbers in the parentheses indicates the measures rank from smallest to biggest values

	Bland-Altmann agreement limit distance	MRI-based SDrms	Gait-based SDrms
Walk - Peak Flexion Moment (N.m/kg)	0.04 -- (1)	0.07 -- (4)	0.07 -- (4)
Walk - Peak Extension Moment (N.m/kg)	0.05 -- (2)	0.07 -- (4)	0.07 -- (4)
Walk - Peak Abduction Moment (N.m/kg)	0.21 -- (7)	0.05 -- (1)	0.05 -- (1)
Walk - Peak Adduction Moment (N.m/kg)	0.21 -- (7)	0.08 -- (6)	0.08 -- (6)
Chair Rise - Peak Extension Moment (N.m/kg)	0.13 -- (3)	0.06 -- (3)	0.06 -- (3)
Chair Rise - Peak Adduction Moment (N.m/kg)	0.2 -- (6)	0.18 -- (9)	0.18 -- (9)
Chair Down - Peak Flexion Moment (N.m/kg)	0.13 -- (3)	0.05 -- (1)	0.05 -- (1)
Chair Down - Peak Abduction Moment (N.m/kg)	0.15 -- (5)	0.14 -- (8)	0.14 -- (8)
Stair Up - Peak Extension Moment (N.m/kg)	0.26 -- (10)	0.32 -- (10)	0.32 -- (10)
Stair Down - Peak Flexion Moment (N.m/kg)	0.25 -- (9)	0.11 -- (6)	0.11 -- (6)

For kinetics, the difference between MRI-based and functional-based is not as distinct as with kinematics. MRI-based outcomes lower SD_{rms} in more measures for kinetics than kinematics. Walk sagittal kinematics and kinetics show the least difference in repeatability with good agreement between the two methods. This may imply that for these measures, choosing one method over the other may not have a big impact on the results, although accuracy has not been assessed in this study. However, for measures like frontal walk moments, where the agreement and repeatability difference are small in kinematics but large in kinetics, it is important to be aware of the difference in sensitivity when deciding on the coordinate system to be used.

5.2.3 What is the repeatability of the kinematic and kinetic outcomes using a MRI-based anatomical system and a standard gait coordinate system? - Conclusions

From this research, it can be said that the answer to this question is non-trivial as different repeatability values between the two methods reveal different conclusions. The literature has indeed shown no particular gold-standard for processing dynamic data, however, for the purposes of this research, the measures used for comparison show gait-based processed data to have smaller SD_{rms} than from MRI-based overall. MRI-based processed data however, seemed to have smaller SD_{rms} values than gait-based for the kinetic measures for some activities.

5.3 Is there a link between qMRI T_2 and contact area values in cartilage?

The battery of quantitative measures used to explore the relationship within the contact area gives insight into tissue behaviour during loading. As these are novel measures, there is no literature to my knowledge that exists and hence cannot be compared directly. The regional-contact maximum and SD difference of the lateral side show higher T_2 relaxation times in the lateral region than the contact for both loaded and unloaded cartilage. This may describe the T_2 increase with outflow of fluid from the matrix in the presence of load. The medial region only follows this trend in the loaded cartilage but only with slight values of 0.5ms. The difference between the medial and lateral measures is most distinct in the regional-contact maximum and SD difference for both loaded and unloaded cartilage (where lateral is a lot more positive). It also follows that the medial compartment has more negative values for SD difference measures than the lateral side (where the SD is smaller in the larger region than the smaller region). Relating this to more clusters seen in the medial contact area than in the lateral, implies that dispersion of fluid under load from the contact or its centroid leads to less variability of T_2 relaxation time where the fluid exudes to the bigger medial region. Another reason for less variability in the larger versus the smaller region in the medial side (more negative SD-difference measures), could be a re-organization of the collagen and PG network in the cartilage matrix under load. Also, the medial region bears more load at the knee than the lateral region [185].

Our T_2-contact measures are all difference measures; thus we can determine if the change observed between regions meets the minimum detectible difference criterias defined by using the confidence interval values (Table 4-21, 4-22). For example, the overall mean difference for lateral compartment loaded cartilage ranged from -3.4 to 19.9 ms, using our confidence interval talbe, only the regional-contact SD difference, regional-contact maximum difference and contact-centroid SD difference (II-T_2-weighted), will be considered measures with a large enough difference at the 80% confidence level. This is because these measures have overall mean values that are larger than the corresponding confidence interval at 80% confidence. This approach can be applied to determine the minimum detectible difference between groups or conditions in future studies that use these novel metrics.

To assess the link between contact area and T_2 relaxation times in this study, cluster areas of notable increase and decrease were evaluated within the contact region (of the loaded and unloaded scenarios) as well as quantitative difference measures between contact area, centroid,

and between the medial or lateral regions. SD_{rms} was used to assess what values may indicate an existing relationship from the repeatability of that measure.

T_2-decrease within the contact region appears to be more consistent across participants than the T_2-increase. Cluster regions within the contact area, present in the loaded knee scenario, occur more than cluster areas within the contact area present in the unloaded knee scenario, with slightly more clusters occurring in the T_2-decrease than T_2-increase. The fact that the loaded contact area is the area over which 20 % BW of the participant was applied, explains why more cluster areas will be seen under this area than in the unloaded contact area over which no load was applied. There are also more clusters seen in the medial contact than in the lateral contact areas implying greater differences between loaded and unloaded contact in the medial than lateral side. This aligns with the fact that the medial side is the more load-bearing compartment of the knee joint [185]. Nishii et al also saw a bigger change between loaded and unloaded cartilage T_2 in the medial than in the lateral tibiofemoral contact region [82].

Assessing the cluster maps within areas of contact reveals some interesting findings about effect of load on T_2 in the full cartilage plate. First, it is interesting to see how the T_2-weighted centroid aligns or is in close proximity to the geometric centroid. This indicates that our T_2 relaxation times within the contact area is like a pressure gradient where the mean T_2 under the contact is closest to the geometric centroid of the contact area. In the cluster maps, more clusters with their centroids were seen in the T_2-increase maps (from unloaded to loaded) than the T_2-decrease maps (from unloaded to loaded). This indicates that loaded cartilage generally has higher T_2 values than unloaded cartilage, especially in the cluster regions. These cluster regions and centroids mostly occurred around the lower edges of the trochlear, and within and around the contact regions. The literature has generally found lower T_2 relaxation times in loaded cartilage than unloaded but none of these studies assessed the full cartilage plate [83, 186]. From our study, we are finding the particular regions where T_2 relaxation time is higher even in loaded cartilage which aligns with the finding that fluid from the ECM exudes when cartilage is loaded and moves to other regions; because of this extra fluid, the T_2 will be higher [187]. The overall mean of the number of clusters that occurred in and around the contact regions (see Table 0-24) shows the clusters in the medial and lateral side being about the same - the most difference was in the negative difference of unloaded contact (0.5 M vs 1 L). There is also seen to be more clusters occurring in and around the contact region of loaded cartilage than the contact region of

unloaded cartilage, indicating that more changes are seen in the contact region of loaded cartilage. The measures with the lowest SD_{rms} were seen to be in the T_2-decrease cluster maps (0.3 - 0.4 vs 0.4 - 0.9 # of clusters) which could make these measures of particular interest in future studies. Assessing these cluster maps as was done in this study, in the study of ACL-injured individuals, will give us more insight into how the distribution of load affects cartilage in ACL-injured compared to healthy individuals. This behaviour can be seen in the T_2 cluster projection map images in Appendix F (also see Figure 0-1 below).

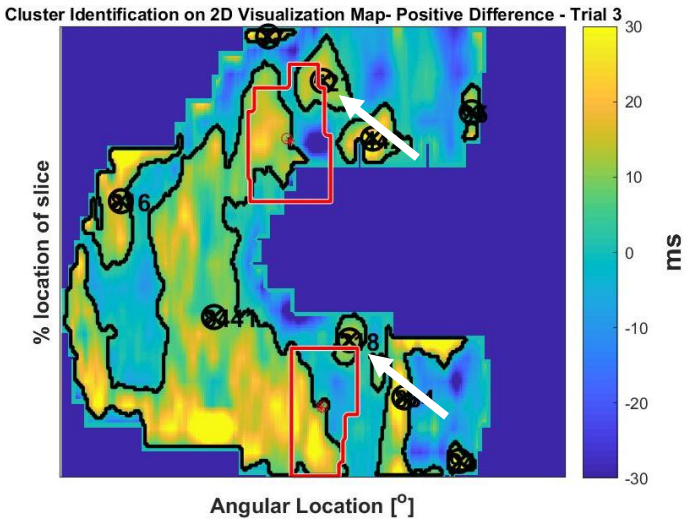

Figure 0-1: An example of a T_2-increase (from unloaded to loaded case) cluster projection map showing cluster centroids away from the centroid of the contact region of loaded cartilage. The red contour indicates the outer boundary of the unloaded contact region. The contact region is seen to overlay over a region where there is no cartilage because cartilage regions not present in loaded and unloaded cartilage are removed. Interpolation of the cartilage map also plays a role in this.

5.3.1 Is there a link between contact area and qMRI T_2 values in cartilage? - Conclusions

Our research shows that there is an existing link between qMRI T_2 and contact area measures. This was demonstrated by the repeatability of the integration measures, one of which is contact-centroid SD difference. These measures are important because they identify a link between qMRI T_2 relaxation time and load distribution over the contact area in cartilage. The link between the measures was also supported by the outcomes of the cluster-contact image analysis which consistently showed cluster centroids around the edges of the contact area and away from the contact centroid. This indicates that these are measures and analysis methods that could be adopted in the study of the ACL-injured individuals.

5.4 Study Limitations

Although every effort was made to create a robust data collection and analysis protocol, the study does have limitations. The major limitations are listed below.

- Some of the T_2 relaxation time data for unloaded cartilage was not processed due to MRI error. This contributed to four missing trials – three in participant 1 and one in participant 2. The repeatability measures may not be as robust for these measures that had 4 participants.
- Our study size was small. One study found that for repeatability studies a minimum of 14 participants with three trials each, is needed [190]. However, the imaging modality and variability in our measures is different from that of this study. It is not clear what we will need in our measures, however, 5 participants may not be enough.
- Ideally, for each trial set, the mean of three good trials is recommended. However, in two of the earlier data acquisition sessions, only two trials were collected and so the mean of only two trials was used in these cases (Participant 1, trial 1 and 2 – chair rise and sit).
- When collecting data of loaded cartilage, it is generally recommended to leave the cartilage unloaded for about an hour before scanning to ensure that all fluid is properly exuded from the cartilage matrix. However, this was not the case in our study due to scheduling constraints of the gait and MRI data collection sessions carried out in tandem. The cartilage not being unloaded for some time probably reduced the effect on the T_2 relaxation time results found when the cartilage was loaded.
- In selecting the second point to create the MRI-based long-axis for the coordinate system, the proximal and distal points for the femur and tibia respectively, were chosen on the most extreme slice. As the position of the field-of-views around the knee was not consistent across the trials and participants, this might have added variability to the system. In future studies, it might be better to pick a consistent slice from a known landmark in the image.
- The MRI-lucent gait cluster marker analysis in Table A-5-1 in the Appendix shows than the MRI-lucent gait markers which were ideally not supposed to move relative to each other between the motion capture and MRI systems did move in some cases. This motion could cause errors in the transformation matrix used to transform the points from the MRI to the motion capture system. This will introduce more variability to the system as the

magnitude of movement within the clusters is not consistent from study to study. Methods to ensure the markers do not move can be employed, including reducing the amount of walking the participant does beforehand between data acquisition in the two systems.

- Further analysis on the functional flexion axis acquired from the gait-system, showed a discrepancy in the flexion axis vector acquired when the femur and tibia cluster markers were closer together (steeper vector than expected) and when they were farther apart. It was important to have the MRI-lucent gait markers close to the knee joint because of the limitation of field-of-view in the MRI data acquisition for the high-resolution scan within a reasonable scan time. The steeper flexion axis vector from closer segment clusters is of concern because this may contribute to more kinematic crosstalk. A way around this limitation for future studies will be to have both MRI-lucent gait markers close to the joint and regular gait markers farther apart just to process the functional flexion axis. The MRI-lucent gait markers will then only be used during the 'T-pose' calibration step.
- In determining the mechanical behaviour of the bungee cords used in the MRI-safe loading rig, we created a linear equation from the test data. However, the displacement of the cords on the rig was sometimes below this range (0.05m). The smaller displacement may be outside the linear range, thus overestimating the applied load. Characterization of the bungee cord behaviour at smaller displacements is suggested.

Chapter 6
CONCLUSION

The conclusion section below gives a general overview of the key findings of our qMRI-mechMRI-gait analysis integrative and repeatability study while highlighting how we fulfilled our study's objectives, the contributions of this work, clinical significance, recommendations for future research, and closing remarks.

6.1 Summary

This research developed a method to acquire and integrate qMRI, mechMRI and gait analysis measures under physiological loading conditions, hence fulfilling objective 1. The novel T_2-contact integrative measures and cluster analysis inside and outside of contact areas were developed for qMRI and mechMRI integration. A method was also developed to integrate mechMRI and gait analysis measures in order to compare their kinematic and kinetic outcomes. The repeatability of all these integrative measures and individual measures of each of the three metrics, was also carried out in healthy individuals, hence fulfilling objective 2.

6.2 Conclusions

The contribution of this work is the development of two integrative pieces of qMRI and mechMRI (T_2-contact measure, clusters in and around contact regions) and mechMRI and gait analysis (comparing MRI-based with gait-based coordinate system outcomes) while assessing the repeatability of the outcome measures in healthy individuals. For the first time, comparison of qMRI metrics has been made between, inside and outside a region of contact. This novel methodology has highlighted two measures – regional-contact maximum difference and regional-contact standard deviation difference – for qMRI-contact analysis, based on repeatability. Through the findings from our comparisons between anatomical and gait-based coordinate systems, we have found the gait-based coordinate system to have better repeatability for kinematics, and in kinetics, we have found it to be activity dependent. In general, our findings recommend the gait-based coordinate system, based on repeatability. The methodology developed and repeatable measures discovered from this research can be applied to and can be used to guide future research in studying the kinematics and kinetics of ACL-injured individuals.

6.3 Clinical Significance

The major contribution of this research is the development of this integrative, repeatable method that can be used to study the ACL-injured population as an early model of OA. Being able to identify repeatable measures and relationships among the three assessment types (qMRI,

mechMRI and gait analysis), will guide future research in assessing the knee mechanics of the ACL-injured population. Although we did not study individuals with ACL-injury, when choosing our measures, we chose those that have been shown to be important in the ACL-injured studies. The reason we took this approach is that if we gain a better understanding of how these relate in the ACL-injured population, it may give us more insight into the progression of PTOA.

6.4 Recommendations for future research

The next steps following this work will be to make an informed decision as to the most important and repeatable measures that should be applied to the study of the ACL-injured population. The outcomes of this research suggest an improvement to controlling the loading conditions for MRI mechanics analysis. One such ways may be to keep the knee unloaded for about an hour before the loaded scans. Also, implementing a method to load the knees at a consistent load and angle should improve the mechMRI outcomes. Due to the constraint of the amount of load that is attainable with the loading rig and motion artifacts, loading the knee immediately prior to scanning may show more distinct load-unload difference in T_2 values which will be useful in the study of ACL-injured individuals.

The integrative method developed from this research focused more on the affiliation between quantitative T_2 relaxation time and contact area. We recommend developing a method to also integrate gait analysis outcomes to T_2 relaxation time and contact area, for example using statistical regional analysis techniques like those used in ecology. Other qMRI metrics could also be explored.

6.5 Closing Remarks:

The primary objective of this work was to provide a basis for integrative qMRI, mechMRI and gait analysis that can be used in the study of the ACL-injured population. Repeatability of several measures from these metrics were assessed to highlight which ones may be most important in the study of ACL-injured individuals. Also, novel repeatable measures have been discovered that can be used to assess the link between qMRI T_2 relaxation times and contact area. The comparison of kinetic and kinematic outcomes of a MRI-based and gait-based coordinate system reveal which method has better repeatability and least sensitive measures to the two coordinate systems. The findings from this study can be used to better guide future studies on the important measures that can be used to better assess the mechanics of ACL-injured individuals and their association to knee PTOA.

REFERENCES:

[1] L. S. Lohmander, A. Ostenberg, M. Englund, and H. Roos, "High prevalence of knee osteoarthritis, pain, and functional limitations in female soccer players twelve years after anterior cruciate ligament injury," (in eng), *Arthritis Rheum,* vol. 50, no. 10, pp. 3145-52, Oct 2004, doi: 10.1002/art.20589.

[2] A. von Porat, E. M. Roos, and H. Roos, "High prevalence of osteoarthritis 14 years after an anterior cruciate ligament tear in male soccer players: a study of radiographic and patient relevant outcomes," (in eng), *Ann Rheum Dis,* vol. 63, no. 3, pp. 269-73, Mar 2004.

[3] L. S. Lohmander, P. M. Englund, L. L. Dahl, and E. M. Roos, "The Long-term Consequence of Anterior Cruciate Ligament and Meniscus Injuries," (in en), *http://dx.doi.org/10.1177/0363546507307396*, other 2016-11-17 2016, doi: 10.1177_0363546507307396.

[4] Z. A. Zarins *et al.*, "Cartilage and meniscus assessment using T1rho and T2 measurements in healthy subjects and patients with osteoarthritis," (in eng), *Osteoarthritis Cartilage,* vol. 18, no. 11, pp. 1408-16, Nov 2010, doi: 10.1016/j.joca.2010.07.012.

[5] R. I. Bolbos, T. M. Link, C. B. Ma, S. Majumdar, and X. Li, "T1rho relaxation time of the meniscus and its relationship with T1rho of adjacent cartilage in knees with acute ACL injuries at 3 T," (in eng), *Osteoarthritis Cartilage,* vol. 17, no. 1, pp. 12-8, Jan 2009, doi: 10.1016/j.joca.2008.05.016.

[6] X. Li *et al.*, "Cartilage in anterior cruciate ligament-reconstructed knees: MR imaging T1{rho} and T2--initial experience with 1-year follow-up," (in eng), *Radiology,* vol. 258, no. 2, pp. 505-14, Feb 2011, doi: 10.1148/radiol.10101006.

[7] M. Son, S. B. Goodman, W. Chen, B. A. Hargreaves, G. E. Gold, and M. E. Levenston, "Regional variation in T1rho and T2 times in osteoarthritic human menisci: correlation with mechanical properties and matrix composition," (in eng), *Osteoarthritis Cartilage,* vol. 21, no. 6, pp. 796-805, Jun 2013, doi: 10.1016/j.joca.2013.03.002.

[8] J. Rautiainen *et al.*, "Multiparametric MRI assessment of human articular cartilage degeneration: Correlation with quantitative histology and mechanical properties," (in eng), *Magn Reson Med,* Aug 7 2014, doi: 10.1002/mrm.25401.

[9] U. D. Monu, C. D. Jordan, B. L. Samuelson, B. A. Hargreaves, G. E. Gold, and E. J. McWalter, "Cluster analysis of quantitative MRI T2 and T1rho relaxation times of cartilage identifies differences between healthy and ACL-injured individuals at 3T," (in eng), *Osteoarthritis Cartilage,* vol. 25, no. 4, pp. 513-520, Apr 2017, doi: 10.1016/j.joca.2016.09.015.

[10] S. A. Ismail, K. Button, M. Simic, R. Van Deursen, and E. Pappas, "Three-dimensional kinematic and kinetic gait deviations in individuals with chronic anterior cruciate ligament deficient knee: A systematic review and meta-analysis," (in eng), *Clin Biomech (Bristol, Avon),* vol. 35, pp. 68-80, Jun 2016, doi: 10.1016/j.clinbiomech.2016.04.002.

[11] M. Kaur, D. C. Ribeiro, J. C. Theis, K. E. Webster, and G. Sole, "Movement Patterns of the Knee During Gait Following ACL Reconstruction: A Systematic Review and Meta-Analysis," (in eng), *Sports Med,* vol. 46, no. 12, pp. 1869-1895, Dec 2016, doi: 10.1007/s40279-016-0510-4.

[12] L. V. Slater, J. M. Hart, A. R. Kelly, and C. M. Kuenze, "Progressive Changes in Walking Kinematics and Kinetics After Anterior Cruciate Ligament Injury and Reconstruction: A Review and Meta-Analysis," (in eng), *J Athl Train,* vol. 52, no. 9, pp. 847-860, Sep 2017, doi: 10.4085/1062-6050-52.6.06.

[13] H. F. Hart *et al.*, "Knee kinematics and joint moments during gait following anterior cruciate ligament reconstruction: a systematic review and meta-analysis," (in eng), *Br J Sports Med,* vol. 50, no. 10, pp. 597-612, May 2016, doi: 10.1136/bjsports-2015-094797.

[14] V. V. Patel *et al.*, "A three-dimensional MRI analysis of knee kinematics," *Journal of Orthopaedic Research,* vol. 22, no. 2, pp. 283-292, 2004, doi: 10.1016/j.orthres.2003.08.015.

[15] R. D. Carpenter, S. Majumdar, and C. B. Ma, "Magnetic resonance imaging of 3-dimensional in vivo tibiofemoral kinematics in anterior cruciate ligament-reconstructed knees," (in eng), *Arthroscopy,* vol. 25, no. 7, pp. 760-6, Jul 2009, doi: 10.1016/j.arthro.2009.01.014.

[16] R. B. Souza *et al.*, "Response of knee cartilage T1rho and T2 relaxation times to in vivo mechanical loading in individuals with and without knee osteoarthritis," *Osteoarthritis and Cartilage,* vol. 22, no. 10, pp. 1367-1376, 2014, doi: 10.1016/j.joca.2014.04.017.

[17] R. D. Carpenter, S. Majumdar, and C. B. Ma, "Magnetic Resonance Imaging of 3-Dimensional In Vivo Tibiofemoral Kinematics in Anterior Cruciate Ligament–Reconstructed Knees," *Arthroscopy: The Journal of Arthroscopic and Related Surgery,* vol. 25, no. 7, pp. 760-766, 2009, doi: 10.1016/j.arthro.2009.01.014.

[18] A. R. Poole, T. Kojima, T. Yasuda, F. Mwale, M. Kobayashi, and S. Laverty, "Composition and structure of articular cartilage: a template for tissue repair," (in eng), *Clin Orthop Relat Res,* no. 391 Suppl, pp. S26-33, Oct 2001.

[19] A. Mobasheri, C. Matta, R. Zakany, and G. Musumeci, "Chondrosenescence: definition, hallmarks and potential role in the pathogenesis of osteoarthritis," (in eng), *Maturitas,* vol. 80, no. 3, pp. 237-44, Mar 2015, doi: 10.1016/j.maturitas.2014.12.003.

[20] G. Musumeci, "The Effect of Mechanical Loading on Articular Cartilage," (in en), *Journal of Functional Morphology and Kinesiology,* Editorial vol. 1, no. 2, pp. 154-161, 2016-04-12 2016, doi: 10.3390/jfmk1020154.

[21] J. A. Buckwalter and H. J. Mankin, "Articular cartilage: tissue design and chondrocyte-matrix interactions," (in eng), *Instr Course Lect,* vol. 47, pp. 477-86, 1998.

[22] A. J. Sophia Fox, A. Bedi, and S. A. Rodeo, "The Basic Science of Articular Cartilage: Structure, Composition, and Function," in *Sports Health,* vol. 1, no. 6), 2009, pp. 461-8.

[23] H. Lorenz and W. Richter, "Osteoarthritis: cellular and molecular changes in degenerating cartilage," (in eng), *Prog Histochem Cytochem,* vol. 40, no. 3, pp. 135-63, 2006, doi: 10.1016/j.proghi.2006.02.003.

[24] Z. Ashkavand, H. Malekinejad, and B. S. Vishwanath, "The pathophysiology of osteoarthritis," *Journal of Pharmacy Research,* vol. 7, no. 1, pp. 132-138, 2013/01/01/ 2013, doi: https://doi.org/10.1016/j.jopr.2013.01.008.

[25] D. Heinegard, "Fell-Muir Lecture: Proteoglycans and more--from molecules to biology," (in eng), *Int J Exp Pathol,* vol. 90, no. 6, pp. 575-86, Dec 2009, doi: 10.1111/j.1365-2613.2009.00695.x.

[26] F. Eckstein, M. Hudelmaier, and R. Putz, "The effects of exercise on human articular cartilage," (in eng), *J Anat,* vol. 208, no. 4, pp. 491-512, Apr 2006, doi: 10.1111/j.1469-7580.2006.00546.x.

[27] S. M. Iqbal *et al.*, "Lubricin/Proteoglycan 4 binds to and regulates the activity of Toll-Like Receptors In Vitro," (in eng), *Sci Rep,* vol. 6, p. 18910, Jan 11 2016, doi: 10.1038/srep18910.

[28] G. Musumeci, F. M. Trovato, K. Pichler, A. M. Weinberg, C. Loreto, and P. Castrogiovanni, "Extra-virgin olive oil diet and mild physical activity prevent cartilage degeneration in an osteoarthritis model: an in vivo and in vitro study on lubricin expression," (in eng), *J Nutr Biochem,* vol. 24, no. 12, pp. 2064-75, Dec 2013.

[29] G. Musumeci *et al.*, "The effects of physical activity on apoptosis and lubricin expression in articular cartilage in rats with glucocorticoid-induced osteoporosis," (in eng), *J Bone Miner Metab,* vol. 31, no. 3, pp. 274-84, May 2013, doi: 10.1007/s00774-012-0414-9.

[30] J. P. Furia, D. M. Lintner, P. Saiz, H. W. Kohl, and P. Noble, "Isometry measurements in the knee with the anterior cruciate ligament intact, sectioned, and reconstructed," (in eng), *Am J Sports Med,* vol. 25, no. 3, pp. 346-52, May-Jun 1997, doi: 10.1177/036354659702500313.

[31] M. Dienst, R. T. Burks, P. E. Greis, and patrick.greis@hsc.utah.edu, "Anatomy and biomechanics of the anterior cruciate ligament," (in English), *Orthopedic Clinics,* vol. 33, no. 4, pp. 605-620, 2002/10/01 2002, doi: 10.1016/S0030-5898(02)00010-X.

[32] E. White *et al.*, "Cruciate ligament avulsion fractures: Anatomy, biomechanics, injury patterns, and approach to management," *A Journal of Practical Imaging Official Journal of the American Society of Emergency Radiology,* vol. 20, no. 5, pp. 429-440, 2013, doi: 10.1007/s10140-013-1121-0.

[33] T. D. Brown, R. C. Johnston, C. L. Saltzman, J. L. Marsh, and J. A. Buckwalter, "Posttraumatic osteoarthritis: A first estimate of incidence, prevalence, and burden of disease," vol. 20, ed, 2006, pp. 739-748.

[34] S. G. Muthuri, D. F. McWilliams, M. Doherty, and W. Zhang, "History of knee injuries and knee osteoarthritis: a meta-analysis of observational studies," *Osteoarthritis and Cartilage,* vol. 19, no. 11, pp. 1286-1293, 2011, doi: 10.1016/j.joca.2011.07.015.

[35] A. Hart, J. Buscombe, A. Malone, and G. Dowd, "Assessment of osteoarthritis after reconstruction of the anterior cruciate ligament - A study using single-photon emission computed tomography at ten years," *J. Bone Joint Surg.-Br. Vol.,* vol. 87B, no. 11, pp. 1483-1487, 2005, doi: 10.1302/0301-620X.87B11.16138.

[36] B. Lebel, C. Hulet, B. Galaud, G. Burdin, B. Locker, and C. Vielpeau, "Arthroscopic Reconstruction of the Anterior Cruciate Ligament Using Bone-Patellar Tendon-Bone Autograft," *The American Journal of Sports Medicine,* vol. 36, no. 7, pp. 1275-1282, 2008, doi: 10.1177/0363546508314721.

[37] P. Neuman, M. Englund, I. Kostogiannis, T. Friden, H. Roos, and L. E. Dahlberg, "Prevalence of Tibiofemoral Osteoarthritis 15 Years after Nonoperative Treatment of Anterior Cruciate Ligament Injury," *The American Journal of Sports Medicine,* vol. 36, no. 9, pp. 1717-1725, 2008, doi: 10.1177/0363546508316770.

[38] H. Wu, T. Hackett, and J. C. Richmond, "Effects of meniscal and articular surface status on knee stability, function, and symptoms after anterior cruciate ligament reconstruction: A long-term prospective study," *American Journal of Sports Medicine,* vol. 30, no. 6, pp. 845-850, 2002, doi: 10.1177/03635465020300061501.

[39] A. Meunier, M. Good, L. Odensten, and L. Meunier, "Long-term results after primary repair or non-surgical treatment of anterior cruciate ligament rupture: A randomized study with a 15-year follow-up," *Scandinavian Journal of Medicine and Science in Sports,* vol. 17, no. 3, pp. 230-237, 2007, doi: 10.1111/j.1600-0838.2006.00547.x.

[40] B. T. Hanypsiak *et al.*, "Twelve-year follow-up on anterior cruciate ligament reconstruction: long-term outcomes of prospectively studied osseous and articular

injuries," *The American journal of sports medicine,* vol. 36, no. 4, p. 671, 2008, doi: 10.1177/0363546508315468.

[41] H. C. Smith *et al.*, "Risk factors for anterior cruciate ligament injury: a review of the literature-part 2: hormonal, genetic, cognitive function, previous injury, and extrinsic risk factors," (in eng), *Sports Health,* vol. 4, no. 2, pp. 155-61, Mar 2012, doi: 10.1177/1941738111428282.

[42] P. Sward, T. Friden, T. Boegard, I. Kostogiannis, P. Neuman, and H. Roos, "Association between varus alignment and post-traumatic osteoarthritis after anterior cruciate ligament injury," (in eng), *Knee Surg Sports Traumatol Arthrosc,* vol. 21, no. 9, pp. 2040-7, Sep 2013, doi: 10.1007/s00167-013-2550-8.

[43] A. Wang *et al.*, "MR T1rho and T2 of meniscus after acute anterior cruciate ligament injuries," (in eng), *Osteoarthritis Cartilage,* vol. 24, no. 4, pp. 631-9, Apr 2016, doi: 10.1016/j.joca.2015.11.012.

[44] H. P. Jones, R. C. Appleyard, S. Mahajan, and G. A. Murrell, "Meniscal and chondral loss in the anterior cruciate ligament injured knee," (in eng), *Sports Med,* vol. 33, no. 14, pp. 1075-89, 2003.

[45] J. Noble and D. L. Hamblen, "The pathology of the degenerate meniscus lesion," *Journal of Bone and Joint Surgery - Series B,* vol. 57, no. 2, pp. 180-186, 1975, doi: 10.1302/0301-620X.57B2.180.

[46] C. Cooper *et al.*, "Mechanical and constitutional risk factors for symptomatic knee osteoarthritis: differences between medial tibiofemoral and patellofemoral disease," *The Journal of rheumatology,* vol. 21, no. 2, p. 307, 1994.

[47] L. D. Bennett and J. C. BucklandWright, "Meniscal and articular cartilage changes in knee osteoarthritis a crosssectional doublecontrast macroradiographic study," *Rheumatology,* vol. 41, no. 8, pp. 917-923, 2002, doi: 10.1093/rheumatology/41.8.917.

[48] H. Lorenz, W. Wenz, M. Ivancic, E. Steck, and W. Richter, "Early and stable upregulation of collagen type II, collagen type I and YKL40 expression levels in cartilage during early experimental osteoarthritis occurs independent of joint location and histological grading," *Arthritis Research & Therapy,* vol. 7, no. 1, pp. R156-R165, 2005, doi: 10.1186/ar1471.

[49] C. McDevitt, E. Gilbertson, and H. Muir, "An experimental model of osteoarthritis; early morphological and biochemical changes," *Journal of Bone and Joint Surgery - Series B,* vol. 59, no. 1, pp. 24-35, 1977, doi: 10.1302/0301-620X.59B1.576611.

[50] M. E. Adams and K. D. Brandt, "Hypertrophic repair of canine articular cartilage in osteoarthritis after anterior cruciate ligament transection," *The Journal of rheumatology,* vol. 18, no. 3, p. 428, 1991.

[51] A. J. Bollet and J. L. Nance, "Biochemical Findings in Normal and Osteoarthritic Articular Cartilage. II. Chondroitin Sulfate Concentration and Chain Length, Water, and Ash Content," *The Journal of clinical investigation,* vol. 45, no. 7, p. 1170, 1966, doi: 10.1172/JCI105423.

[52] M. Englund, A. Guermazi, and L. S. Lohmander, "The Meniscus in Knee Osteoarthritis," *Rheumatic Disease Clinics of North America,* vol. 35, no. 3, pp. 579-590, 2009, doi: 10.1016/j.rdc.2009.08.004.

[53] M. Englund *et al.*, "Meniscal tear in knees without surgery and the development of radiographic osteoarthritis among middle-aged and elderly persons: The multicenter osteoarthritis study," *Arthritis & Rheumatism,* vol. 60, no. 3, pp. 831-839, 2009, doi: 10.1002/art.24383.

[54] M. Englund, "The Role of the Meniscus in Osteoarthritis Genesis," *Rheumatic Disease Clinics of North America,* vol. 34, no. 3, pp. 573-579, 2008, doi: 10.1016/j.rdc.2008.05.009.
[55] C. Ding *et al.*, "Meniscal tear as an osteoarthritis risk factor in a largely non-osteoarthritic cohort: a cross-sectional study," *The Journal of rheumatology,* vol. 34, no. 4, p. 776, 2007.
[56] C. Pauli *et al.*, "Macroscopic and histopathologic analysis of human knee menisci in aging and osteoarthritis," *Osteoarthritis and Cartilage,* vol. 19, no. 9, pp. 1132-1141, 2011, doi: 10.1016/j.joca.2011.05.008.
[57] J. S. Lawrence, "The Epidemiology of Chronic Rheumatism," *Annals of the Rheumatic Diseases,* vol. 23, no. 1, p. 81, 1964, doi: 10.1136/ard.23.1.81-b.
[58] J. H. Kellgren and J. S. Lawrence, "Radiological Assessment of Osteo-Arthrosis," *Annals of the Rheumatic Diseases,* vol. 16, no. 4, p. 494, 1957, doi: 10.1136/ard.16.4.494.
[59] M. Hannan, D. Felson, and T. Pincus, "Analysis of the discordance between radiographic changes and knee pain in osteoarthritis of the knee," *J. Rheumatol.,* vol. 27, no. 6, pp. 1513-1517, 2000.
[60] N. Klocke *et al.*, "Comparison of T1ρ, dGEMRIC, and Quantitative T2 MRI in Pre-Operative ACL Rupture Patients," (in eng), *Acad Radiol,* vol. 20, no. 1, pp. 99-107, Jan 2013, doi: 10.1016/j.acra.2012.07.009.
[61] T. C. Dunn, Y. Lu, H. Jin, M. D. Ries, and S. Majumdar, "T2 relaxation time of cartilage at MR imaging: Comparison with severity of knee osteoarthritis," *Radiology,* vol. 232, no. 2, pp. 592-598, 2004, doi: 10.1148/radiol.2322030976.
[62] K. E. Keenan *et al.*, "Prediction of glycosaminoglycan content in human cartilage by age, T1ρ and T2 MRI," *Osteoarthritis and Cartilage,* vol. 19, no. 2, pp. 171-179, 2011, doi: 10.1016/j.joca.2010.11.009.
[63] I. Rauscher *et al.*, "Meniscal measurements of T1rho and T2 at MR imaging in healthy subjects and patients with osteoarthritis," (in eng), *Radiology,* vol. 249, no. 2, pp. 591-600, Nov 2008, doi: 10.1148/radiol.2492071870.
[64] H. Nishioka *et al.*, "T1ρ and T2 mapping reveal the in vivo extracellular matrix of articular cartilage," *Journal of Magnetic Resonance Imaging,* vol. 35, no. 1, pp. 147-155, 2012, doi: 10.1002/jmri.22811.
[65] M. Venn and A. Maroudas, "Chemical composition and swelling of normal and osteoarthrotic femoral head cartilage. I. Chemical composition," *Annals of the Rheumatic Diseases,* vol. 36, no. 2, p. 121, 1977, doi: 10.1136/ard.36.2.121.
[66] A. P. Prasad, L. Nardo, J. Schooler, G. B. Joseph, and T. M. Link, "T 1ρ and T 2 relaxation times predict progression of knee osteoarthritis," *Osteoarthritis and Cartilage,* vol. 21, no. 1, pp. 69-76, 2013, doi: 10.1016/j.joca.2012.09.011.
[67] A. Van Ginckel, P. Verdonk, J. M. K. Victor, and E. Witvrouw, "Cartilage Status in Relation to Return to Sports After Anterior Cruciate Ligament Reconstruction," vol. 29, ed, 2013, pp. e112-e112.
[68] X. Li *et al.*, "In vivo T(1rho) and T(2) mapping of articular cartilage in osteoarthritis of the knee using 3 T MRI," (in eng), *Osteoarthritis Cartilage,* vol. 15, no. 7, pp. 789-97, Jul 2007, doi: 10.1016/j.joca.2007.01.011.
[69] K. K. Hovis *et al.*, "Non-traumatic anterior cruciate ligament abnormalities and their relationship to osteoarthritis using morphological grading and cartilage T2 relaxation times: data from the Osteoarthritis Initiative (OAI)," (in eng), *Skeletal Radiol,* vol. 41, no. 11, pp. 1435-43, Nov 2012, doi: 10.1007/s00256-012-1379-4.

[70] V. Pedoia, X. Li, F. Su, N. Calixto, and S. Majumdar, "Fully automatic analysis of the knee articular cartilage T1rho relaxation time using voxel-based relaxometry," (in eng), *J Magn Reson Imaging,* vol. 43, no. 4, pp. 970-80, Apr 2016, doi: 10.1002/jmri.25065.

[71] "Whole-Organ Magnetic Resonance Imaging Score (WORMS) of the knee in osteoarthritis - ScienceDirect." http://www.sciencedirect.com/science/article/pii/S1063458403002917 (accessed.

[72] X. Li *et al.*, "Simultaneous acquisition of T1rho and T2 quantification in knee cartilage: repeatability and diurnal variation," (in eng), *J Magn Reson Imaging,* vol. 39, no. 5, pp. 1287-93, May 2014, doi: 10.1002/jmri.24253.

[73] T. J. Mosher *et al.*, "Knee articular cartilage damage in osteoarthritis: analysis of MR image biomarker reproducibility in ACRIN-PA 4001 multicenter trial," (in eng), *Radiology,* vol. 258, no. 3, pp. 832-42, Mar 2011, doi: 10.1148/radiol.10101174.

[74] C. Glaser *et al.*, "Global and regional reproducibility of T2 relaxation time measurements in human patellar cartilage," (in eng), *Magn Reson Med,* vol. 56, no. 3, pp. 527-34, Sep 2006, doi: 10.1002/mrm.21005.

[75] C. D. Jordan *et al.*, "Variability of CubeQuant T1rho, Quantitative DESS T2, and Cones Sodium MRI in Knee Cartilage," (in eng), *Osteoarthritis Cartilage,* vol. 22, no. 10, pp. 1559-67, Oct 2014, doi: 10.1016/j.joca.2014.06.001.

[76] S. J. Matzat, E. J. McWalter, F. Kogan, W. Chen, and G. E. Gold, "T2 Relaxation time quantitation differs between pulse sequences in articular cartilage," (in eng), *J Magn Reson Imaging,* vol. 42, no. 1, pp. 105-13, Jul 2015, doi: 10.1002/jmri.24757.

[77] A. Prasad, L. Nardo, J. Schooler, G. Joseph, and T. Link, "T1ρ and T2 relaxation times predict progression of knee osteoarthritis," (in eng), *Osteoarthritis Cartilage,* vol. 21, no. 1, pp. 69-76, Jan 2013, doi: 10.1016/j.joca.2012.09.011.

[78] E. Staroswiecki, K. L. Granlund, M. T. Alley, G. E. Gold, and B. A. Hargreaves, "Simultaneous estimation of T(2) and apparent diffusion coefficient in human articular cartilage in vivo with a modified three-dimensional double echo steady state (DESS) sequence at 3 T," (in eng), *Magn Reson Med,* vol. 67, no. 4, pp. 1086-96, Apr 2012, doi: 10.1002/mrm.23090.

[79] R. R. Regatte, S. V. S. Akella, J. H. Lonner, J. B. Kneeland, and R. Reddy, "T1rho relaxation mapping in human osteoarthritis (OA) cartilage: comparison of T1rho with T2," *Journal of magnetic resonance imaging : JMRI,* vol. 23, no. 4, p. 547, 2006.

[80] V. C. Mow, M. H. Holmes, and W. Michael Lai, "Fluid transport and mechanical properties of articular cartilage: A review," *Journal of Biomechanics,* vol. 17, no. 5, pp. 377-394, 1984, doi: 10.1016/0021-9290(84)90031-9.

[81] V. C. Mow, S. C. Kuei, W. M. Lai, and C. G. Armstrong, "Biphasic creep and stress relaxation of articular cartilage in compression? Theory and experiments," *Journal of biomechanical engineering,* vol. 102, no. 1, p. 73, 1980.

[82] T. Nishii, K. Kuroda, Y. Matsuoka, T. Sahara, and H. Yoshikawa, "Change in knee cartilage T2 in response to mechanical loading," *Journal of Magnetic Resonance Imaging,* vol. 28, no. 1, pp. 175-180, 2008, doi: 10.1002/jmri.21418.

[83] E. Schoenbauer *et al.*, "Cartilage evaluation with biochemical MR imaging using in vivo Knee compression at 3 T-comparison of patients after cartilage repair with healthy volunteers," *Journal of Biomechanics,* vol. 48, no. 12, pp. 3349-3355, 2015, doi: 10.1016/j.jbiomech.2015.06.016.

[84] C. G. Armstrong and V. C. Mow, "Variations in the intrinsic mechanical properties of human articular cartilage with age, degeneration, and water content," *The Journal of bone and joint surgery. American volume,* vol. 64, no. 1, p. 88, 1982, doi: 10.2106/00004623-198264010-00013.

[85] M. VC, "Structure and function of articular cartilage and meniscus.," in *Basic orthopedic biomechanics and mechanobiology.*, C. F. GU Wy, Ed., ed. Philadelphia: Lip-pincott Williams & Wilkins, 2005, pp. 181-237.

[86] D. Kumar, A. Kothari, R. B. Souza, S. Wu, C. B. Ma, and X. Li, "Frontal plane knee mechanics and medial cartilage MR relaxation times in individuals with ACL reconstruction : A pilot study," (in eng), *Knee,* vol. 21, no. 5, pp. 881-5, Oct 2014, doi: 10.1016/j.knee.2014.06.005.

[87] B. Haughom, W. Schairer, R. B. Souza, D. Carpenter, C. B. Ma, and X. Li, "Abnormal tibiofemoral kinematics following ACL reconstruction are associated with early cartilage matrix degeneration measured by MRI T1rho," (in eng), *Knee,* vol. 19, no. 4, pp. 482-7, Aug 2012, doi: 10.1016/j.knee.2011.06.015.

[88] A. E. Ellison and E. E. Berg, "Embryology, anatomy, and function of the anterior cruciate ligament," *The Orthopedic clinics of North America,* vol. 16, no. 1, p. 3, 1985.

[89] I. A. Kapandji, *The physiology of the joints*, 6th ed., English ed.. ed. Edinburgh ; New York: Edinburgh ; New York : Churchill Livingstone, 2007.

[90] J. M. Scarvell, P. N. Smith, K. M. Refshauge, H. R. Galloway, and K. R. Woods, "Association between abnormal kinematics and degenerative change in knees of people with chronic anterior cruciate ligament deficiency: a magnetic resonance imaging study," (in eng), *Aust J Physiother,* vol. 51, no. 4, pp. 233-40, 2005.

[91] J. M. Deneweth, M. J. Bey, S. G. McLean, T. R. Lock, P. A. Kolowich, and S. Tashman, "Tibiofemoral joint kinematics of the anterior cruciate ligament-reconstructed knee during a single-legged hop landing," *The American journal of sports medicine,* vol. 38, no. 9, p. 1820, 2010, doi: 10.1177/0363546510365531.

[92] L. E. DeFrate, R. Papannagari, T. J. Gill, J. M. Moses, N. P. Pathare, and G. Li, "The 6 degrees of freedom kinematics of the knee after anterior cruciate ligament deficiency: an in vivo imaging analysis.(Clinical report)," *The American Journal of Sports Medicine,* vol. 34, no. 8, p. 1240, 2006, doi: 10.1177/0363546506287299.

[93] G. Li, S. K. Van de Velde, and T. J. Gill, "Evaluation of kinematics of anterior cruciate ligament-deficient knees with use of advanced imaging techniques, three-dimensional modeling techniques, and robotics," *Journal of Bone and Joint Surgery,* vol. 91, no. Supplement 1, p. 108, 2009, doi: 10.2106/JBJS.H.01382.

[94] H. Mannel, F. Marin, L. Claes, and L. Dürselen, "Anterior cruciate ligament rupture translates the axes of motion within the knee," *Clinical biomechanics (Bristol, Avon),* vol. 19, no. 2, p. 130, 2004, doi: 10.1016/j.clinbiomech.2003.11.007.

[95] S. J. Shefelbine *et al.*, "MRI analysis of in vivo meniscal and tibiofemoral kinematics in ACL-deficient and normal knees," (in eng), *J Orthop Res,* vol. 24, no. 6, pp. 1208-17, Jun 2006, doi: 10.1002/jor.20139.

[96] A. D. Georgoulis, A. Papadonikolakis, C. D. Papageorgiou, A. Mitsou, and N. Stergiou, "Three-dimensional tibiofemoral kinematics of the anterior cruciate ligament-deficient and reconstructed knee during walking," vol. 31, ed, 2003, pp. 75-79.

[97] S. Brandsson, J. Karlsson, B. I. Eriksson, and J. Kärrholm, "Kinematics after tear in the anterior cruciate ligament: Dynamic bilateral radiostereometric studies in 11 patients,"

Acta Orthopaedica Scandinavica, vol. 72, no. 4, pp. 372-378, 2001, doi: 10.1080/000164701753542032.

[98] J. Waite, D. Beard, C. Dodd, D. Murray, and H. Gill, "In vivo kinematics of the ACL-deficient limb during running and cutting," *Knee Surgery, Sports Traumatology, Arthroscopy,* vol. 13, no. 5, pp. 377-384, 2005, doi: 10.1007/s00167-004-0569-6.

[99] W. L. Jenkins, S. W. Munns, G. Jayaraman, K. L. Wertzberger, and K. Neely, "A measurement of anterior tibial displacement in the closed and open kinetic chain," *Journal of Orthopaedic and Sports Physical Therapy,* vol. 25, no. 1, pp. 49-56, 1997, doi: 10.2519/jospt.1997.25.1.49.

[100] J. Dargel, M. Gotter, K. Mader, D. Pennig, J. Koebke, and R. Schmidt-Wiethoff, "Biomechanics of the anterior cruciate ligament and implications for surgical reconstruction," in *Strategies Trauma Limb Reconstr*, vol. 2, no. 1), 2007, pp. 1-12.

[101] B. Barenius, S. Ponzer, A. Shalabi, R. Bujak, L. Norlen, and K. Eriksson, "Increased risk of osteoarthritis after anterior cruciate ligament reconstruction: a 14-year follow-up study of a randomized controlled trial," (in eng), *Am J Sports Med,* vol. 42, no. 5, pp. 1049-57, May 2014, doi: 10.1177/0363546514526139.

[102] R. von Eisenhart-Rothe *et al.*, "Femoro-tibial and menisco-tibial translation patterns in patients with unilateral anterior cruciate ligament deficiency--a potential cause of secondary meniscal tears," (in eng), *J Orthop Res*, vol. 22, no. 2, pp. 275-82, Mar 2004, doi: 10.1016/j.orthres.2003.08.009.

[103] M. Logan, E. Dunstan, J. Robinson, A. Williams, W. Gedroyc, and M. Freeman, "Tibiofemoral kinematics of the anterior cruciate ligament (ACL)-deficient weightbearing, living knee employing vertical access open "interventional" multiple resonance imaging," (in eng), *Am J Sports Med,* vol. 32, no. 3, pp. 720-6, Apr-May 2004, doi: 10.1177/0095399703258771.

[104] J. M. Scarvell, P. N. Smith, K. M. Refshauge, H. R. Galloway, and K. R. Woods, "Comparison of kinematic analysis by mapping tibiofemoral contact with movement of the femoral condylar centres in healthy and anterior cruciate ligament injured knees," (in eng), *J Orthop Res,* vol. 22, no. 5, pp. 955-62, Sep 2004, doi: 10.1016/j.orthres.2003.12.016.

[105] A. G. d'Entremont and D. R. Wilson, "Joint mechanics measurement using magnetic resonance imaging," (in eng), *Top Magn Reson Imaging,* vol. 21, no. 5, pp. 325-34, Oct 2010, doi: 10.1097/RMR.0b013e31823fb2b9.

[106] G. Hares, J. Eschweiler, and K. Radermacher, "Combined magnetic resonance imaging approach for the assessment of in vivo knee joint kinematics under full weight-bearing conditions," *Proceedings of the Institution of Mechanical Engineers,* vol. 229, no. 6, p. 439, 2015, doi: 10.1177/0954411915585863.

[107] S. Tashman, D. Collon, K. Anderson, P. Kolowich, and W. Anderst, "Abnormal rotational knee motion during running after anterior cruciate ligament reconstruction," *Am. J. Sports Med.,* vol. 32, no. 4, pp. 975-983, 2004, doi: 10.1177/0363546503261709.

[108] E. J. McWalter, D. J. Hunter, and D. R. Wilson, "The effect of load magnitude on three-dimensional patellar kinematics in vivo," (in eng), *J Biomech,* vol. 43, no. 10, pp. 1890-7, Jul 20 2010, doi: 10.1016/j.jbiomech.2010.03.027.

[109] J. M. Scarvell, P. N. Smith, K. M. Refshauge, H. Galloway, and K. Woods, "Comparison of kinematics in the healthy and ACL injured knee using MRI," (in eng), *J Biomech,* vol. 38, no. 2, pp. 255-62, Feb 2005, doi: 10.1016/j.jbiomech.2004.02.012.

[110] F. T. Sheehan and J. E. Drace, "Quantitative MR measures of three-dimensional patellar kinematics as a research and diagnostic tool," (in eng), *Med Sci Sports Exerc,* vol. 31, no. 10, pp. 1399-405, Oct 1999, doi: 10.1097/00005768-199910000-00007.

[111] A. J. Rebmann and F. T. Sheehan, "Precise 3D skeletal kinematics using fast phase contrast magnetic resonance imaging," (in eng), *J Magn Reson Imaging,* vol. 17, no. 2, pp. 206-13, Feb 2003, doi: 10.1002/jmri.10253.

[112] J. M. Scarvell, P. N. Smith, K. M. Refshauge, and H. R. Galloway, "Magnetic Resonance Imaging Analysis of Kinematics in Osteoarthritic Knees," *The Journal of Arthroplasty,* vol. 22, no. 3, pp. 383-393, 2007, doi: 10.1016/j.arth.2006.06.006.

[113] H. N. Chen, K. Yang, Q. R. Dong, and Y. Wang, "Assessment of tibial rotation and meniscal movement using kinematic magnetic resonance imaging," *Journal of Orthopaedic Surgery and Research,* vol. 9, no. 1, p. <xocs:firstpage xmlns:xocs=""/>, 2014, doi: 10.1186/s13018-014-0065-8.

[114] S. Brandsson, J. Karlsson, L. Swärd, J. Kartus, B. I. Eriksson, and J. Kärrholm, "Kinematics and laxity of the knee joint after anterior cruciate ligament reconstruction. Pre- and postoperative radiostereometric studies," *American Journal of Sports Medicine,* vol. 30, no. 3, pp. 361-367, 2002, doi: 10.1177/03635465020300031001.

[115] H. Jonsson, J. Kärrholm, and L. G. Elmqvist, "Kinematics of active knee extension after tear of the anterior cruciate ligament," *The American journal of sports medicine,* vol. 17, no. 6, p. 796, 1989, doi: 10.1177/036354658901700613.

[116] E. S. Grood and W. J. Suntay, "A joint coordinate system for the clinical description of three-dimensional motions: application to the knee," (in eng), *J Biomech Eng,* vol. 105, no. 2, pp. 136-44, May 1983.

[117] B. A. MacWilliams and R. B. Davis, "Addressing some misperceptions of the joint coordinate system," (in eng), *J Biomech Eng,* vol. 135, no. 5, p. 54506, May 2013, doi: 10.1115/1.4024142.

[118] G. Wu *et al.*, "ISB recommendation on definitions of joint coordinate system of various joints for the reporting of human joint motion--part I: ankle, hip, and spine. International Society of Biomechanics," in *J Biomech*, vol. 35, no. 4). United States, 2002, pp. 543-8.

[119] D. L. Churchill, S. J. Incavo, C. C. Johnson, and B. D. Beynnon, "The transepicondylar axis approximates the optimal flexion axis of the knee," (in eng), *Clin Orthop Relat Res,* no. 356, pp. 111-8, Nov 1998, doi: 10.1097/00003086-199811000-00016.

[120] M. Stokdijk, M. Biegstraaten, W. Ormel, Y. A. de Boer, H. E. Veeger, and P. M. Rozing, "Determining the optimal flexion-extension axis of the elbow in vivo - a study of interobserver and intraobserver reliability," (in eng), *J Biomech,* vol. 33, no. 9, pp. 1139-45, Sep 2000, doi: 10.1016/s0021-9290(00)00079-8.

[121] N. M. Lenz, A. Mane, L. P. Maletsky, and N. A. Morton, "The effects of femoral fixed body coordinate system definition on knee kinematic description," (in eng), *J Biomech Eng,* vol. 130, no. 2, p. 021014, Apr 2008, doi: 10.1115/1.2898713.

[122] R. M. Ehrig, W. R. Taylor, G. N. Duda, and M. O. Heller, "A survey of formal methods for determining functional joint axes," (in eng), *J Biomech,* vol. 40, no. 10, pp. 2150-7, 2007, doi: 10.1016/j.jbiomech.2006.10.026.

[123] T. F. Besier, D. L. Sturnieks, J. A. Alderson, and D. G. Lloyd, "Repeatability of gait data using a functional hip joint centre and a mean helical knee axis," (in eng), *J Biomech,* vol. 36, no. 8, pp. 1159-68, Aug 2003, doi: 10.1016/s0021-9290(03)00087-3.

[124] R. Stagni, A. Leardini, A. Cappozzo, M. Grazia Benedetti, and A. Cappello, "Effects of hip joint centre mislocation on gait analysis results," (in eng), *J Biomech,* vol. 33, no. 11, pp. 1479-87, Nov 2000, doi: 10.1016/s0021-9290(00)00093-2.

[125] P. Bulgheroni, M. V. Bulgheroni, L. Andrini, P. Guffanti, and A. Giughello, "Gait patterns after anterior cruciate ligament reconstruction," *Knee Surgery, Sports Traumatology, Arthroscopy,* vol. 5, no. 1, pp. 14-21, 1997, doi: 10.1007/s001670050018.

[126] Z. Knoll, L. Kocsis, and R. Kiss, "Gait patterns before and after anterior cruciate ligament reconstruction," *Knee Surgery, Sports Traumatology, Arthroscopy,* vol. 12, no. 1, pp. 7-14, 2004, doi: 10.1007/s00167-003-0440-1.

[127] A. Gokeler, T. Schmalz, E. Knopf, J. Freiwald, and S. Blumentritt, "The relationship between isokinetic quadriceps strength and laxity on gait analysis parameters in anterior cruciate ligament reconstructed knees," *Knee Surgery, Sports Traumatology, Arthroscopy,* vol. 11, no. 6, pp. 372-378, 2003, doi: 10.1007/s00167-003-0432-1.

[128] G. Vairo, J. Myers, T. Sell, F. Fu, C. Harner, and S. Lephart, "Neuromuscular and biomechanical landing performance subsequent to ipsilateral semitendinosus and gracilis autograft anterior cruciate ligament reconstruction," *Knee Surgery, Sports Traumatology, Arthroscopy,* vol. 16, no. 1, pp. 2-14, 2008, doi: 10.1007/s00167-007-0427-4.

[129] A. Porat, M. Henriksson, E. Holmström, C. Thorstensson, L. Mattsson, and E. Roos, "Knee kinematics and kinetics during gait, step and hop in males with a 16 years old ACL injury compared with matched controls," *Knee Surgery, Sports Traumatology, Arthroscopy,* vol. 14, no. 6, pp. 546-554, 2006, doi: 10.1007/s00167-006-0071-4.

[130] S. Ristanis, G. Giakas, C. Papageorgiou, T. Moraiti, N. Stergiou, and A. Georgoulis, "The effects of anterior cruciate ligament reconstruction on tibial rotation during pivoting after descending stairs," *Knee Surgery, Sports Traumatology, Arthroscopy,* vol. 11, no. 6, pp. 360-365, 2003, doi: 10.1007/s00167-003-0428-x.

[131] S. Ristanis, N. Stergiou, K. Patras, H. S. Vasiliadis, G. Giakas, and A. D. Georgoulis, "Excessive Tibial Rotation During High-Demand Activities Is Not Restored by Anterior Cruciate Ligament Reconstruction.(Report)," *Arthroscopy: The Journal of Arthroscopic and Related Surgery,* vol. 21, no. 11, p. 1323, 2005, doi: 10.1016/j.arthro.2005.08.032.

[132] T. E. Hewett *et al.*, "Biomechanical measures of neuromuscular control and valgus loading of the knee predict anterior cruciate ligament injury risk in female athletes: a prospective study," *The American journal of sports medicine,* vol. 33, no. 4, p. 492, 2005, doi: 10.1177/0363546504269591.

[133] F. R. Noyes, O. D. Schipplein, T. P. Andriacchi, S. R. Saddemi, and M. Weise, "The anterior cruciate ligament-deficient knee with varus alignment. An analysis of gait adaptations and dynamic joint loadings," *The American journal of sports medicine,* vol. 20, no. 6, p. 707, 1992, doi: 10.1177/036354659202000612.

[134] C. L. Ardern, K. E. Webster, N. F. Taylor, and J. A. Feller, "Return to the preinjury level of competitive sport after anterior cruciate ligament reconstruction surgery: two-thirds of patients have not returned by 12 months after surgery.(Clinical report)," *The American Journal of Sports Medicine,* vol. 39, no. 3, p. 538, 2011, doi: 10.1177/0363546510384798.

[135] C. Hui, L. J. Salmon, A. Kok, S. Maeno, J. Linklater, and L. A. Pinczewski, "Fifteen-year outcome of endoscopic anterior cruciate ligament reconstruction with patellar tendon autograft for "isolated" anterior cruciate ligament tear," *The American journal of sports medicine,* vol. 39, no. 1, p. 89, 2011, doi: 10.1177/0363546510379975.

[136] F. Su *et al.*, "Cartilage morphology and T1rho and T2 quantification in ACL-reconstructed knees: a 2-year follow-up," (in eng), *Osteoarthritis Cartilage,* vol. 21, no. 8, pp. 1058-67, Aug 2013, doi: 10.1016/j.joca.2013.05.010.

[137] H. G. Potter, S. K. Jain, Y. Ma, B. R. Black, S. Fung, and S. Lyman, "Cartilage injury after acute, isolated anterior cruciate ligament tear: immediate and longitudinal effect with clinical/MRI follow-up," (in eng), *Am J Sports Med,* vol. 40, no. 2, pp. 276-85, Feb 2012, doi: 10.1177/0363546511423380.

[138] E. N. Chua *et al.*, "Motion Task Selection for Kinematic Evaluation After Anterior Cruciate Ligament Reconstruction: A Systematic Review," *Arthroscopy: The Journal of Arthroscopic and Related Surgery,* vol. 32, no. 7, pp. 1453-1465, 2016, doi: 10.1016/j.arthro.2016.01.057.

[139] D. L. Benoit, D. K. Ramsey, M. Lamontagne, L. Xu, P. Wretenberg, and P. Renstrom, "Effect of skin movement artifact on knee kinematics during gait and cutting motions measured in vivo," (in eng), *Gait Posture,* vol. 24, no. 2, pp. 152-64, Oct 2006, doi: 10.1016/j.gaitpost.2005.04.012.

[140] J. L. McGinley, R. Baker, R. Wolfe, and M. E. Morris, "The reliability of three-dimensional kinematic gait measurements: A systematic review," *Gait & Posture,* vol. 29, no. 3, pp. 360-369, 2009, doi: 10.1016/j.gaitpost.2008.09.003.

[141] S. M. Robbins, J. L. Astephen Wilson, D. J. Rutherford, and C. L. Hubley-Kozey, "Reliability of principal components and discrete parameters of knee angle and moment gait waveforms in individuals with moderate knee osteoarthritis," (in eng), *Gait Posture,* vol. 38, no. 3, pp. 421-7, Jul 2013, doi: 10.1016/j.gaitpost.2013.01.001.

[142] M. P. Kadaba, H. K. Ramakrishnan, M. E. Wootten, J. Gainey, G. Gorton, and G. V. B. Cochran, "Repeatability of kinematic, kinetic, and electromyographic data in normal adult gait," *Journal of Orthopaedic Research,* vol. 7, no. 6, pp. 849-860, 1989, doi: 10.1002/jor.1100070611.

[143] M. L. van der Linden, P. J. Rowe, and R. W. Nutton, "Between-day repeatability of knee kinematics during functional tasks recorded using flexible electrogoniometry," (in eng), *Gait Posture,* vol. 28, no. 2, pp. 292-6, Aug 2008, doi: 10.1016/j.gaitpost.2008.01.009.

[144] L. Scheys *et al.*, "Three-dimensional knee kinematics by conventional gait analysis for eleven motor tasks of daily living: typical patterns and repeatability," (in eng), *J Appl Biomech,* vol. 29, no. 2, pp. 214-28, Apr 2013, doi: 10.1123/jab.29.2.214.

[145] A. Protopapadaki, W. I. Drechsler, M. C. Cramp, F. J. Coutts, and O. M. Scott, "Hip, knee, ankle kinematics and kinetics during stair ascent and descent in healthy young individuals," (in eng), *Clin Biomech (Bristol, Avon),* vol. 22, no. 2, pp. 203-10, Feb 2007, doi: 10.1016/j.clinbiomech.2006.09.010.

[146] M. HAJIZADEH, A. H. OSKOUEI, F. GHALICHI, and G. SOLE, "INTRA-SESSION RELIABILITY AND REPEATABILITY OF KNEE KINEMATICS IN SUBJECTS WITH ACL DEFICIENCY DURING STAIR ASCENT," (in en), *https://doi.org/10.1142/S0219519417500920*, research-article 2017-09-28 2017, doi: 10.1142/S0219519417500920.

[147] P. A. Costigan, K. J. Deluzio, and U. P. Wyss, "Knee and hip kinetics during normal stair climbing," (in eng), *Gait Posture,* vol. 16, no. 1, pp. 31-7, Aug 2002, doi: 10.1016/s0966-6362(01)00201-6.

[148] W. Gilleard, J. Crosbie, and R. Smith, "Rising to stand from a chair: symmetry, and frontal and transverse plane kinematics and kinetics," (in eng), *Gait Posture,* vol. 27, no. 1, pp. 8-15, Jan 2008, doi: 10.1016/j.gaitpost.2006.11.002.

[149] D. Suriyaamarit and S. Boonyong, "Mechanical work, kinematics, and kinetics during sit-to-stand in children with and without spastic diplegic cerebral palsy," (in eng), *Gait Posture,* vol. 67, pp. 85-90, Jan 2019, doi: 10.1016/j.gaitpost.2018.09.030.

[150] F. Alenezi, L. Herrington, P. Jones, and R. Jones, "The reliability of biomechanical variables collected during single leg squat and landing tasks," (in eng), *J Electromyogr Kinesiol,* vol. 24, no. 5, pp. 718-21, Oct 2014, doi: 10.1016/j.jelekin.2014.07.007.

[151] D. M. Hooper, M. C. Morrissey, W. I. Drechsler, N. C. Clark, F. J. Coutts, and T. B. McAuliffe, "Gait analysis 6 and 12 months after anterior cruciate ligament reconstruction surgery," (in eng), *Clin Orthop Relat Res,* no. 403, pp. 168-78, Oct 2002, doi: 10.1097/00003086-200210000-00025.

[152] M. Spanjaard, N. D. Reeves, J. H. van Dieen, V. Baltzopoulos, and C. N. Maganaris, "Lower-limb biomechanics during stair descent: influence of step-height and body mass," (in eng), *J Exp Biol,* vol. 211, no. Pt 9, pp. 1368-75, May 2008, doi: 10.1242/jeb.014589.

[153] A. H, "Multiple Correlation Coefficient," in *Enccyclopedia of measurement and statistics*, S. NJ, Ed., ed, pp. 648 -651.

[154] K. K. Itoh C., Wakayama S., "Comparison of intraclass correlation coefficient and the coefficient of multiple correlation in the reliability of gait analysis - Physiotherapy," *Physiotherapy,* vol. 102, no. S1, 1, p. e83, 2016, doi: doi:10.1016/j.physio.2016.10.082.

[155] G. SM, M. SW, H. PA, and B. L, "Incidence of anterior cruciate ligament injury and other knee ligament injuries: a national population-based study," *Journal of science and medicine in sport,* vol. 12, no. 6, 2009 Nov 2009, doi: 10.1016/j.jsams.2008.07.005.

[156] D. WR and S. KP, "Predictors of activity level 2 years after anterior cruciate ligament reconstruction (ACLR): a Multicenter Orthopaedic Outcomes Network (MOON) ACLR cohort study," *The American journal of sports medicine,* vol. 38, no. 10, 2010 Oct 2010, doi: 10.1177/0363546510370280.

[157] W. J. Hurd, M. J. Axe, and L. Snyder-Mackler, "Influence of Age, Gender, and Injury Mechanism on the Development of Dynamic Knee Stability After Acute ACL Rupture," (in eng), *J Orthop Sports Phys Ther,* vol. 38, no. 2, pp. 36-41, Feb 2008, doi: 10.2519/jospt.2008.2609.

[158] B. RH *et al.,* "Return to play and future ACL injury risk after ACL reconstruction in soccer athletes from the Multicenter Orthopaedic Outcomes Network (MOON) group," *The American journal of sports medicine,* vol. 40, no. 11, 2012 Nov 2012, doi: 10.1177/0363546512459476.

[159] S. KD, G. T, and H. M, "Incidence of subsequent injury to either knee within 5 years after anterior cruciate ligament reconstruction with patellar tendon autograft," *The American journal of sports medicine,* vol. 37, no. 2, 2009 Feb 2009, doi: 10.1177/0363546508325665.

[160] D. S. S, H. EH, and S.-M. L, "Sex-specific gait adaptations prior to and up to 6 months after anterior cruciate ligament reconstruction," *The Journal of orthopaedic and sports physical therapy,* vol. 45, no. 3, 2015 Mar 2015, doi: 10.2519/jospt.2015.5062.

[161] K. D *et al.,* "Are There Sex Differences in Knee Cartilage Composition and Walking Mechanics in Healthy and Osteoarthritis Populations?," *Clinical orthopaedics and related research,* vol. 473, no. 8, 2015 Aug 2015, doi: 10.1007/s11999-015-4212-2.

[162] M. A. Samaan *et al.*, "Cyclops lesions are associated with altered gait patterns and medial knee joint cartilage degeneration at 1 year after ACL-reconstruction," (in eng), *J Orthop Res*, vol. 35, no. 10, pp. 2275-2281, Oct 2017, doi: 10.1002/jor.23530.
[163] H. L. Teng *et al.*, "Gait Characteristics Associated With a Greater Increase in Medial Knee Cartilage T1rho and T2 Relaxation Times in Patients Undergoing Anterior Cruciate Ligament Reconstruction," (in eng), *Am J Sports Med*, vol. 45, no. 14, pp. 3262-3271, Dec 2017, doi: 10.1177/0363546517723007.
[164] D. Kumar *et al.*, "Frontal Plane Knee Mechanics and Early Cartilage Degeneration in People With Anterior Cruciate Ligament Reconstruction: A Longitudinal Study," (in eng), *Am J Sports Med*, vol. 46, no. 2, pp. 378-387, Feb 2018, doi: 10.1177/0363546517739605.
[165] M. Zaid *et al.*, "Abnormal tibial position is correlated to early degenerative changes one year following ACL reconstruction," *Journal of Orthopaedic Research*, vol. 33, no. 7, pp. 1079-1086, 2015, doi: 10.1002/jor.22867.
[166] D. A. Lansdown *et al.*, "A comprehensive in vivo kinematic, quantitative MRI and functional evaluation following ACL reconstruction--A comparison between mini-two incision and anteromedial portal femoral tunnel drilling," (in eng), *Knee*, vol. 22, no. 6, pp. 547-53, Dec 2015, doi: 10.1016/j.knee.2014.12.005.
[167] B. Sveinsson, A. Chaudhari, G. Gold, and B. Hargreaves, "A Simple Analytic Method for Estimating T2 in the Knee from DESS," (in eng), *Magn Reson Imaging*, vol. 38, pp. 63-70, May 2017, doi: 10.1016/j.mri.2016.12.018.
[168] J. F. O'Brien, R. E. Bodenheimer, Jr. (Bobby), G. J. Brostow, and J. K. Hodgins, "Automatic Joint Parameter Estimation from Magnetic Motion Capture Data," (in en_US), Technical Report 1999 1999, doi: http://hdl.handle.net/1853/3408.
[169] E. J. McWalter, C. M. O'Kane, D. P. Fitzpatrick, and D. R. Wilson, "Validation of an MRI-based method to assess patellofemoral joint contact areas in loaded knee flexion in vivo," (in eng), *J Magn Reson Imaging*, vol. 39, no. 4, pp. 978-87, Apr 2014, doi: 10.1002/jmri.24240.
[170] I. Soderkvist and P. A. Wedin, "Determining the movements of the skeleton using well-configured markers," (in eng), *J Biomech*, vol. 26, no. 12, pp. 1473-7, Dec 1993, doi: 10.1016/0021-9290(93)90098-y.
[171] H. N, P. G, V. d. P. M, S.-O. N, D. N, and d. G. J, "A Reproducible Method for Studying Three-Dimensional Knee Kinematics," *Journal of biomechanics*, vol. 38, no. 9, 2005 Sep 2005, doi: 10.1016/j.jbiomech.2005.05.013.
[172] C. Reinschmidt. "readme1.htm." Human Performance Laboratory, University of Calgary. https://isbweb.org/software/movanal/kinemat/ (accessed June 11, 2020).
[173] P. de Leva, "Adjustments to Zatsiorsky-Seluyanov's segment inertia parameters," (in eng), *J Biomech*, vol. 29, no. 9, pp. 1223-30, Sep 1996, doi: 10.1016/0021-9290(95)00178-6.
[174] T. H *et al.*, "Quantitative T2-Mapping and T2 ∗-Mapping Evaluation of Changes in Cartilage Matrix After Acute Anterior Cruciate Ligament Rupture and the Correlation Between the Results of Both Methods," *BioMed research international*, vol. 2018, 05/17/2018 2018, doi: 10.1155/2018/7985672.
[175] T. J. Mosher *et al.*, "Change in knee cartilage T2 at MR imaging after running: a feasibility study," (in eng), *Radiology*, vol. 234, no. 1, pp. 245-9, Jan 2005, doi: 10.1148/radiol.2341040041.
[176] J. M. Scarvell, P. N. Smith, K. M. Refshauge, H. R. Galloway, and K. R. Woods, "Association between abnormal kinematics and degenerative change in knees of people

with chronic anterior cruciate ligament deficiency: A magnetic resonance imaging study," *Australian Journal of Physiotherapy*, vol. 51, no. 4, pp. 233-240, 2005, doi: 10.1016/S0004-9514(05)70004-0.

[177] U. Della Croce, A. Leardini, L. Chiari, and A. Cappozzo, "Human movement analysis using stereophotogrammetry. Part 4: assessment of anatomical landmark misplacement and its effects on joint kinematics," (in eng), *Gait Posture*, vol. 21, no. 2, pp. 226-37, Feb 2005, doi: 10.1016/j.gaitpost.2004.05.003.

[178] J. P. Holden, W. S. Selbie, and S. J. Stanhope, "A proposed test to support the clinical movement analysis laboratory accreditation process," (in eng), *Gait Posture*, vol. 17, no. 3, pp. 205-13, Jun 2003, doi: 10.1016/s0966-6362(02)00088-7.

[179] D. Giavarina, "Understanding Bland Altman analysis," (in eng), *Biochem Med (Zagreb)*, vol. 25, no. 2, pp. 141-51, 2015, doi: 10.11613/bm.2015.015.

[180] A. Leardini, L. Chiari, U. Della Croce, and A. Cappozzo, "Human movement analysis using stereophotogrammetry. Part 3. Soft tissue artifact assessment and compensation," (in eng), *Gait Posture*, vol. 21, no. 2, pp. 212-25, Feb 2005, doi: 10.1016/j.gaitpost.2004.05.002.

[181] J. P. Holden and S. J. Stanhope, "The effect of variation in knee center location estimates on net knee joint moments," (in eng), *Gait Posture*, vol. 7, no. 1, pp. 1-6, Jan 1 1998, doi: 10.1016/s0966-6362(97)00026-x.

[182] A. Leardini *et al.*, "Validation of a functional method for the estimation of hip joint centre location," (in eng), *J Biomech*, vol. 32, no. 1, pp. 99-103, Jan 1999, doi: 10.1016/s0021-9290(98)00148-1.

[183] V. Camomilla, A. Cereatti, A. G. Cutti, S. Fantozzi, R. Stagni, and G. Vannozzi, "Methodological factors affecting joint moments estimation in clinical gait analysis: a systematic review," in *Biomed Eng Online*, vol. 16, 2017.

[184] J. Richards, J. Selfe, J. Sinclair, K. May, and G. Thomas, "The effect of different decline angles on the biomechanics of double limb squats and the implications to clinical and training practice," in *J Hum Kinet*, vol. 52, 2016, pp. 125-38.

[185] A. Salih and I. Simsek, *Comparative Kinesiology of the Human Body*. 2020.

[186] V. Juras *et al.*, "Kinematic biomechanical assessment of human articular cartilage transplants in the knee using 3-T MRI: an in vivo reproducibility study," (in eng), *Eur Radiol*, vol. 19, no. 5, pp. 1246-52, May 2009, doi: 10.1007/s00330-008-1242-0.

[187] T. J. Mosher and B. J. Dardzinski, "Cartilage MRI T2 relaxation time mapping: overview and applications," (in eng), *Semin Musculoskelet Radiol*, vol. 8, no. 4, pp. 355-68, Dec 2004, doi: 10.1055/s-2004-861764.

[188] S. Sánchez-García, C. García-Peña, M. X. Duque-López, T. Juárez-Cedillo, A. R. Cortés-Núñez, and S. Reyes-Beaman, "Anthropometric measures and nutritional status in a healthy elderly population," in *BMC Public Health*, vol. 7, 2007, p. 2.

[189] D. Winter, *Biomechanics and Motor Control of Human Movement, 4th Edition*, 4th Edition ed. Hoboken,NJ: John Wiley & Sons, Ltd, 2009, p. 384.

Appendix A: Methods Section – Supplementary Material

The figures below show supplementary data from the methods section.

A-1: Initial Designs for Loading Rig

As described in section 3.3, I led a team of summer students in the loading rig design process. In this process different loading rig designs were initially proposed. The figures A-1-1 – A-1-3 below show these different loading rig designs.

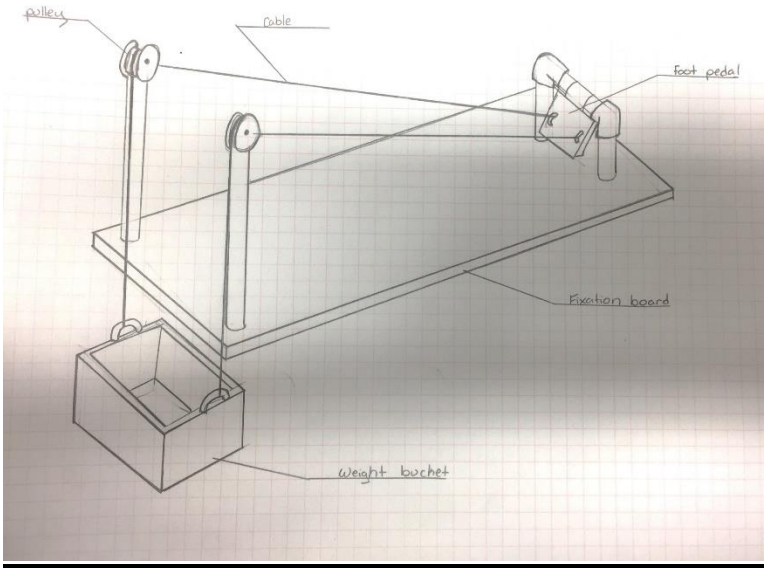

Figure A-1-1: 'SLIK' loading rig design by Chelsey Thorson and Madeline Martel

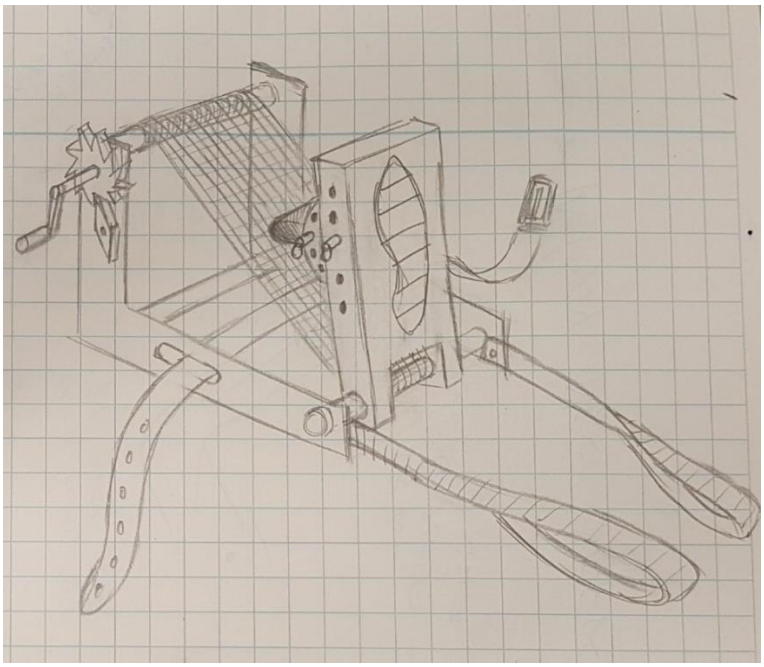

Figure A-1-2: 'Tennis Pedal' loading rig design by Alvaro Espinosa

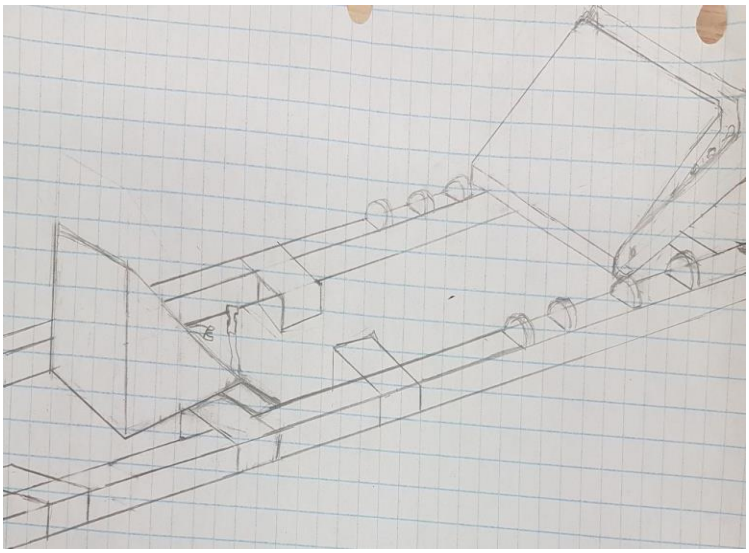

Figure A-1-3: 'Spring Adjustable Rig' loading rig design by Ibukun Elebute

A-2: Loading Rig Design

The rig was designed and constructed in order to study the knee in loaded flexion in the MRI. First, design constraints were identified. The four points considered were:

a) **Functionality:** The loading rig had to be able to generate between 20-30 percent of the individual's body weight at the knee. This load was chosen as tolerable to individuals with knee injury. It corresponds to loads experienced during the swing phase of gait. Further, lower loads are required in the supine position due to difficulty in maintaining loads in such a position as compared to standing. Our group has found that maintaining high loads in this position can result in motion artifacts in the MRI images; the 20-30% body weight load is manageable for individuals with knee injury or disease.

b) **Compatibility:** All materials used in the design of the loading rig had to be non-ferromagnetic and non-metallic. This is important both for safety in the MRI room and to ensure artifact free images.

c) **Compactness:** The MRI machine available for the purpose of this project was a short-bore Tesla system (MAGNETOM skyra, Siemens Healthcare, Erlangen, Germany). It was necessary to have a loading rig compact enough to be able to fit within the bore of the machine with enough clearance such that it would not disrupt the MRI table movement or make the participant uncomfortable.

d) **Simplicity:** A simple, stand-alone design that could be constructed would allow for easy storage and use in other MRI systems in the future if required.

Having all the above constraints in mind, several potential designs were drafted with the help of a team undergraduate summer students whom I led through the design process. After several design iterations (see Appendix A-1), a final decision was made based on how well it fit the design constraints. Figure A-2-1 below is a labeled image of the final design decision.

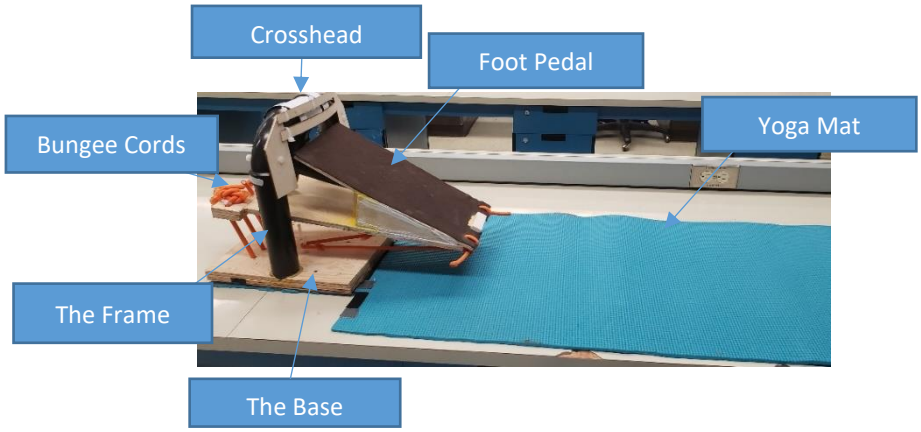

Figure A-2-1: Labelled MRI-safe loading Rig. When the foot is applied to the foot pedal, cross-head rotates around the frame, allowing the attached bungee cords, held down to the base, to be stretched hence causing resistance and force to be generated at the participant's knee.

Parts and Materials Used

As can be seen in Figure A-2-1 above, the loading rig structure was made of a foot pedal, a frame, a base, a rotating part, and springs (bungee cords).

a) Foot Pedal: The foot of the participant was placed on the pedal so that they can apply force to the loading rig. The foot pedal had a stopper at the base to ensure that the participant's heel does not slip off the bottom while applying the load. The pedal also had a base that extends to the back of the rig, with holes that allow the bungee cords to be attached to the base of the rig

b) Cross-head: The cross-head was used as a fulcrum to enable the applied load from the foot to be translated to the bungee cords. When the foot was applied to the pedal, the pedal rotates about the cross-head and then the bungee cords were stretched.

c) **Frame:** The frame contained the cross-head and side supports and provides overall structure to the rig.

d) **Base:** This part of the rig acted as a platform to contain the frame and also acted as an attachment to the yoga mat (6mm blue yoga mat, Renew) used to keep the participant in place. Holes were made on the base help to keep the frame in place. With attachment strips (Velcro, 10lb industrial strength strips) applied to the bottom of the base, the loading rig could be attached to the yoga mat. With this in place, the participant could lie on the yoga mat and apply force to the loading rig without the loading rig slipping in the MRI.

e) **Bungee cords:** The bungee cords were attached through the holes in the loading rig base and pedal create the load at the prescribed foot pedal angle. The bungee cords (Stinson 6186 36" stretch cord) were knotted on either end of the holes, so that when the pedal was pressed, the elasticity produced a resistance that generated the desired load at the knee. More details on the mechanical properties of the bungee cords are detailed in the sections below.

Determining Spring Load from Desired Load at Knee

For the purpose of generalizing the different elastic materials tested, they will be described as springs. The functionality constraint for the loading rig was to be able to generate approximately 20% of body weight at the knee joint. In order to incorporate this into the loading rig design, the load generated at the springs needed to be determined from the desired load at the knee. These values were generated for a mass range of between 40 to 100 kg, which was approximately the range of the 5^{th} percentile male to the 95^{th} percentile male from anthropometric data [188] . Working with the maximum mass value of 100 kg, 20% of this in newtons works out to be 200 N as the desired load generated at the knee. Figure A-2-2 below shows all the forces considered to determine the desired load at the spring given the desired load at the knee was to be a maximum of 200 N. This knee force of 200N was simplified to be a 2-D case because only an axial load is being applied.

With segmental static equilibrium equations, the resultant moments and forces of each rigid body segment (femur, tibia and foot) were determined. Anthropometric data assumptions were made for segment lengths [189]. The equations below show how the desired force required

at the springs was calculated. Knowing the total maximum desired force at the spring helped to determine the desired attributes of the spring that should be used for the rig. From the calculation, the desired maximum total spring force (corresponding to 20% of 1000N at the knee) was found to be 145N.

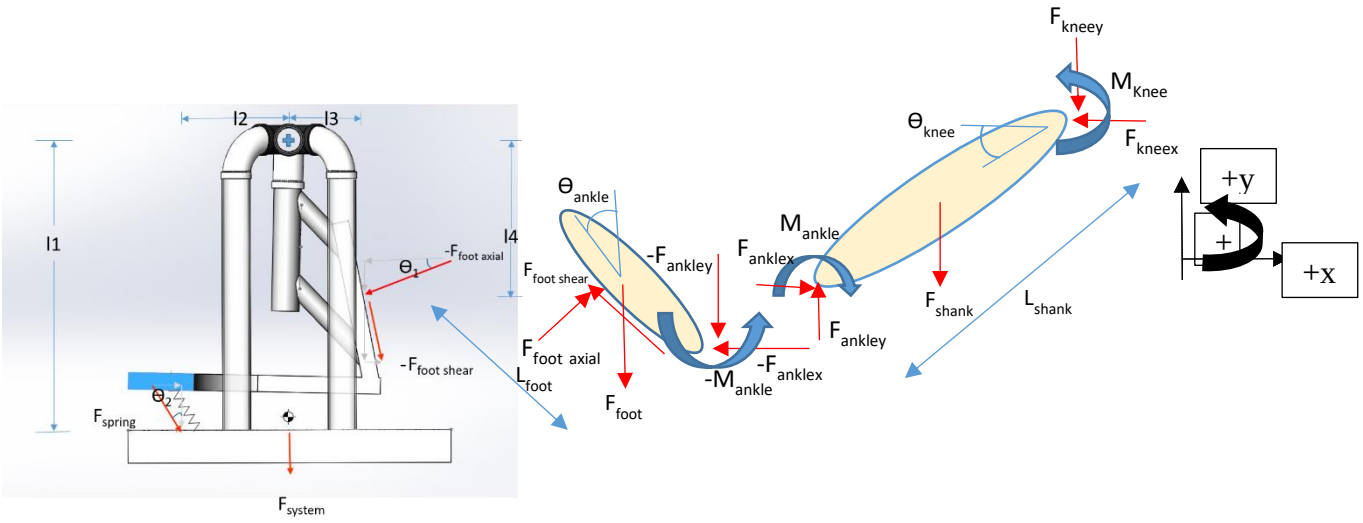

Figure A-2-2: Lower limb segments and loading rig with reaction forces needed to work out required force at springs

$\sum \boldsymbol{F_x(shank-foot)}: F_{ankle-x} + (-F_{R-knee} \times \cos(\theta_{knee})) = 0 - - - - - (A-2-1)$

$\sum \boldsymbol{F_y(shank-foot)}: F_{ankle-y} - F_{shank} + (-F_{R-knee} \times \sin(\theta_{knee})) = 0 - - - - - (A-2-2)$

$\sum \boldsymbol{M(knee)}: (F_{ankle-x} \times L_{shank} \times \sin(\theta_{knee})) - (F_{ankle-y} \times L_{shank} \times \cos(\theta_{knee})) + (F_{shank} \times (\frac{L_{shank}}{2}) \times \cos(\theta_{knee})) - M_{ankle} + M_{knee} = 0 - - - - - (A-2-3)$

$\sum \boldsymbol{F_x(foot-rig)}: -F_{ankle-x} + (F_{foot-axial} \cos(\theta_{ankle})) - (F_{foot-shear} \sin(\theta_{ankle})) = 0 - - - - - (A-2-4)$

$\sum \boldsymbol{F_y(foot-rig)}: -F_{ankle-y} + (F_{foot-axial} \sin(\theta_{ankle})) + (F_{foot-shear} \cos(\theta_{ankle})) = 0 - - - - - (A-2-5)$

$\sum \boldsymbol{M(rig\ fulcrum)}: -F_{foot-axial}(cos(\theta_1) \times l_4 - \sin(\theta_1) \times l_3) - F_{foot-shear}(sin(\theta_1) \times l_4 - \cos(\theta_1) \times l_3) - F_{spring}(cos(\theta_2) \times l_2 - \sin(\theta_2) \times l_1) = 0 - - - - - - (A-2-6)$

The 6 equations above were used to find the following unknowns: M_{knee}, M_{ankle}, F_{ankle}, $F_{foot\text{-}axial}$, $F_{foot\text{-}shear}$ and F_{spring}.

Determining the spring to be used

Given the resultant force required, several potential springs were tested for linear elastic behavior that would yield the desired total spring force with the minimal number of individual springs. To test the elastic behavior, the deflection of the spring was plotted versus the uniform increase in force applied to the spring. We assumed that all the cords were the same and therefore had the same mechanical properties. Since the cords were to be arranged in parallel (side by side), the resultant force was additive. Thus, the number of springs needed to achieve the desired loads was also considered. The result of the load-deflection plot can be seen in Figure A-2-3 below. The same plots for the other springs can be seen in Appendix A-3. While the bungee cord spring was chosen, two other springs had a similar number of minimal springs to reach the desired spring load. The bungee cord spring was chosen because it took up the least space and had a more secure mode of attachment to the loading rig. The force-displacement equation of this spring in the linear elastic region was found to be:

Force (N) = 105.05 (N/m) x displacement (m) + 11.905 N ---------- (A-2-7)

We determined that a reasonable displacement of the springs with load applied at the foot is 5 cm. With this displacement value inserted into the equation and our maximum total spring force of 145N, it worked out that nine bungee cord springs were needed to generate the maximum amount of load at the knee (200N). The number of springs for the maximum desired load defined how many holes were to be drilled on the loading rig to accommodate the cords.

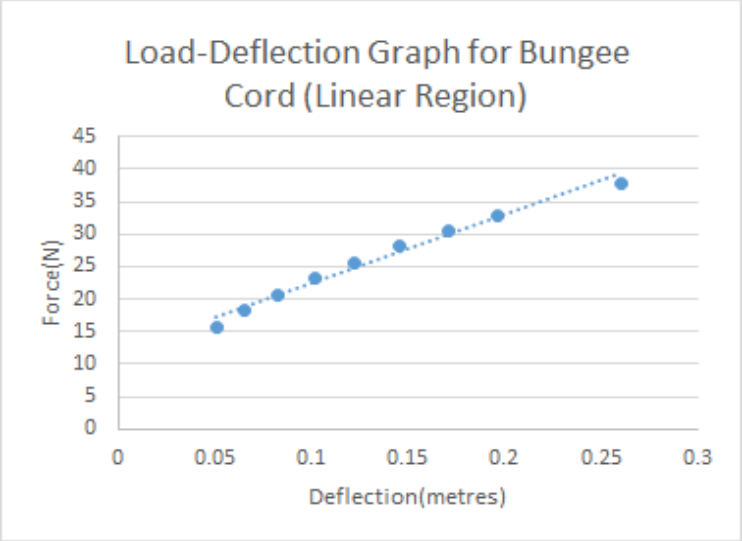

Figure A-2-3: Load-deflection graph for chosen bungee cords, to determine spring equation in linear-elastic region

Adjusting the Loads per Individual

Using the equations discussed above, custom code (Matlab, the Mathworks, Natwick, USA) was created to determine the number of springs required to achieve the desired knee load based on the mass of the individual. The axial load that should be generated at the foot plate was also calculated. To ensure that the rig delivered the prescribed load, a calibration was carried out. Specifically, the rig was set up with the prescribed number of cords and a force gauge (Omega, DFG35-200) attached to a custom-made aluminum foot was used to press on the pedal (see **Error! Reference source not found.** below). The aluminum foot was pushed by hand until the f orce gauge reading matched that from the custom code. A visual cue (simply a line that lined up with a slot) was placed at this position so that the participant would know exactly at what angle to hold the pedal to achieve the prescribed load. A white dry-erase sheet was used to mark the line so that it could be changed in a participant-specific manner. In the MRI scanner, each individual was simply instructed to maintain the pre-loaded position of the rig while the load was released. **Error! Reference source not found.** below shows the load-cell with aluminum foot b eing pressed onto the rig with the visual cue.

Figure A-2-4: Force gauge being applied with custom-made aluminum foot to mark out angle of tilt on visual cue per individual

A-3: Force-deflection plots for other elastic material (springs)

Described in section 3.3.3, several potential springs were tested for linear elastic behavior that will yield the desired total spring force with the minimal number of individual springs. The figures below show the spring images and plots used for this experiment.

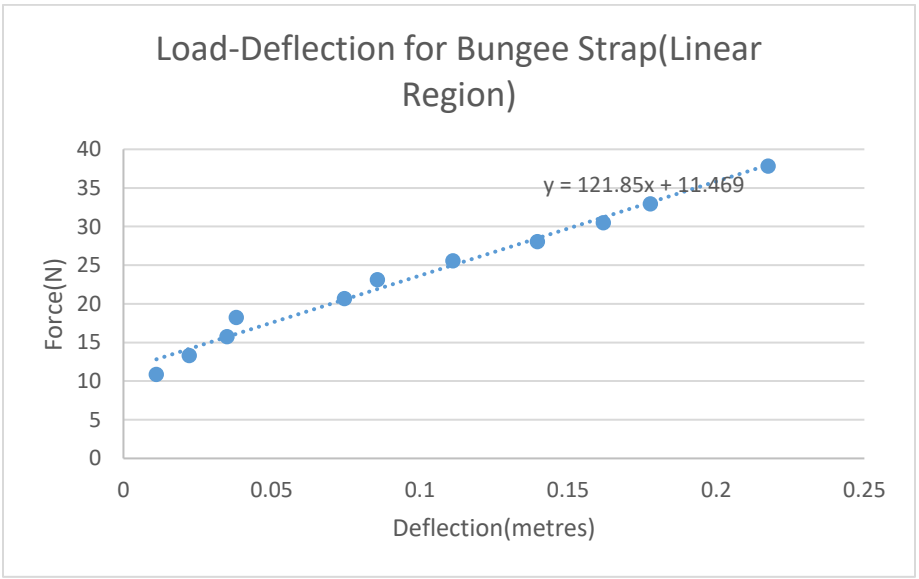

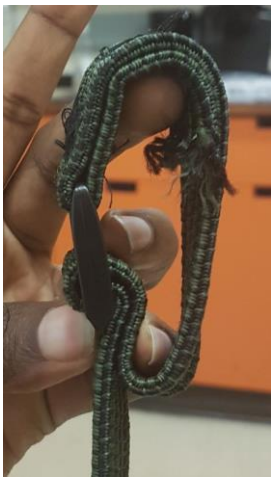

Figure A-3-1: Load-deflection plot and image for bungee strap elastic material

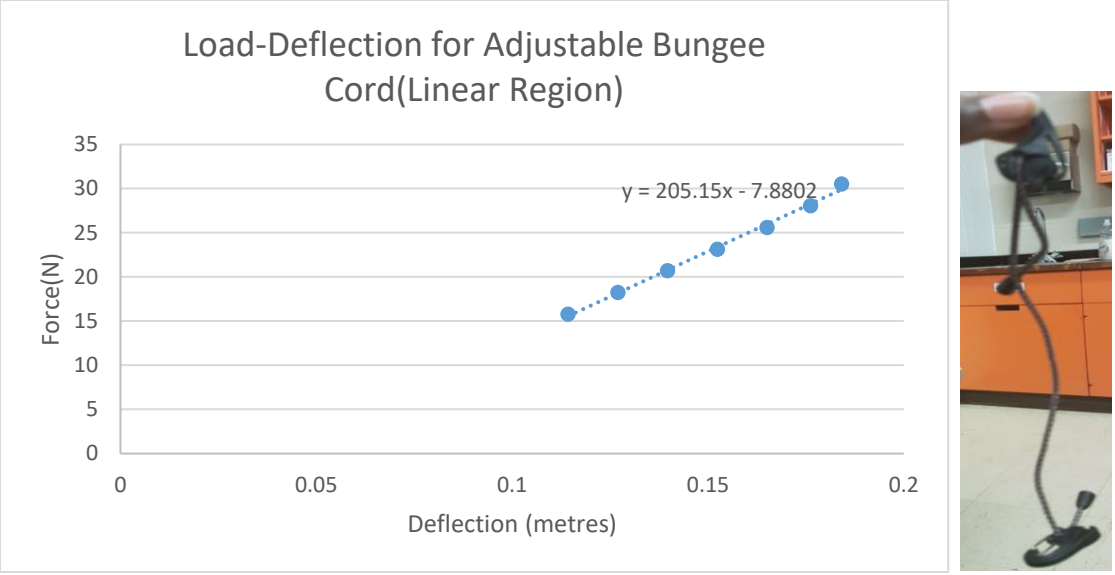

Figure A-3-2: Load-deflection plot and image for adjustable bungee cord elastic material

A-4: T_2 Cluster Sensitivity Analysis

A cluster size of 12 mm^2 and intensity-difference of 5 ms, was used as the thresholds for this project. This was based on work from previous work in our group. The sensitivity experiment was done to verify that these thresholds will still be valid for our study. The sensitivity analysis below assesses how the clusters changed with varying pixel-difference area and fixed intensity-difference at the defined threshold and varying intensity-difference with a fixed pixel-difference area size at the defined threshold. The outcome of this sensitivity analysis shows that the thresholds can be used as the maps are seen to nit significantly change with these thresholds and varying the other parameter (Figure A-4-1).

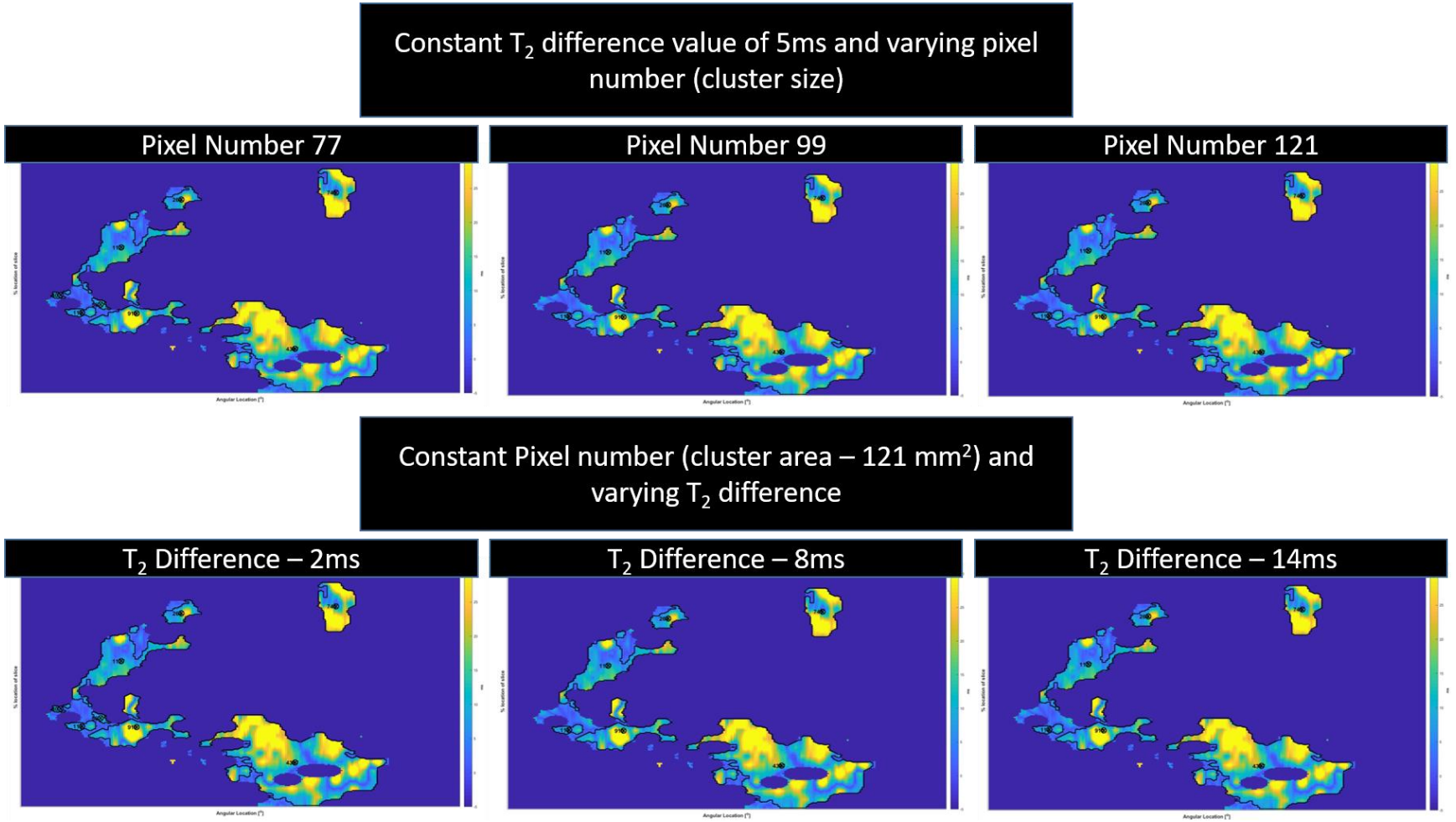

Figure A-4-1: Cluster map sensitivity analysis

A-5: More Details on Determining the Best Approach for Determining the Marker Centroid Position.

To be able to successfully transform MRI-based points to the gait system, it was important to ensure that the centroid of the MRI-lucent markers approximately coincide with the gait marker. This was tested by placing the prepared MRI-lucent gait markers into an agar phantom for visualization. The gait marker centroid was defined by segmenting the sphere which appeared as signal void (black) on the MRI image (see Figure A-5-1 below). The volume centroid was found using the region of interest (ROI) module in packaged image processing software (Analyze 12.0, Analyze Direct, Overland Park, KS, USA). Next, the MRI ellipsoid marker centroid was visually-determined. From Figure A-5-1 below, the centroid positions for both the MRI-lucent and gait marker can be seen. The absolute difference between the two centroid positions was approximately 2.5 mm. The centroid difference for this test was acquired from the same system (MRI), however, in practice, the centroid for the gait markers for tracking, is generated from the gait system. To be able to account for this 2.5mm difference in centroid positions, an extra point on each of the markers, along the long symmetrical axis of the ellipsoid was selected. It was however of concern that there may be a discrepancy between determining the centroid position of the markers in the motion capture system and the way it was done in this experiment from MRI.

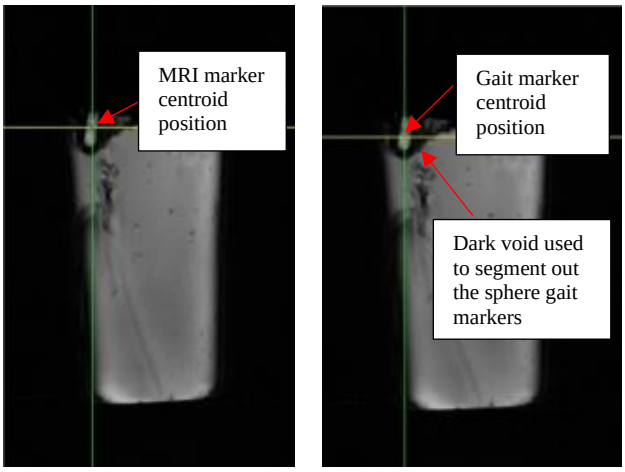

Figure A-5-1: MRI-lucent gait marker inserted in agar phantom. Left: MRI-marker centroid position Right: Gait-marker centroid position – both sagittal view

An additional test was carried out to see which of the methods of determining the centroid (with the corrected 2.5mm centroid and the visually-determined centroid), was farthest away from the motion-capture-system-determined centroid. To do this, a local marker cluster (4 markers) coordinate system was created from the reported marker position vectors of the motion-capture-determined centroid, the visually-determined centroid and the 2.5mm-corrected-centroid. Table A-5-1 below shows the outcome of this analysis. As can be seen, the 2.5mm-corrected-centroid difference from the motion-capture-determined centroid, was consistently higher than that of the visually-determined centroid in all four markers. From this analysis, we decided to go with the visually-determined method of determining the centroid position of the ellipsoid MRI markers without including the 2.5mm correction.

Table A-5-1: Absolute difference values in mm of marker cluster centroids difference between visually-determined and 5mm-correctod centroids and centroids from the motion-capture system

	Absolute difference between motion-capture determined & visually-determined centroid positions (mm)	**Absolute difference between motion-capture determined & 2.5 mm-corrected centroid positions (mm)**
Marker 1	4.2×10^{-14}	4.5×10^{-14}
Marker 2	4.6	6.3
Marker 3	5.8	6.8
Marker 4	9.5	10

A-6: MRI-lucent Gait Marker Design

The MRI-lucent gait markers played a key role in integrating the data from the MRI and gait systems. The goal of this was to have a set of fiducial markers that were visible in both the MRI and gait coordinate spaces. For the markers to be seen in the MR images, the markers had to be MRI-lucent which implies it had to be made of a substance that contained hydrogen and had MRI properties within the range of human tissue so as not to affect the dynamic range of the images. For it to be visualized in the motion capture system, it had to have a reflective feature so that it could be easily identified by the infrared cameras. A few options were considered to meet these requirements:

a) To modify an already existing gait marker to have MRI-lucent features i.e insert MRI-lucent fluid into a hollow gait marker.
b) To modify an already existing MRI marker to have reflective features i.e add on reflective tape an MRI marker
c) To design a custom marker with both desired features

After several designs, the final and working approach of creating an MRI-lucent gait marker was to integrate product ellipsoid MRI marker (MR. SPOT ™ – 092/122, Beekley Medical, Bristol, CT, USA) and an existing hollow sphere gait marker (14mm-SBXV-H, X-base, hollow sphere with Velcro, MoCap Solutions, LLC, USA). This was done by placing the ellipsoid MRI markers, that are 15mm wide and 20 mm long into the 14mm diameter hollow sphere gait marker (see Figure A-6-1 below). The sizing created a snug fit so the MRI marker would not move relative to the gait marker.

Figure A-6-1: a) Left - MRI marker inserted into the hollow gait marker. B) Right - MRI marker

Appendix B: qMRI Results – Supplementary Material

The figures and tables below show all supplementary material for the qMRI results section including the tables that show the corresponding mean T_2 values and T_2 cartilage projection maps for all 15 trials of our study (three trials for each of five participants). Note that for three trials in participant 1 and 1 trial in participant 2 for the loaded cartilage scenario, there are no values or images due to MRI sequence error in these cases during data acquisition.

B-1: qMRI All-Trial Tables

Table B-1-1: Mean qMRI T_2 values for general, medial, lateral and trochlear regions at loaded and unloaded positions and their difference

	Participant 1			Participant 2			Participant 3			Participant 4			Participant 5		
	Trial 1	Trial 2	Trial 3	Trial 1	Trial 2	Trial 3	Trial 1	Trial 2	Trial 3	Trial 1	Trial 2	Trial 3	Trial 1	Trial 2	Trial 3
	General														
Loaded (Values)	24.6	28.2	24.5	23.8	24.9	24.3	30.0	31.4	31.0	25.4	23.2	21.9	32.9	27.4	30.2
Unloaded (Values)					31.5	22.3	26.5	27.7	26.2	23.4	23.7	30.4	27.9	27.1	26.3
Difference (Values)					-6.6	2.0	3.5	3.7	4.8	1.9	-0.5	-8.5	5.0	0.3	3.8
	Medial														
Loaded (Values)	29.8	34.5	22.5	19.3	22.1	18.6	30.1	31.4	28.3	23.3	26.6	19.4	29.2	27.5	27.8
Unloaded (Values)					31.7	20.8	27.1	30.2	27.8	24.6	21.6	30.2	25.5	27.7	23.5
Difference (Values)					-9.6	-2.2	3.0	1.2	0.4	-1.3	5.0	-10.8	3.8	-0.1	4.3
	Lateral														
Loaded (Values)	22.2	24.0	26.3	28.1	23.4	24.8	34.6	35.2	32.2	29.1	25.5	22.2	31.7	29.7	27.1
Unloaded (Values)					32.0	25.5	26.6	28.3	26.8	23.4	27.1	31.1	28.4	24.9	27.6
Difference (Values)					-8.6	-0.7	8.0	6.9	5.4	5.7	-1.7	-8.9	3.3	4.8	-0.5
	Trochlear														
Loaded (Values)	22.8	27.2	25.4	22.4	28.5	27.6	25.0	26.0	31.5	23.5	19.3	23.3	34.6	25.0	34.1
Unloaded (Values)					26.7	20.3	27.0	24.4	24.1	21.9	22.8	28.9	29.2	27.8	26.9
Difference (Values)					1.7	7.3	-2.0	1.5	7.4	1.6	-3.4	-5.5	5.3	-2.8	7.2

B-2: qMRI T_2 Projection Maps for three trials each of five participants

Below figure shows the T_2 projection map results for all three trials of each participant.

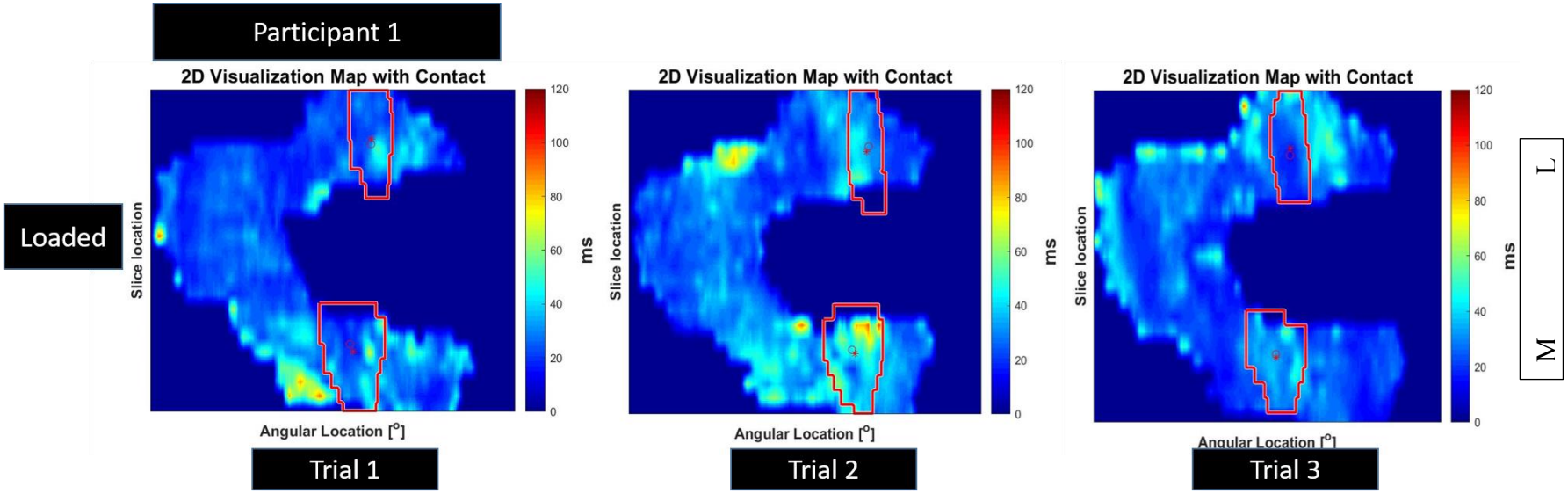

Figure B-2-1: T_2 Projection Maps of Loaded cartilage for Three Trials of Participant 1. The T_2 Projection maps of the unloaded cartilage is not available for this participant due to MRI sequence error.

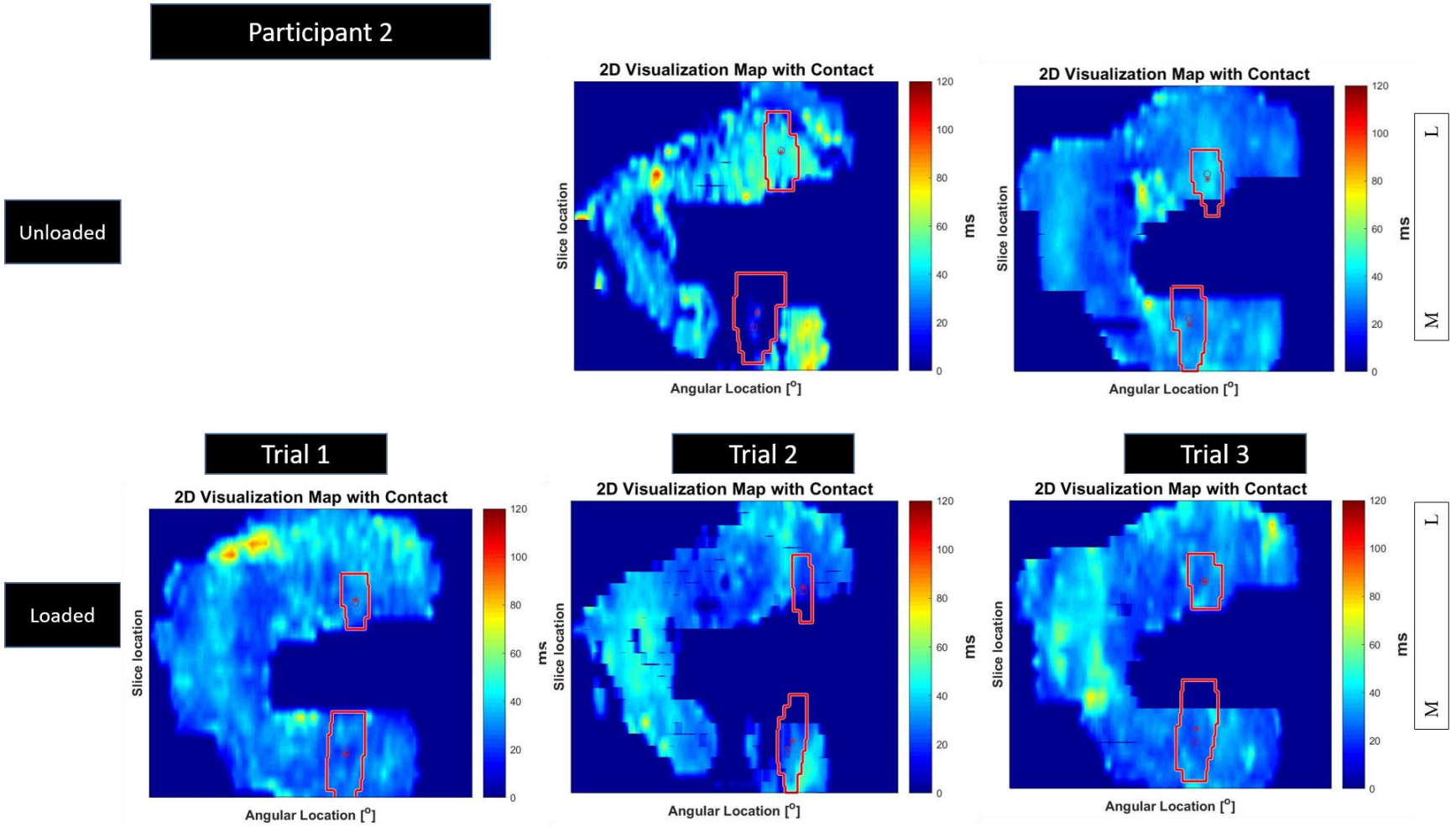

Figure B-2-2: T_2 Projection Maps of Loaded and Unloaded cartilage for Three Trials of Participant 2. One of the trials of the T_2 Projection maps of the unloaded cartilage is not available for this participant due to MRI sequence error.

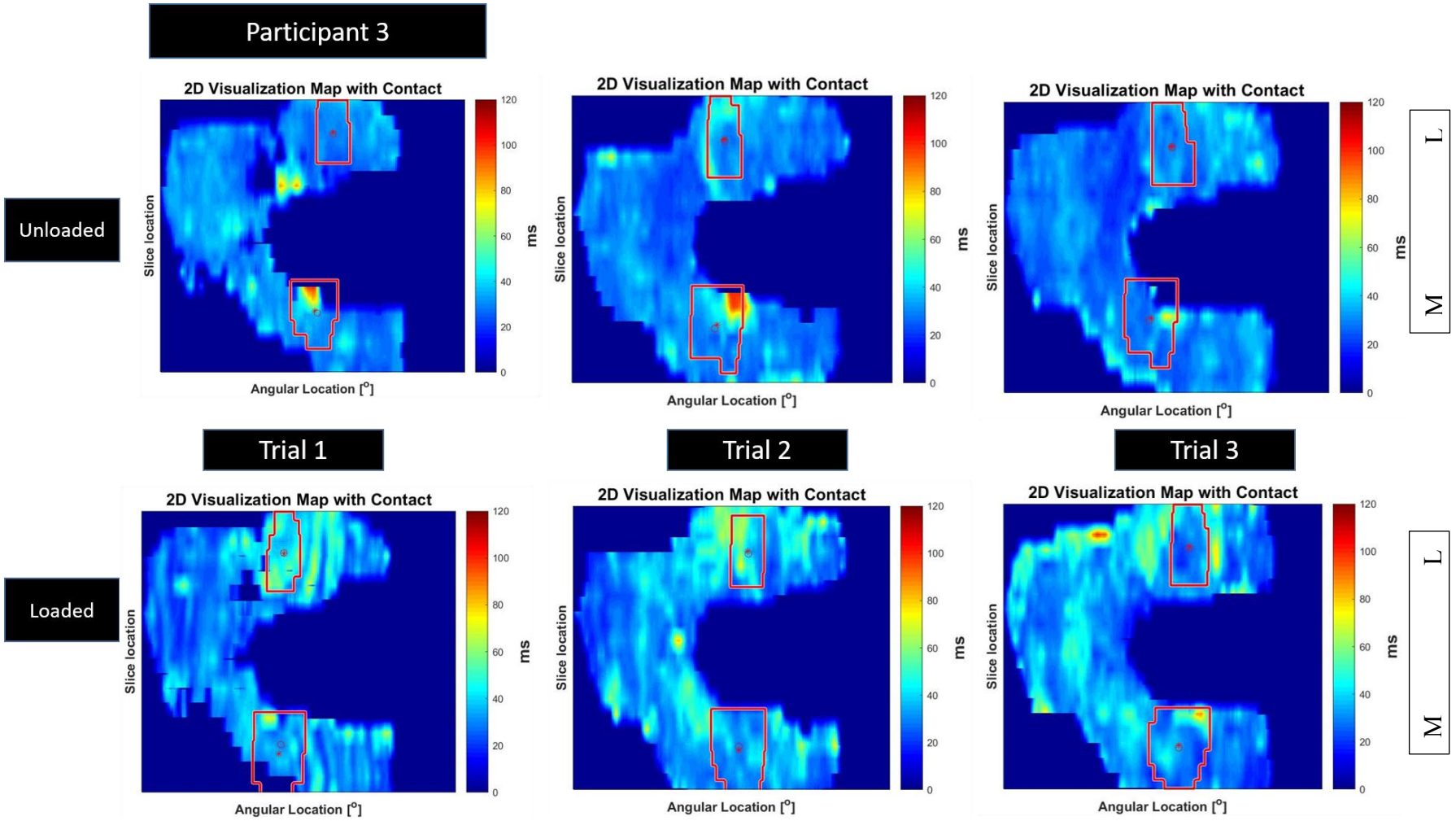

Figure B-2-3: T_2 Projection Maps of Loaded and Unloaded cartilage for Three Trials of Participant 3.

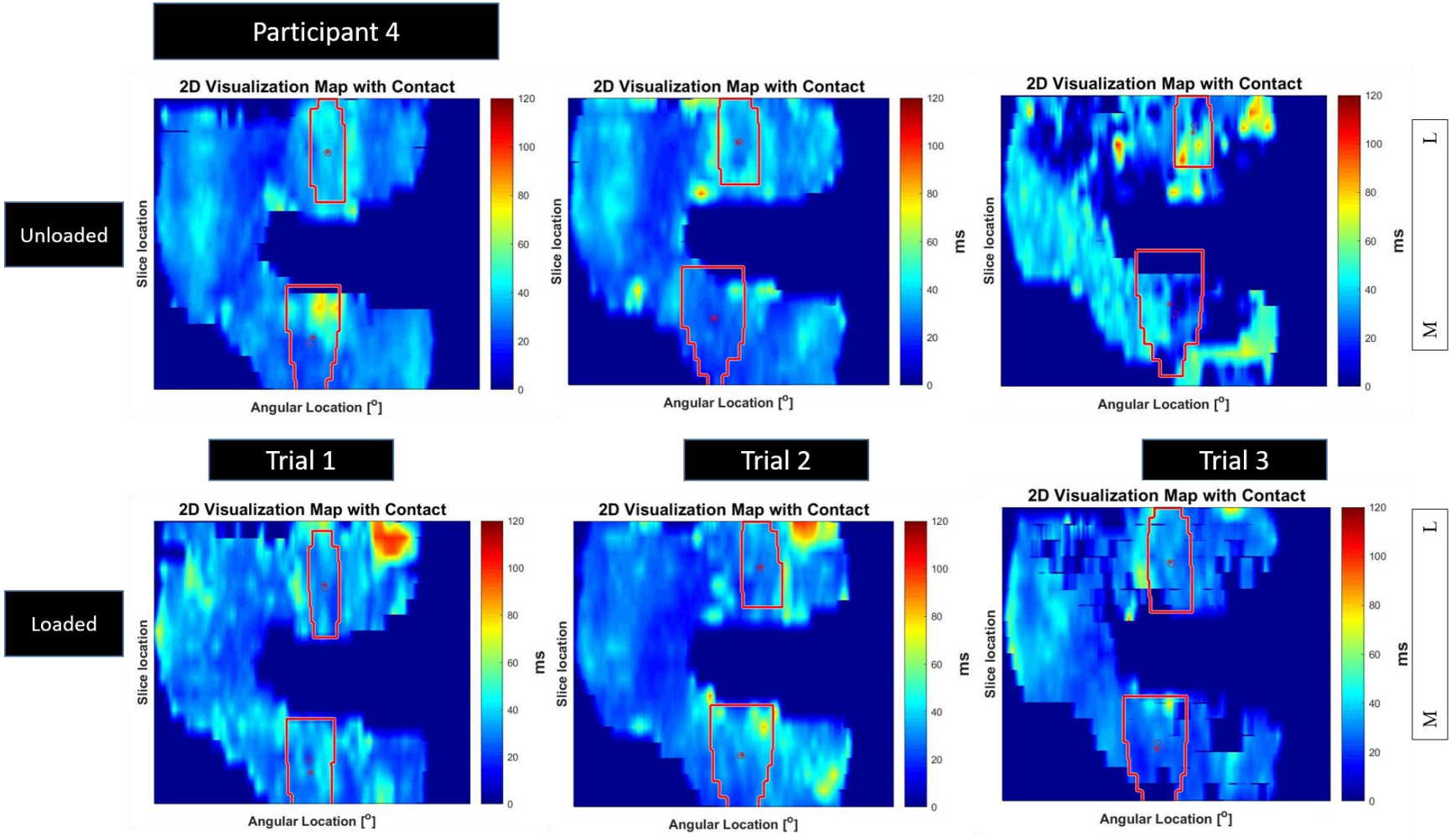

Figure B-2-4: T_2 Projection Maps of Loaded and Unloaded cartilage for Three Trials of Participant 4.

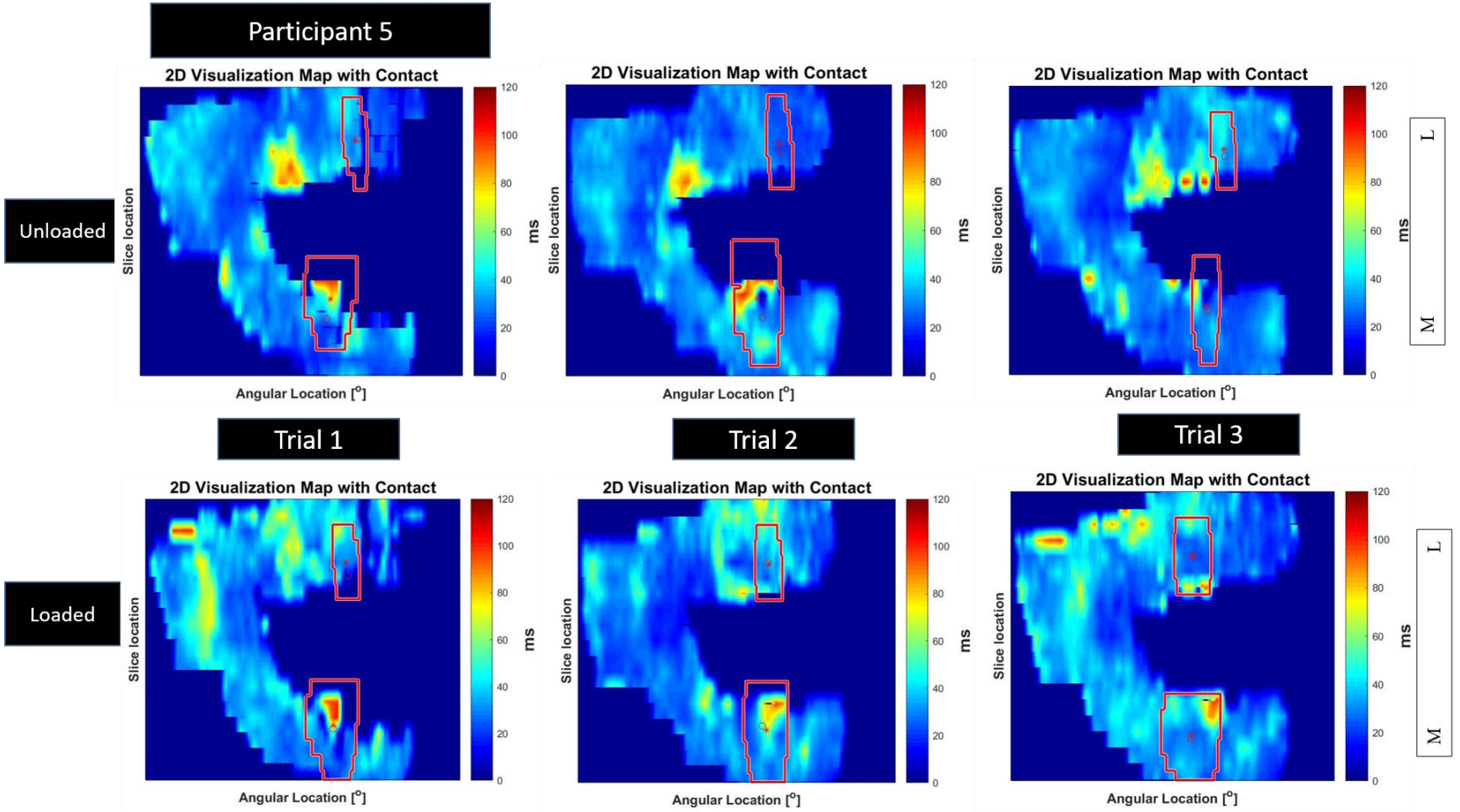

Figure B-2-5: T_2 Projection Maps of Loaded and Unloaded cartilage for Three Trials of Participant 5.

Appendix C: mechMRI Results - Supplementary Material

The figures and tables below show all supplementary material for the mechMRI results section including the tables and figures that show the corresponding contact centroid translation, contact area and point-cloud images for all 15 trials of our study (three trials for each of five participants).

C-1: mechMRI (Contact Centroid Translation and Contact Area) All-Trial Tables

The tables below show the values for medial and lateral contact area centroid translation for three limb position movements as well as the contact area for each limb position for all 15 trials.

Table C-1-1: Medial and lateral contact centroid translation (absolute distance) – one-to-two (fully extended to lower flexion angle), one-to-three (fully extended to higher flexion angle), two-to-three (lower to higher flexion angle)

	Participant 1			Participant 2			Participant 3			Participant 4			Participant 5		
	Trial 1	Trial 2	Trial 3	Trial 1	Trial 2	Trial 3	Trial 1	Trial 2	Trial 3	Trial 1	Trial 2	Trial 3	Trial 1	Trial 2	Trial 3
	Medial														
One-to-Two - mm	16.4	7.9	19.3	1.8	5.2	13.3	14.1	10.6	9.3	15.5	9.9	10.8	12.0	5.0	10.4
One-to-Three - mm	22.3	21.0	24.0	18.3	16.7	24.1	26.4	22.4	16.8	26.3	15.2	16.0	17.5	17.8	18.9
Two-to-Three - mm	6.3	14.0	7.0	19.7	12.0	10.9	12.7	12.0	8.0	10.8	5.5	5.2	6.0	13.1	9.6
	Lateral														
One-to-Two - mm	10.5	8.3	11.3	1.9	6.7	13.4	10.2	7.3	6.1	10.5	5.0	8.2	9.0	7.4	5.6
One-to-Three - mm	13.3	10.7	13.5	11.7	14.0	17.2	18.6	15.8	13.5	16.9	8.7	10.7	11.3	12.6	12.8
Two-to-Three - mm	10.3	5.1	2.7	10.0	8.0	3.7	9.4	9.8	8.7	6.6	3.8	2.5	2.5	6.3	7.4

Table C-1-2: Medial and lateral contact area values at three limb orientations. Flexion Angle 1 – Low flexion angle. Flexion Angle 2 – High flexion angle

	Participant 1			Participant 2			Participant 3			Participant 4			Participant 5		
	Trial 1	Trial 2	Trial 3	Trial 1	Trial 2	Trial 3	Trial 1	Trial 2	Trial 3	Trial 1	Trial 2	Trial 3	Trial 1	Trial 2	Trial 3
Fully Extended (Degrees)	0.0	0.0	0.0	0.0	0.0	0.0	0.0	0.0	0.0	0.0	0.0	0.0	0.0	0.0	0.0
Medial Contact Area (mm^2)	339.5	394.4	507.2	438.3	399.1	425.0	284.6	272.8	278.9	465.5	409.8	417.0	410.5	401.6	364.4
Lateral Contact Area (mm^2)	346.7	520.7	514.9	336.6	340.9	350.2	204.7	222.1	210.8	227.3	194.5	186.5	205.6	178.7	203.2
Low Flexion Angle (Degrees)	27.9	18.6	32.0	23.2	27.3	27.9	26.0	16.1	16.9	26.3	10.9	15.1	18.0	13.9	21.8
Medial Contact Area (mm^2)	480.3	520.7	429.6	667.1	398.3	498.7	342.0	396.4	336.1	661.1	679.2	802.4	480.4	553.3	454.2
Lateral Contact Area (mm^2)	467.7	322.1	443.6	276.4	261.9	210.0	161.5	178.9	187.0	326.6	299.0	271.5	196.2	176.6	161.1
High Flexion Angle (Degrees)	35.7	35.7	40.1	32.5	36.8	34.1	55.6	43.4	31.2	39.1	19.1	26.4	29.2	29.1	37.1
Medial Contact Area (mm^2)	540.1	597.9	295.0	489.7	375.1	427.2	302.9	312.9	271.7	358.5	427.7	361.6	446.9	451.4	417.7
Lateral Contact Area (mm^2)	373.5	354.0	270.7	235.1	238.1	204.1	267.0	235.9	271.0	353.3	313.7	306.0	160.4	143.7	174.1

C-2: Femur-contact point cloud images for three trials each of five participants

The point cloud plots of femur and contact below show the contact areas and centroid position for the medial and lateral sides for all three trials of each participant. The red contact area represents the contact at fully extended position. The yellow represents the contact area at the lower flexion angle and the blue represents the contact area at the higher flexion angle. For the centroids, the white dot represents the centroid position for the fully extended knee position, the purple represents the centroid for the lower flexion angle position and the green represents the centroid for the higher flexion angle.

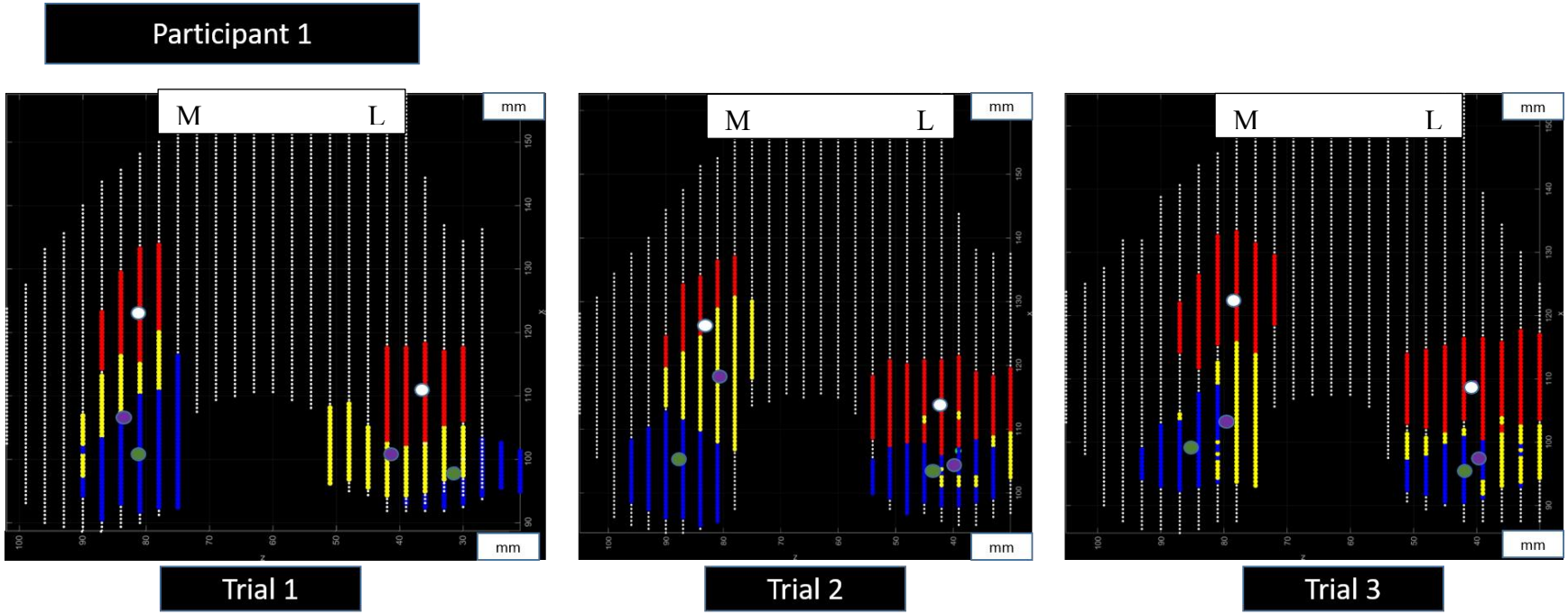

Figure C-2-1: Front-view point cloud images of femur, contact and contact centroids of medial and lateral sides for all three trials of participant 1

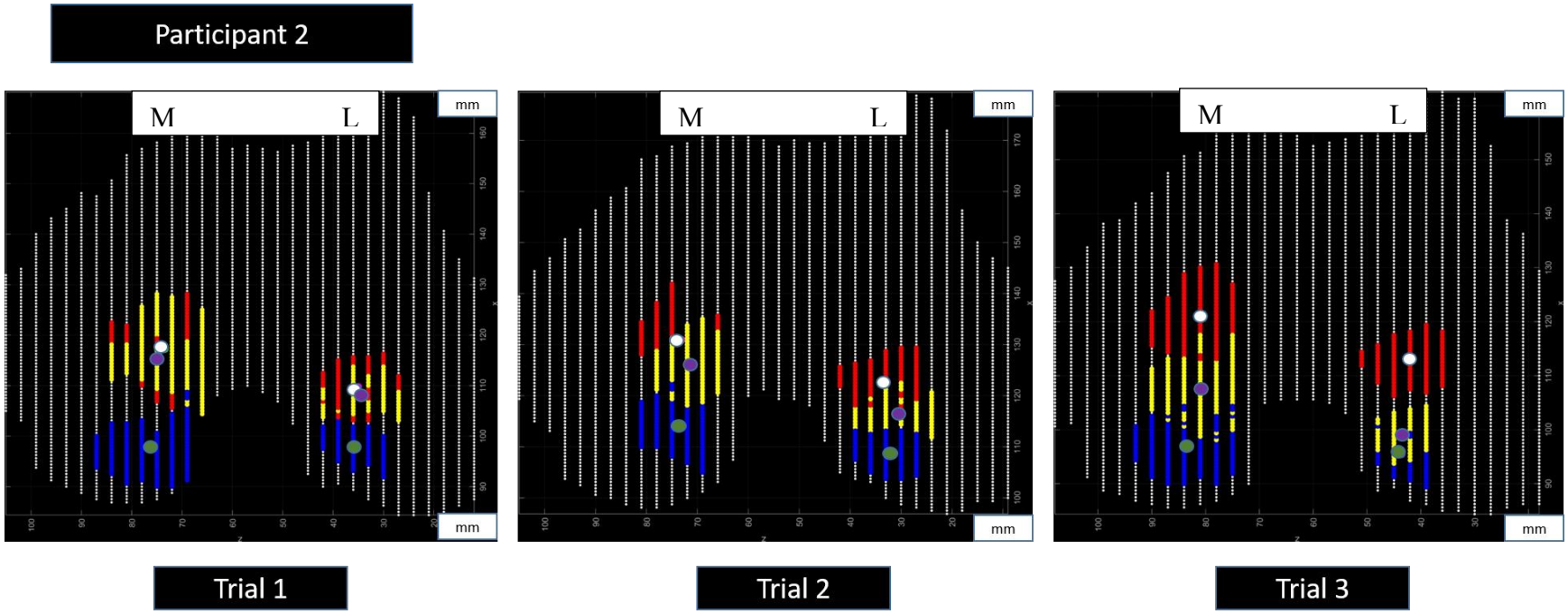

Figure C-2-2: Front-view point cloud images of femur, contact and contact centroids of medial and lateral sides for all three trials of participant 2

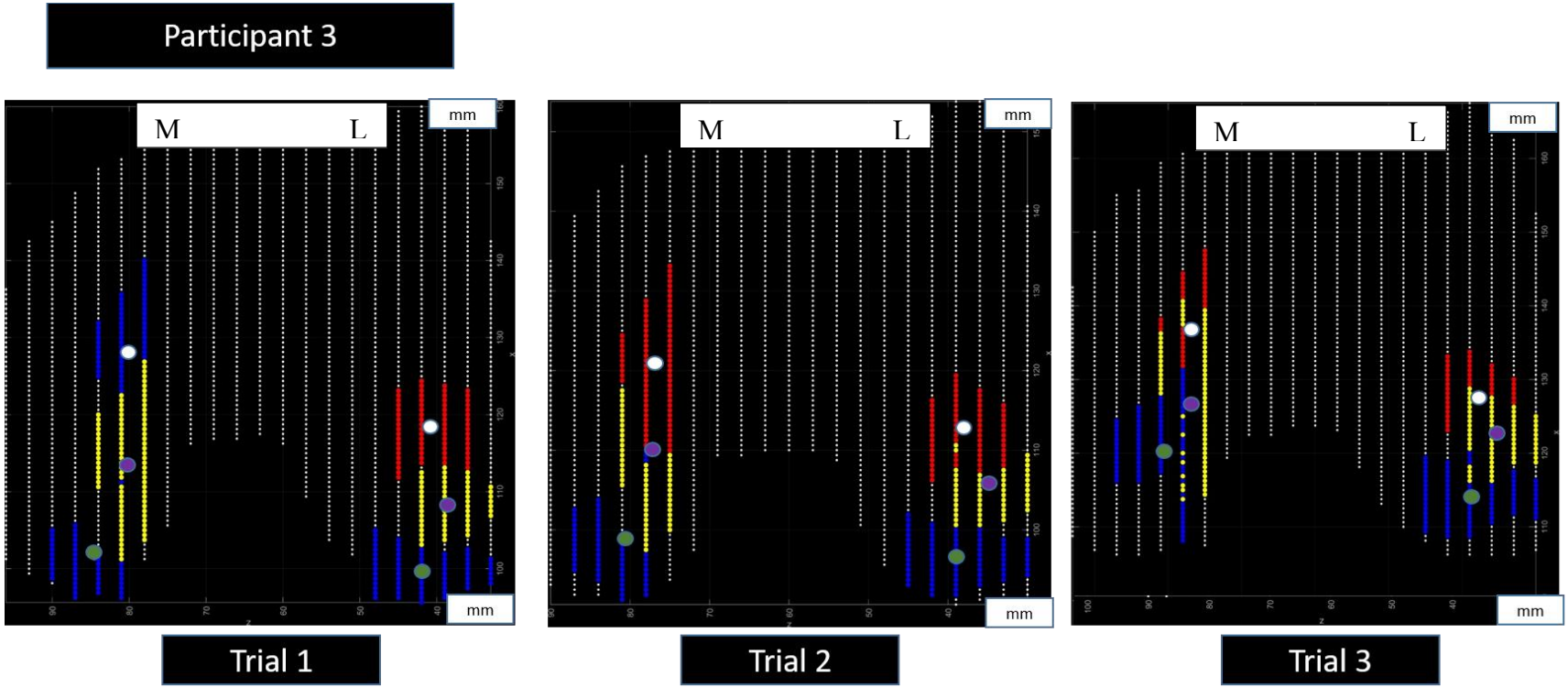

Figure C-2-1: Front-view point cloud images of femur, contact and contact centroids of medial and lateral sides for all three trials of participant 3

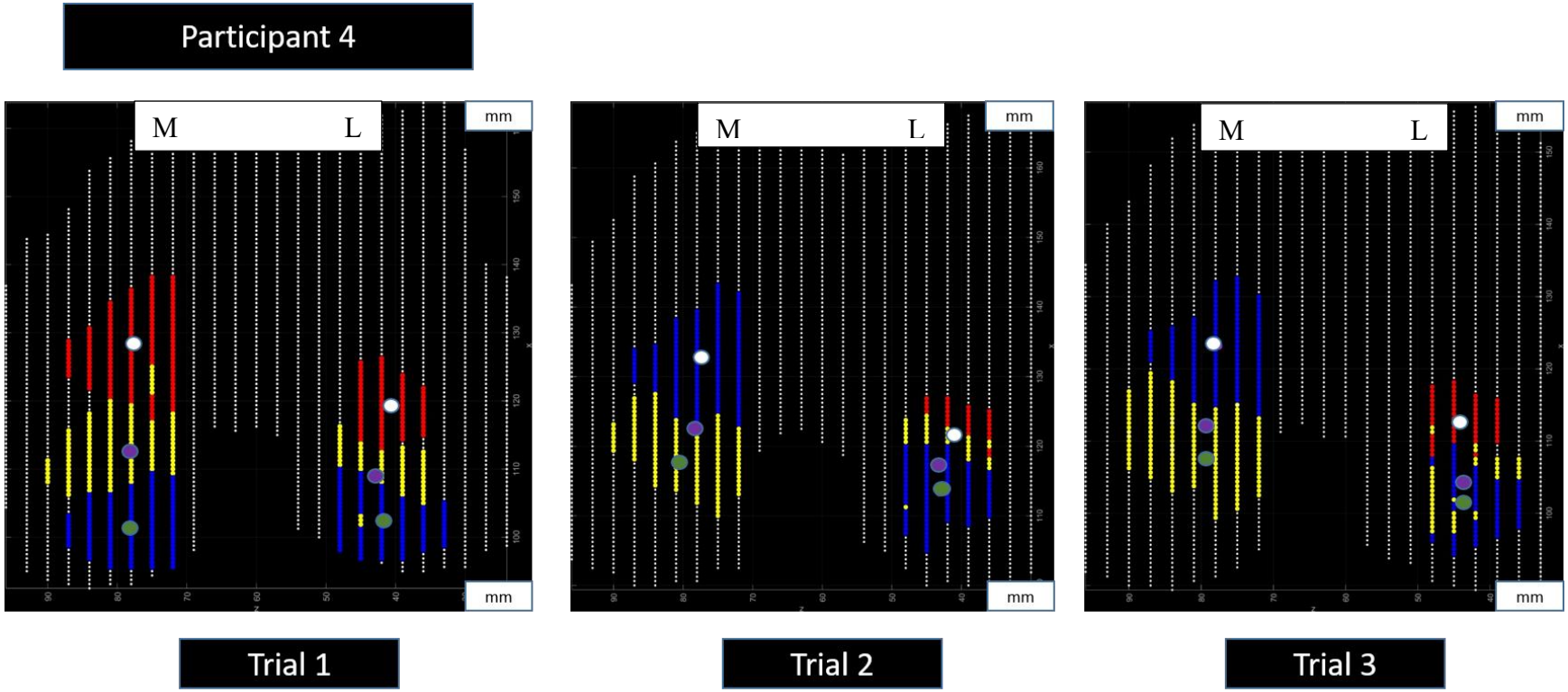

Figure C-2-1: Front-view point cloud images of femur, contact and contact centroids of medial and lateral sides for all three trials of participant 4

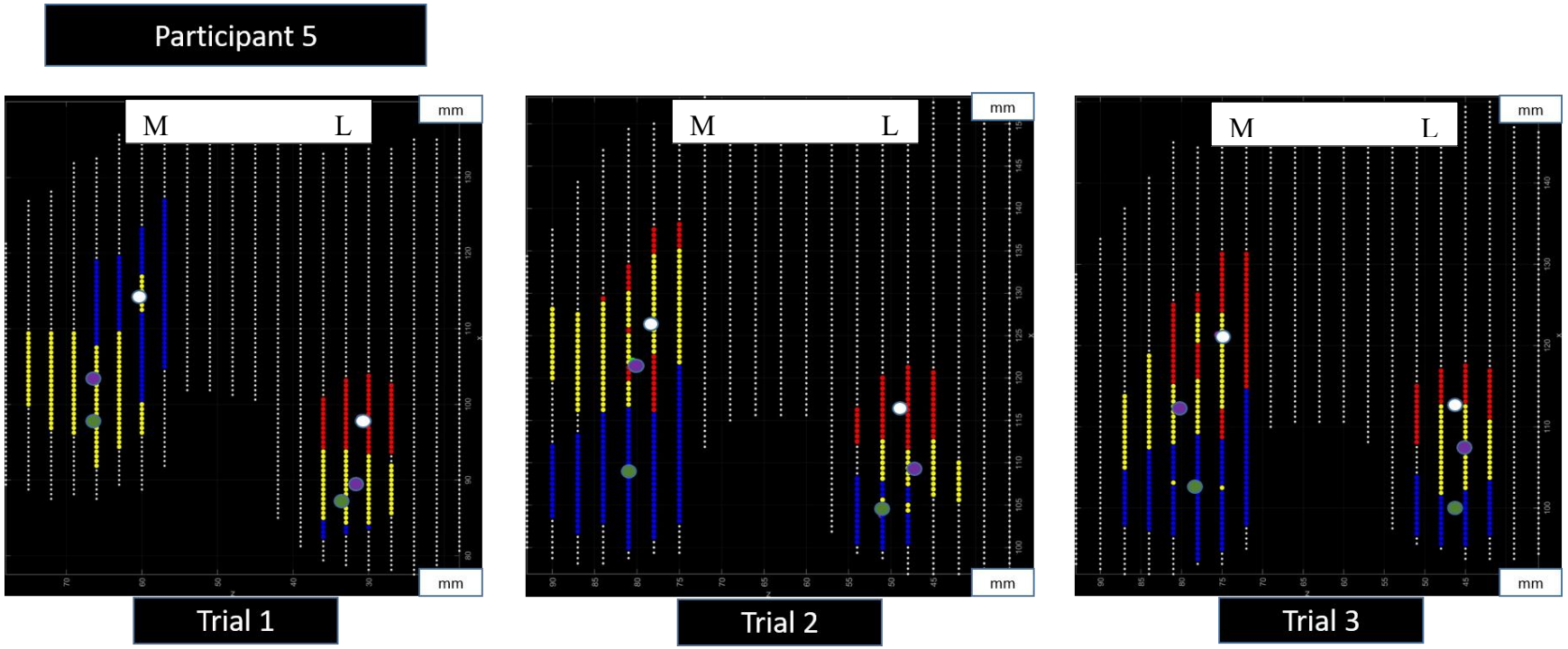

Figure C-2-1: Front-view point cloud images of femur, contact and contact centroids of medial and lateral sides for all three trials of participant 5

Appendix D: Gait Analysis Results - Supplementary Material

The tables and figures below show all supplementary material for the gait analysis results section including the tables and figures that show the corresponding kinematic and kinetic measures for all 15 trials of our study (three trials for each of five participants) as well as sample peak points selected for each measure.

D-1: All-Trial Table for Gait Analysis Measures

The tables below show the values for the kinematic and kinetic measures of MRI-based and Gait-based outcomes for all 15 trials.

Table D-1-1: MRI-based kinematics for walking, chair and stair tasks

	Participant 1			Participant 2			Participant 3			Participant 4			Participant 5		
	Trial 1	Trial 2	Trial 3	Trial 1	Trial 2	Trial 3	Trial 1	Trial 2	Trial 3	Trial 1	Trial 2	Trial 3	Trial 1	Trial 2	Trial 3
Walk - Peak Flexion Angle (degrees)	25.5	28.7	21.8	19.6	20.8	21.8	14.2	15.8	17.2	14.6	5.4	1.6	3.4	5.5	3.9
Walk - Peak Extension Angle (degrees)	6.9	11.3	4.0	7.6	3.5	2.2	5.0	2.0	0.6	3.1	2.6	4.8	11.7	8.9	10.0
Walk - Peak Adduction Angle (degrees)	4.4	10.0	7.4	13.5	14.6	13.8	13.6	8.6	5.4	11.0	1.9	0.7	6.6	0.3	1.7
Walk - Peak Abduction Angle (degrees)	0.7	5.6	3.5	5.2	3.7	3.1	3.8	1.6	3.4	1.7	0.8	2.6	2.7	3.1	0.3
Stair Up - Peak Extension Angle (degrees)	56.4	42.5	55.4	56.8	45.7	56.0	50.0	55.6	57.4	52.2	49.4	34.8	67.4	55.3	54.9
Stair Down - Peak Flexion Angle (degrees)	77.8	62.6	73.1	77.0	79.9	76.5	74.9	74.6	81.1	79.8	76.6	60.4	100.5	80.3	80.3

Table D-1-2: MRI-based kinetics for walking, chair and stair tasks

	Participant 1			Participant 2			Participant 3			Participant 4			Participant 5		
	Trial 1	Trial 2	Trial 3	Trial 1	Trial 2	Trial 3	Trial 1	Trial 2	Trial 3	Trial 1	Trial 2	Trial 3	Trial 1	Trial 2	Trial 3
Walk - Peak Flexion Moment (N.m/kg)	0.14	0.17	0.15	0.02	0.03	0.05	0.06	0.07	0.08	0.03	0.01	0.00	0.00	0.15	0.13
Walk - Peak Extension Moment (N.m/kg)	0.29	0.27	0.25	0.25	0.24	0.24	0.34	0.24	0.39	0.23	0.19	0.27	0.16	0.12	0.12
Walk - Peak Abduction Moment (N.m/kg)	0.47	0.45	0.47	0.58	0.14	0.21	0.55	0.45	0.25	0.65	0.88	1.00	0.49	0.54	0.51
Walk - Peak Adduction Moment (N.m/kg)	0.81	0.74	0.71	0.85	0.39	0.62	1.40	1.00	0.68	0.82	0.96	1.20	0.82	0.98	0.95
Chair Rise - Peak Extension Moment (N.m/kg)	0.43	0.44	0.43	0.62	0.77	0.79	0.52	0.71	0.69	1.10	0.70	0.67	0.52	0.50	0.57
Chair Rise - Peak Adduction Moment (N.m/kg)	0.12	0.26	0.19	0.30	0.19	0.22	0.24	0.49	0.48	0.61	0.74	0.92	0.35	0.21	0.21
Chair Down - Peak Flexion Moment (N.m/kg)	0.34	0.36	0.39	0.41	0.51	0.54	0.51	0.53	0.86	0.81	0.57	0.46	0.33	0.27	0.49
Chair Down - Peak Abduction Moment (N.m/kg)	0.11	0.28	0.44	0.17	0.08	0.15	0.49	0.56	0.36	0.51	0.62	0.65	0.15	0.24	0.15
Stair Up - Peak Extension Moment (N.m/kg)	0.27	0.42	0.32	0.44	0.54	0.14	1.20	0.97	1.40	1.60	1.10	1.10	0.50	0.33	0.50
Stair Down - Peak Flexion Moment (N.m/kg)	1.20	0.52	0.52	0.12	0.97	1.10	1.40	1.20	1.50	0.93	0.42	0.58	0.23	0.13	0.21

Table D-1-3: Gait-based kinematics for walking, chair and stair tasks

	Participant 1			Participant 2			Participant 3			Participant 4			Participant 5		
	Trial 1	Trial 2	Trial 3	Trial 1	Trial 2	Trial 3	Trial 1	Trial 2	Trial 3	Trial 1	Trial 2	Trial 3	Trial 1	Trial 2	Trial 3
Walk - Peak Flexion Angle (Degrees)	24.1	22.4	21.7	17.1	18.6	15.7	17.7	16.6	19.0	15.7	1.2	5.3	14.1	13.4	11.5
Walk - Peak Extension Angle (Degrees)	5.3	3.7	4.0	3.5	1.7	4.7	2.4	2.3	0.2	3.0	1.9	1.3	0.6	0.6	0.3
Walk - Peak Adduction Angle (Degrees)	1.5	0.8	7.4	2.3	0.7	1.3	0.2	0.2	0.1	5.0	1.6	0.7	0.3	7.1	1.9
Walk - Peak Abduction Angle (Degrees)	1.4	3.5	3.5	3.5	2.5	1.9	1.4	0.9	1.5	0.8	0.1	0.5	1.2	2.1	1.2
Stair Up - Peak Extension Angle (Degrees)	53.9	34.5	55.3	54.3	64.3	49.9	54.1	56.8	59.3	51.6	54.9	53.7	68.2	65.1	64.7
Stair Down - Peak Flexion Angle (Degrees)	75.4	54.9	73.1	71.9	75.9	69.2	77.7	74.7	82.9	78.1	79.4	74.9	97.6	90.4	88.6

Table D-1-4: Gait-based kinetics for walking, chair and stair tasks

	Participant 1			Participant 2			Participant 3			Participant 4			Participant 5		
	Trial 1	Trial 2	Trial 3	Trial 1	Trial 2	Trial 3	Trial 1	Trial 2	Trial 3	Trial 1	Trial 2	Trial 3	Trial 1	Trial 2	Trial 3
Walk - Peak Flexion Moment (N.m/kg)	0.20	0.20	0.29	0.09	0.09	0.24	0.04	0.04	0.04	0.04	0.00	0.01	0.12	0.02	0.1
Walk - Peak Extension Moment (N.m/kg)	0.41	0.26	0.24	0.18	0.32	0.30	0.17	0.13	0.21	0.17	0.23	0.15	0.26	0.23	0.32
Walk - Peak Abduction Moment (N.m/kg)	0.19	0.16	0.16	0.18	0.18	0.16	0.23	0.11	0.12	0.19	0.31	0.23	0.16	0.16	0.11
Walk - Peak Adduction Moment (N.m/kg)	0.30	0.34	0.31	0.36	0.41	0.52	0.64	0.38	0.41	0.24	0.35	0.31	0.25	0.33	0.19
Chair Rise - Peak Extension Moment (N.m/kg)	0.17	0.08	0.16	0.28	0.23	0.22	0.06	0.17	0.29	0.12	0.14	0.11	0.09	0.09	0.09
Chair Rise - Peak Adduction Moment (N.m/kg)	0.44	0.34	0.47	0.47	0.72	0.75	0.50	0.81	0.41	1.10	0.10	0.79	0.36	0.39	0.41
Chair Down - Peak Flexion Moment (N.m/kg)	0.86	0.11	0.19	0.07	0.20	0.16	0.26	0.28	0.20	0.12	0.08	0.12	0.09	0.18	0.09
Chair Down - Peak Abduction Moment (N.m/kg)	0.32	0.45	0.51	0.26	0.41	0.49	0.57	0.67	0.55	0.87	0.83	0.54	0.22	0.24	0.33
Stair Up - Peak Extension Moment (N.m/kg)	0.30	0.20	0.47	0.63	0.52	0.01	1.10	0.90	1.30	1.50	0.10	1.20	0.33	0.23	0.43
Stair Down - Peak Flexion Moment (N.m/kg)	0.61	0.84	0.82	0.79	0.95	0.58	0.75	0.67	0.57	0.42	0.46	0.40	0.46	0.52	0.49

D-2: Gait Analysis Plot Peak Position – Kinematics

The following images show the VICON image and corresponding peak of the plot, exemplifying the peak points chosen for kinematic analyses measures including walk peak extension angle, peak flexion angle, peak abduction and peak adduction angle. For stair activity – stair ascent peak extension angle and stair descent peak flexion angle

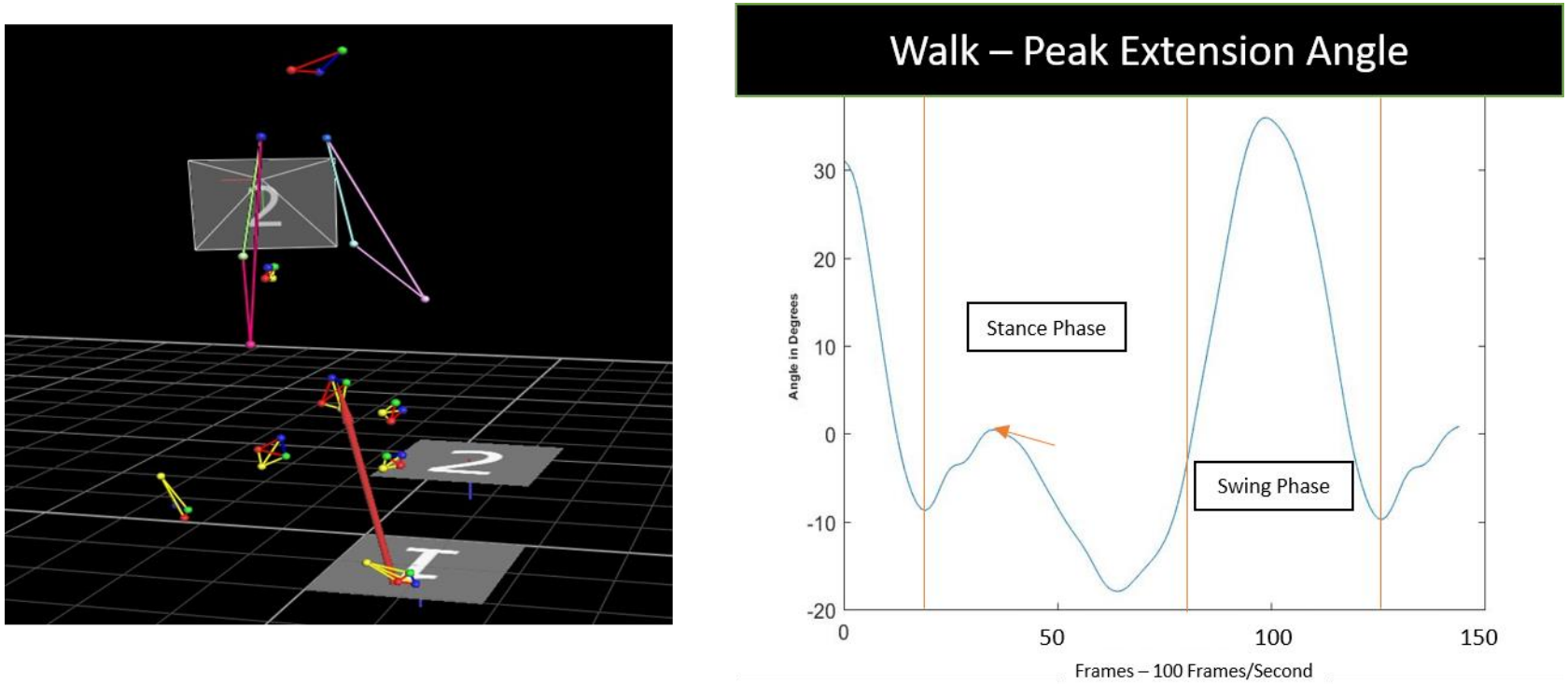

Figure D-2-1: VICON image and corresponding peak of the plot for walk peak extension angle (shown with red arrow)

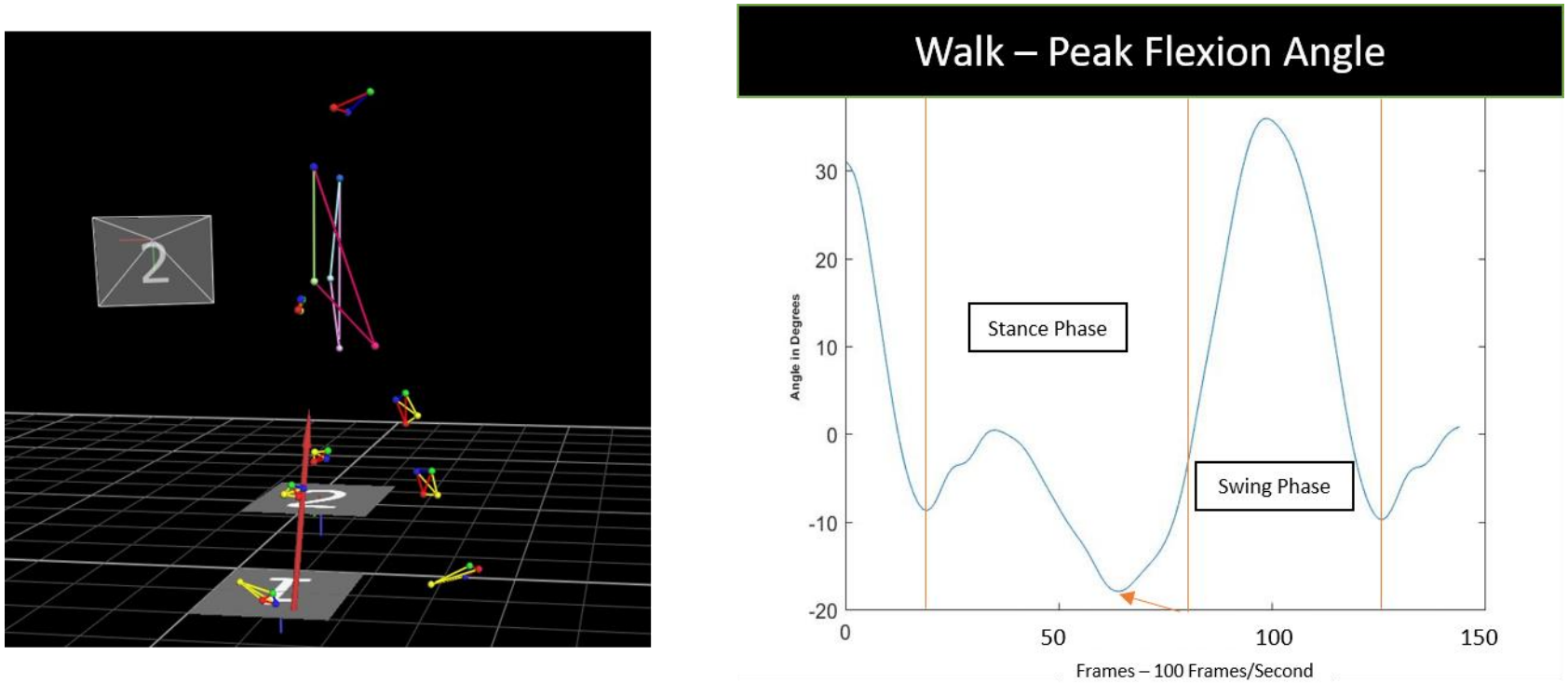

Figure D-2-2: VICON image and corresponding peak of the plot for walk peak flexion angle (shown with red arrow)

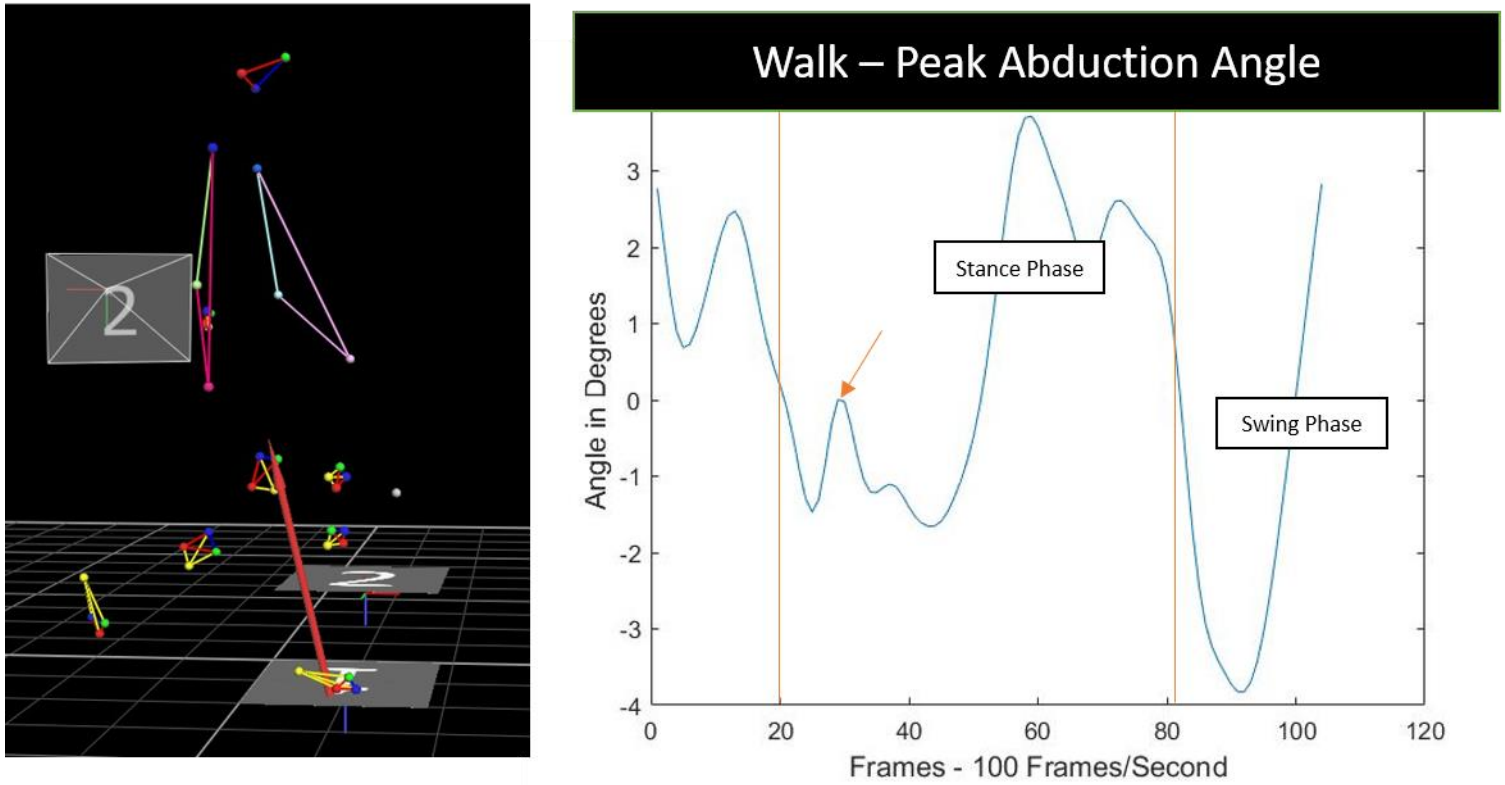

Figure D-2-3: VICON image and corresponding peak of the plot for walk peak flexion angle (shown with red arrow)

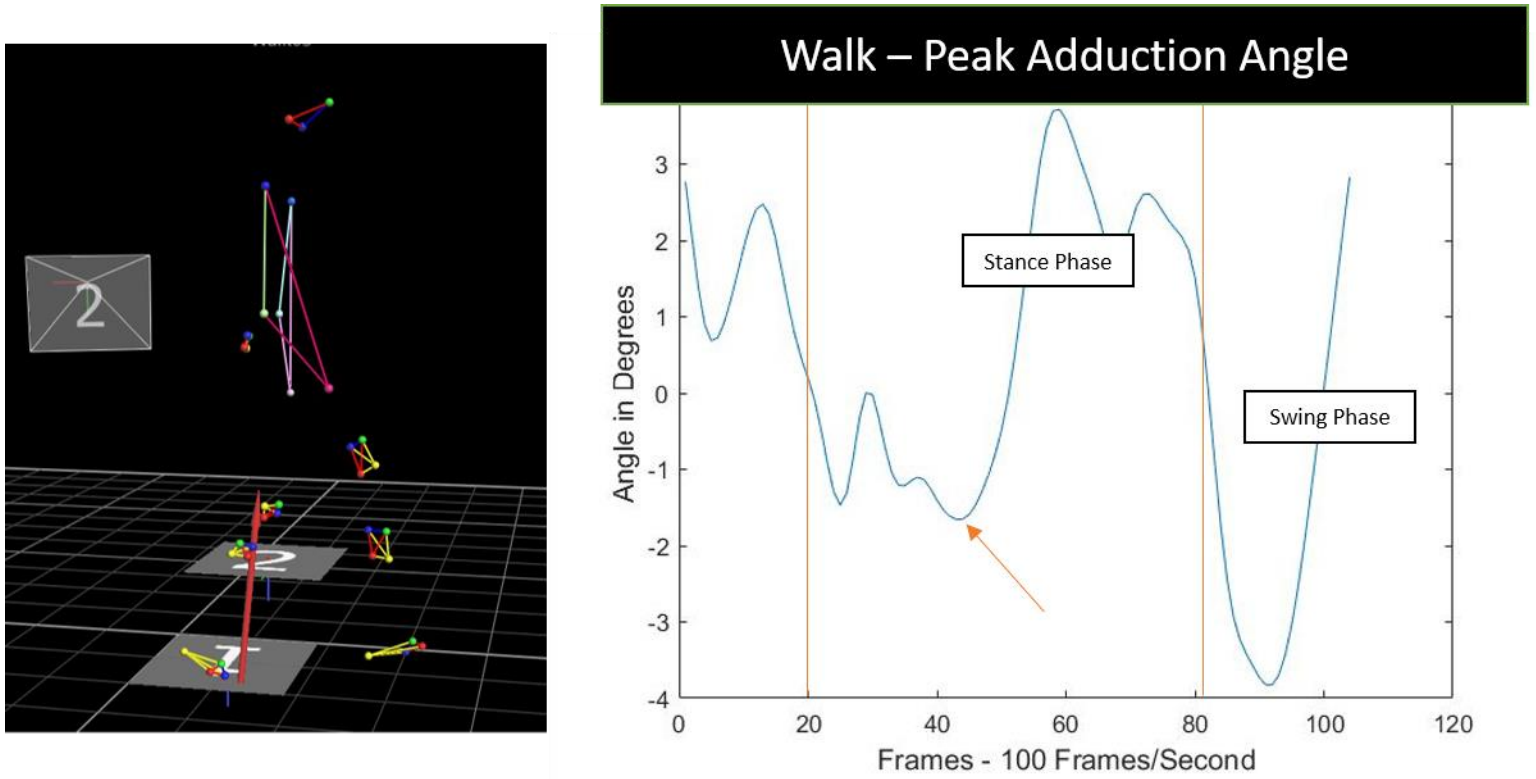

Figure D-2-4: VICON image and corresponding peak of the plot for walk peak flexion angle (shown with red arrow)

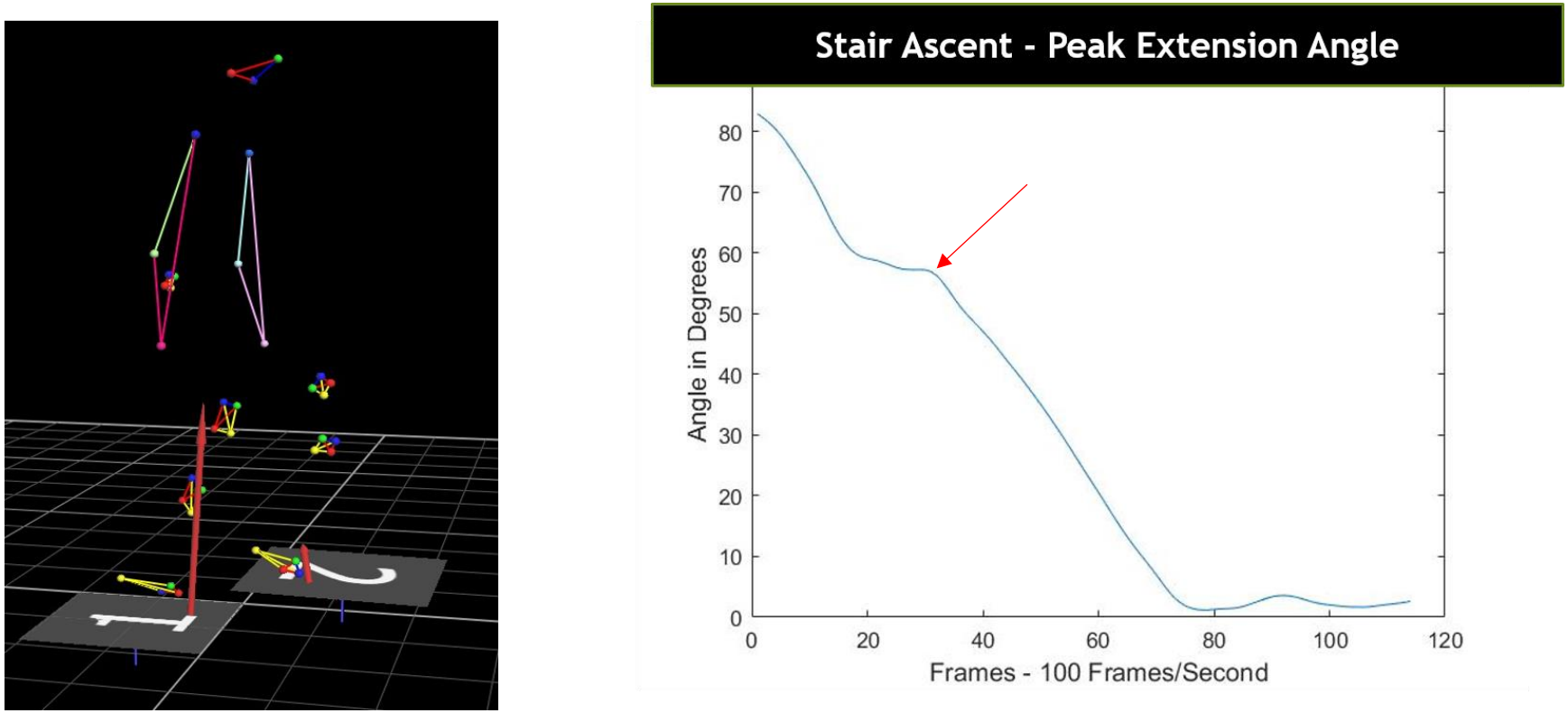

Figure D-2-5: VICON image and corresponding peak of the plot for walk peak flexion angle (shown with red arrow)

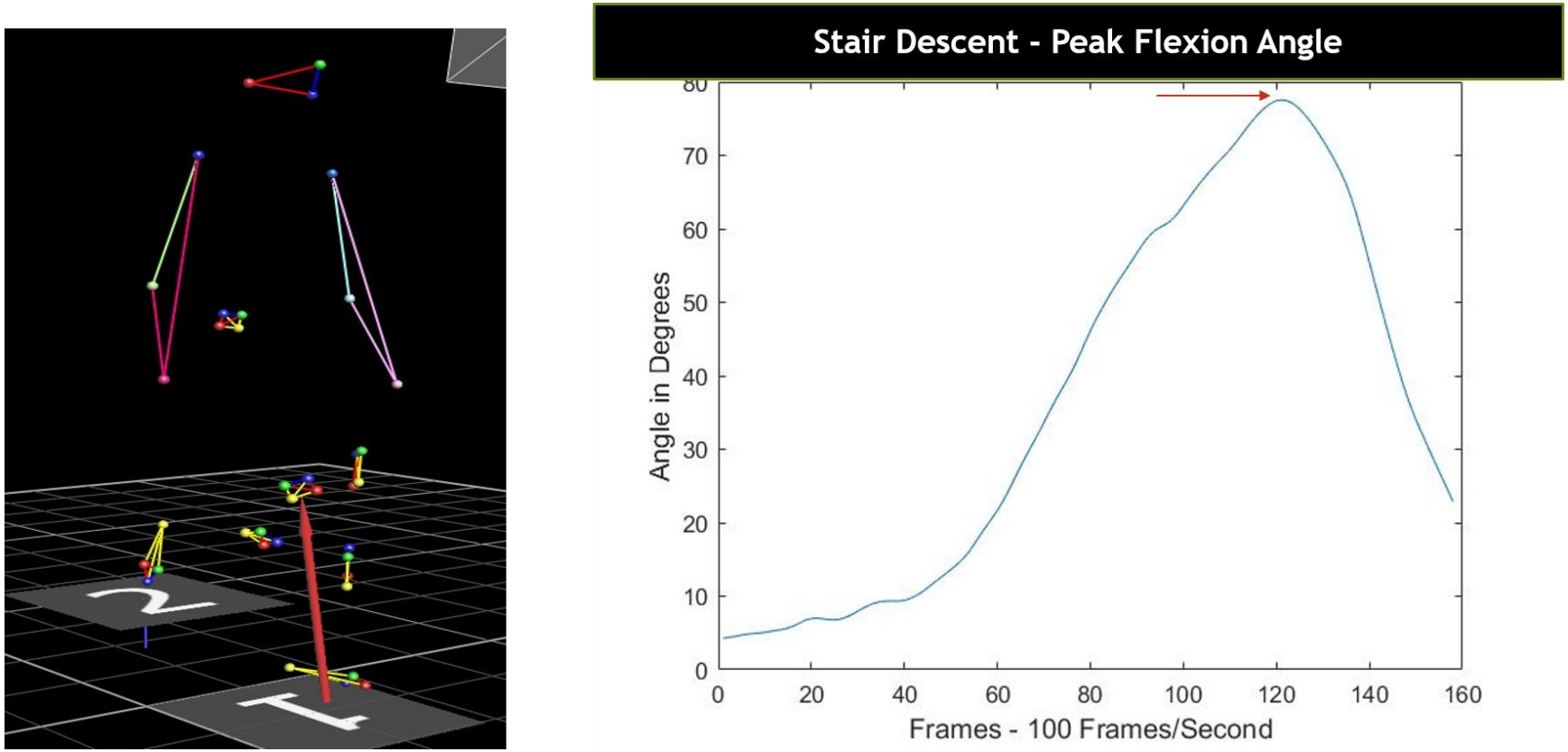

Figure D-2-6: VICON image and corresponding peak of the plot for walk peak flexion angle (shown with red arrow)

Appendix D-3: Gait Analysis Plot Peak Position – Kinetics

The following images show the VICON image and corresponding peak of the plot, exemplifying the peak points chosen for kinetic analyses measures including walk peak flexion moment, peak extension moment, peak abduction and peak adduction moment. For the chair activity – Chair rise peak extension and adduction moments and chair sit peak flexion moment, chair sit peak abduction moment. Foer the stair activity – Stair ascent peak extension moment and stair descent peak flexion moment

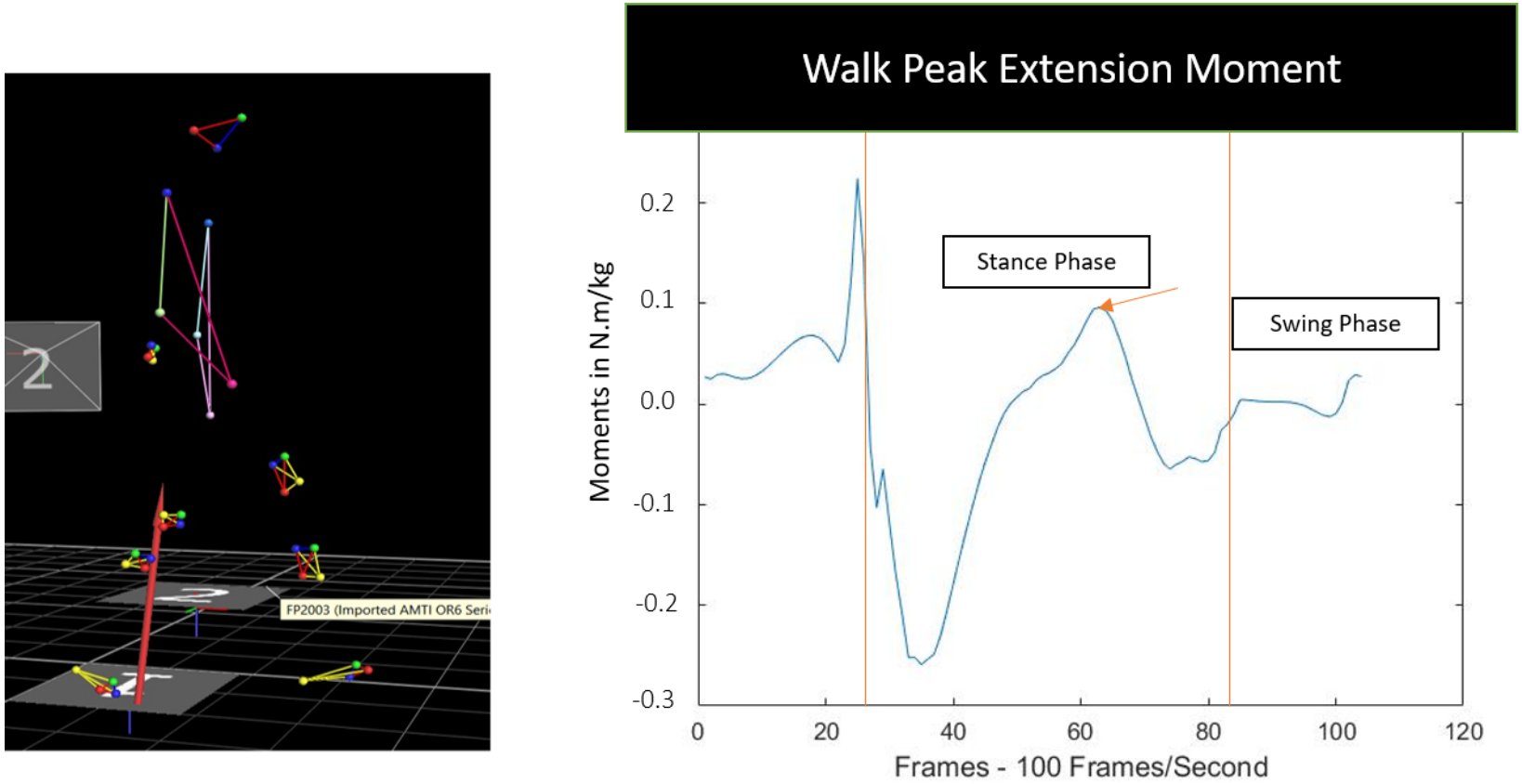

Figure D-3-1: VICON image and corresponding peak of the plot for walk peak extension moment (shown with red arrow)

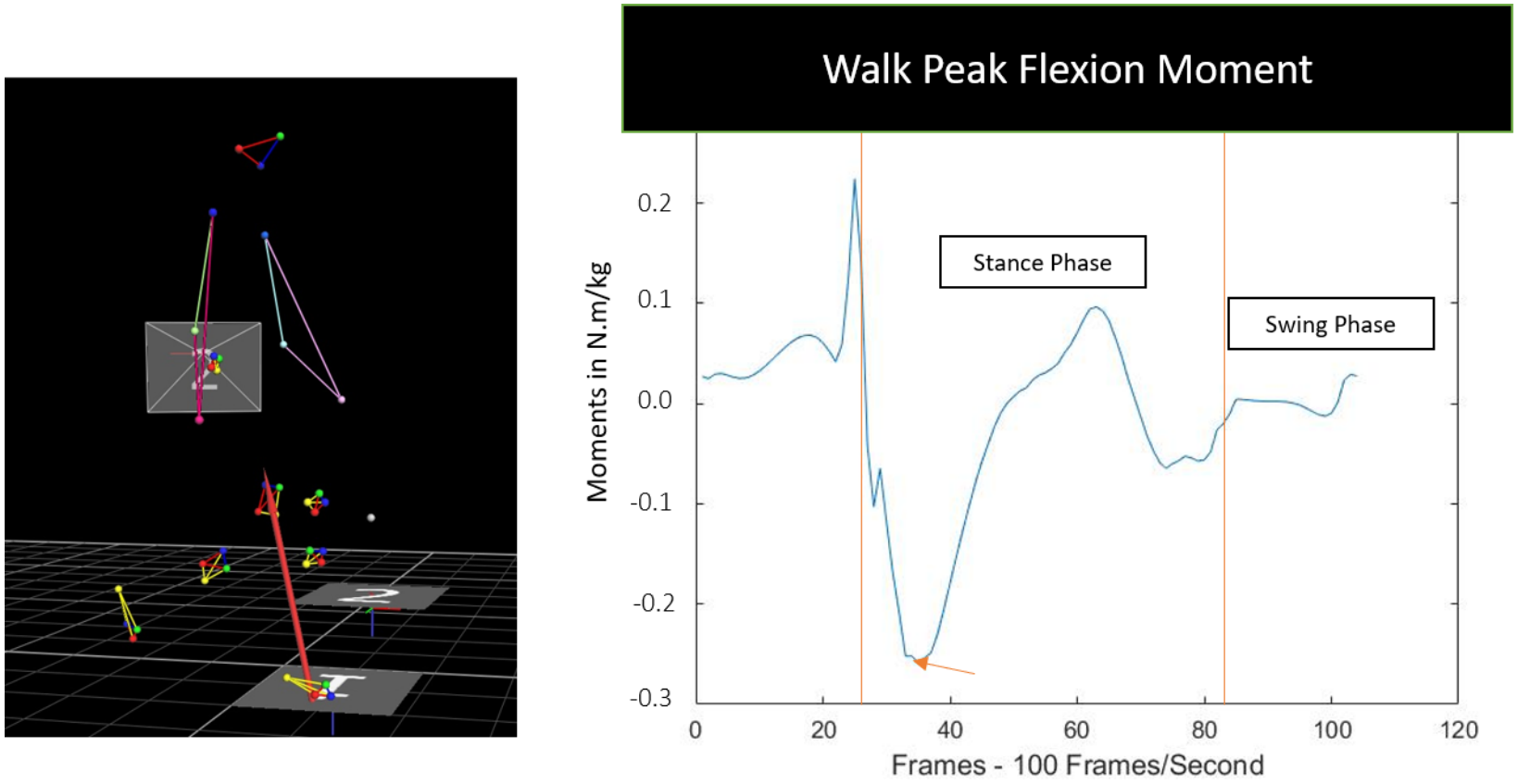

Figure D-3-2: VICON image and corresponding peak of the plot for walk peak flexion moment (shown with red arrow)

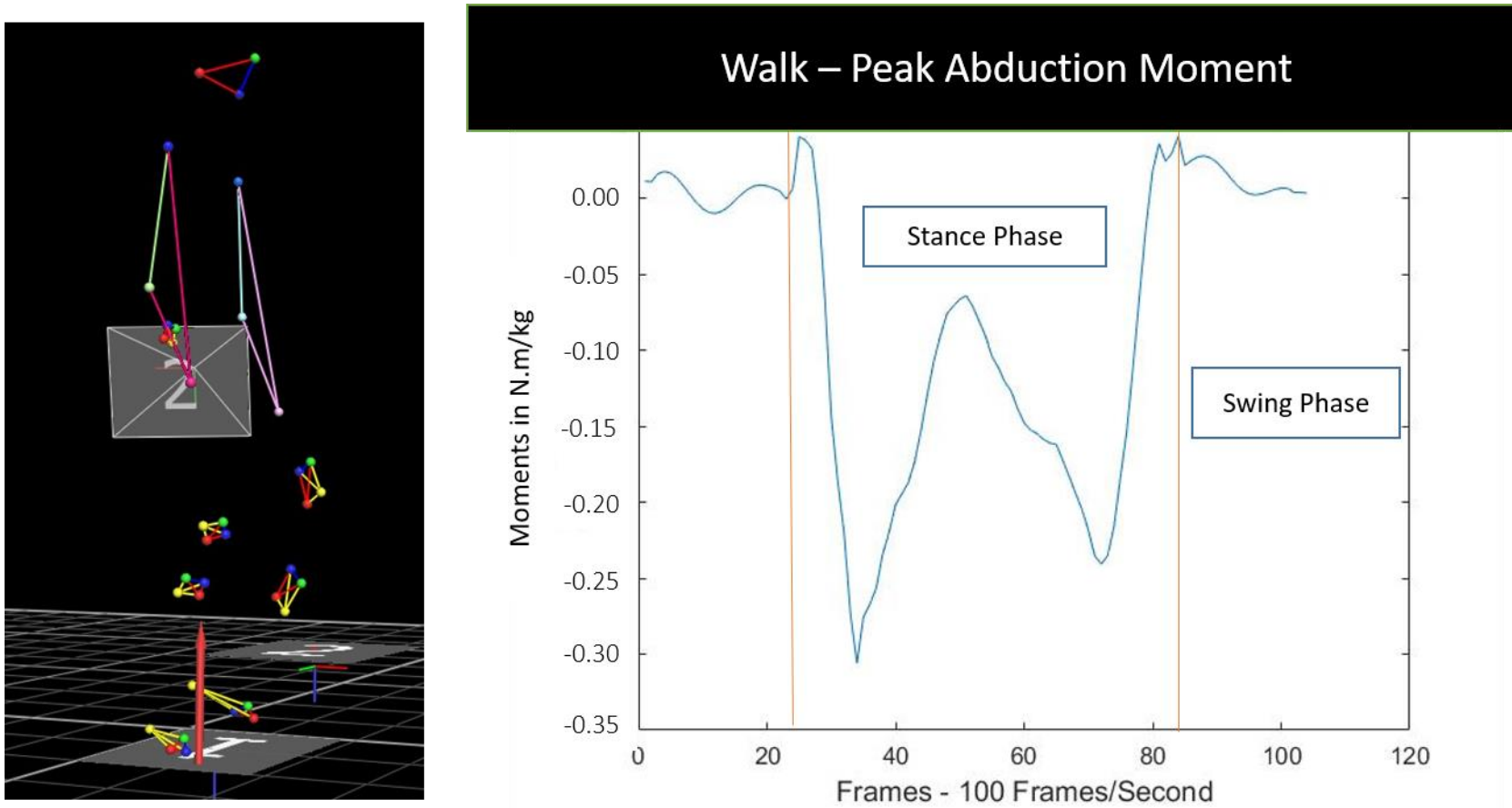

Figure D-3-3: VICON image and corresponding peak of the plot for walk peak abduction moment (shown with red arrow)

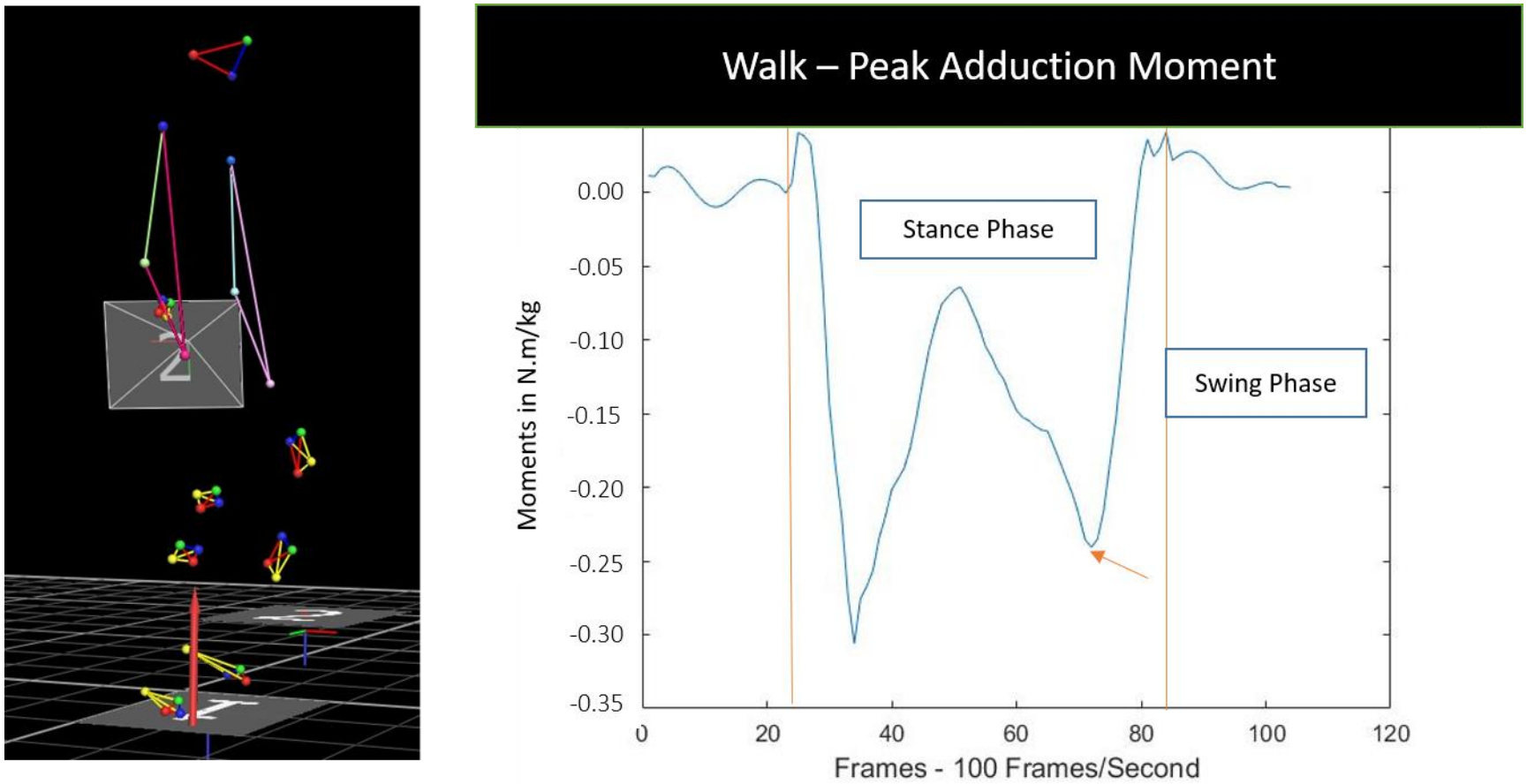

Figure D-3-4: VICON image and corresponding peak of the plot for walk peak adduction moment (shown with red arrow)

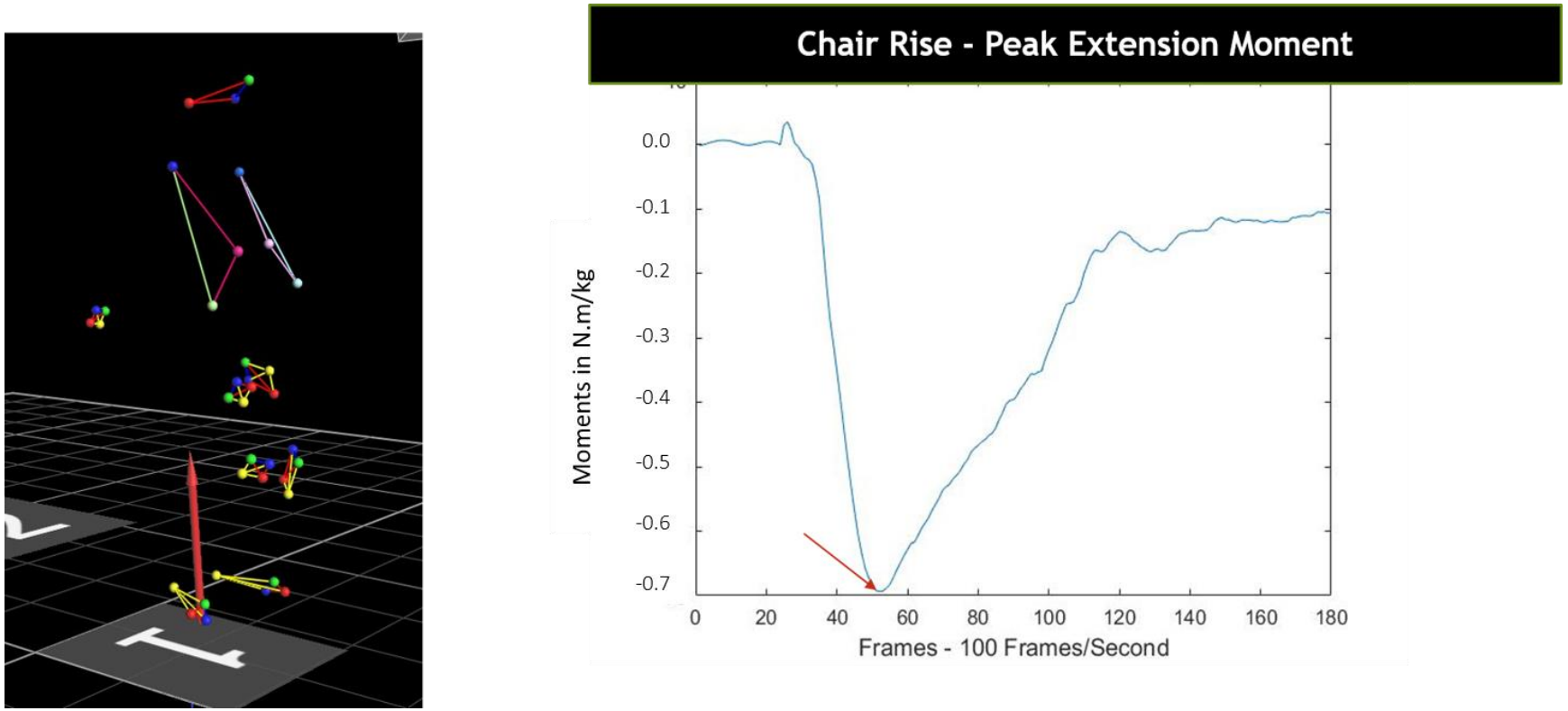

Figure D-3-5: VICON image and corresponding peak of the plot for chair rise peak extension moment (shown with red arrow)

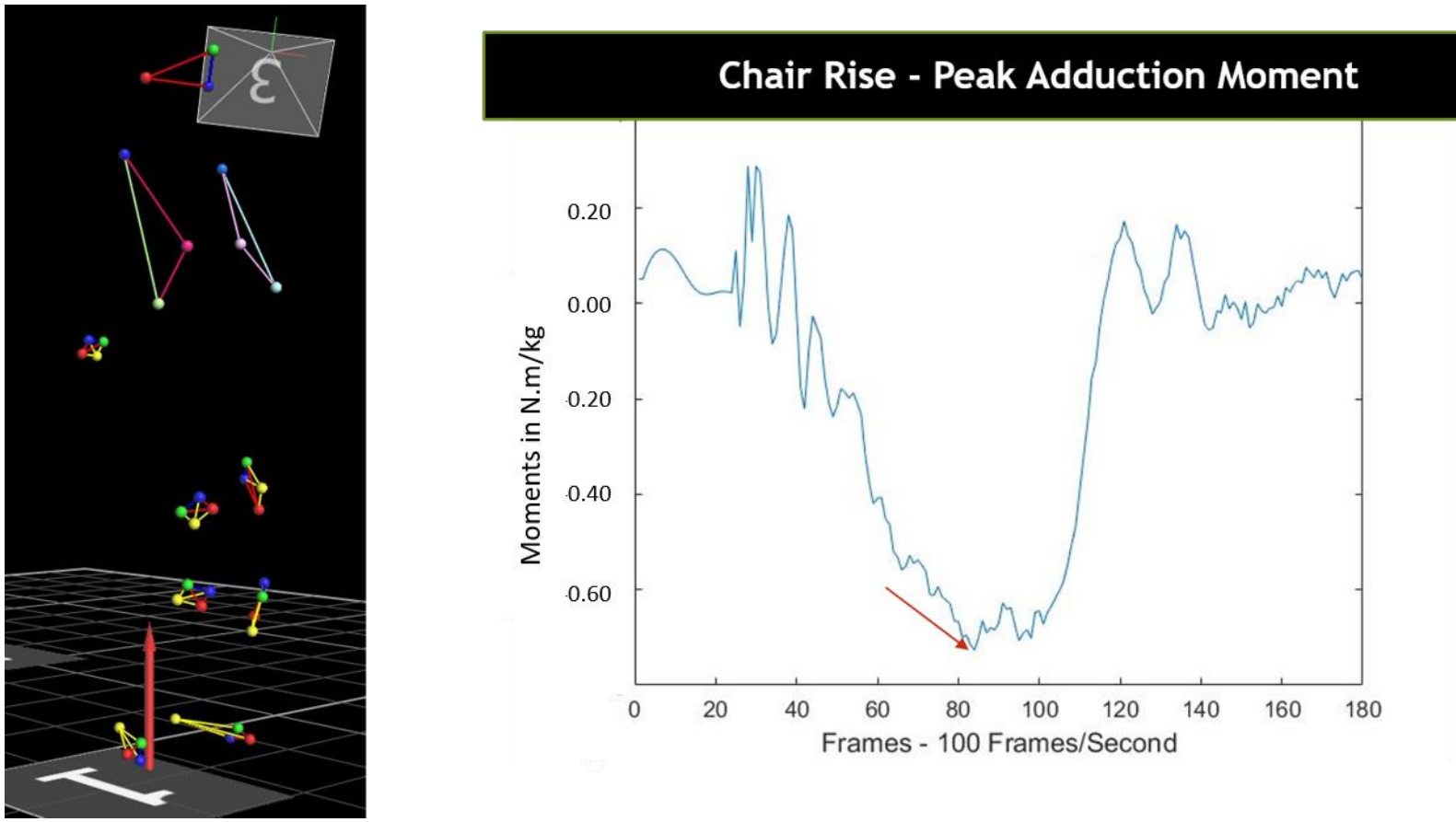

Figure D-3-6: VICON image and corresponding peak of the plot for walk peak abduction moment (shown with red arrow)

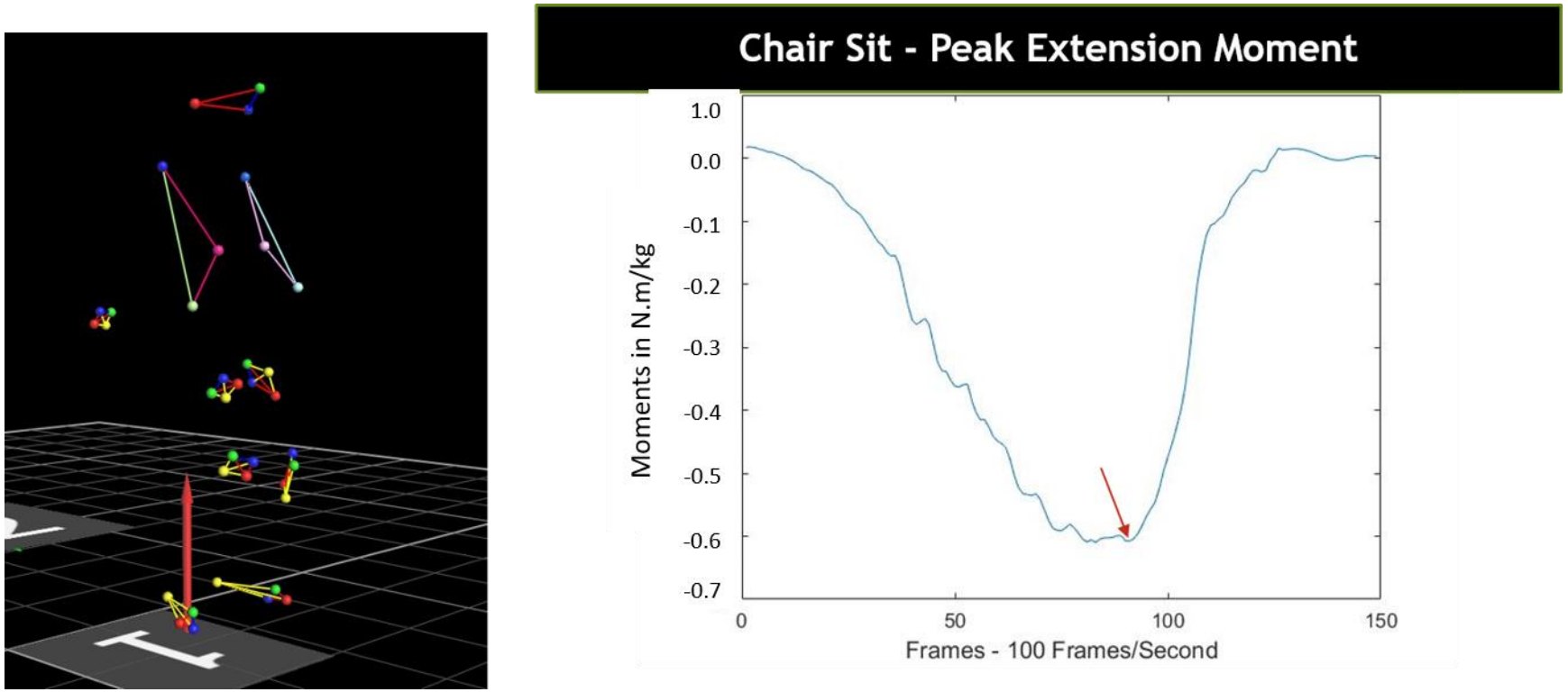

Figure D-3-7: VICON image and corresponding peak of the plot for chair sit peak extension moment (shown with red arrow)

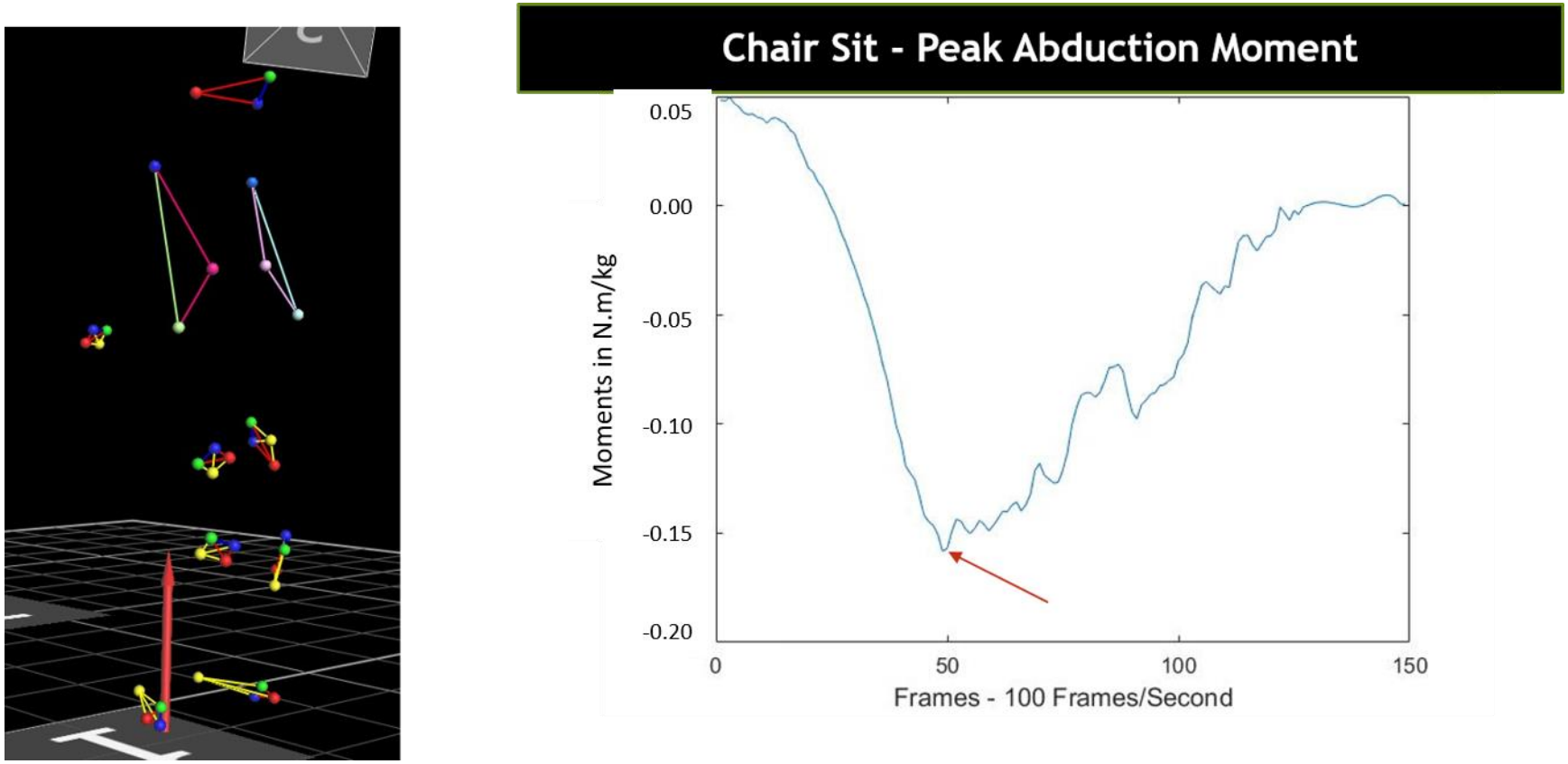

Figure D-3-8: VICON image and corresponding peak of the plot for chair sit peak abduction moment (shown with red arrow)

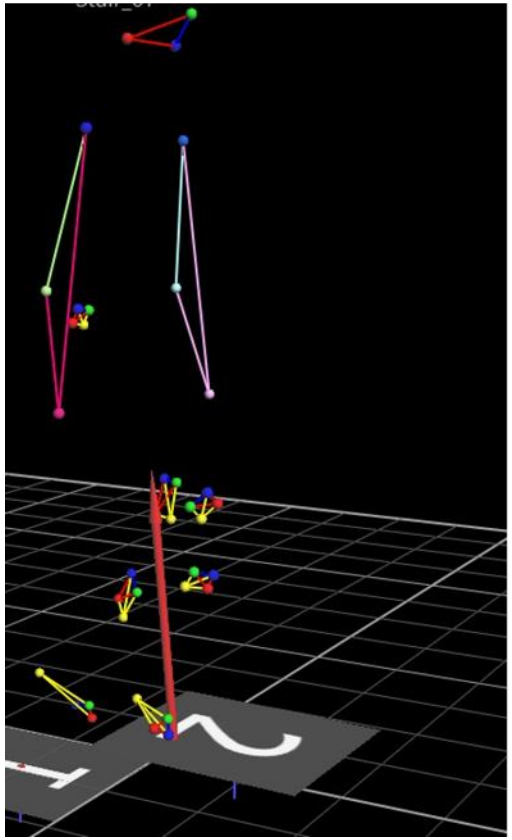

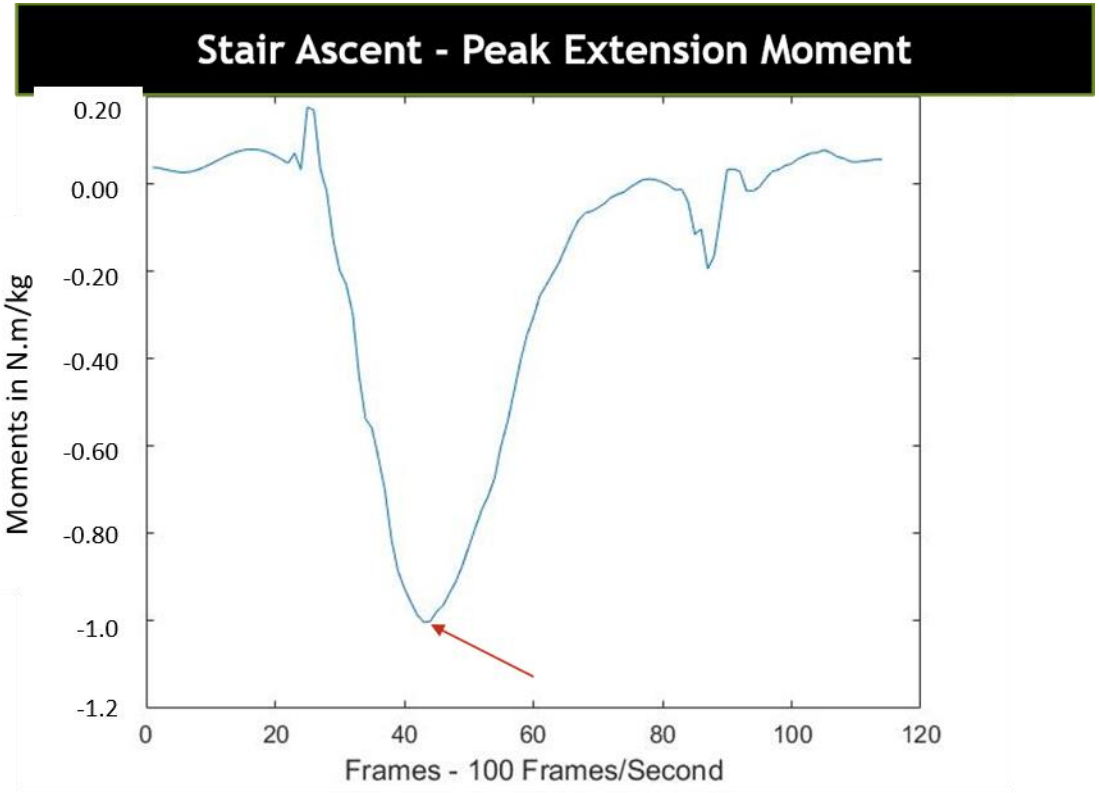

Figure D-3-9: VICON image and corresponding peak of the plot for stair ascent peak extension moment (shown with red arrow)

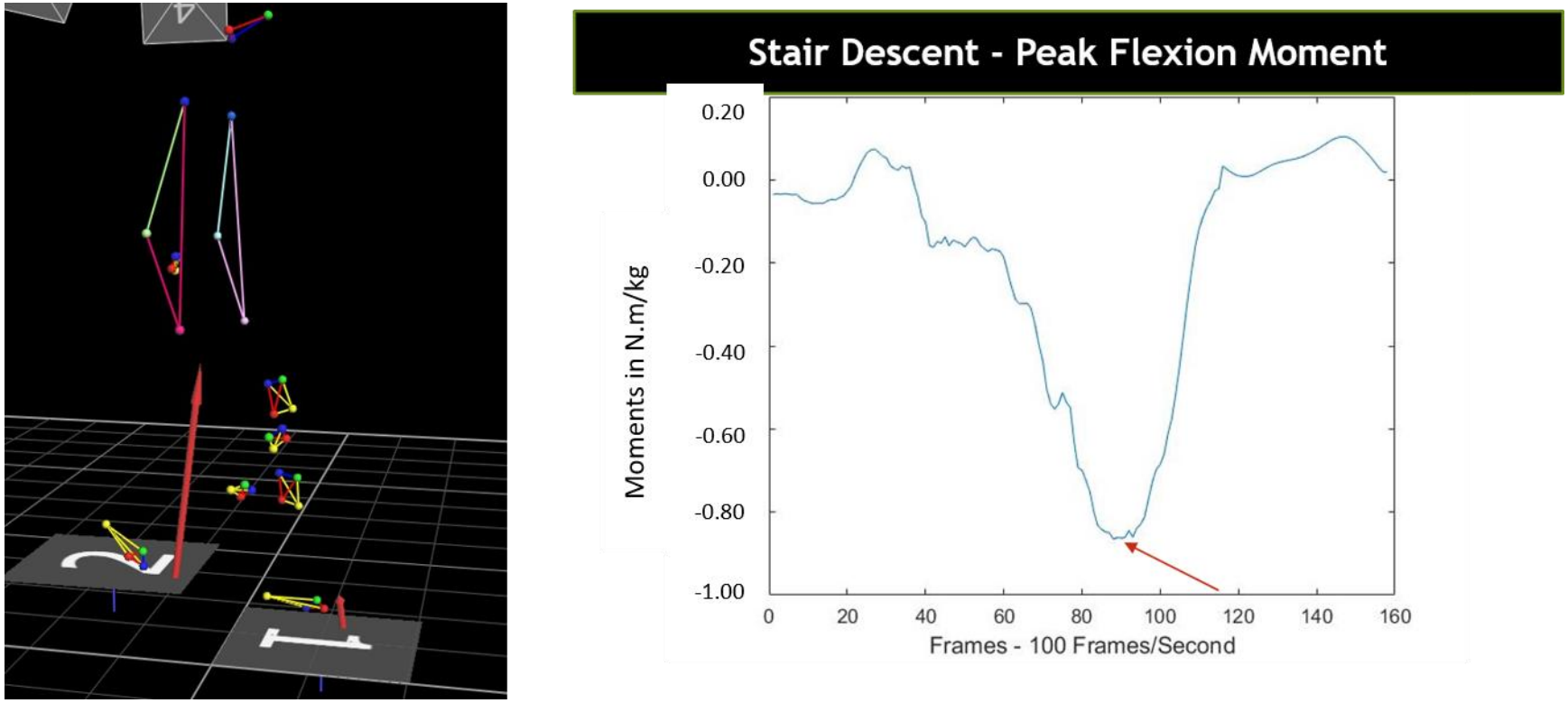

Figure D-3-10: VICON image and corresponding peak of the plot for stair descent peak extension moment (shown with red arrow)

Appendix E: MRI-Gait Comparison Results – Supplementary Material

The figures below show Bland-Altman plots all kinematic and kinetic measures.

E1: Bland-Altman Plots for Kinematic Measures

The figures in this section show the Bland-Altman plots, comparing the MRI-based and gait-based kinematic outcomes for all three trials of five participants (15 points in plot). The kinematic outcomes with plots below include walk peak extension angle, peak flexion angle, peak abduction and peak adduction angle. For stair activity – stair ascent peak extension angle and stair descent peak flexion angle

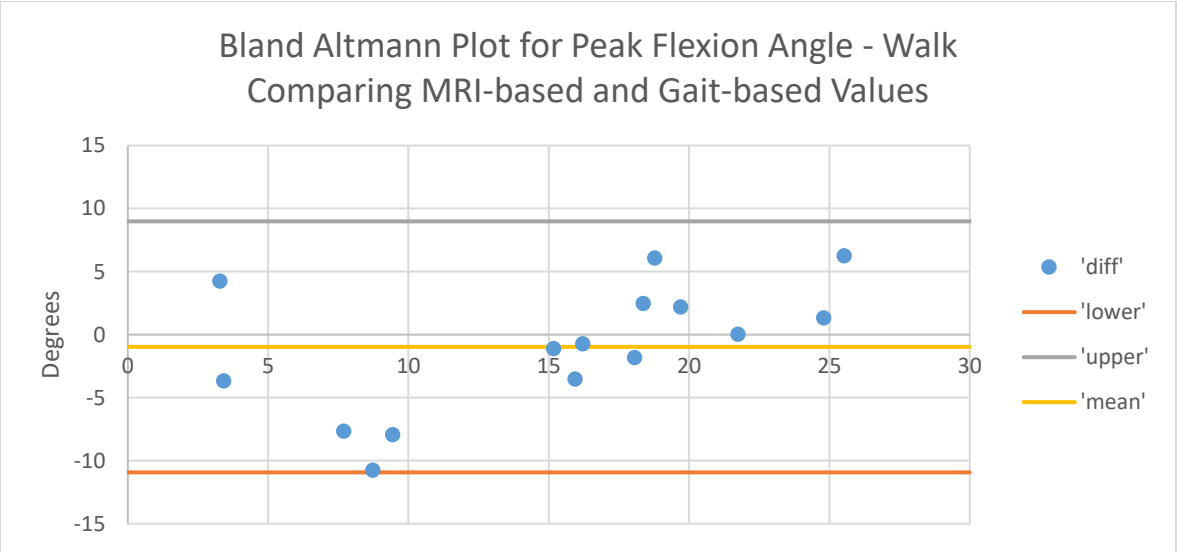

Figure E-1-1: Bland-Altman plot for walk peak knee flexion angle - comparing MRI-based and gait-based outcomes

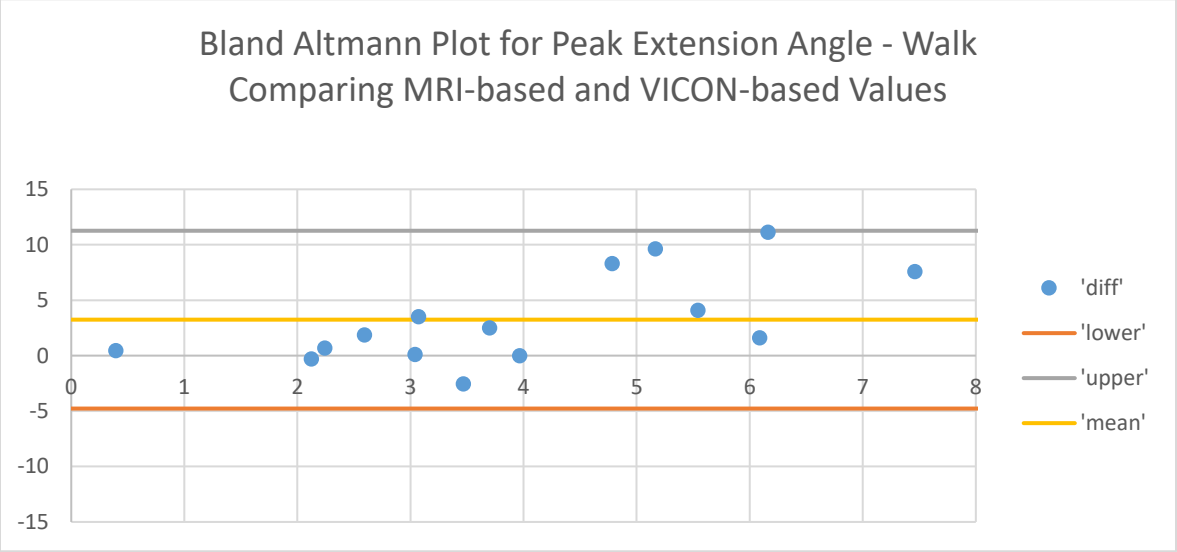

Figure E-1-2: Bland-Altman plot for walk peak knee extension angle - comparing MRI-based and gait-based outcomes

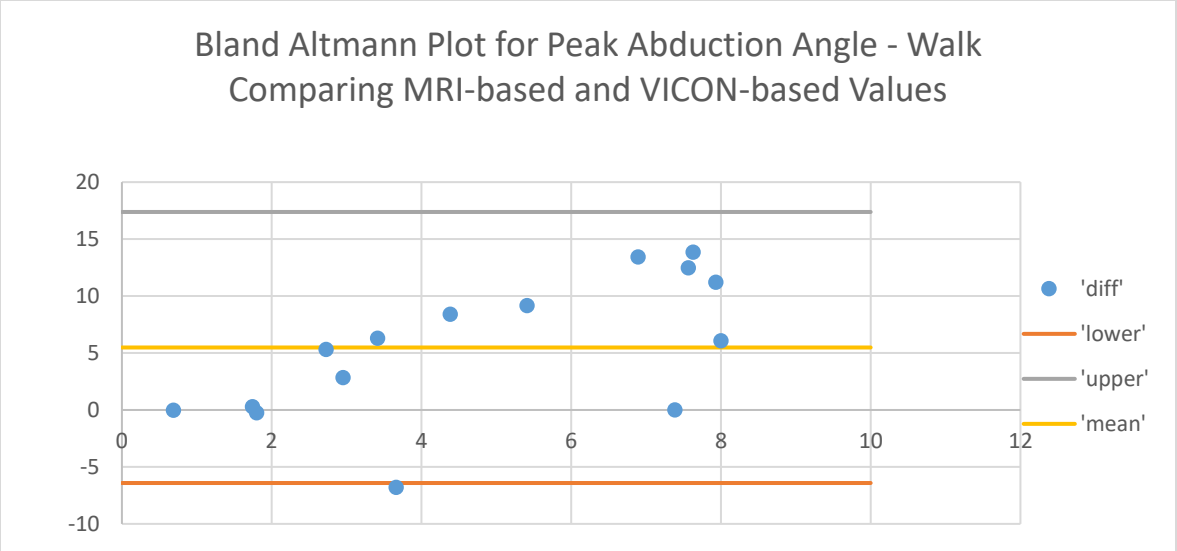

Figure E-1-3: Bland-Altman plot for walk peak knee abduction angle - comparing MRI-based and gait-based outcomes

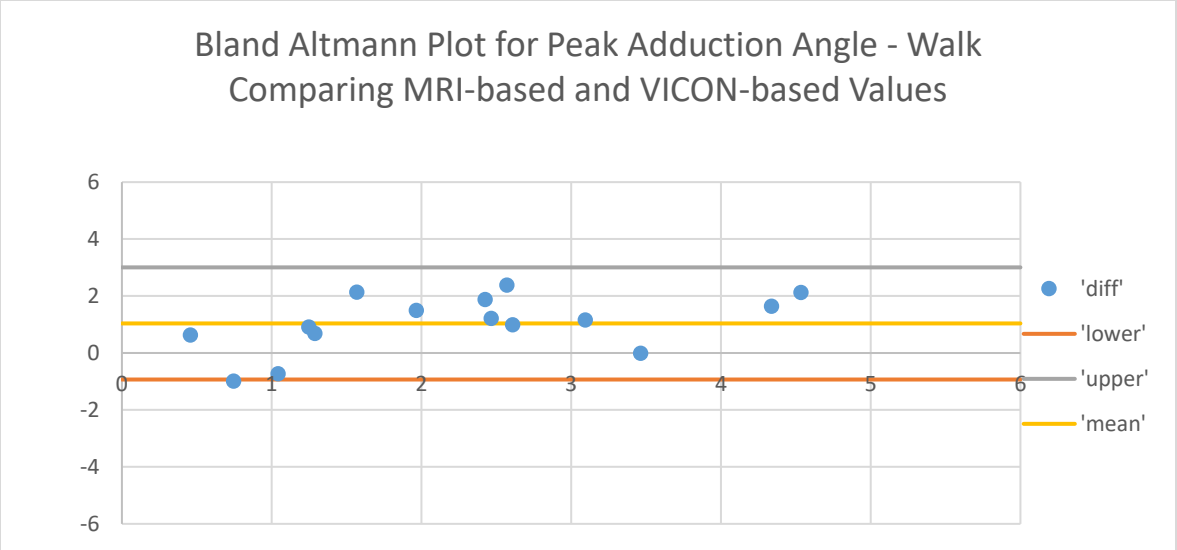

Figure E-1-4: Bland-Altman plot for walk peak knee adduction angle - comparing MRI-based and gait-based outcomes

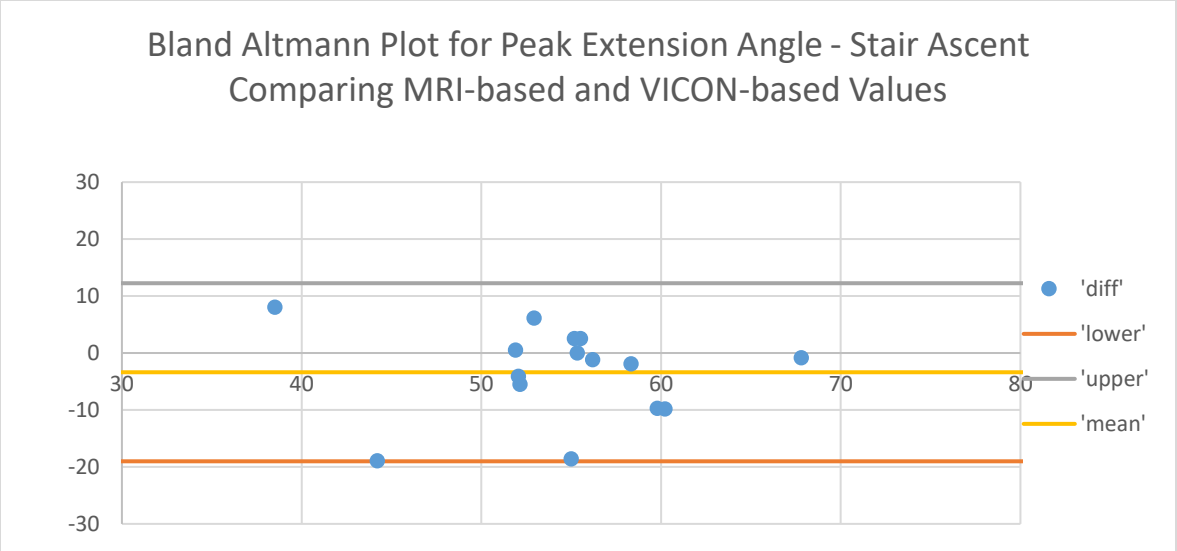

Figure E-1-5: Bland-Altman plot for stair ascent peak knee extension angle - comparing MRI-based and gait-based outcomes

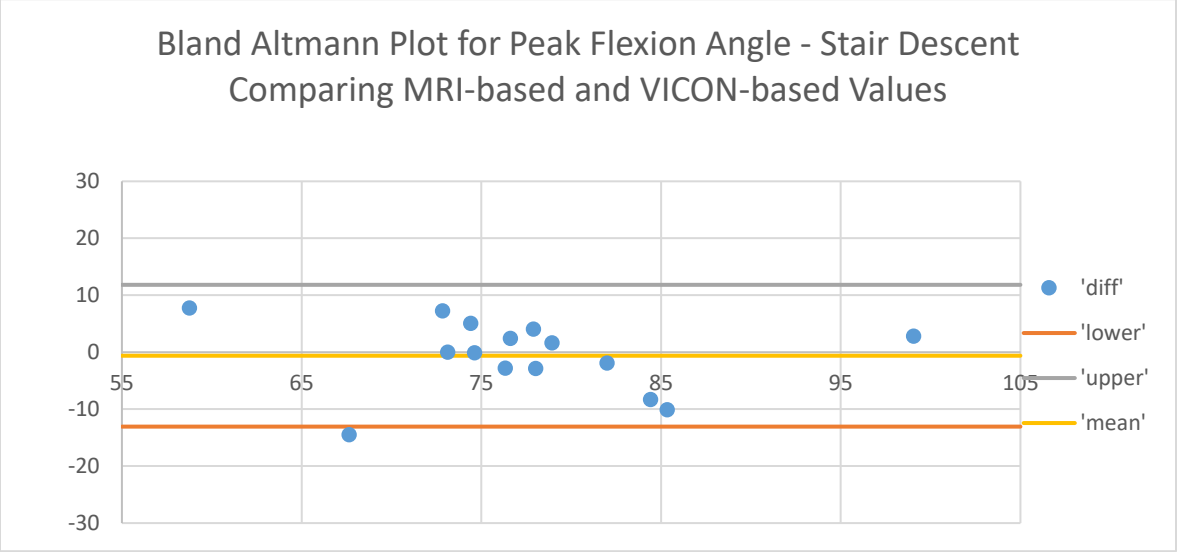

Figure E-1-6: Bland-Altman plot for stair descent peak knee flexion angle - comparing MRI-based and gait-based outcomes

E-2: Bland-Altman Plots for Kinetic Measures

The figures in this section show the Bland-Altman plots, comparing the MRI-based and gait-based kinetic outcomes for all three trials of five participants (15 points in plot). The kinetic analyses measures including walk peak flexion moment, peak extension moment, peak abduction and peak adduction moment. For the chair activity – chair rise peak extension and adduction moments and chair sit peak flexion moment, chair sit peak abduction moment. For the stair activity – stair ascent peak extension moment and stair descent peak flexion moment.

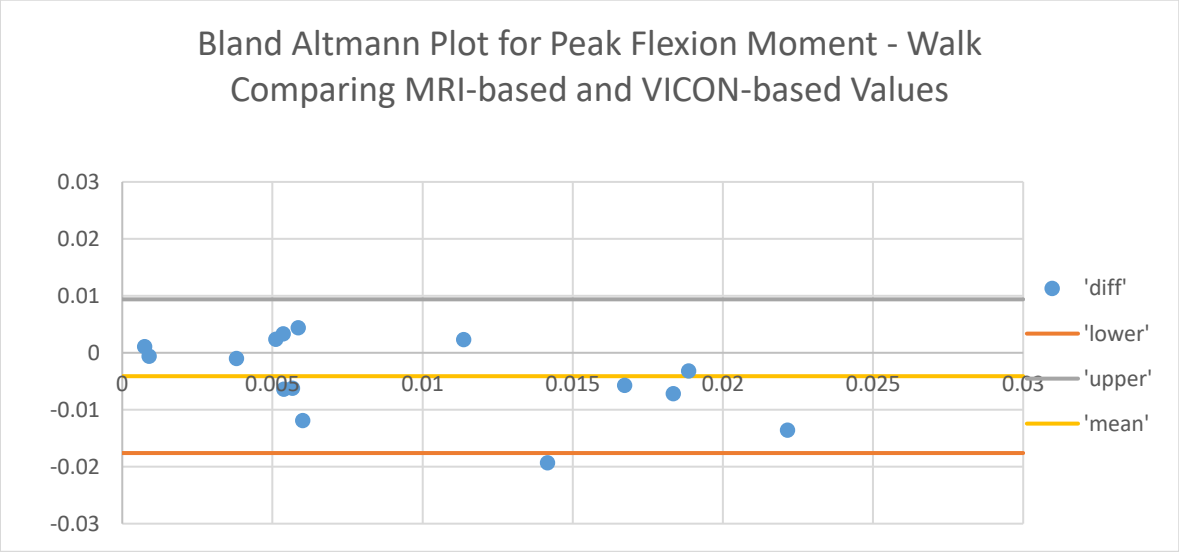

Figure E-2-1: Bland-Altman plot for walk peak knee flexion moment - comparing MRI-based and gait-based outcomes

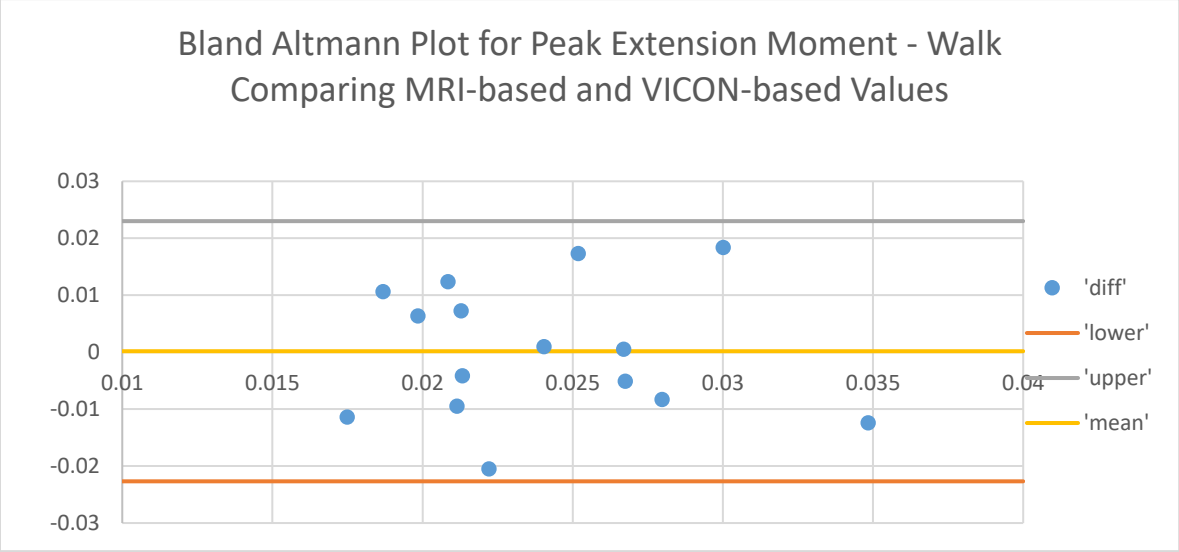

Figure E-2-2: Bland-Altman plot for walk peak knee extension moment - comparing MRI-based and gait-based outcomes

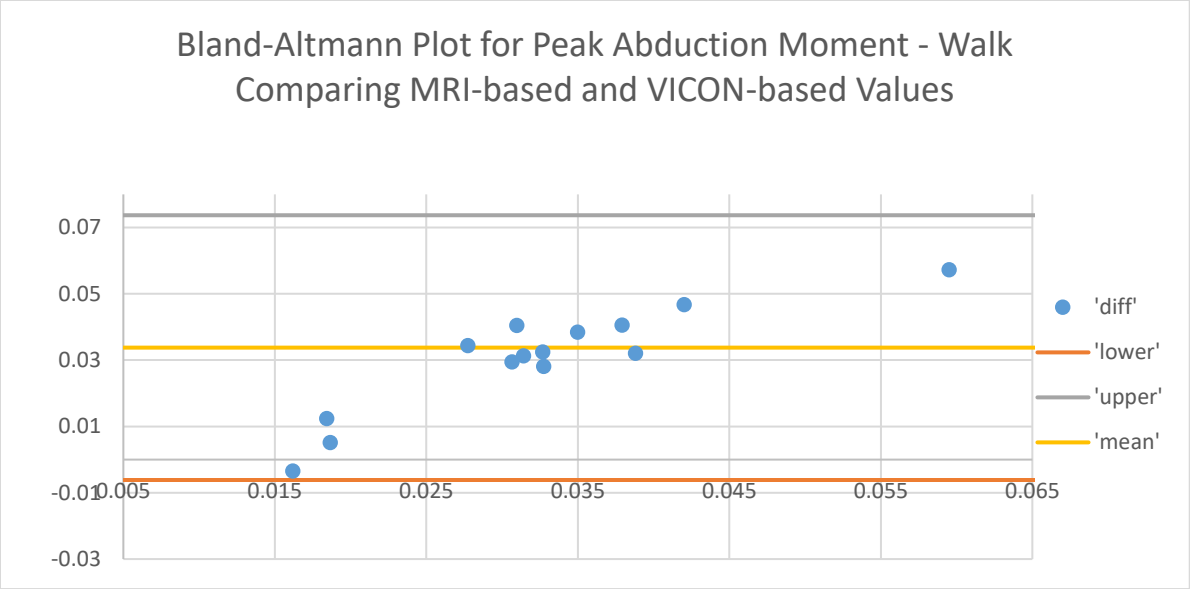

Figure E-2-3: Bland-Altman plot for walk peak knee abduction moment - comparing MRI-based and gait-based outcomes

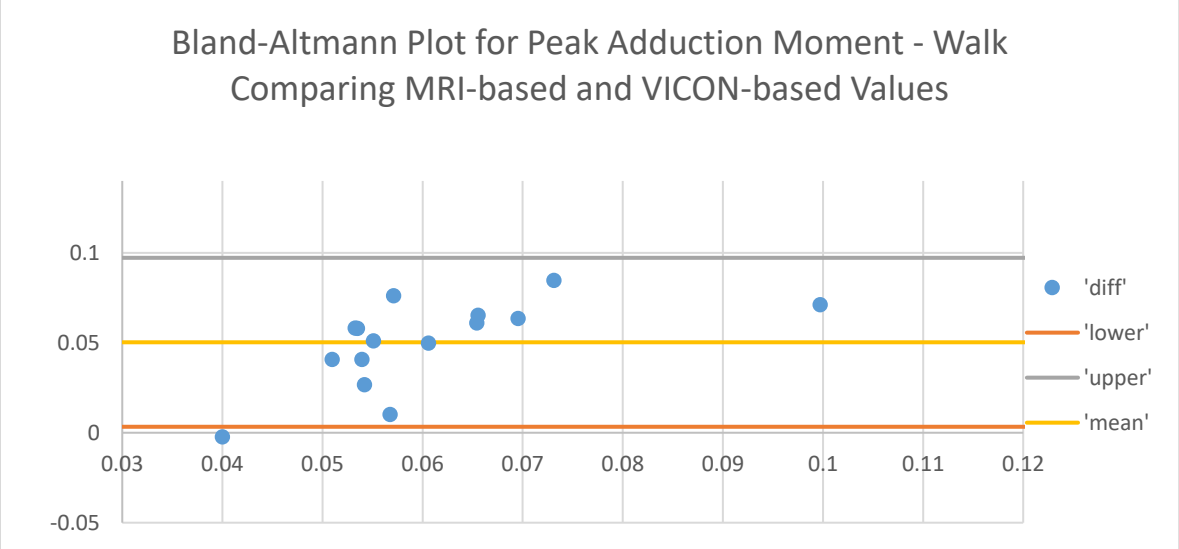

Figure E-2-4: Bland-Altman plot for walk peak knee adduction moment - comparing MRI-based and gait-based outcomes

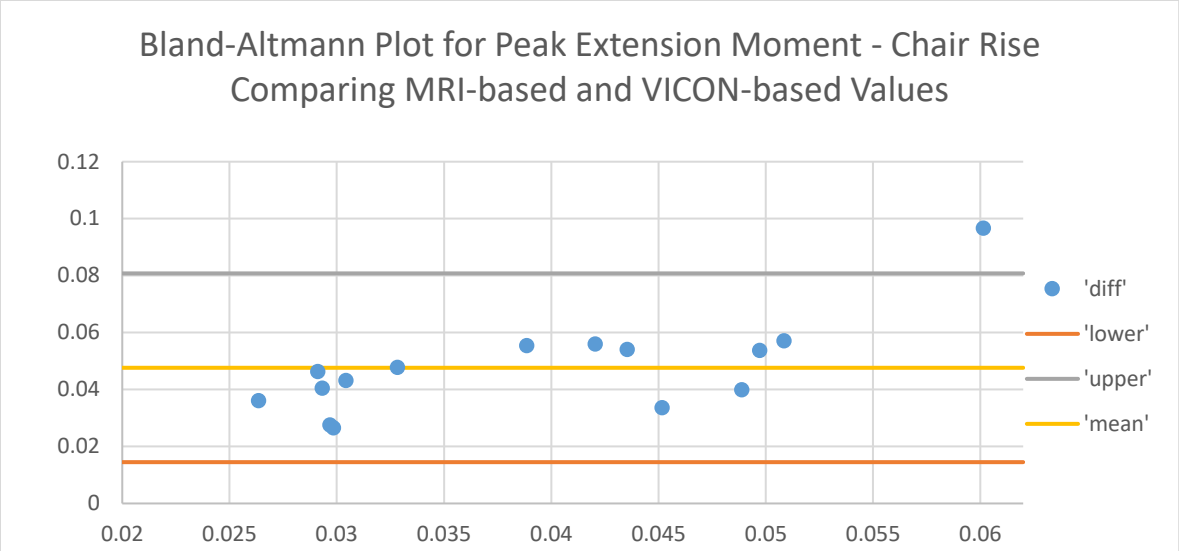

Figure E-2-5: Bland-Altman plot for chair rise peak knee extension moment - comparing MRI-based and gait-based outcomes

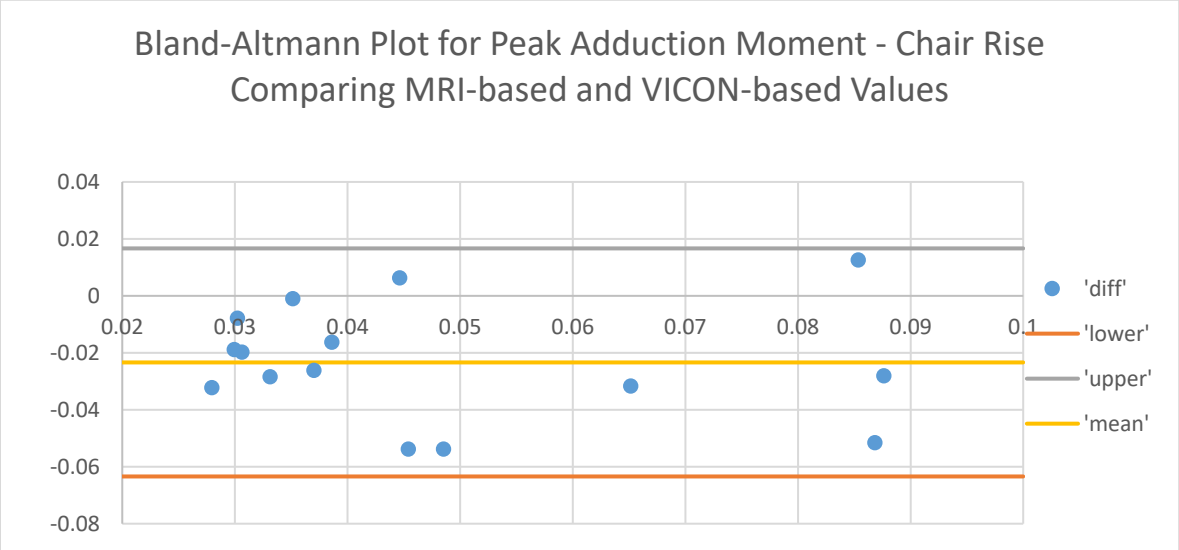

Figure E-2-6: Bland-Altman plot for chair rise peak knee adduction moment - comparing MRI-based and gait-based outcomes

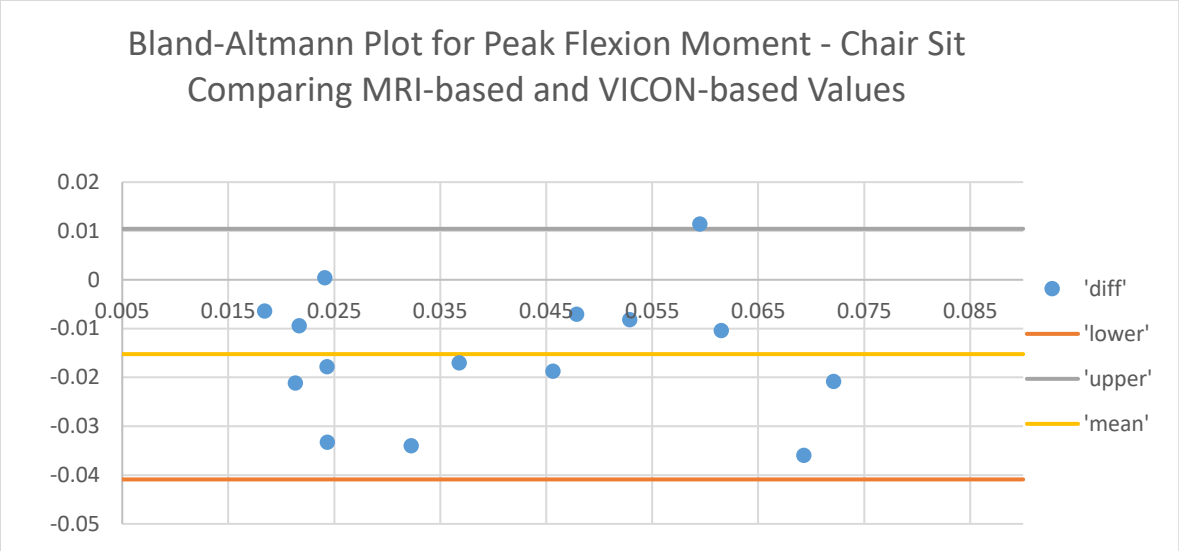

Figure E-2-7: Bland-Altman plot for chair sit peak knee flexion moment - comparing MRI-based and gait-based outcomes

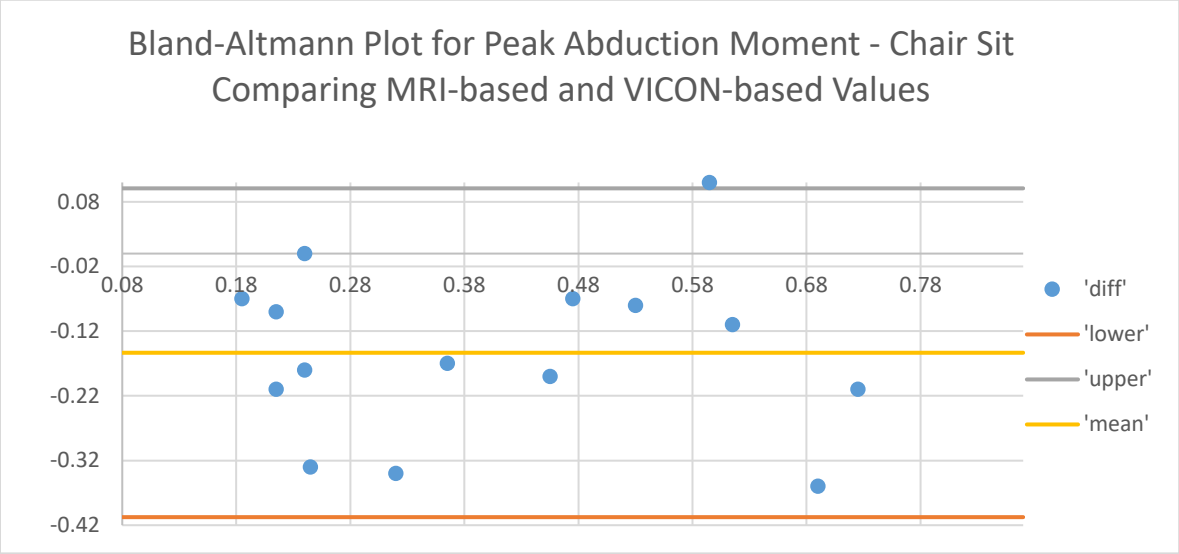

Figure E-2-8: Bland-Altman plot for chair sit peak knee abduction moment - comparing MRI-based and gait-based outcomes

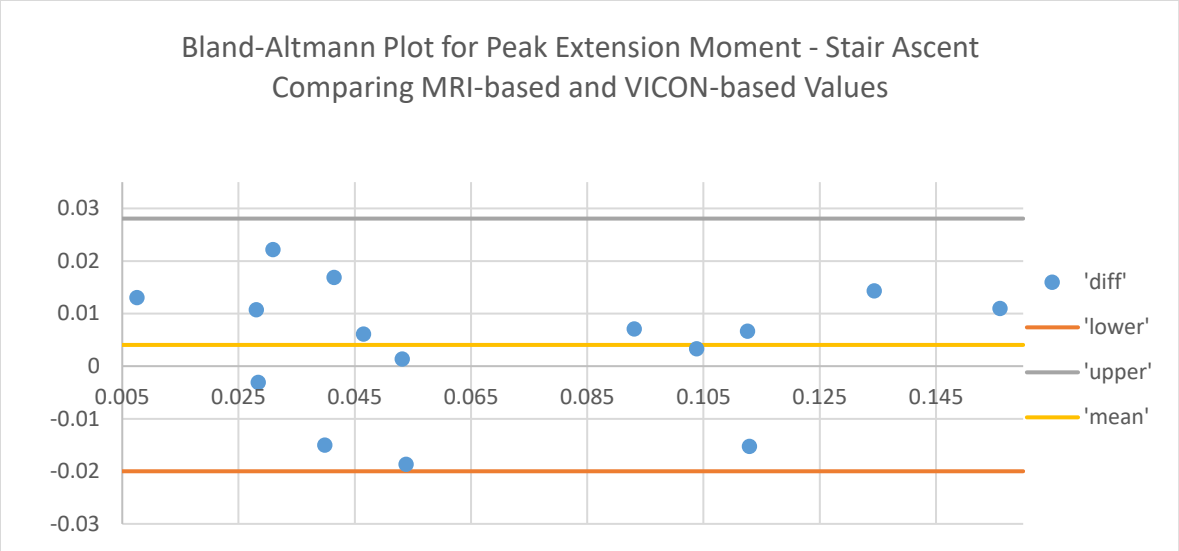

Figure E-2-9: Bland-Altman plot for stair ascent peak knee extension moment - comparing MRI-based and gait-based outcomes

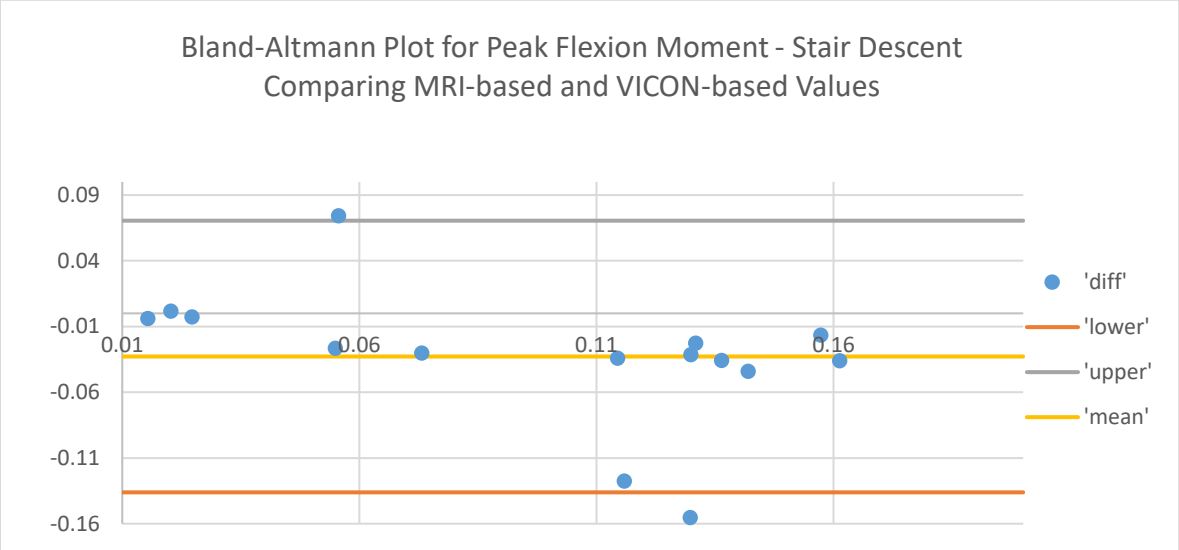

Figure E-2-10: Bland-Altman plot for stair descent peak knee flexion moment - comparing MRI-based and gait-based outcomes

Appendix F: qMRI-Contact Integration Results – Supplementary Material

The tables and figures below show the values of all the 15 trials including the T_2-contact novel measures for medial and lateral sides, the number of cluster centroids in and contact regions and the cluster maps for increasing and decreasing T_2 in cartilage from unloaded to loaded cases.

F1: All- Trial Tables

The tables below show the T_2-contact measures for the medial and lateral sides as well as the number of cluster centroids in and around the contact area. Note that for three trials in participant 1 and 1 trial in participant 2 for the loaded cartilage scenario, there are no values or images due to MRI sequence error in these cases during data acquisition.

Table F-1-1: qMRI T_2 contact integration outcomes for loaded and unloaded cases in the medial compartment

	Participant 1			Participant 2			Participant 3			Participant 4			Participant 5		
	Trial 1	Trial 2	Trial 3	Trial 1	Trial 2	Trial 3	Trial 1	Trial 2	Trial 3	Trial 1	Trial 2	Trial 3	Trial 1	Trial 2	Trial 3
	Medial Loaded														
Regional-Contact Mean Diff (ms)	3.1	-11.5	-11.1	7.4	-3.9	8.5	-3.5	0.8	-2.2	-6.9	-3.1	-5.7	-4.7	0.5	-3.7
Regional-Contact S.D Diff (ms)	3.2	-1.9	0.0	2.9	0.0	3.7	0.1	4.6	2.6	1.2	1.4	-1.3	-9.2	-0.7	1.6
Regional-Contact Max Diff (ms)	22.9	-8.7	-6.1	25.6	3.8	19.7	-5.7	24.6	2.4	11.8	9.9	-32.3	-20.4	-6.1	-32.6
Regional-Contact Min Diff (ms)	-1.2	-1.2	-2.3	0.0	-0.4	-0.1	-0.3	-0.2	-2.3	-0.5	-0.1	-0.1	0.0	-0.2	-0.9
Contact-Centroid Mean Diff (ms)	-3.7	-13.1	3.6	-8.5	-19.7	-6.4	2.0	4.2	7.6	5.4	4.3	7.0	-4.0	2.2	-2.1
Contact-Centroid S.D (ms)	-8.6	-13.5	-6.7	-4.0	-8.9	-3.9	-8.2	-7.4	-7.6	-8.2	-12.1	-9.7	-21.3	-12.7	-9.8
Contact-Centroid Mean Diff - Weighted (ms)	-7.0	2.5	3.2	-12.8	-9.5	-5.8	3.0	-1.0	6.3	-11.1	5.6	2.2	29.3	12.5	-3.1
Contact-Centroid S.D - Weighted (ms)	-10.5	-12.9	-6.5	-7.8	-12.7	-4.0	-10.8	-8.8	-7.7	-7.6	-10.9	-9.4	-16.1	-5.5	-8.7
	Medial Unloaded														
Regional-Contact Mean Diff (ms)					26.3	9.9	-5.9	-8.6	-2.9	-6.7	-1.3	5.4	-3.9	-6.0	0.3
Regional-Contact S.D Diff (ms)					13.5	4.2	-2.2	-3.9	-0.7	-4.1	3.1	3.3	-3.9	-7.0	-3.1
Regional-Contact Max Diff (ms)					55.9	41.1	-30.9	-33.1	-28.4	-20.1	9.4	14.7	-20.1	-38.0	-3.9
Regional-Contact Min Diff (ms)					0.2	-0.1	-0.3	-2.3	-0.3	0.1	-0.3	0.0	-0.3	-0.2	0.1
Contact-Centroid Mean Diff (ms)					-4.9	-6.8	-2.3	-3.0	-4.3	2.1	-0.5	18.8	-7.8	6.2	3.9
Contact-Centroid S.D (ms)					-2.5	-4.3	-11.3	-14.2	-9.7	-12.9	-7.1	-13.7	-14.3	-16.1	-12.2
Contact-Centroid Mean Diff - Weighted (ms)					4.6	14.1	-0.1	-4.2	-0.3	-24.7	-2.3	-18.6	-4.7	-6.6	-5.9
Contact-Centroid S.D - Weighted (ms)					-4.2	-7.1	-11.0	-13.0	-9.6	-13.0	-7.3	-9.3	-11.0	-16.5	-10.7

Table F-1-2: qMRI T_2 contact integration outcomes for loaded and unloaded cases in the lateral compartment

	Participant 1			Participant 2			Participant 3			Participant 4			Participant 5		
	Trial 1	Trial 2	Trial 3	Trial 1	Trial 2	Trial 3	Trial 1	Trial 2	Trial 3	Trial 1	Trial 2	Trial 3	Trial 1	Trial 2	Trial 3
	Lateral Loaded														
Regional-Contact Mean Diff (ms)	-4.5	-8.8	0.5	2.7	3.5	-4.9	-12.5	-12.5	-2.0	2.8	-2.4	-5.0	0.2	-3.0	-2.7
Regional-Contact S.D Diff (ms)	1.8	-1.0	4.4	1.6	2.9	5.4	6.1	2.9	8.3	12.4	11.2	4.2	0.6	3.6	4.5
Regional-Contact Max Diff (ms)	7.4	7.2	24.7	20.2	17.2	33.3	1.0	1.3	25.6	41.8	54.8	20.0	0.1	24.5	19.8
Regional-Contact Min Diff (ms)	-1.8	-1.9	-9.4	0.0	-0.6	-3.0	-11.0	-14.9	-15.7	-0.2	-1.9	-0.1	0.0	-0.5	-2.0
Contact-Centroid Mean Diff (ms)	-3.6	-4.5	-9.3	-3.2	2.5	-2.1	-15.4	-10.6	-5.1	3.2	-4.2	10.9	5.8	-6.8	-3.4
Contact-Centroid S.D (ms)	-7.5	-8.9	-7.2	-9.0	-6.5	-4.8	-6.6	-10.4	-6.6	-8.3	-6.8	-7.9	-14.5	-11.1	-10.7
Contact-Centroid Mean Diff - Weighted (ms)	6.4	1.3	-10.3	-4.0	-4.7	-0.6	-1.0	-4.1	-6.7	-8.3	-4.1	10.5	-20.9	-1.6	-3.3
Contact-Centroid S.D - Weighted (ms)	-3.8	-9.0	-7.7	-6.6	-6.1	-5.0	-7.2	-10.7	-6.9	-5.9	-5.5	-8.1	-12.7	-11.0	-11.1
	Lateral Unloaded														
Regional-Contact Mean Diff (ms)	0.0	0.0	0.0	0.0	-11.3	-7.5	-5.1	-12.8	-4.6	-11.4	-9.5	-13.1	-1.8	6.5	-2.2
Regional-Contact S.D Diff (ms)	0.0	0.0	0.0	0.0	4.1	1.0	5.1	1.9	7.5	1.3	3.3	2.7	7.7	6.2	0.6
Regional-Contact Max Diff (ms)	0.0	0.0	0.0	0.0	15.5	36.0	21.5	-10.6	22.8	4.2	3.6	0.8	42.5	58.2	29.9
Regional-Contact Min Diff (ms)	0.0	0.0	0.0	0.0	-1.1	-0.2	-4.9	-16.0	-12.4	-0.4	-2.0	-2.1	-0.3	-0.1	-0.3
Contact-Centroid Mean Diff (ms)	0.0	0.0	0.0	0.0	4.0	9.9	-1.5	-3.7	-0.1	2.9	2.1	-12.3	0.8	14.2	3.3
Contact-Centroid S.D (ms)	0.0	0.0	0.0	0.0	-10.2	-9.6	-7.4	-7.2	-3.5	-8.2	-7.9	-15.6	-9.0	-7.2	-13.5
Contact-Centroid Mean Diff - Weighted (ms)	0.0	0.0	0.0	0.0	1.6	7.0	-0.2	-9.8	-0.8	-10.0	-2.6	-16.3	-9.5	-0.7	-3.0
Contact-Centroid S.D - Weighted (ms)	5.2	0.0	0.0	0.0	-9.1	-6.6	-7.3	-8.0	-3.7	-5.1	-9.7	-14.1	-8.6	-5.9	-11.8

Table F-1-3: Number of positive and negative cluster regions present within the loaded and unloaded contact areas. M - medial side, L - lateral side

	Participant 1			Participant 2			Participant 3			Participant 4			Participant 5		
	Trial 1	Trial 2	Trial 3	Trial 1	Trial 2	Trial 3	Trial 1	Trial 2	Trial 3	Trial 1	Trial 2	Trial 3	Trial 1	Trial 2	Trial 3
	Unloaded Contact														
T_2-increase (from unloaded to loaded)					1M, 1L	0M, 1L	1M, 0L	2M, 0L	1M, 0L	2M, 0L	1M, 0L	3M, 0L	1M, 0L	2M, 0L	1M, 0L
T_2-decrease (from unloaded to loaded)					1M, 0L	2M, 1L	2M, 0L	1M, 1L	1M, 0L	1M, 2L	1M, 1L	1M, 1L	2M, 0L	1M, 0L	2M, 1L
	Loaded Contact														
T_2-increase (from unloaded to loaded)					0M, 0L	1M, 1L	3M, 1L	3M, 0L	2M, 2L	2M, 0L	1M, 0L	2M, 2L	1M, 0L	2M, 1L	2M, 0L
T_2-decrease (from unloaded to loaded)					1M, 0L	2M, 1L	2M, 1L	2M, 2L	2M, 1L	1M, 2L	1M, 1L	1M, 1L	2M, 0L	1M, 1L	3M, 1L

F2: Cluster Maps with Contact Images

The following figures show the difference cluster maps for increasing and decreasing T_2 from unloaded cartilage to loaded cartilage for all three trials of 5 participants. The cluster maps with loaded and unloaded contact are displayed for each participant. The missing images for participant one and the first trial of participant are due to MRI sequence errors for these trials.

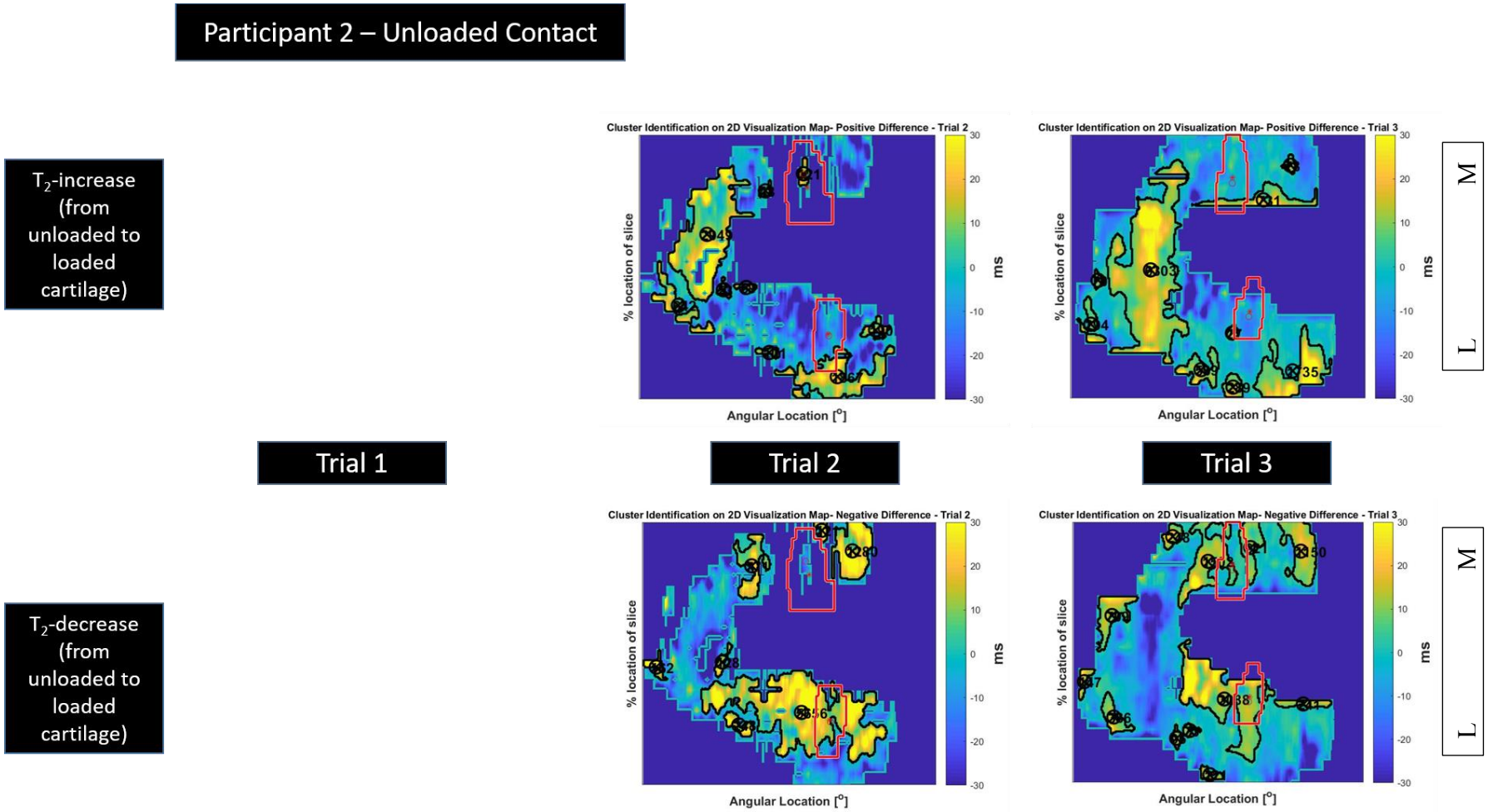

Figure F-2-1: T_2-increasing and T_2-decreasing cluster maps for participant 2 – unloaded contact

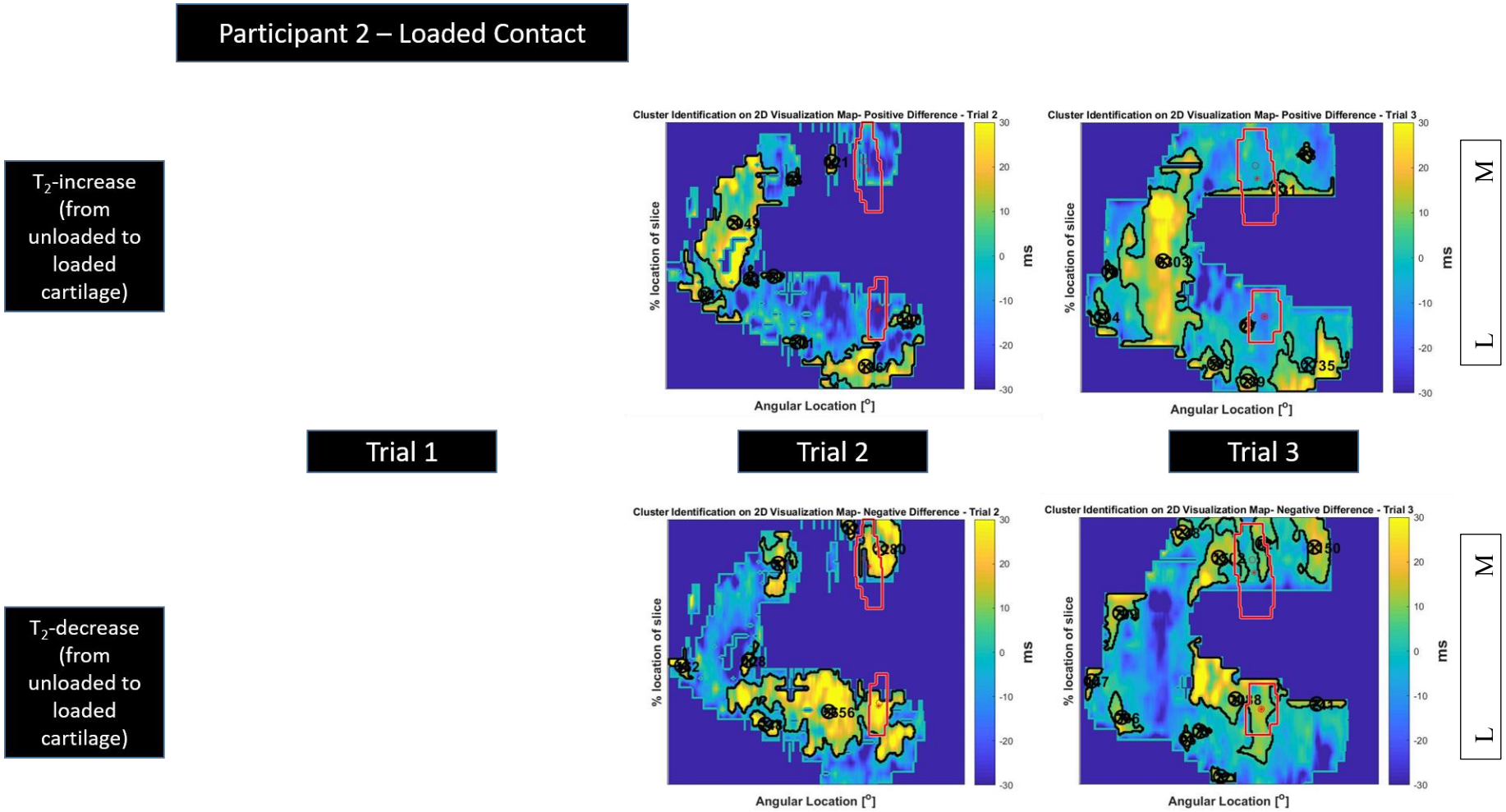

Figure F-2-2: T_2-increasing and T_2-decreasing cluster maps for participant 2 – loaded contact

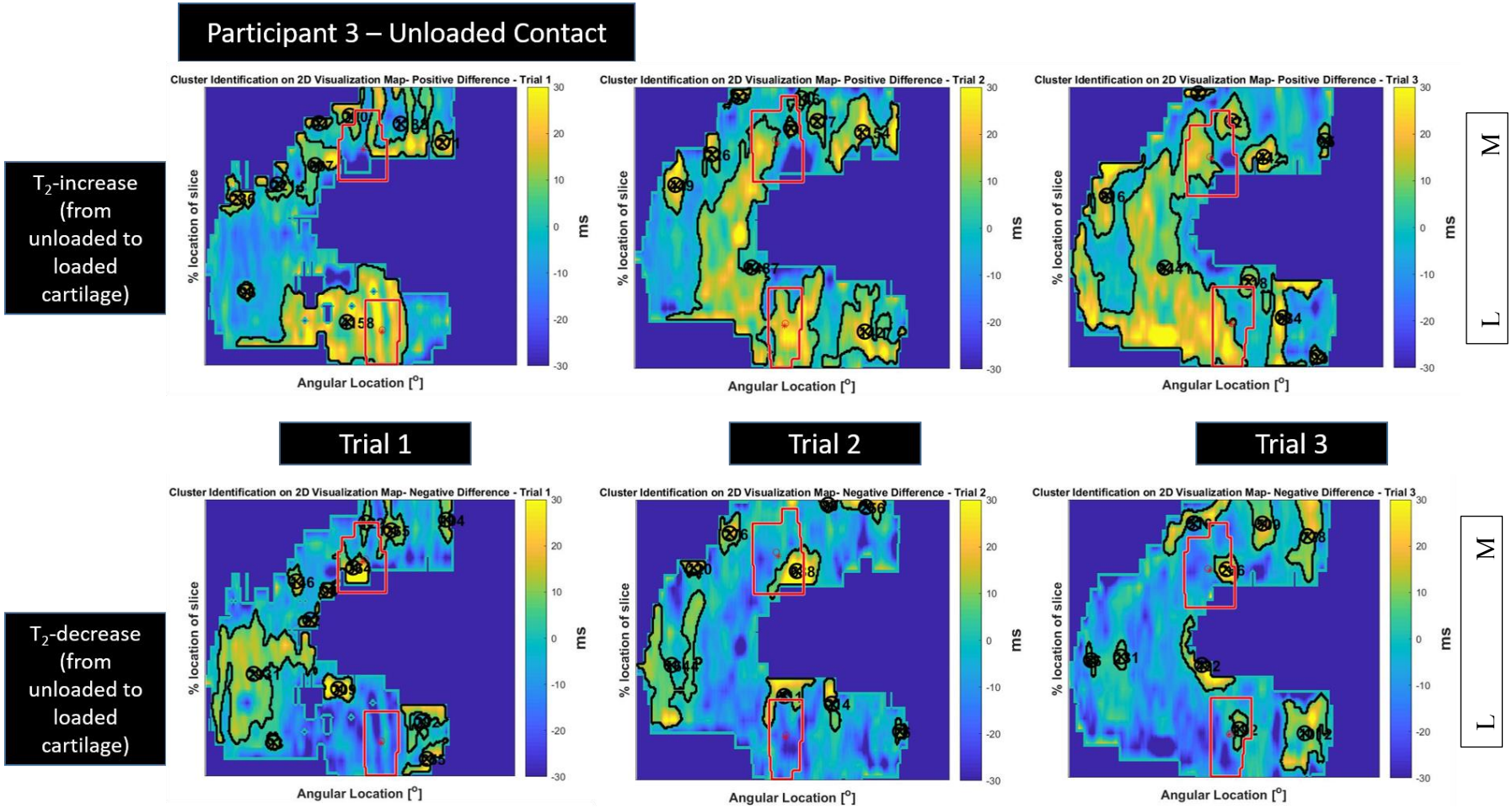

Figure F-2-3: T_2-increasing and T_2-decreasing cluster maps for participant 3 – unloaded contact

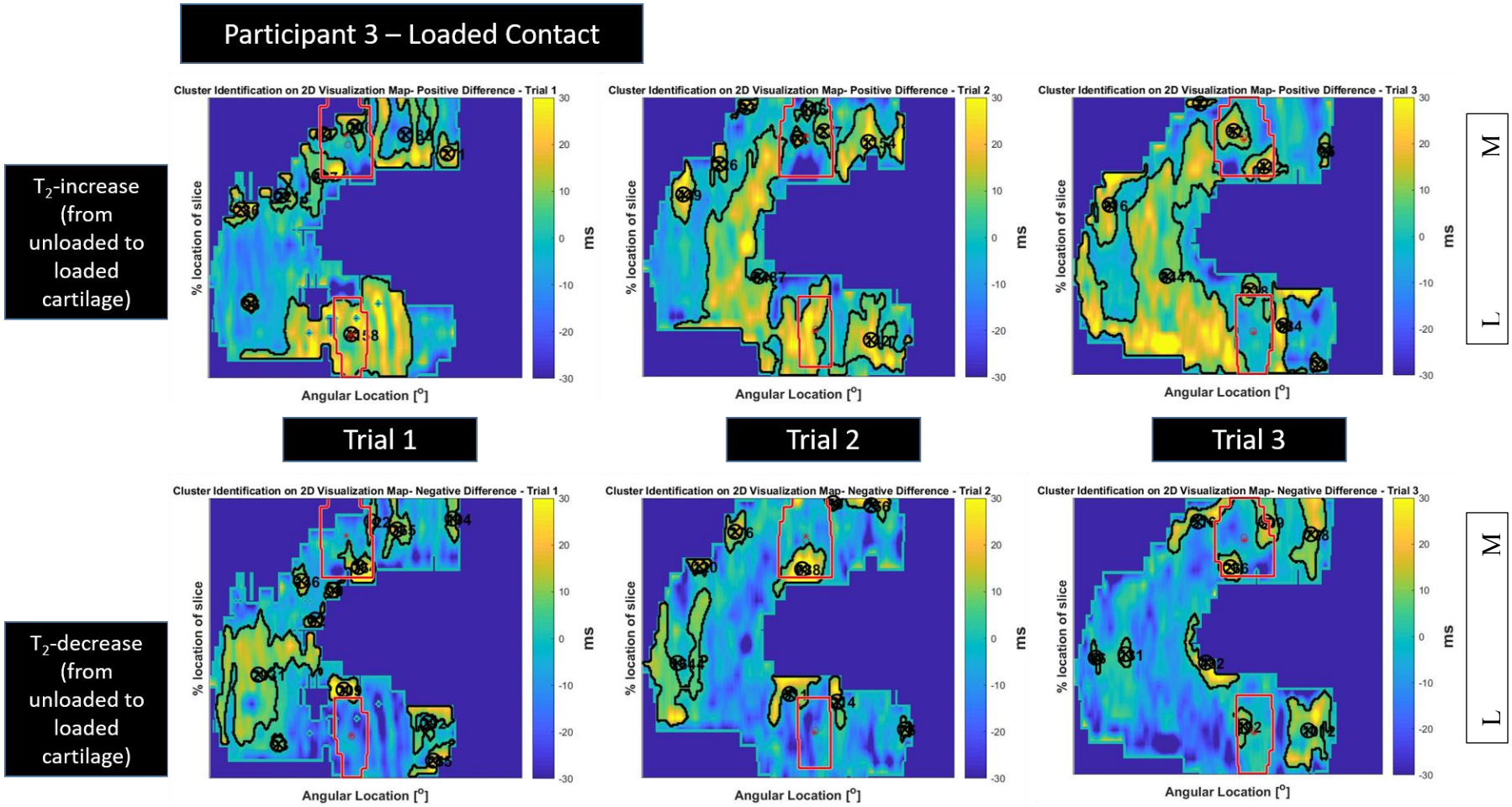

Figure F-2-4: T_2-increasing and T_2-decreasing cluster maps for participant 3 – loaded contact

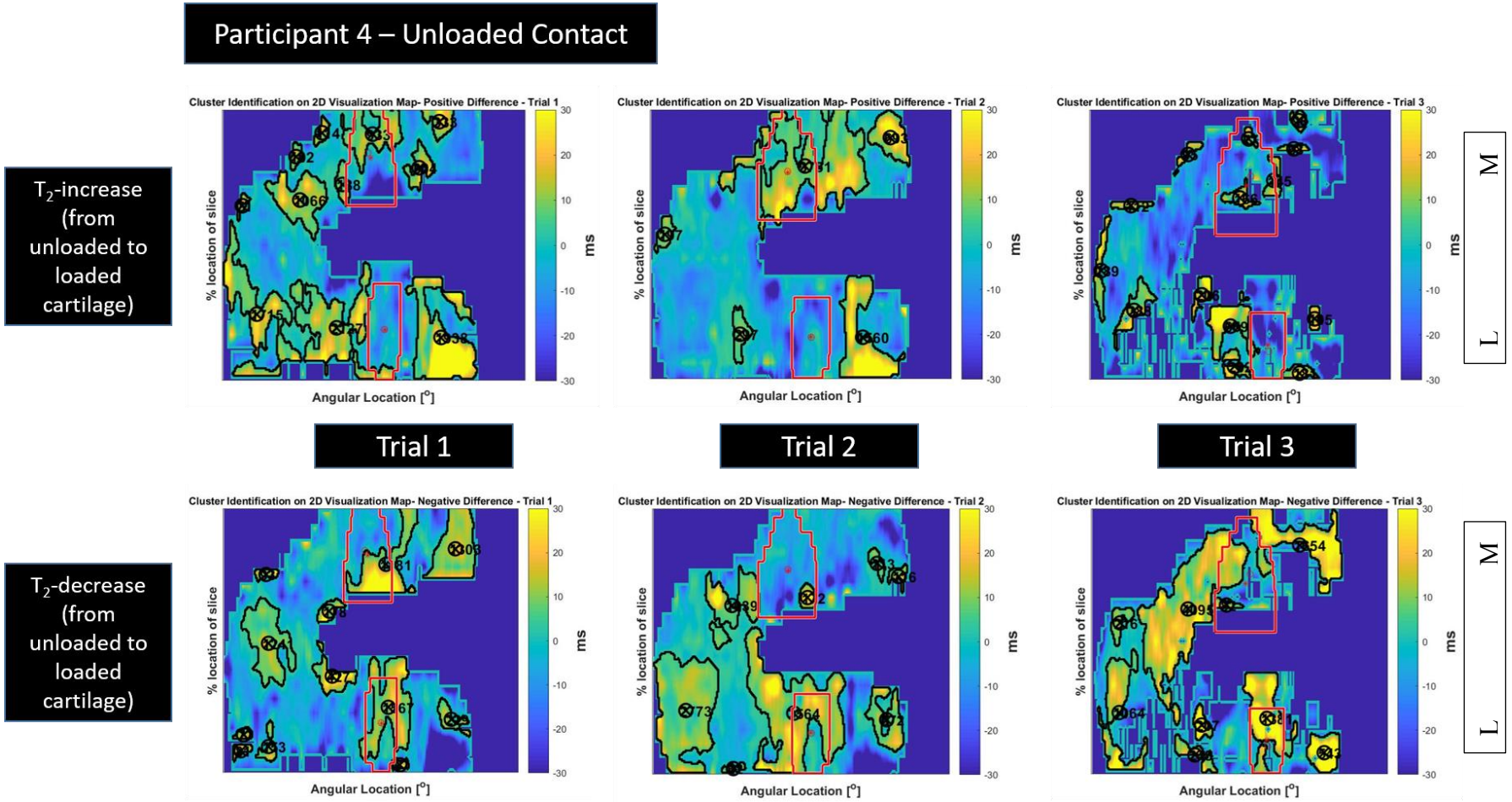

Figure F-2-5: T_2-increasing and T_2-decreasing cluster maps for participant 4 – unloaded contact

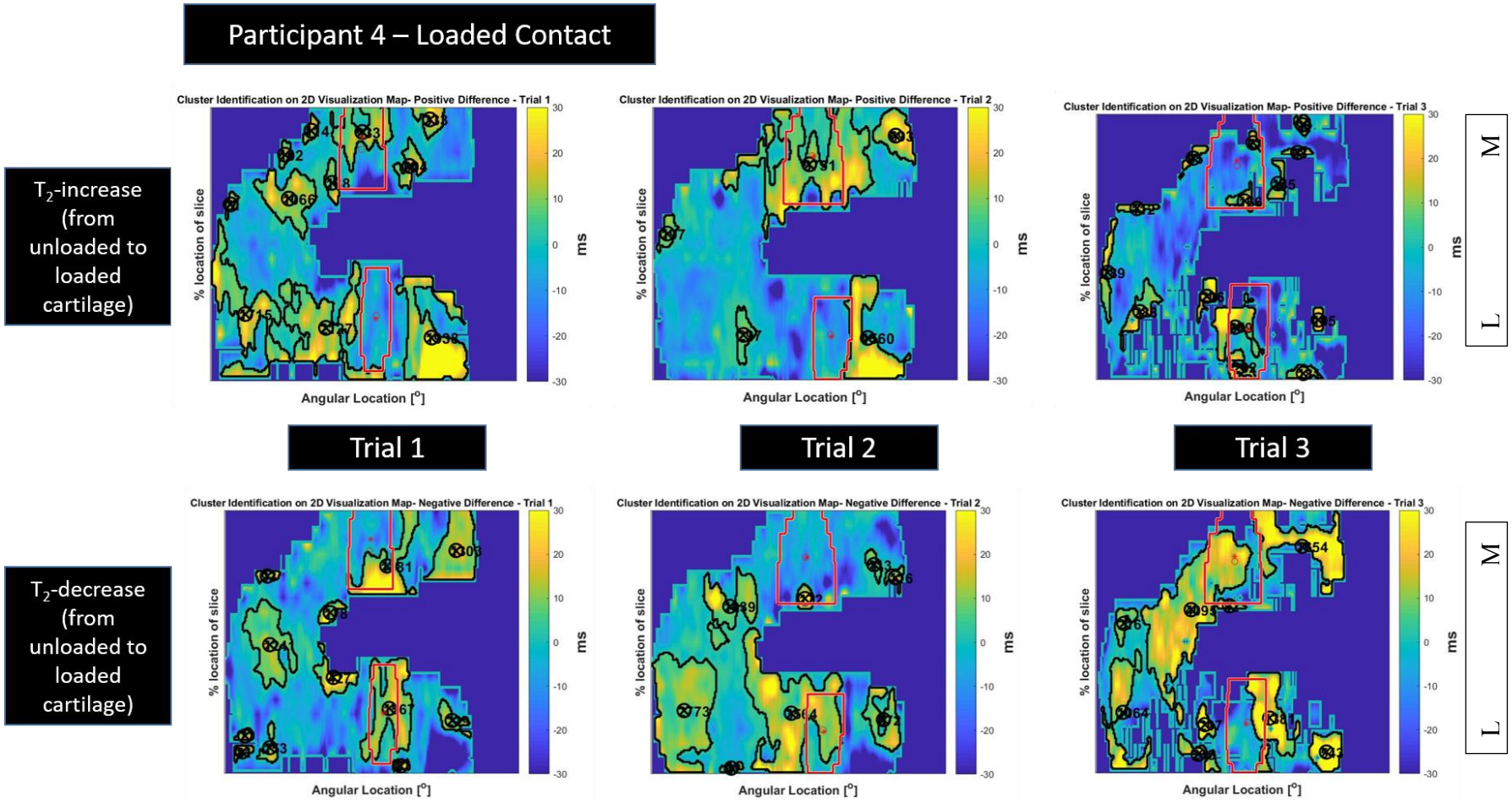

Figure F-2-6: T_2-increasing and T_2-decreasing cluster maps for participant 4 – loaded contact

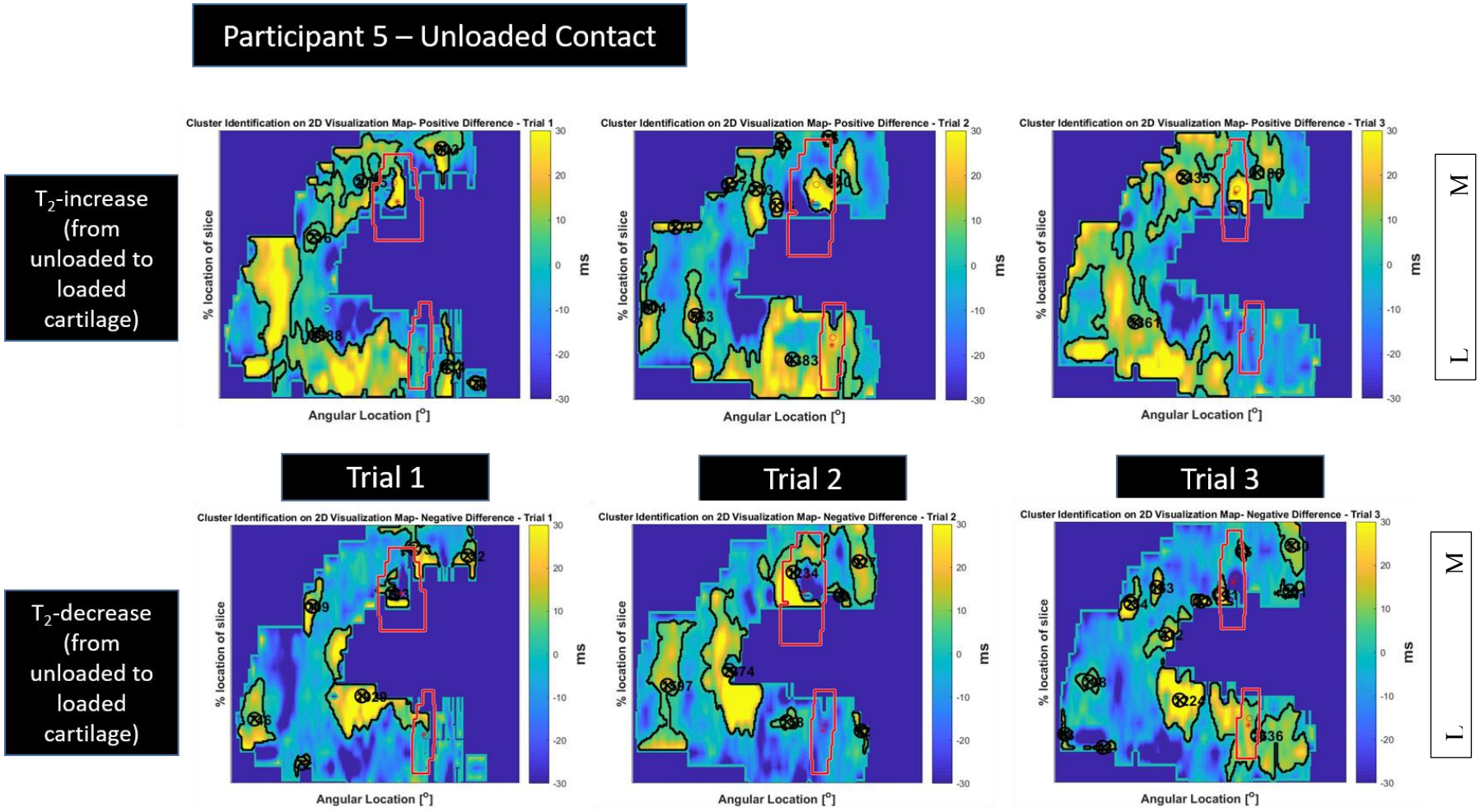

Figure F-2-7: T_2-increasing and T_2-decreasing cluster maps for participant 5 – unloaded contact

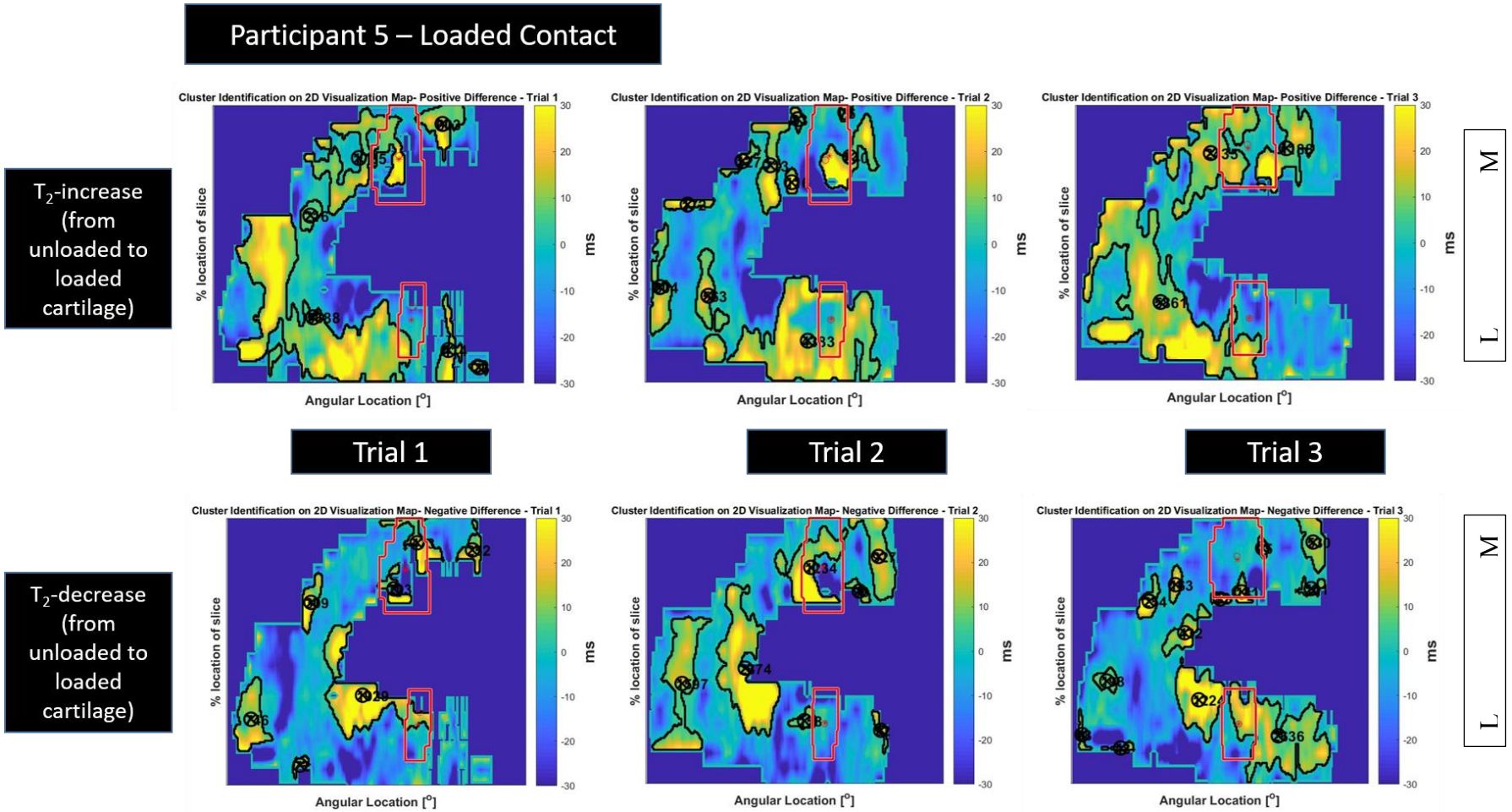

Figure F-2-8: T_2-increasing and T_2-decreasing cluster maps for participant 5 – loaded contact

Appendix G: Consent Form and Ethics Approval

UNIVERSITY OF SASKATCHEWAN

PARTICIPANT INFORMATION AND CONSENT FORM

STUDY TITLE: Validation of a Non-Invasive Tool to Assess Joint and Tissue Mechanics Simultaneously - Healthy Volunteer Study

PRINCIPAL INVESTIGATOR (PI):
Emily McWalter, PhD
Assistant Professor, Department of Mechanical Engineering
University of Saskatchewan
57 Campus Drive, Saskatoon, SK, S7N 5A9
phone: (306) 966-5298
email: emily.mcwalter@usask.ca

SUB-INVESTIGATOR
Joel Lanovaz, PhD
joel.lanovaz@usask.ca

STUDENT RESEARCHER
Lumeng Cui
cuilumeng135@gmail.com

SPONSOR:
The Arthritis Society of Canada

Ibukun Elebute
ioe760@mail.usask.ca

INTRODUCTION
You are invited to participate in this study because you are a healthy individual with no history of knee pain, knee injury, knee surgery, or musculoskeletal disease or disorder.

Your participation is voluntary. It is up to you to decide whether or not you wish to take part. If you decide to participate, you are still free to withdraw at any time and without giving any reasons for your decision. If you do not wish to participate, you will not affect your employment or academic standing.

Please take time to read the following information carefully. You can ask the study principal investigator or staff to explain any information that you do not clearly understand. You may ask as many questions as you need. Please feel free to discuss this with your family, friends or family physician before you decide.

WHO IS CONDUCTING THE STUDY?
The study is being conducted by Dr. McWalter, her co-investigators, and her students at the University of Saskatchewan. The sponsor of this study, The Arthritis Society of Canada, will reimburse Dr. McWalter and the University of Saskatchewan for the costs of undertaking this study. However, neither the institution nor any of the investigators or staff will receive any direct financial benefit from conducting this study.

WHY IS THIS STUDY BEING DONE?
This study is being done because we need more validated and robust research tools that can tell us about how knee joints work.

WHO CAN PARTICIPATE IN THIS STUDY?
You are eligible to participate in this study if you are a healthy individual with no history of knee pain, knee injury, knee surgery, or musculoskeletal disease.

You may not participate in this study if you have any contraindications for MRI including but not limited to a cardiac pacemaker, implanted metal, pregnancy, and claustrophobia.

WHAT DOES THE STUDY INVOLVE?

This is a repeatability study, meaning that we need to determine if we are able to obtain the same numbers each time we collect data. All participants will repeat the entire study procedure three times in order to check this.

Each participant will fill out a questionnaire asking basic information (sex, height, weight, date of birth, etc). This information will be used to identify any potential bias in the data; for example, results of a group of all young individuals may differ from those of a group of older individuals. This is information is important to report to the scientific community.

Each participant will also undergo the following procedures THREE TIMES:

1) **MRI of the knee in a relaxed position:** This MRI exam consist of a series of scans of your knee that will last approximately one hour and five minutes. There will be small markers attached at various locations around your knee using double sided tape during these scans. The MRI exam will take place at the Royal University Hospital.
2) **MRI of the knee while pressing on a pedal:** A MRI-safe pedal will be placed into the MRI system. You will be positioned in the scanner with your foot on the pedal. A series of six scans will be obtained while you push on this pedal. These scans will be no more than 3 minutes each and you will have a three minute break between scans. One of the research team members will be providing you with detailed instructions throughout this process. There will be small markers attached at various locations around your knee using double sided tape during these scans. This exam will take approximately 45 minutes. The MRI exam will take place at the Royal University Hospital.
3) **Motion tracking:** You will be asked to carry out a series of activities including, , walking, climbing stairs, walking down stairs, rising from a chair, drop (40 cm box), single leg drop, single leg hop, counter-movement jump, pivots, side-step cutting, running, jogging, squats, and seated knee extensions in the biomechanics lab. You will have small markers placed at points from your back to your foot using double sided tape for the duration of this test. We will collect movement and force data during the activities. Each activity will be repeated three times. The motion tracking tests will take approximately 1 hour. Motion tracking will take place at the Physical Activity Complex at the University of Saskatchewan.

Note: The overall procedure may not occur in the order shown above.

Your commitment will be no more than four hours for each of the three data collection sessions; therefore, your total participation for this study will be no more than 12 hours. Ideally the sessions will take place on three consecutive days; however, due to scheduling of the MRI this may not be possible. At most, all three sessions will occur within a two-week time period.

OPTION OF HAVING DATA STORED IN A RESEARCH DATABASE

The researchers are creating a database that may be used to answer additional research questions in the future. The purpose of this is to use the research data to its fullest extent in the long term. For example, a larger study of patients with diseases of the knee may need to be compared to a group of individuals with healthy knees; instead of collecting data from healthy individuals again, we could use the data collected for the present study. Examples of other potential studies that may be conducted include knee osteoarthritis, anterior cruciate ligament injury (ACL), meniscus injury, changes in tissue health with age, and changes in tissue health with exercise.

Having your information included in this database is optional and does not impact your participation in the present study. The data will be stored until the lead investigator, Dr. Emily McWalter, either retires or leaves the University of Saskatchewan at which point it will be destroyed. The database will consist of only de-identified data, i.e. your name will not be included in the database; however, the database will be password protected on an encrypted computer. No de-identification key will be maintained for this database. For the present study, the data is de-identified at the collection stage (i.e. only a study ID identifies your MRI and Motion Tracking data); for the database, the study ID will be removed from your data and only the name of the original study will be included in the database. Only Dr. McWalter's research team and collaborators at the University of Saskatchewan will have access to the database. Prior to using your data in any subsequent research studies, approval by the University of Saskatchewan Research Ethics Board will be obtained but you will not be contacted to reaffirm consent.

WHAT ARE THE BENEFITS OF PARTICIPATING IN THIS STUDY?

If you choose to participate in this study, there will not be direct benefits to you. It is hoped the information gained from this study can be used in the future to benefit other people with knee injury or disease. Once the study is complete, a summary of the study results and published data can be provided to you upon request; contact Dr. Emily McWalter via phone or email (contact information on first page).

The study may lead to the development of commercial products but there are no plans to share with you any financial profits resulting from the use of your samples or data.

WHAT ARE THE POSSIBLE RISKS AND DISCOMFORTS?

To date, there are no known long-term health risks associated with having a MRI procedure. The extended length of you MRI session could result in you becoming uncomfortable lying still during the scan or a brief elevation in your body temperature. The MRI technologist or researcher operating the system will visually monitor you throughout the procedure and will communicate with you via telecom system throughout the MRI exam.

There are no known long-term health risks associated with the motion tracking or force measurement portion of the study.

WHAT HAPPENS IF I DECIDE TO WITHDRAW?

Your participation in this research is voluntary. You may withdraw from this study at any time. You do not have to provide a reason. Your future medical care, employment or academic status will not be affected.

If you choose to enter the study and then decide to withdraw at a later time, all data collected about you during your enrolment will be retained for analysis.

CAN I BE ASKED TO LEAVE THE STUDY?

The principal investigator may decide to discontinue the study at any time, or withdraw you from the study at any time if it is felt to be in your best interests. You may be withdrawn from the study if staying in the study would be harmful, you fail to follow instructions, you become pregnant, or the study is cancelled by the sponsor for administrative or other reasons.

WHAT HAPPENS IF SOMETHING GOES WRONG?

In the case of a medical emergency related to the study, you should seek immediate care and, as soon as possible, notify the principal investigator. Necessary medical treatment will be made available at no cost to you. By signing this document, you do not waive any of your legal rights against the sponsor, investigators or anyone else

WHAT HAPPENS AFTER THE COMPLETION OF THE STUDY?
The results of the study in the form of a brief summary and/or published data will be available, upon request, after the completion of the entire project in 2020 from the Principal Investigator.

WHAT WILL THE STUDY COST ME?
You will not be charged for any research-related procedures. You will not be paid for participating in this study. Parking costs will be reimbursed.

WILL MY PARTICIPATION BE KEPT CONFIDENTIAL?
In Saskatchewan, the Health Information Protection Act (HIPA) defines how the privacy of your personal health information must be maintained so that your privacy will be respected. Your name will not be attached to any information, nor mentioned in any study report, nor be made available to anyone except the research team. A de-identification key that associates your name with a study ID will be stored securely (in a password protected file on an encrypted computer under the supervision of the principal investigator) and will only be accessible by research team members. Data collected by the study team will be retained for a minimum of 5 years after the final results are published. It is the intention of the research team to publish results of this research in scientific journals and to present the findings at related conferences and workshops, but your identity will not be revealed. Research records identifying you may be inspected by the University of Saskatchewan Biomedical Research Ethics Board in the presence of the Principal Investigator for quality assurance and monitoring purposes. The MRI protocols used in this study consist of research sequences, therefore your MRI results will not be used by the study team or your doctors to guide medical decisions regarding your care. The MRI images will only be kept as part of your study data and will not become part of your medical record.

WHO DO I CONTACT IF I HAVE QUESTIONS ABOUT THE STUDY?
If you have any questions or desire further information about this study before or during participation, you can contact Dr. Emily McWalter at 306-966-5298.

If you have any concerns about your rights as a research participant and/or your experiences while participating in this study, contact the Chair of the University of Saskatchewan Research Ethics Board, at 306-*966-2975(out of town calls 1-888-966-2975)*. The Research Ethics Board is a group of individuals (scientists, physicians, ethicists, lawyers and members of the community) that provide an independent review of human research studies. This study has been reviewed and approved on ethical grounds by the University of Saskatchewan Research Ethics Board.

UNIVERSITY OF SASKATCHEWAN

PARTICIPANT CONSENT TO PARTICIPATE

Study Title: Validation of a Non-Invasive Tool to Assess Joint and Tissue Mechanics Simultaneously - Healthy Volunteer Study

- I have read the information in this consent form.
- I understand the purpose and procedures and the possible risks and benefits of the study.
- I was given sufficient time to think about it.
- I had the opportunity to ask questions and have received satisfactory answers.
- I understand that I am free to withdraw from this study at any time for any reason and the decision to stop taking part will not affect my future relationships.
- I give permission to the use and disclosure of my de-identified information collected for the research purposes described in this form.
- I understand that by signing this document I do not waive any of my legal rights.
- I will be given a signed copy of this consent form.

I agree to participate in this study:

Printed name of participant:	Signature	Date
Printed name of person obtaining consent:	Signature	Date

☐ I agree to be contacted about research projects in the future.

☐ I give permission for the data collected to be stored in a database and used for similar, related research studies not described in this form knowing that my identity will remain confidential.

UNIVERSITY OF SASKATCHEWAN

Biomedical Research Ethics Board (Bio-REB)

Certificate of Re-Approval

PRINCIPAL INVESTIGATOR	DEPARTMENT	Bio #
Emily McWalter	Mechanical Engineering	16-326

INSTITUTION(S) WHERE RESEARCH WILL BE CARRIED OUT

Royal University Hospital 103 Hospital Drive Saskatoon SK S7N 0W8	University of Saskatchewan Saskatoon SK	Physical Activity Complex (PAC) University of Saskatchewan Saskatoon SK

STUDENT RESEARCHER(S)
Lumeng Cui, Ibukun Elebute

FUNDER(S)
ARTHRITIS SOCIETY
UNIVERSITY OF SASKATCHEWAN

TITLE
Validation of a Non-Invasive Tool to Assess Joint and Tissue Mechanics Simultaneously – Healthy Volunteer Study

RE-APPROVED ON	EXPIRY DATE
03-Jan-2018	02-Jan-2019

Delegated Review ☒ Full Board Meeting ☐

IRB 1 Registration #00001471 ☐ IRB 2 Registration #00008358 ☐ Not Applicable ☒

CERTIFICATION
The University of Saskatchewan Biomedical Research Ethics Board (Bio-REB) has reviewed the above-named research study. The study was found to be acceptable on scientific and ethical grounds. The principal investigator has the responsibility for any other administrative or regulatory approvals that may pertain to this research study, and for ensuring that the authorized research is carried out according to governing law. This approval is valid for the specified period provided there is no change to the approved protocol or consent process.

FIRST TIME REVIEW AND CONTINUING APPROVAL
The University of Saskatchewan Biomedical Research Ethics Board reviews above minimal studies at a full-board (face-to-face meeting. Any research classified as minimal risk is reviewed through the delegated (subcommittee) review process. The initial Certificate of Approval includes the approval period the REB has assigned to a study. The Status Report form must be submitted within one month prior to the assigned expiry date. The researcher shall indicate to the REB any specific requirements of the sponsoring organizations (e.g. requirement for full-board review and approval) for the continuing review process deemed necessary for that project. For more information visit https://vpresearch.usask.ca/researchers/ethics1.php.

REB ATTESTATION
In respect to clinical trials, the University of Saskatchewan Research Ethics Board complies with the membership requirements for Research Ethics Boards defined in Part 4 of the Natural Health Products Regulations and Part C Division 5 of the Food and Drug Regulations and carries out its functions in a manner consistent with Good Clinical Practices. Members of the Bio-REB who are named as investigators, do not participate in the discussion related to, nor vote on such studies when presented to the Bio-REB. This approval and the views of this REB have been documented in writing. The University of Saskatchewan Biomedical Research Ethics Board is constituted and operates in accordance with the current version of the *Tri-Council Policy Statement: Ethical Conduct for Research Involving Humans* (TCPS2 2014).

Gordon McKay, PhD., Chair
Biomedical Research Ethics Board
University of Saskatchewan

Please send all correspondence to:

Research Services and Ethics Office
University of Saskatchewan
Room 223 – Thorvaldson Building
110 Science Place
Saskatoon, SK Canada S7N 5C9

Appendix H: Copyright Permission

ALL DETAILS

ISSN:	1522-9653	Publisher:	W.B. SAUNDERS CO. LTD.
Type of Use:	Republish in a thesis/dissertation	Portion:	Image/photo/illustration

LICENSED CONTENT

Publication Title	Osteoarthritis and cartilage	Rightsholder	Elsevier Science & Technology Journals
Article Title	Cluster analysis of quantitative MRI T2 ...	Publication Type	e-Journal
Author/Editor	Osteoarthritis Research Society.	URL	http://www.harcourt-international.com...
Date	12/31/1992	Start Page	513
Language	English	Issue	4
Country	United Kingdom of Great Britain and N...	Volume	25

REQUEST DETAILS

Portion Type	Image/photo/illustration	Distribution	Worldwide
Number of images / photos / illustrations	1	Translation	Original language of publication
Format (select all that apply)	Electronic	Copies for the disabled?	No
Who will republish the content?	Academic institution	Minor editing privileges?	Yes
Duration of Use	Life of current edition	Incidental promotional use?	No
Lifetime Unit Quantity	Up to 250,000	Currency	CAD
Rights Requested	Main product		

NEW WORK DETAILS

Title	Repeatability of an Integrative Method ...	Institution name	University of Saskatchewan
Instructor name	Dr. Emily McWallter	Expected presentation date	2020-09-07

ADDITIONAL DETAILS

The requesting person / organization to appear on the license	Ibukunoluwa Elebute

REUSE CONTENT DETAILS

Title, description or numeric reference of the portion(s)	Figure 1i	Title of the article/chapter the portion is from	Cluster analysis of quantitative MRI T2 ...
Editor of portion(s)	Monu, U.D.; Jordan, C.D.; Samuelson, B...	Author of portion(s)	Monu, U.D.; Jordan, C.D.; Samuelson, B...
Volume of serial or monograph	25	Issue, if republishing an article from a serial	4
Page or page range of portion	513-520	Publication date of portion	2017-03-31